Chemogenetic Inhibition of Sensory Neuron Excitability Attenuates Pain-Like Behaviours

Huimin Hu

Green Templeton College

University of Oxford

A thesis submitted for the degree of

Doctor of Philosophy

Nuffield Department of Clinical Neuroscience

Trinity Term 2025

Dedication

This work, a journey through pain and silence, is dedicated

to Daniel and my family, in whom I found my peace,

and to my podcast, *Dasein*, the space where I learned to respond.

Acknowledgements

I am certain that life is indeed a long, long voyage, its ultimate meaning found in experiencing, unlocking, and becoming. My time at Oxford has been a voyage of the self, its destination not merely this thesis, but a clearer version of myself.

Looking back on this journey, a fascinating dialogue emerged between my research and my personal exploration. My research was on Pain and Silence. The former was the stimulus, while the latter, Silence, was the very Response I sought to achieve. Evolution has equipped us with instinctive Reactions to stimuli, but these do not necessarily lead to happiness. Between stimulus and reaction, there is a space. In that space is our power to choose our response. In our response lies our growth and our freedom.

My doctoral studies thus became a journey of transformation, undertaken within the cell in the lab and within the depths of my own self: a journey from a passive Reaction to the active creation of a Response, even if that Response is the no-response of Silence.

This voyage was made possible by those who illuminated the path. My deepest gratitude goes to my supervisors. To my primary supervisor, Professor David Bennett: as the guide for this journey, your vision cleared the fog, and your steadfast support, especially during moments of doubt, provided the safety net that gave me the courage to grow. To Dr Steven Middleton: thank you for imparting your practical wisdom and for giving me the academic freedom to translate ideas into practice. To Professor Annina Schmid: your strength and agency as a woman were a profound inspiration, a theme I have treasured and explored in my podcast.

A fantastic voyage is also impossible without professional guides and warm fellow travellers. I offer my heartfelt thanks to Dr Tina Wei for her expert guidance. I am deeply

grateful to all past and present members of the Bennett Lab, who cultivated a research atmosphere that was rigorous, collaborative, and deeply humane. Thank you (in alphabetical order) to: Adham Farah, Alex Clark, Alexander Davies, Allison Barry, Andreas Themistocleous, Claire Johnson, Emily Gordon, Georgios Baskozos, Helen Johnson, Jimena Perez Sanchez, Jishi John, Joel Fundaun, John Dawes, Kira Werder, Kiran Dhillon, Lucy Dove, Lucy Ridgway, Lyndsey Mugford, Maddalena Comini, Mandy Tseng, Maria Renke, Mariya Misheva, Mathilde Pascal, Miles Peck, Mosab Ali Awadelkareem, Ning Zhu, Oliver Sandy-hindmarch, Omar Alzahrany, Reza Taghipour, Roberto Bellanti, Sana Zuberi, Shuaiwei Wang, Simon Rinaldi, Teodora Trendafilova, and Wenqianglong Li (Ayden Lee).

Among them, a special thank you goes to Dr Pao-Sheng Chang (Paul), who was not only a generous collaborator but a dear friend in the lab, always there for discussion and mutual support.

I am also grateful for the wider Oxford community. To the Principal of Green Templeton College (GTC), Sir Michael Dixon; my College Advisor, Professor Sue Burge; and my College Coach Tutor, Dr Andromachi Athanasopoulou, thank you for representing the pastoral care that made this large university feel like a home. This sense of being seen was amplified when the Nuffield Department of Clinical Neurosciences (NDCN) and GTC featured my story on their websites, a gesture of support that gave me immense strength.

Beyond the microscope, this journey was illuminated by deep friendships and shared thoughts. My thoughts found a sanctuary in my podcast, *Dasein*, co-created with my dear friend, Claire Fang. To our fifty thousand listeners, thank you for transforming solitary reflection into a shared resonance. The most precious treasures of this voyage are the

friendships forged at Oxford. Thank you, Claire, for building a kingdom of thought with me and for sharing in life's countless moments. My heartfelt thanks also go to my dear friends (in alphabetical order): Betty Wan, Demi Jin, Huishu Wang, Linshan Chu, Lily Su, Mary Zhou, Natalia Chen, Noel Shin, Xinyi Shen, Yibo Wang, and all the others not named who filled this road with vibrant colour.

Finally, I thank my staunchest support and my warmest harbour. To my partner, Daniel Dai: You are not a passing traveller on my life's journey, but my anchor of ataraxia and the still point of the turning world. In this tumultuous voyage, you were my one, eternal constant, sharing my anxieties and celebrating my most minor triumphs. With your love and patience, you created a sanctuary where my spirit could rest, always knowing there was a centre for me to return to.

The logbook for this voyage is now written, but the journey of self-discovery is endless. Carrying all of this with me, I set forth once more.

Declaration

I hereby declare that this thesis is my own original research, conducted independently under the supervision of Professor David Bennett and Dr Steve Middleton. All contributions from collaborators have been explicitly acknowledged within the thesis. My specific contributions to the research presented herein are as follows:

For Chapter 2: I was responsible for performing and analysing the immunohistochemistry (IHC) and in situ hybridisation (RNAscope) experiments. I also contributed to the analysis of behavioural data. The data from this chapter have been published in the journal *Pain* (Middleton et al., 2023), on which I am a co-author.

For Chapter 3: After the initial neonatal injections and tissue harvesting by Dr Steve Middleton, I independently performed all further experiments.

For Chapter 4: I designed and independently executed all experimental work presented in this chapter, under the joint guidance of Dr Steve Middleton and Dr Tina Wei.

For Chapter 5: The human induced pluripotent stem cell (hiPSC) lines were a generous gift from Dr Alex Clark and Dr Pao Sheng Chang. Under the guidance of Dr Steve Middleton, I performed all the remaining experiments for this chapter.

Contents

Word count: 40923 (excluding figure legends, references and appendices)

Page count: 283

Abstract

Chronic pain, particularly neuropathic pain and migraine, represents a significant clinical challenge, underpinned by the hyperexcitability of peripheral sensory neurons. Existing therapies offer limited efficacy and substantial side effects, creating an urgent need for novel strategies that can precisely and reversibly modulate pathological neuronal activity. This thesis aimed to develop and validate a chemogenetics-based gene therapy platform for targeted silencing of the peripheral sensory system, offering a new therapeutic avenue for chronic pain.

The research followed a logical progression from foundational validation to translational application. Initial proof-of-concept was established by silencing Nav1.8-positive sensory neurons using the inhibitory chemogenetic tool, GluCl.CreON. This strategy effectively alleviated nociceptive pain while preserving normal tactile sensation, confirming the theoretical viability of subtype-specific analgesia.

However, this success highlighted the limitations of conventional adeno-associated virus (AAV) delivery. To overcome bottlenecks in coverage and invasiveness, we pioneered a neonatal subcutaneous (nSC) injection strategy. This method exploits the transient permeability of the neonatal blood-nerve barrier to achieve simultaneous, efficient (~50% transduction), and stable gene delivery to multi-level dorsal root ganglia (DRG) and the trigeminal ganglia (TG) with a single, minimally invasive injection.

This efficient delivery platform enabled the application of a clinically promising, fully humanised chemogenetic tool, PSAM^4-GlyR, in a nitroglycerin-induced model of chronic migraine. The combined strategy successfully reversed established mechanical

allodynia and orofacial hypersensitivity, providing the first causal evidence for using a humanised chemogenetic tool to treat craniofacial pain.

Finally, to bridge the species translational gap, we performed human-centric validation using sensory neurons derived from human induced pluripotent stem cells (hiPSCs). We systematically evaluated 13 AAV serotypes, revealing a clear trade-off between efficacy and safety. While the engineered AAV-PHP.S was most efficient, it exhibited significant neurotoxicity. In contrast, the natural serotype AAV9 offered a superior safety profile with good transduction efficiency, suggesting a wider therapeutic window.

In summary, this thesis establishes a complete technological pipeline, from tool optimisation and delivery innovation to in vivo validation and preclinical human cell assessment. This work provides a powerful methodological toolkit for sensory neuroscience and lays a robust foundation for developing precise, reversible gene therapies for chronic pain and migraine.

Chapter I General Introduction

1. The Sensory Nervous System

The somatosensory system is the neural foundation that enables an organism to perceive its internal and external environments, generate adaptive behaviours, and maintain homeostasis. It is responsible for transducing diverse forms of physical energy, such as mechanical, thermal, and chemical stimuli from the skin, muscles, joints, and viscera, into the electrochemical signals of the central nervous system (CNS). This process gives rise to a rich array of sensory modalities, including touch, proprioception, temperature sensation, itch, and pain (Basbaum et al., 2009). The integrity of this system is critical for survival; it guides our interactions with the environment and, through the sensation of pain, provides an essential alarm system that triggers protective reflexes in the face of potential or actual tissue damage. However, this system undergoes profound plastic changes following development, disease, or injury. While these changes are adaptive in some contexts, in others, they can evolve into intractable chronic pathological states (Denk & McMahon, 2012; R.-R. Ji et al., 2018).

At a functional level, one of the most fundamental organisational forms through which the nervous system processes information and generates responses is the reflex arc. The afferent pathway is responsible for gathering sensory information (e.g., touch, temperature, noxious stimuli) from peripheral receptors and transmitting it to the CNS, constituting the first input step of the sensory circuit. Conversely, the efferent pathway conveys commands (e.g., motor orders) from the CNS to effectors (e.g., muscles or glands) to execute specific actions or physiological responses, forming the output signal. At the core of the sensory afferent pathway are the primary sensory neurons. These

neurons are the messengers connecting the body to the brain, and their cell body location and structural properties determine how sensory information is initially collected and processed (Almeida et al., 2004; Dewey, 1896).

1.1. Dorsal Root Ganglia (DRG) and Trigeminal Ganglia (TG)

At the origin of the sensory signal transduction pathway, the cell bodies (somata) of primary sensory neurons congregate in specific ganglia, forming critical information gateways between the periphery and the central nervous system. For sensations from the trunk and limbs, these somata are located in the dorsal root ganglia (DRG), which are arranged in pairs along the spinal column. Situated adjacent to the intervertebral foramina, DRG neurons are pseudounipolar. Their peripheral axons extend to various parts of the body to form receptor endings. In contrast, their central axons pass through the dorsal root to enter the spinal dorsal horn, where they form synaptic connections with second-order neurons (J.-K. Cheng & Ji, 2008; Haberberger et al., 2019; Krames, 2014).

For the head and facial regions, the corresponding sensory functions are undertaken by the trigeminal ganglion (TG). The TG, also known as the Gasserian ganglion, is located in Meckel's cave within the middle cranial fossa. It serves as the sole peripheral hub for all somatic sensations from the face and head, including pain, touch, and temperature. Consequently, dysfunction of the TG is intimately linked to a variety of intractable craniofacial pain syndromes, such as migraine and trigeminal neuralgia (Messlinger & Russo, 2019; Rappaport & Devor, 1994).

Both the DRG and TG share an anatomical feature of great significance for neuromodulation: their neuronal somata are enveloped by a relatively permeable blood-nerve barrier (BNB). Compared to the dense blood-brain barrier (BBB) within the CNS, the BNB of the DRG/TG allows for the permeation of larger molecules. This

characteristic is a double-edged sword. On one hand, it renders DRG/TG neurons more susceptible to insults from circulating inflammatory mediators, metabolic by-products, and toxins, making them vulnerable targets in various pathological states. On the other hand, it provides a valuable window for therapeutic intervention, making it possible to target drugs or gene therapy vectors (such as adeno-associated viruses) to primary sensory neurons via systemic or local administration (Reinhold & Rittner, 2020; Sapunar et al., 2012; Sun et al., 2024). How to leverage this window to achieve widespread, efficient, and stable gene delivery to sensory ganglia throughout the body, rather than merely local or incomplete coverage, remains a significant technical hurdle, which is one of the key challenges this thesis aims to overcome.

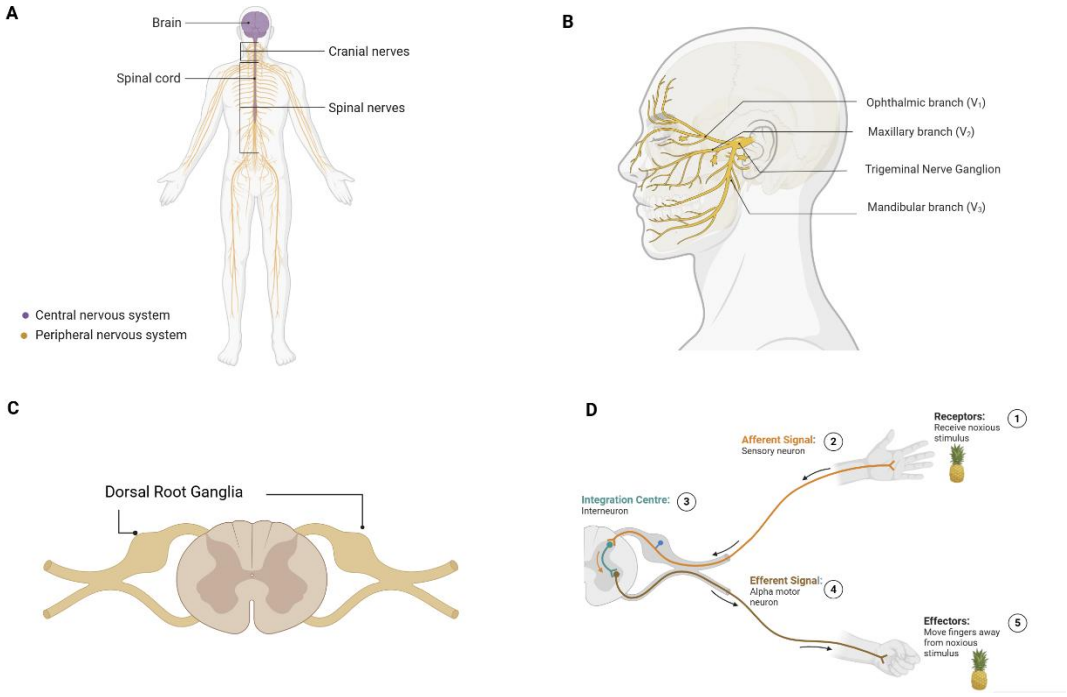

Figure 1.1. Overview of the Peripheral Nervous System (PNS) and its connections to central neural circuits.

A. Schematic overview of the human nervous system, illustrating the central nervous system (CNS; brain and spinal cord, purple) and the peripheral nervous system (PNS;

cranial and spinal nerves, yellow).

B. Anatomical representation of the trigeminal nerve, highlighting the cranial PNS connection to the CNS via the trigeminal nerve ganglion.

C. Cross-section of the spinal cord showing the dorsal root ganglia (DRG), which serve as the primary sensory gateway for spinal nerves connecting the periphery to the CNS.

D. A basic spinal reflex arc illustrating a functional sensorimotor circuit. Peripheral receptors detect noxious stimuli, transmitting afferent signals via sensory neurons to the integration centre in the spinal cord, which subsequently activates efferent alpha motor neurons to elicit a physiological response.

2. Sensory Neuron Heterogeneity

The DRG and TG are not homogeneous cell clusters; instead, they are complex assemblies of sensory neuron subpopulations with high functional and molecular heterogeneity. Based on axon diameter, degree of myelination, and conduction velocity, these neurons can be broadly classified into three types: Aβ-fibres, which are thickly myelinated and transmit non-noxious sensations like light touch; Aδ-fibres, which are thinly myelinated, with some mediating sensations associated with acute, fast, sharp pain and others transmitting light touch (Aδ-LTMRs, also named D-Hairs); and C-fibres, which are unmyelinated and transmit slow, ache-like pain, as well as thermal and itch sensations. Amongst these, Aδ- and C-fibre neurons are collectively known as nociceptors. They are the primary afferent neurons responsible for detecting high-threshold, potentially tissue-damaging stimuli and initiating the neural pathways that transmit this information toward the central nervous system. Sufficient activation of these pathways is considered a prerequisite for the sensation of pain (Basbaum et al., 2009).

At the molecular level, these subpopulations establish their functional specificity by expressing unique combinations of ion channels, receptors, and neuropeptides. For example, the voltage-gated sodium channel Nav1.8 (encoded by the SCN10A gene) is selectively and highly expressed in most nociceptors. It is crucial for maintaining their repetitive firing, making it a key target in pain research (Dib-Hajj et al., 2010). This clear, subpopulation-based division provides a solid biological basis for achieving modality-specific analgesia. This strategy involves precisely targeting and inhibiting the nociceptor subpopulations responsible for transmitting pain signals (e.g., Nav1.8-positive neurons) to alleviate pain whilst preserving normal tactile sensation. However, this simple classification framework, along with traditional drug development strategies that have pinned their hopes on targeting single molecules (such as Nav1.7), is far from sufficient to explain the precision of sensory information encoding, nor has it adequately addressed the pervasive challenges in the treatment of chronic pain (Kingwell, 2019).

Over the past decade, the revolutionary development of single-cell/single-nucleus RNA sequencing (sc/snRNA-seq) and spatial transcriptomics technologies has dramatically reshaped our understanding of DRG and TG neuron diversity. These techniques reduce the reliance on a few markers and instead analyse the complete transcriptomes of tens of thousands of individual neurons, revealing a molecular map far more refined and complex than traditional classifications. Studies have shown that DRG/TG neurons can be deconstructed into more than a dozen, or even over twenty, transcriptionally distinct cell types or subtype clusters. Each cluster is defined by its unique gene expression signature and corresponds to specific functional, morphological, and physiological properties (Qi et al., 2024; Usoskin et al., 2015; Zeisel et al., 2018).

2.1 The Mouse DRG Atlas and its Functional Decoding

Pioneering studies first established a molecular classification system for DRG neurons in mouse models (see Figure 1.2). These studies divided DRG neurons into several major branches including neuropeptide-expressing peptidergic (PEP) nociceptors, marked by genes such as Calca (CGRP), Tac1, and the neurotrophin receptor TrkA; non-peptidergic (NP) nociceptors expressing MrgprD and the receptor tyrosine kinase Ret, which encompass pruriceptor subpopulations expressing specific members like MrgprA3; C-fibre low-threshold mechanoreceptors (C-LTMRs) expressing tyrosine hydroxylase (Th) and Vglut3; TRPM8-expressing cold thermoreceptors; various low-threshold mechanoreceptors, such as Aδ-fibre D-hair afferents expressing TrkB and Aβ-fibre SA/RA-LTMRs expressing TrkC and MafA; and proprioceptors expressing Pvalb and TrkC. More recently, single-cell RNA sequencing (scRNA-seq) has further resolved these classes into finer subgroups, such as PSPEP1-8 for peptidergic and PSNP1-6 for non-peptidergic neurons (Sharma et al., 2020; Usoskin et al., 2015; Zeisel et al., 2018). These molecularly defined subtypes show a high degree of concordance with classical functional classifications (e.g., sensory modality, fibre class, and electrophysiological properties) but provide an unprecedented level of molecular detail and resolution.

Recently, Qi et al. (2024) constructed a DRG genetic toolkit. Based on subtype-specific genes, they developed Cre/Flp and other genetic tools to enable the labelling of specific neuron subpopulations. Through morphological reconstruction and in vivo electrophysiological recordings of these labelled neurons, they discovered that different subtypes have unique coverage areas and branching patterns for their axon terminals in the skin. They also exhibit distinct response thresholds and dynamic ranges to mechanical and thermal stimuli. These findings support a population code model of sensory encoding, wherein different sensory neuron subtypes tile the sensory space. Through their unique

tuning properties and combinatorial activity, they collectively encode the vast complexity of stimuli found in the natural world (Ma, 2012; Qi et al., 2024).

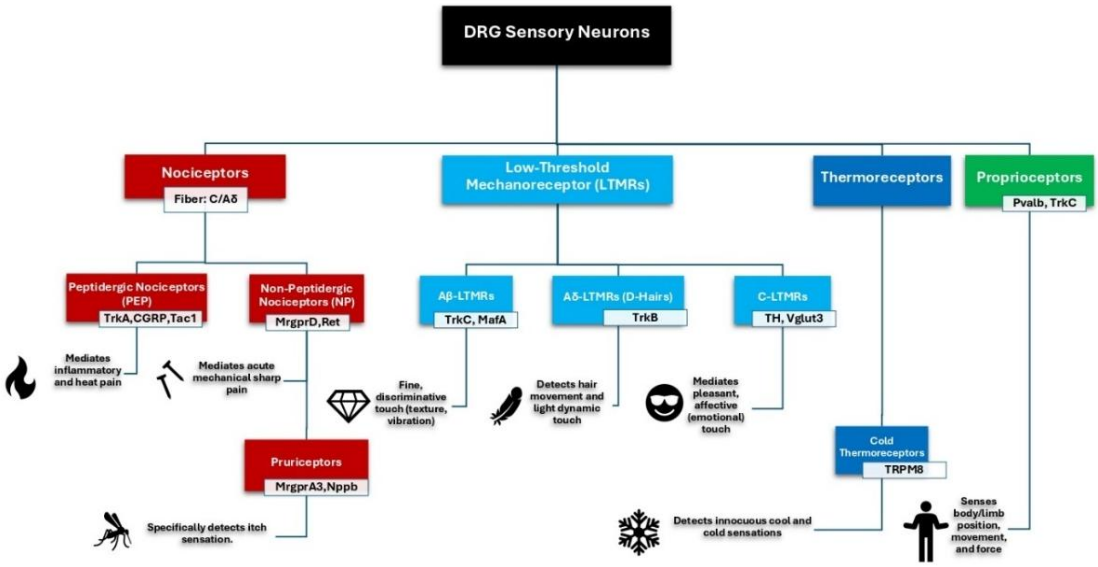

Figure 1.2. Schematic of the molecular classification of DRG sensory neurons. This diagram illustrates the major classes and subpopulations of dorsal root ganglion (DRG) sensory neurons, categorised based on their unique molecular markers, primary sensory functions, and nerve fibre types. Neurons are divided into four major functional categories: nociceptors (red-toned), low-threshold mechanoreceptors (LTMRs, blue-toned), thermoreceptors (cyan-toned), and proprioceptors (green-toned).

Key molecular markers and primary functions for each subtype are listed. Nociceptors are further divided into the neuropeptide-expressing peptidergic (PEP) subclass and the non-peptidergic (NP) subclass, the latter of which includes pruriceptors that specifically mediate itch. LTMRs are classified according to their fibre type and function into Aβ-LTMRs, Aδ-LTMRs, and C-LTMRs, which mediate fine touch, hair movement sensation, and affective touch, respectively.

2.2 The Human DRG Atlas and Cross-Species Insights

Single-cell studies of human sensory neurons face greater challenges due to the difficulty in obtaining human DRG tissue and the fact that the neurons have large, lipid-rich somata that are easily damaged during dissociation. Early studies primarily relied on single-nucleus sequencing or the limited resolution of Visium spatial transcriptomics (Nguyen et al., 2021). Tavares-Ferreira et al. (2022) used spatial transcriptomics to analyse DRGs from eight organ donors, identifying 12 classes of sensory neurons, including five types of C-fibre nociceptors. They also provided the first evidence of potential sex differences in the human DRG; for example, in a nociceptor subpopulation enriched with itch receptors, the expression of calcitonin gene-related peptide alpha (CALCA) was significantly higher in females (Tavares-Ferreira et al., 2022).

More recently, Yu et al. (2024) combined laser capture microdissection (LCM) to isolate individual neuron somata with Smart-seq2 deep sequencing technology, successfully obtaining high-quality human DRG single-cell transcriptome data, with an average of over 9,000 genes detected per neuron. Combined with high-resolution 10x Xenium spatial transcriptomics and RNAscope in situ hybridisation validation, they classified human DRG neurons into 16 fine-grained subtypes. This high-resolution atlas has made critical cross-species comparisons possible. The study found that non-nociceptive neurons (such as TRPM8+ cold thermoreceptors, LTMRs) and proprioceptors exhibit high conservation among humans, monkeys, and mice. In contrast, C-fibre and A-fibre nociceptors show the most significant interspecific divergence. For instance, humans appear to possess a more diverse array of A-fibre nociceptors, including a unique subpopulation named hPEP.PIEZO, which has exceptionally high expression of the PIEZO2 gene, is notable. The researchers speculate that it may be specialised to sense mechanical forces from blood vessels or viscera, possibly as an adaptation to the larger

body size and unique physiological demands of upright walking in humans. Furthermore, the study identified instances of functional homology with different molecular markers. For example, the specific marker for human C-LTMRs is CASQ2, whereas the classic corresponding markers in mice, TH and SLC17A8, are almost unexpressed in humans (Tavares-Ferreira et al., 2022; Yu et al., 2024).

2.3 Specialisation of the Trigeminal System

Although the DRG and TG share the basic blueprint for most sensory neuron subtypes in terms of macro-structure and fundamental function, the TG, as the independent afferent hub for the highly complex craniofacial region, has evolved specialisations. Its neurons specifically innervate the cornea, nasal cavity, oral mucosa, teeth, and the dural vascular system, which is crucial for intracranial pain. For example, single-cell sequencing of mouse dental primary afferent (DPA) neurons revealed that these neurons comprise various multimodal peptidergic nociceptors. Driven by the nerve growth factor (NGF) signalling pathway, they exhibit sensitisation, leading to pain signals in response to low-threshold mechanical stimuli, which precisely reflects the clinical features of dental pulp pain (Lee et al., 2023).

High-throughput single-cell sequencing has further elucidated the cellular ecosystem within the TG. The neuron subtypes largely correspond to those in the DRG, including peptidergic (PEP) and non-peptidergic (NP) nociceptors, C-fibre low-threshold mechanoreceptors (C-LTMRs), TRPM8+ cold thermoreceptors, and various A-fibre neurons (NF subtypes) (Nguyen et al., 2017; L. Yang et al., 2022). Non-neuronal cells include satellite glial cells (SGCs) that tightly envelop neuron somata, myelinating and non-myelinating Schwann cells responsible for myelination, fibroblasts that form the endo- and perineurial connective tissues, as well as vascular and immune cells. These

cells collectively constitute a complex and dynamic microenvironment (Morchio et al., 2024; L. Yang et al., 2022).

In trigeminal neuralgia (TN) and nerve injury, the pathological changes are dramatic. On one hand, animal models reveal that nerve compression can induce dynamic changes of demyelination and remyelination in Schwann cells, accompanied by the involvement of cell death pathways such as ferroptosis. Moreover, neurons actively regulate the pathological responses of glial cells through ligand-receptor signalling (e.g., Sema5a/Plxnb3) (Wei et al., 2024). On the other hand, direct studies of human traumatic trigeminal neuromas have found that the presence or absence of pain is closely associated with the expansion of pro-inflammatory endothelial cells within the nerve and the overexpression of immune molecules such as HLA-A, CXCL2, and CXCL8. This reveals that, following nerve injury in humans, a persistent pro-inflammatory microenvironment driven by the interplay of neural, immune, and vascular cells is a key factor in the chronification of pain (Morchio et al., 2024).

In migraine, human genetic studies (GWAS) have found that risk loci are functionally enriched in multiple cell types of the TG, including peptidergic (PEP) and non-peptidergic (NP) nociceptors, SST+ neurons, and satellite glial cells. This aligns with the transcriptional activation observed across multiple cell types (neurons, glia, vascular cells) in mouse headache models, collectively indicating that migraine is a disorder involving the dysfunction of a complex cellular interaction network within the TG (L. Yang et al., 2022), and it projects to the brain stem.

In summary, the heterogeneity of sensory neurons is far too complex to be captured by single markers. Research based on multi-species, multi-platform single-cell and spatial omics provides unprecedented opportunities for the imaging, functional manipulation,

and therapeutic intervention of specific neuron subpopulations. For example, it enables the development of drugs that target only specific nociceptor subtypes to treat a particular type of pain (such as mechanical or cold pain) and provides key molecular coordinates for evaluating and optimising cross-species translational research strategies.

3. The Challenge of Chronic Pain

Chronic pain is defined as pain that persists or recurs for more than three months, constituting a disease state rather than merely a symptom. It is estimated that over 20% of the global population is affected by chronic pain. It severely impairs patients' physical function, emotional health, and overall quality of life, while imposing a tremendous socioeconomic burden (Baskozos et al., 2023; Breivik et al., 2006; Mills et al., 2019; Van Hecke et al., 2014). Chronic pain often coexists with depression, anxiety, sleep disorders, and cognitive decline, creating a vicious cycle (Descalzi et al., 2017; Finnerup et al., 2021).

3.1 The Pathophysiology of Neuropathic Pain

According to the International Association for the Study of Pain (IASP), neuropathic pain is caused by a lesion or disease of the somatosensory nervous system (Costigan et al., 2009). Unlike acute nociceptive pain, which serves as a physiological alarm, the generation and transmission processes in neuropathic pain become abnormal. Patients may experience spontaneous burning, shooting, or electric shock-like pain in the absence of any external stimulus. Concurrently, they may feel severe pain in response to normally non-painful stimuli (such as the light touch of clothing), a phenomenon known as allodynia. Furthermore, their response to painful stimuli may be disproportionately amplified, a condition called hyperalgesia (Colloca et al., 2017; Finnerup et al., 2021).

The core pathophysiological basis of neuropathic pain is a series of profound and lasting maladaptive neuroplastic changes that occur throughout the sensory signalling pathway. These changes span the peripheral and central nervous systems and primarily involve two major processes: peripheral sensitisation and central sensitisation.

Peripheral pathology begins in the periphery. Within the DRG and TG, nerve injury triggers the infiltration of immune cells (such as macrophages) and the activation of resident satellite glial cells (SGCs). These cells release a plethora of sensitising substances, including tumour necrosis factor-alpha (TNF-α), interleukin-1β (IL-1β), and nerve growth factor (NGF), forming a "sensitising soup" (Hanani, 2005; Hanani & Spray, 2020; Ren & Dubner, 2010). Simultaneously, injury signals initiate endogenous transcriptional and epigenetic reprogramming, leading to the upregulation of expression and function of a range of pro-excitatory ion channels and receptors (e.g., voltage-gated sodium channels Nav1.7/1.8/1.9, hyperpolarisation-activated cyclic nucleotide-gated channels (HCN), and transient receptor potential channels TRPV1/TRPA1), while inhibitory mechanisms (such as various potassium channels) are downregulated. These molecular changes collectively lower the firing threshold of neurons and lead to spontaneous and ectopic discharges (Deval & Lingueglia, 2015; Dib-Hajj et al., 2010; Giorgi et al., 2019; He et al., 2019; Koivisto et al., 2024). At the structural level, axonal transport within neurons is disrupted, and their peripheral projections undergo remodelling, such as abnormal axonal sprouting and re-innervation. There is also evidence of neuronal cell death following injury. All these factors combine to alter connectivity between the peripheral and central nervous systems (Basbaum et al., 2009; Cooper et al., 2024; N. Gao et al., 2024; Y. Ji et al., 2022; Testa et al., 2024).

The persistent, abnormal afferent signals originating from the periphery continuously bombard second-order neurons in the spinal dorsal horn and brainstem. This barrage,

along with neuroinflammatory responses mediated by microglia and astrocytes within the CNS, synergistically enhances central synaptic transmission efficiency and expands neuronal network excitability. This ultimately leads to the establishment and maintenance of central sensitisation, whereby the central system's capacity to process incoming signals is amplified, causing even normal inputs to be interpreted as pain (Denk & McMahon, 2012; Ghosh & Pan, 2022; Meacham et al., 2017).

3.2 Trigeminal Neuralgia (TN)

Trigeminal neuralgia is another classic example of craniofacial neuropathic pain, characterised by brief, sudden, electric shock-like attacks of severe facial pain. Its aetiology is diverse; the most common classical form is caused by neurovascular compression, while secondary forms arise from lesions to the trigeminal root entry zone (REZ) due to multiple sclerosis or other pathologies. There is also an idiopathic form with no known cause (Zakrzewska & Linskey, 2014). Although the initiating factors vary, they all lead to focal demyelination, axonal loss, and local inflammation. These peripheral structural pathologies directly result in abnormal function of trigeminal axons. Demyelinated nociceptive axons become hyperexcitable, generating spontaneous ectopic impulses and causing ephaptic transmission (crosstalk) between nociceptive and non-nociceptive fibres. This persistent abnormal neural activity from the periphery then induces central sensitisation through over-excitation or causes deafferentation hypersensitivity through axonal loss (Ashina et al., 2024; Love & Coakham, 2001). The pathology of TN clearly points to the trigeminal pathway, underscoring the rationale for targeting peripheral sensory ganglia for intervention.

3.3 Limitations of Neuropathic Pain Treatment and Translational Challenges

Despite a deepening understanding of the pathophysiology of neuropathic pain, the clinical treatment landscape remains far from satisfactory.

Firstly, existing therapies struggle to balance efficacy and tolerability. As early as 2005, a seminal review by Finnerup et al. used the Number Needed to Treat (NNT) framework to systematically demonstrate that even the most effective drugs at the time, tricyclic antidepressants (TCAs), required treating several patients for one to achieve significant pain relief (Finnerup et al., 2005). This conclusion has been repeatedly corroborated in nearly two decades of subsequent research. Currently, first- and second-line drugs for neuropathic pain, such as calcium channel α2δ subunit ligands (gabapentin/pregabalin), TCAs, and serotonin-norepinephrine reuptake inhibitors (SNRIs), exhibit significant variability in efficacy depending on the individual and the aetiology (Finnerup et al., 2015, 2021; NICE, 2020; Soliman et al., 2025). Moreover, these drugs are commonly associated with central side effects like dizziness and somnolence, which prevent many patients from reaching an effective therapeutic dose (Derry et al., 2019). Although opioids have definite analgesic effects, their use in chronic non-cancer pain is strictly limited due to risks of addiction, abuse, respiratory depression, and long-term use-induced hyperalgesia (Busse et al., 2018).

As the first-line drug for classical trigeminal neuralgia (TN), the efficacy of carbamazepine is often compromised by its severe side effects. In addition to common sedation and ataxia, there is a risk of the life-threatening Stevens-Johnson syndrome (associated with the HLA-B1502 gene in specific Asian populations). Consequently, up to 27% of patients are forced to reduce their dose due to adverse reactions, and the slightly

better-tolerated oxcarbazepine also has its limitations. Ultimately, treatment failure or intolerance compels patients to turn to second-line drugs with weaker evidence or to invasive surgical procedures (Ashina et al., 2024).

Secondly, despite a wealth of basic research yielding numerous new analgesic targets, clinical translation has been fraught with setbacks. Classic examples include NK1 (neurokinin) receptor antagonists, which, despite showing promise in rodents, failed to demonstrate consistent and reproducible analgesic benefits in human pain trials (Hill, 2000; Rupniak & Kramer, 2017). Although the development of Nav1.7 voltage-gated sodium channel inhibitors was historically challenged by issues of achieving sufficient target occupancy and functional inhibition (Eagles et al., 2022; Kingwell, 2019). A more significant contemporary hurdle has become managing the on-target side effects of potent inhibitors. Notably, because Nav1.7 plays a crucial role in postganglionic sympathetic nerve function in humans, its inhibition can disrupt the sympathetic nervous system, which has emerged as a key factor limiting their clinical therapeutic window (Kim et al., 2024). TRPV1 antagonists, while effective preclinically, commonly cause hyperthermia and other thermoregulatory side effects in clinical studies (Talavera et al., 2020). FAAH inhibitors have shown limited overall efficacy, and a severe safety incident in a Phase I trial significantly impacted the translational prospects of this mechanism (Kaur et al., 2016). These failures and limitations collectively reflect core translational barriers, including inadequate pharmacokinetics and target occupancy, cross-species differences in physiology and pathways, and insufficient safety margins.

3.4 Chronic Migraine

Chronic migraine is another disabling condition originating from the dysfunction of the sensory nervous system. Its core pathophysiological process involves the activation of the trigeminovascular system. During a migraine attack, neurons in the trigeminal

ganglion (TG) are activated, releasing various neuropeptides, including calcitonin gene-related peptide (CGRP). CGRP acts on receptors on cranial blood vessels (especially dural vessels), causing vasodilation and plasma extravasation, which triggers neurogenic inflammation. This process not only activates and sensitises dural nociceptors, but the persistent afferent signals also lead to central sensitisation of second- and third-order neurons in the trigeminal pathway. This ultimately manifests as pulsating headache, photophobia, phonophobia, and cephalic allodynia, where normal touch to the scalp is perceived as painful (Edvinsson, Haanes, et al., 2018; Goadsby et al., 2017).

The success of monoclonal antibodies and small-molecule antagonists (gepants) targeting CGRP or its receptor in the prevention and acute treatment of migraine is a paradigm of bench-to-bedside translation. It also validates the TG as an effective intervention target for headache and craniofacial pain (Tso & Goadsby, 2017). However, CGRP-targeted drugs are not without their limitations. Their potential interference with normal physiological functions, such as the cardiovascular system, highlights an inherent limitation of systemic pharmacological interventions.

To study the mechanisms of migraine and test new treatments, researchers have developed various animal models. Among them, the repeated systemic administration of nitroglycerin (NTG) is a widely used model. In the body, NTG is metabolised to produce nitric oxide (NO). NO can directly enhance the excitability of TG neurons and promote CGRP release by activating the soluble guanylate cyclase (sGC) - cyclic guanosine monophosphate (cGMP) signalling pathway. This model can reliably reproduce several key features of migraine in animals, including delayed-onset mechanical allodynia (assessed by facial von Frey testing or licking behaviour) and the activation of central structures like the trigeminal nucleus caudalis (TNC), as indicated by the upregulation of immediate-early genes such as c-Fos (Pradhan et al., 2014; Tardiolo et al., 2019). This

makes the NTG model a valuable tool for testing intervention hypotheses aimed at suppressing the activity of peripheral TG neurons to alleviate central sensitisation and pain-like behaviours.

3.5 The Therapeutic Rationale: Functional Silencing versus Deafferentation

The development of novel therapies for chronic pain relies on a crucial distinction: the difference between functional silencing (quieting the nerve) and structural deafferentation (cutting the nerve). A key premise of our approach is that neuropathic pain is driven by peripheral ectopic discharge. Following nerve injury, pathological spontaneous activity arises not only in the injured axons but, crucially, in the uninjured nociceptors within the same nerve bundle, driven by inflammatory signalling and dysregulated ion channels (Devor, 2009; G. Wu et al., 2001). These ectopic discharges bombard the central nervous system, maintaining sensitisation and pain perception (Waxman & Zamponi, 2014).

Historically, surgical attempts to eliminate this input by physically severing nerve pathways (rhizotomy) have often failed, leading to anaesthesia dolorosa (painful numbness) (Tasker, 1987). The mechanism for this failure is the total loss of sensory input: when the brain loses all afferent signals—including touch and proprioception—it undergoes maladaptive cortical reorganisation, effectively hallucinating pain in the deafferented region (Flor et al., 1995).

Therefore, to reduce pain without causing deafferentation syndromes, we must selectively silence nociceptors while preserving Low-Threshold Mechanoreceptors (LTMRs). Evidence that this strategy is likely to work in humans comes from both human genetics and pharmacology. First, humans with loss-of-function mutations in NaV1.7 (a

channel essential for nociceptor firing) experience complete insensitivity to pain without suffering from deafferentation pain or touch deficits, proving that molecular silencing of nociceptors is safe and effective in humans (Cox et al., 2006). Second, topical lidocaine patches, which dampen peripheral excitability without severing nerves, are a first-line treatment for post-herpetic neuralgia (Finnerup et al., 2015). Another approach utilises engineered silencing tools to mimic these effects with greater cell-type specificity. Recent rodent studies have confirmed that such selective silencing of nociceptors effectively reverses hypersensitivity while preserving Aβ-mediated touch, providing a robust translational rationale (Middleton et al., 2023; Weir et al., 2017).

4. Neuromodulation via Chemogenetic Tools

Traditional pharmacology often relies on modulating single molecular targets. Because these targets are shared across multiple cell types, it is difficult to inhibit pathological neurons without affecting cells that maintain normal function, leading to a conflict between efficacy and safety. A new strategy, therefore, is to move beyond molecular selectivity and shift to the cellular/circuit level, aiming to directly, reversibly, and precisely control the electrical activity of the pathological neuronal populations that initiate and maintain pain. Chemogenetics provides the tools to realise this strategy. Through genetic engineering, chemogenetics expresses designer receptors in specific cell populations. These receptors are inert to endogenous neurotransmitters but can be specifically activated or inhibited by exogenous, otherwise physiologically inert designer drugs, thereby enabling remote, reversible, and cell-type-specific control of neuronal activity (Atasoy & Sternson, 2018; Roth, 2016; Sternson & Roth, 2014). A summary of

the key chemogenetic tools discussed below, including their mechanisms of action and primary limitations, is provided in Table 1.1.

4.1 GPCR-Based Metabotropic Systems - DREADDs

The most widely used system in the field of chemogenetics is Designer Receptors Exclusively Activated by Designer Drugs (DREADDs). The core principle involves expressing genetically engineered G protein-coupled receptors (GPCRs) and using exclusive small-molecule ligands to remotely and precisely control the activity of specific neurons. This control is not achieved by directly altering ion channels but through the activation of complex intracellular second messenger cascades, resulting in an indirect but long-lasting modulation of neuronal excitability (Roth, 2016; Urban & Roth, 2015).

The DREADDs system primarily includes two functional modules: excitatory and inhibitory control. The representative excitatory receptor is the Gq-coupled hM3Dq. When its exclusive ligand (such as CNO or the high-affinity, high-selectivity DCZ) binds, hM3Dq activates the Gq–PLC pathway, cleaving PIP2 into IP3 and DAG. IP3 promotes Ca2+ release from the endoplasmic reticulum, and the significant rise in intracellular Ca2+ causes depolarisation and increases the firing rate (Alexander et al., 2009; Armbruster et al., 2007; Nagai et al., 2020). In contrast, the classic inhibitory receptor is the Gi-coupled hM4Di. Upon activation, hM4Di releases Gβγ subunits that directly activate G-protein-coupled inwardly rectifying potassium (GIRK) channels, leading to K+ efflux and membrane hyperpolarisation, thereby silencing neuronal activity (Armbruster et al., 2007; Stachniak et al., 2014; Wess et al., 2013).

To achieve independent, multidimensional control over different neuronal populations within the same animal, researchers have developed further systems like KORD. KORD is an engineered κ-opioid receptor coupled to the Gi pathway, with a mechanism of action

similar to hM4Di, achieving inhibition via GIRK-mediated hyperpolarisation. Its key advantage is that it is activated by an entirely different ligand, salvinorin B (SalB). This allows researchers to co-express hM3Dq and KORD in the same animal. By coordinating the timing and dosage of their respective ligands (CNO or SalB), they can achieve multiplexed (parallel or sequential, excitatory and inhibitory) manipulation of neural activity and behaviour (Atasoy & Sternson, 2018; Vardy et al., 2015).

However, as research has progressed, the inherent limitations of DREADDs in the context of sensory neuron modulation have become increasingly apparent. The primary challenge stems from their complex ligand pharmacology and the risk of central off-target effects. The classic ligand, clozapine-N-oxide (CNO), can be retro-metabolised to clozapine in both rodents and primates (Gomez et al., 2017; Raper et al., 2017). As an antipsychotic drug, clozapine has broad receptor activity, which can confound the causal interpretation of behavioural outcomes. To address these challenges, the scientific community has proposed a series of improved strategies, such as developing new-generation ligands (e.g., perlapine), introducing the more potent and PET-traceable Deschloroclozapine (DCZ), and emphasising the necessity of rigorous pharmacological control experiments (Chen et al., 2015; Nagai et al., 2020). The latest HCAD/FCH-2296413 system has achieved a key breakthrough in reducing central off-target effects through a peripheral restriction strategy (Kang et al., 2024). Nevertheless, although these improved methods have optimised the ligand and receptor, they still operate within the GPCR-based framework.

A deeper challenge of this framework is that its effects are highly dependent on the context of the cell's endogenous effectors. For instance, the inhibitory mechanism of hM4Di relies on endogenous GIRK channels. However, the expression levels and functional activity of GIRK in mouse DRG neurons are weak, severely limiting the inhibitory efficacy of hM4Di in this cell population (Nockemann et al., 2013).

It is important to acknowledge, however, that this limitation is not universal across all sensory ganglia. Indeed, the efficacy of hM4Di appears to be preserved in the trigeminal ganglion (TG). Korczeniewska et al. (2022) demonstrated that hM4Di activation in TG neurons effectively attenuated mechanical hypersensitivity and c-Fos expression in the trigeminal nucleus caudalis in a neuropathic model. Nevertheless, this tissue-specific divergence highlights a fundamental constraint: the utility of Gi-DREADDs is inherently heterogeneous and strictly contingent on the variable repertoire of endogenous ion channels in the target population (Korczeniewska et al., 2022).

Furthermore, the expression of the receptor itself can cause interference. It has been reported that the overexpression of hM4Di, even without ligand activation, can trigger changes in ion channel function and transcription (Saloman et al., 2016). Finally, from a broader perspective, all GPCR-based modulation exhibits slow reaction kinetics on the order of minutes. Its effects are susceptible to the cell's real-time state, signalling network crosstalk, and the potential for receptor desensitisation or signal plasticity with long-term use. These factors collectively determine that the DREADDs system struggles to meet the demand for rapid, precise, and highly robust neuromodulation required for sensory neuron research (Atasoy & Sternson, 2018).

4.2 Systems Based on Engineered Ligand-Gated Ion Channels (LGICs)

In stark contrast to the indirect and slow nature of metabotropic tools, ionotropic chemogenetic tools (LGICs) offer a fast and direct method of control. The receptors in these tools are ion channels themselves, and their gating does not depend on complex intracellular signalling cascades that may be altered in pathological states. Consequently, they can directly modulate membrane conductance, producing rapid and highly

predictable electrophysiological effects, making them an ideal choice for precise mechanistic analysis and disease intervention (Atasoy & Sternson, 2018; Roth, 2016).

Two major classes of chemogenetic ion channels can modulate cellular activity. One system is composed of the glutamate-gated chloride channel (GluCl) from C. elegans and its ligand ivermectin, which can achieve efficient and reversible neural silencing in mammalian neurons and can be engineered for enhanced sensitivity (Lerchner et al., 2007; Weir et al., 2017). A more advanced class of representatives is the PSAM/PSEM (Pharmacologically Selective Actuator/Effector Modules) system. This system is based on an elegant modular design, where the recognition module (PSAM) is derived from the ligand-binding domain of the human α7 nicotinic acetylcholine receptor. It is engineered to no longer respond to endogenous neurotransmitters but instead to specifically recognise the clinically approved drug varenicline with nanomolar affinity. The coupled effector module (PSEM) is a freely interchangeable ion channel pore. For example, using the chloride pore of the glycine receptor (GlyR) creates an inhibitory tool, whilst using the cation pore of the 5-HT3 receptor creates an excitatory tool. This strategy, which integrates humanised design, functional modularity, and activation by a clinical drug, endows the system with low immunogenicity potential, high functional flexibility, and significant clinical translation convenience (Magnus et al., 2011, 2019).

A powerful and recent evolution of this PSAM/PSEM design philosophy is the development of cocaine chemogenetics (Gomez et al., 2025). Building directly on the same modular strategy, researchers engineered the α7 nAChR ligand-binding domain to be exclusively activated by cocaine itself, rather than an external drug like varenicline. By fusing this cocaine-sensing domain to excitatory (5-HT3) or inhibitory (GlyR) pores, they created tools that function as biosensor-actuators. These channels establish an artificial, closed-loop feedback system that is only engaged during the dynamic window

of drug exposure in the brain. This represents a conceptual leap, enabling researchers to programme a physiological response that directly opposes the action of an addictive drug, a technique the authors term synthetic physiology.

This study ultimately chose to focus on the ionotropic GluCl and PSAM/PSEM systems, a decision based on the unique physiological properties of sensory neurons and the demands of the research. Their core advantage lies in their ability to leverage the distinct chloride physiology of sensory neurons to achieve robust inhibition. Unlike most central neurons, sensory neurons of the DRG/TG highly express NKCC1 and have low expression of KCC2, resulting in a high intracellular chloride concentration and a depolarised chloride equilibrium potential (ECl). In this context, activating a chloride channel (such as GluCl or the glycine receptor pore of PSAM4-GlyR) may only cause a slight membrane depolarisation. However, the more critical effect is a dramatic increase in membrane conductance and a decrease in input resistance, creating a potent shunting inhibition that effectively clamps the membrane potential below the action potential threshold, thereby silencing the neuron (Prescott et al., 2006; Price et al., 2009). Furthermore, the ligands for both GluCl (ivermectin) and PSAM4-GlyR (varenicline) are already in widespread clinical use, and the humanised design of PSAM/PSEM reduces potential immunogenicity. Therefore, selecting ionotropic chemogenetic tools, which bypass endogenous signalling pathways and achieve a clamping inhibition by directly altering membrane conductance, represents a more robust and predictable strategy for silencing sensory neurons, particularly those in a pathological state where signalling cascades may be remodelled.

A

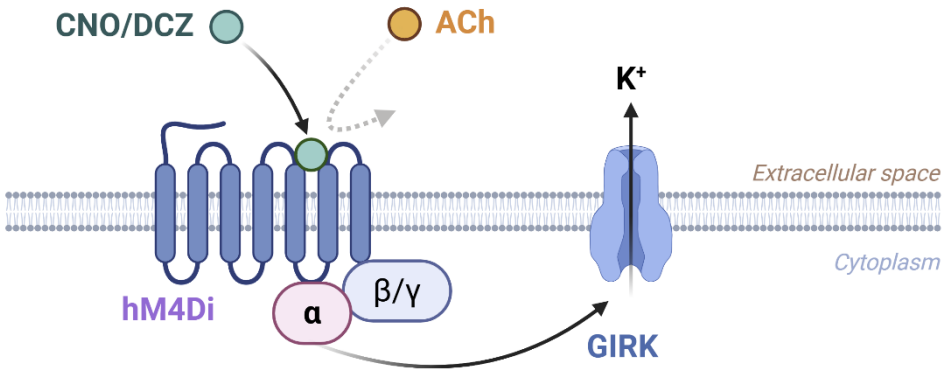
CNO/DCZ
ACh
K+
Extracellular space
Cytoplasm
hM4Di
α
β/γ
GIRK

B

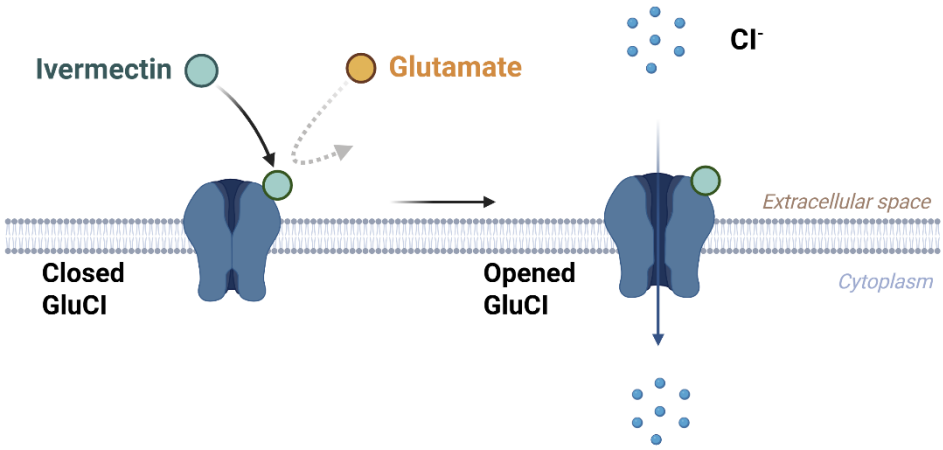
Cl-
Ivermectin
Glutamate
Extracellular space
Cytoplasm
Closed
GluCl
Opened
GluCl

C

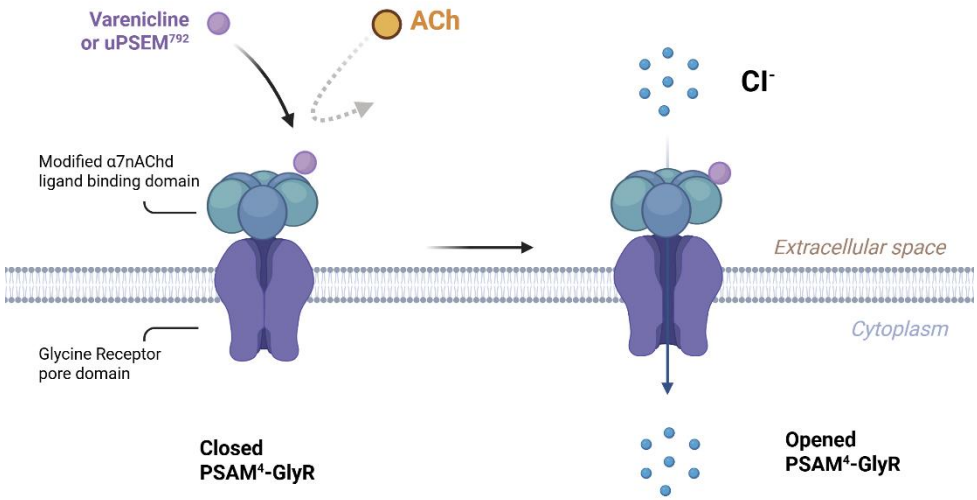
Varenicline
or uPSEM792
ACh
Cl-
Modified α7nAChd
ligand binding domain
Extracellular space
Cytoplasm
Glycine Receptor
pore domain
Closed
PSAM4-GlyR
Opened
PSAM4-GlyR

Figure 1.3. Schematic mechanisms of commonly used inhibitory chemogenetic and pharmacogenetic tools.

A. The hM4Di (DREADD) system. hM4Di is an engineered Gi/o-coupled receptor that is insensitive to its endogenous ligand, acetylcholine (ACh). Upon binding with specific exogenous designer drugs, such as CNO or DCZ, it activates the G-protein pathway. The released β/γ subunits open G protein-coupled inwardly rectifying potassium (GIRK) channels, leading to K^+ efflux, membrane hyperpolarisation, and subsequent neuronal inhibition.

B. The GluCl system. GluCl is an invertebrate-derived glutamate-gated chloride channel. The exogenous administration of Ivermectin specifically binds to and opens the GluCl channel, increasing chloride (Cl^-) conductance. This inhibits neuronal activity primarily through shunting inhibition, which attenuates incoming excitatory currents.

C. The PSAM^4-GlyR system. This chimeric ion channel consists of a modified α7 nicotinic ACh receptor ligand-binding domain (insensitive to endogenous ACh) fused to the pore domain of a glycine receptor (GlyR). Binding of orthogonal ligands, such as Varenicline or uPSEM^{792}, triggers channel opening and Cl^- influx, leading to neuronal inhibition via shunting inhibition.

4.3 Translational Potential

While chemogenetics initially emerged as a fundamental research tool for dissecting neural circuits, its potential for clinical translation has recently garnered significant attention within the biotechnology industry. Conventional pharmacological interventions for neurological disorders often face limitations regarding target specificity, systemic side

effects due to off-target engagement, and high development costs. In contrast, chemogenetics employs a strategy combining gene therapy with small-molecule drugs to achieve high spatiotemporal resolution in modulating specific pathological neurons, offering a novel therapeutic paradigm for intractable neurological conditions. Recent commercial acquisitions and the release of preclinical data indicate that this technology is transitioning from laboratory models towards the early stages of clinical application.

Firstly, gene therapies targeting Trigeminal Neuralgia (TN) and refractory epilepsy have become a primary focus for translation. In November 2022, Kriya Therapeutics acquired Redpin Therapeutics—a company specialising in chemogenetic therapies originally developed in the Scott Sternson laboratory. This strategic move underscores the perceived commercial and clinical value of this technology in treating neuropathologies (Kriya Therapeutics, 2022). Redpin's core platform utilises engineered ion channels modified to respond exclusively to varenicline, an FDA-approved smoking cessation drug (Magnus et al., 2019). By delivering these channels specifically to pathogenic neurons via viral vectors, the strategy aims to allow clinicians to selectively inhibit overactive neurons (such as those in epileptic foci or pain pathways) or activate underactive ones using an oral medication, whilst minimising the impact on the function of surrounding healthy cells.

Secondly, chemogenetic intervention for Focal Epilepsy has also achieved critical *in vivo* proof of concept. Data presented by Klein et al. (2021) at the American Epilepsy Society (AES) Annual Meeting demonstrated the potential efficacy of a platform developed by Coda Biotherapeutics. This study, conducted by the Ivan Soltesz laboratory at Stanford University, utilised an adeno-associated virus (AAV) vector to deliver an engineered inhibitory receptor, which was subsequently activated by a novel oral small-molecule ligand. In a live model recapitulating the feature of human temporal lobe epilepsy, the

results indicated that the system could specifically inhibit neurons in the seizure focus in a dose-dependent manner, significantly reducing the frequency of spontaneous seizures (Klein et al., 2021).

In summary, with the advancement of development pipelines by biotechnology firms such as Redpin and Coda, chemogenetics is attempting to address the translational hurdles involved in moving from rodent models to non-human primates and humans. These industrial developments suggest that, through precise peripheral or central gene delivery combined with orthogonal pharmacological modulation, chemogenetics holds promise as a clinical avenue for addressing refractory conditions such as neuropathic pain and epilepsy.

5. Gene Delivery Methods

The success of any chemogenetic or gene therapy strategy depends on a vector system that can deliver the tool gene to target cells efficiently, broadly, safely, and specifically. To achieve this, academia and industry have developed a diverse toolbox of vectors, which can be broadly divided into viral and non-viral systems. For a comparative overview of the main viral delivery routes and their specific physiological constraints, please refer to Table 1.2.

5.1 Overview of Gene Delivery Vectors

Non-viral Vectors

Lipid Nanoparticles (LNPs) encapsulate nucleic acids (such as mRNA, siRNA, or DNA) within nanoscale particles composed of cationic or ionisable lipids, helper lipids, cholesterol, and PEGylated lipids. Their tremendous success in the mRNA COVID-19

vaccines has demonstrated their vast potential as a gene delivery platform. The main advantages of LNPs are their low immunogenicity (as they contain no viral proteins), relatively simple manufacturing, suitability for repeat administration, and lack of a strict packaging capacity limit. However, the primary challenges currently facing LNP technology are achieving efficient and specific targeting to particular cell types (especially central and peripheral neurons), overcoming various physiological barriers, and ensuring effective intracellular release and long term expression of the nucleic acid after delivery (High & Roncarolo, 2019; Hou et al., 2021; Khare et al., 2021; Xu et al., 2022).

Other Viral Vectors

Viral vectors leverage nature's highly evolved mechanisms for delivering genetic material. Besides AAV, which will be the focus of this study, several other viral vectors have distinct characteristics. Lentiviruses, for instance, offer a large packaging capacity (approx. 8–10 kb) and can efficiently transduce non-dividing cells like neurons; however, their tendency to integrate into the host genome, while enabling stable long-term expression, carries an inherent risk of insertional mutagenesis (Milone & O'Doherty, 2018; Naldini, 2015). Similarly, adenoviruses can deliver large gene payloads with high efficiency. However, their application in neuromodulation is often limited by the strong host immune responses they can provoke, which may cause inflammation and hinder repeat administration (Hackett & Crystal, 2025). These inherent trade-offs between efficiency, durability, safety, and immunogenicity highlight the necessity of developing a vector that strikes an optimal balance for in vivo therapeutic applications, especially within the sensitive environment of the nervous system.

5.2 Adeno-Associated Virus (AAV): The Leading Platform and Its Formidable Challenges

Among the many available options, recombinant adeno-associated virus (rAAV) has emerged as the leading platform for in vivo gene therapy, due to the unique balance it strikes between safety and efficacy. AAV belongs to the Parvoviridae family and is a non-enveloped, single-stranded DNA virus. Wild-type AAV does not cause human disease and requires a helper virus for its replication, endowing it with a high degree of biological safety (Naso et al., 2017).

In gene therapy, rAAV is constructed by removing the AAV genes responsible for replication (rep) and capsid protein expression (cap) and replacing them with an expression cassette containing a promoter, the gene of interest, and a polyadenylation signal. These recombinant genomes are then packaged into viral capsids in producer cells to form rAAV vectors (Grieger et al., 2016). rAAV enters a cell by binding its capsid proteins to receptors on the target cell surface. Following uncoating, its single-stranded DNA genome enters the nucleus, where the complementary strand is synthesised to form double-stranded DNA. The vast majority of these double-stranded DNA molecules persist as stable, non-integrating circular episomes. This allows for long-term, stable expression of the carried gene while minimising the risk of insertional mutagenesis (Bell et al., 2005; Li & Samulski, 2020; Samulski & Muzyczka, 2014). The AAV capsid proteins determine its serotype, and different serotypes exhibit distinct tissue preferences (tropisms), providing a basis for targeted delivery (Issa et al., 2023).

These successes include Luxturna (based on AAV2) for treating RPE65 gene-related retinal diseases (Bennett et al., 2016; Darrow, 2019; U.S. Food and Drug Administration, 2017); Zolgensma (based on AAV9), a one-time gene-replacement therapy for spinal

muscular atrophy (Day et al., 2021; Mendell et al., 2017; U.S. Food and Drug Administration, 2019); and Roctavian, which uses AAV to supplement clotting factors in patients with haemophilia (Ozelo et al., 2022; Pasi et al., 2020; U.S. Food and Drug Administration, 2023).

Despite these promising prospects, AAV as a therapeutic tool faces multiple challenges from production to clinical application, limiting its development. Firstly, at the production level, the large-scale, high-purity preparation of rAAV remains technically complex and costly (Grieger et al., 2016; High & Roncarolo, 2019). In terms of physical properties, the AAV packaging capacity of approximately 4.7 kb restricts its ability to deliver significant genes or carry complex regulatory elements (Dong et al., 1996). Regarding safety, although rAAV predominantly exists in a non-integrating, episomal form, low-frequency genomic integration events and their potential carcinogenic risks still require long-term monitoring and evaluation (Bell et al., 2005; Nault et al., 2015). Furthermore, high-dose AAV injections can trigger strong immune responses against the viral capsid or therapeutic protein, affecting long-term efficacy and safety (Mingozzi & High, 2013; Muhuri et al., 2021).

On one hand, the immune barrier presents a direct challenge. Pre-existing neutralising antibodies against various AAVs are common in the human population, with levels and types varying by region and age, and can significantly impair the efficacy of in vivo administration (Boutin et al., 2010; Calcedo & Wilson, 2013). Moreover, the animal models used in preclinical research to assess and address this issue have their own complex immune backgrounds. Researchers once widely considered experimental animals raised in Specific Pathogen-Free (SPF) environments to be ‘immunologically naïve' and used them as idealised, clean platforms. However, studies have found that even

commercially sourced SPF mice may randomly harbour neutralising antibodies sufficient to block AAV transduction (Rapti et al., 2012). This uncontrollable 'background noise' deprives experimental models of their value as reliable benchmarks. It makes it difficult for researchers to distinguish whether poor vector performance or immune interference caused a failure, thereby leading to the inadvertent over- or underestimation of their application prospects in a real-world human context.

On the other hand, a more intractable problem is the formidable cross-species translational chasm. AAV tissue tropism and cell-type preference exhibit significant species differences. A well-known example is the AAV-PHP.B family, which was initially found to cross the blood-brain barrier in C57BL/6J mice efficiently but was subsequently shown to have significantly diminished or even absent superior neurotropism in other mouse strains, and especially in non-human primates (NHPs) (Hordeaux et al., 2018; Mingozzi & High, 2013). A recent comprehensive study that systematically compared AAV tropism in C57BL/6 mice, BALB/c mice, and crab-eating macaques further confirmed these widespread interspecies differences, clearly indicating that conclusions drawn from a single mouse strain cannot be directly extrapolated to NHPs without further verification (Fang et al., 2025). These differences arise from a combination of factors, including capsid-receptor interactions, innate immune backgrounds, properties of the blood-nerve and central nervous system barriers, and body scale, making it extremely difficult to translate delivery protocols from mice to the clinic directly.

To bridge this translational gap, sensory neurons derived from human induced pluripotent stem cells (hiPSCs) provide a scalable, reproducible, and clinically relevant in vitro platform (Chambers et al., 2012; Clark et al., 2017). This platform can be used to systematically compare the overall performance of different AAVs (natural and engineered) in terms of transduction efficiency, neuronal health, and axonal integrity, as

well as for functional safety assessment at the pharmacological and electrophysiological levels. This offers a crucial pathway to screen and validate AAV vectors in the most relevant human cell models, thereby bridging the gap between basic research and clinical application.

Another specific challenge, central to the focus of this study, is delivery to the dorsal root ganglia (DRG) and trigeminal ganglia (TG). For a long time, achieving efficient delivery to the DRG/TG has been a persistent problem, with existing routes having significant shortcomings in coverage, safety, and clinical feasibility. Intrathecal (i.t.) injection provides inconsistent coverage with high inter-individual variability; intraganglionic direct injection is highly invasive and offers limited spread; retrograde transport from the periphery is inefficient; and systemic intravenous injection in adult individuals is inefficient due to the blood-nerve barrier and first-pass hepatic clearance (O'Donnell et al., 2024; Schuster et al., 2014; Towne et al., 2009; Yuan et al., 2023; H. Zheng et al., 2010). The limitations of these existing methods collectively underscore the urgent need for a novel delivery paradigm—one that is minimally invasive, highly reproducible, provides systemic coverage with a single administration, and leverages the physiological window of the immature BNB. This is precisely the core objective of the neonatal subcutaneous (nSC) injection protocol to be established and validated in Chapter Three of this thesis.

6. Thesis Aims and Chapter Overview

Based on the preceding analysis of clinical needs, existing tools, and translational challenges, this thesis aims to construct and validate a clinically translatable, chemogenetics-based platform for the precise neuromodulation and selective inhibition of peripheral sensory neuron function. To achieve this goal, we have designed a

progressive experimental framework that sequentially addresses key issues such as functional tool optimisation, gene delivery method establishment, in vivo efficacy evaluation, disease model application, and human cell validation. This framework aims to build a complete evidence base from basic research to preclinical application.

Chapter Two will be dedicated to the optimisation and proof-of-concept validation of the functional tool. This chapter will construct and validate a Cre-dependent inhibitory chemogenetic tool (GluCl.CreON) and use a Nav1.8-Cre mouse model to target its expression to nociceptors. The core scientific question is whether the selective functional silencing of this neuronal subpopulation can effectively inhibit pain signals whilst preserving normal tactile perception, thereby completing the foundational proof-of-concept for subpopulation targeting, functional reversibility, and modality specificity.

Chapter Three will focus on exploring an efficient in vivo gene delivery method. To overcome the limitations of traditional strategies in terms of coverage, invasiveness, and stability, this chapter will develop and systematically evaluate a novel neonatal subcutaneous (nSC) single injection protocol. We hypothesise that by leveraging the physiological window of the BNB in neonatal animals, we can achieve simultaneous, widespread, and efficient gene transduction of sensory ganglia (DRG) and trigeminal ganglia (TG) throughout the body, thus establishing a low-invasion, highly reproducible methodological platform for subsequent functional studies.

Chapter Four will focus on the application of the humanised PSAM/PSEM system in the DRG and TG. This chapter will combine the nSC delivery strategy with the PSAM4-GlyR system to achieve widespread transduction of sensory neurons throughout the mouse. The research focus will extend from the DRG to the craniofacial sensory system, with a primary emphasis on evaluating the in vivo reversible silencing at the TG level.

We will systematically test the effects of this tool in the TG for the first time and apply it to a chronic migraine-like animal model to examine its potential therapeutic efficacy.

Chapter Five aims to complete the human cell-based vector evaluation for clinical translation. Recognising that the difference in AAV vector targeting efficiency between species is a core obstacle for gene therapy to reach the clinic, this chapter will conduct studies on sensory neurons differentiated from hiPSCs. We will systematically compare various natural and engineered AAV serotypes, comprehensively evaluating their performance in terms of transduction efficiency, neuronal health, and functional integrity. This will provide a data-driven, optimised virus vector selection protocol based on human cell data for the future application of this technology in humans.

In summary, this thesis, centred on the theme of chemogenetics-mediated precise peripheral inhibition, aims to build and validate a chemogenetic modulation platform systematically. It extends its application from the well-studied dorsal root ganglia (DRG) into the trigeminal system, a critical area where such studies have been far fewer. Through tool engineering optimisation, breakthroughs in in vivo delivery, quantitative functional validation, disease model confirmation, and a translational leap to human cell-level evaluation, this work aims to provide a solid theoretical foundation and technical reserve for developing novel analgesic therapies.

Table 1.1: Overview of Key Chemogenetic Systems

System Type	Representative Tools	Key Ligand(s)	Primary Effect	Key Limitation
GPCR-based (Metabotropic)	**hM3Dq**	CNO, DCZ	**Excitation**	Slow kinetics; Metabolic side-effects of CNO.
	hM4Di / KORD	CNO, DCZ / Salvinorin B	**Inhibition**	Efficacy depends on endogenous GIRK levels (poor in DRG).
LGIC-based (Ionotropic)	**GluCl**	Ivermectin	**Silencing** (Shunting Inhibition)	Ligand (IVM) has a long half-life and requires specific dosing.
	PSAM / PSEM	Varenicline	**Tunable** (Excitation or Inhibition, depending on pore)	Requires specific ion pore selection (e.g., GlyR for Cl-).

Table 1.2: Comparison of Viral Gene Delivery Routes to Sensory Ganglia

Delivery Route	Target Access	Advantages	Major Constraints
Intrathecal (i.t.)	DRG via CSF	Bypasses the Blood-Brain Barrier (BBB); reduced systemic toxicity.	Invasive; variable viral spread; limited transduction of distal ganglia.
Intraganglionic (Direct)	Specific DRG/TG	High local viral titer; minimal off-target effects.	Highly invasive (surgical); risk of mechanical nerve injury; limited to a single ganglion.
Systemic (i.v.) - Adult	Whole-body DRG/TG	Non-invasive; broad potential coverage.	Restricted by the Blood-Nerve Barrier (BNB); high liver clearance; requires massive viral doses.
Systemic (nSC/i.v.) - Neonatal	Whole-body DRG/TG	**High efficiency** due to immature BNB; widespread transduction.	Limited temporal window (developmental stage); technically demanding in neonates.

Chapter II Building an Optimised GluCl.CreON Chemogenetic Toolbox to Selectively Silence Nav1.8-Positive Sensory Neurons

Abstract

Neuropathic pain is a chronic pathological condition caused by a lesion or disease affecting the somatosensory nervous system, and it represents a significant challenge in modern medicine (Baron et al., 2010). In recent years, the development of chemogenetic tools has provided new approaches for precise control of specific neuronal populations, creating opportunities to understand neuropathic pain mechanisms and develop targeted therapeutic strategies (Atasoy & Sternson, 2018). This chapter introduces the development and proof-of-concept use of a novel chemogenetic tool, GluCl.CreON, and explores its application in selectively silencing Nav1.8-positive sensory neurons, thereby providing a powerful tool for analysing the differential contributions of sensory neuron populations in pain processing.

1. Introduction

1.1 Chemogenetics In Sensory Neurons

The pathological foundation of chronic pain is persistent, maladaptive plasticity in the sensory pathways (Basbaum et al., 2009; R.-R. Ji et al., 2018). The dorsal root ganglion (DRG) plays a key role in both the initiation and maintenance of chronic pain states

(Krames, 2014). Following a peripheral nerve injury, a complex cascade of events unfolds within the DRG. Satellite glial and immune cells become activated, establishing a pro-inflammatory neuro-immune microenvironment by releasing a plethora of sensitising substances such as TNF-α and IL-1β (Hanani, 2005; McGinnis & Ji, 2023; Ren & Dubner, 2010). Concurrently, the sensory neurons themselves undergo profound intrinsic changes, including marked alterations to their gene expression profiles and shifts in their connectivity with peripheral targets. This neuro-immune signalling, coupled with intrinsic neuronal modifications, alters the expression and function of key molecules, such as pro-excitatory ion channels (e.g., Nav1.7 and TRPV1). This ultimately causes ectopic spontaneous firing and lowers the activation threshold of neurons, establishing a state of sustained peripheral hypersensitisation (Deval & Lingueglia, 2015; Dib-Hajj et al., 2010; R.-R. Ji et al., 2016; Koivisto et al., 2024). These persistent, abnormal afferent signals are then amplified within the spinal cord through central sensitisation before ascending to the brain, where they can distort sensation and negatively affect circuits related to emotion and cognition. This entire process helps explain why some pain becomes refractory, or difficult to treat (Kuner & Kuner, 2021). Current treatments, whether pharmacological approaches (such as gabapentinoids, tricyclic antidepressants, and opioid analgesics) or interventional modalities (including spinal cord or dorsal root ganglion stimulation), have limited efficacy. They are often complicated by side effects, risk of addiction, and a lack of cellular specificity, which creates a strong need for new neuromodulation technologies (Finnerup et al., 2015, 2021; Huygen et al., 2020, 2024; NICE, 2020).

Chemogenetics is a promising technology that can help solve this problem. Its core principle is to genetically introduce engineered receptors into target cells that are insensitive to endogenous ligands but can be activated by specific designer molecules

that are otherwise pharmacologically inert (Atasoy & Sternson, 2018; Roth, 2016). Chemogenetic tools that directly control neuronal activity can be classified into two main categories. The first includes systems based on G protein-coupled receptors (GPCRs), such as Designer Receptors Exclusively Activated by Designer Drugs (DREADDs), which work by activating internal cell signalling pathways (Armbruster et al., 2007). The second includes systems based on engineered ligand-gated ion channels (LGICs), such as the Glutamate-gated Chloride Channel (GluCl), which work by directly changing the cell's membrane conductance (Magnus et al., 2011; Weir et al., 2017).

Despite their widespread use, GPCR-based systems like the inhibitory DREADD (hM4Di) have clear limitations for silencing sensory neurons. The inhibitory mechanism of hM4Di relies on activation of endogenous G-protein-gated inward-rectifying potassium channels (GIRKs). However, studies have shown that these channels have low expression and activity in mouse DRG neurons, a fact that constrains the inhibitory capacity of hM4Di in this population (Nockemann et al., 2013). Furthermore, potential off-target effects make the results difficult to interpret. For example, the common ligand Clozapine N-oxide (CNO) can be back converted in vivo to clozapine, a centrally active antipsychotic drug that can introduce confounding pharmacological effects (Gomez et al., 2017; MacLaren et al., 2016; Raper et al., 2017). Other issues have also been reported. Overexpression of the hM4Di receptor itself may alter neurons' natural properties, and alternative systems, such as KORD, use ligands with rapid clearance rates, limiting their utility for long-term inhibition (Saloman et al., 2016; Vardy et al., 2015).

To address these challenges, scientists have proposed improved strategies, such as developing new-generation ligands like perlapine and Deschloroclozapine (DCZ) and, most recently, designing peripherally restricted systems to minimise central off-target

effects (Chen et al., 2015; Kang et al., 2024; Nagai et al., 2020). Although these advanced methods represent significant optimisations of the ligand and receptor, they still operate within the GPCR-based framework and are thus constrained by a reliance on indirect modulation via endogenous cellular machinery.

These collective limitations underscore the need for alternative strategies that can achieve robust and durable inhibition of sensory neurons without relying on endogenous signalling cascades. In this context, the GluCl system is a promising research direction. Previous studies have already shown that GluCl can effectively inhibit neurons in the mammalian central nervous system (Lerchner et al., 2007), and protein engineering has improved its sensitivity to the ligand ivermectin (Frazier et al., 2013). Our lab's early work also confirmed this system's potential in DRG neurons (Weir et al., 2017). Building on this solid foundation, this chapter aims to optimise the GluCl system, improving its usefulness as a research tool and exploring its potential for future clinical applications.

1.2 Glutamate-Gated Chloride Channel (GluCl) System

The glutamate-gated chloride channel (GluCl) is a member of the cysteine (Cys) loop receptor superfamily, an inhibitory channel expressed in invertebrates but not in mammals. In chemogenetic applications, GluCl has been designed to be unresponsive to endogenous glutamate but sensitive to the insecticide ivermectin (IVM) (Slimko et al., 2002). The receptor is encoded by two subunits, GluClα and GluClβ, and their co-expression is required to form functional channels. IVM activates this channel, increasing chloride conductance and suppressing neuronal excitability, enabling robust neuronal silencing (Frazier et al., 2013; Lerchner et al., 2007; Slimko et al., 2002). Beyond basic chemogenetic silencing, ivermectin-gated inhibitory channels have also been adapted for disease-oriented applications, including epilepsy (Lieb et al., 2018, 2019).

The development of GluCl as a chemogenetic tool proceeded through several key stages. Slimko et al. (2002) first expressed C. elegans GluCl in cultured rodent hippocampal neurons and showed that IVM application robustly silenced neuronal firing in vitro. Subsequent work demonstrated in vivo feasibility, with the GluClv1.0/IVM system enabling reversible silencing of striatal neurons in behaving mice (Lerchner et al., 2007; Slimko et al., 2002).

However, early GluCl systems had several practical limitations that motivated further optimisation. In vivo performance of GluClv1.0 was constrained primarily by properties of the ligand IVM, which is limited and variable penetration across the blood–brain barrier and relatively slow pharmacokinetics, together with variability arising from suboptimal β-subunit surface expression (Atasoy & Sternson, 2018; Lerchner et al., 2007). To address these issues, an improved GluClv2.0 was engineered (Frazier et al., 2013). The enhanced design incorporated a gain-of-function mutation in the α subunit (L9′F) that significantly improved IVM sensitivity. Surface expression was optimised through replacement of an arginine-based ER retention motif in the β subunit (RSR to AAA). Additionally, monomeric fluorescent tags were integrated to prevent the deleterious dimerisation effects on channel function. These strategic modifications collectively increased both sensitivity and consistency, ultimately enabling the use of lower effective IVM doses in vivo.

Building on these advances, our laboratory's research was the first to apply GluClv2.0 to the sensory nervous system, demonstrating its effectiveness in inhibiting DRG neuron activity and alleviating neuropathic pain (Weir et al., 2017). However, even the improved GluClv2.0 system could not yet selectively target specific neuronal subpopulations, limiting its application in dissecting pain circuits. The high heterogeneity of sensory

neurons requires more precise tools to distinguish the functional contributions of different subpopulations, especially in pain pathways.

To address this key limitation, it became necessary to develop a GluCl system that could selectively target molecularly defined neuronal subpopulations. This need led to the development of the Cre-dependent GluCl system (GluCl.CreON) (Middleton et al., 2023), an innovative tool that enables precise targeting and control of specific neuronal subpopulations using Cre/lox technology, thereby enhancing the study of sensory processing and pain mechanisms.

1.3 Considerations of Chloride Ion Dynamics in DRG Neurons

Understanding the mechanisms of chloride ion (Cl^-) dynamic changes in dorsal root ganglion (DRG) neurons is critical for optimising the effectiveness of the glutamate-gated chloride channel (GluCl) as a pain inhibition tool. Traditionally, it was thought that cation channels mainly regulate the excitability of primary sensory neurons. However, recent studies have shown that Cl^- plays an important yet often overlooked role in pain perception (Wilke et al., 2020).

DRG neurons maintain an unusually high intracellular chloride concentration (30-50 mM), significantly higher than central neurons (approximately 5-10 mM). This high intracellular chloride concentration is maintained by several key transport mechanisms. Firstly, the high expression and sustained activity of the Na^+-K^+-$2Cl^-$ cotransporter 1 (NKCC1) continuously pump chloride into the cell. Secondly, a relative lack of the K^+-Cl^- cotransporter 2 (KCC2) results in a low capacity for chloride extrusion. Furthermore, while transporters such as KCC1 and KCC3 are expressed, they are mainly active during cell swelling and show low activity under isotonic conditions. Finally, the Na^+-independent Cl^--HCO_3^- anion exchanger AE3, expressed in most DRG neurons, also

contributes to chloride accumulation. (Gamba, 2005; Pfeffer et al., 2009; Rivera et al., 1999; Sung et al., 2000).

This ion distribution results in a chloride equilibrium potential (ECl^-) higher than the resting membrane potential. Activation of chloride channels causes chloride efflux and cell depolarisation, rather than the hyperpolarisation commonly seen in central neurons (Funk et al., 2008). However, the functional consequence of this depolarisation is not simply excitation. When depolarisation is slow and moderate, it can reduce neuronal excitability through inactivation of voltage-gated sodium channels; only when depolarisation is rapid and strong (ECl^- close to action potential threshold) might it promote action potential generation (Prescott et al., 2006). More importantly, activation of chloride channels significantly increases membrane conductance, reducing membrane input resistance, producing a "shunt inhibition" mechanism. This "shunting" effect can effectively weaken the impact of excitatory inputs without significant changes in membrane potential (Price et al., 2009). Compared to hyperpolarising inhibition, shunt inhibition is more economical in terms of energy metabolism and allows for more precise local inhibitory control.

GluCl utilises this unique Cl^- dynamic feature in DRG neurons to achieve neuronal silencing. Our laboratory's in vivo experiments have shown that when GluCl is activated by ivermectin (IVM), it causes significant chloride conductance; this greatly increased membrane conductance leads to significantly reduced input resistance, primarily blocking neuronal activity through shunt inhibition; the current threshold (rheobase) required for neurons to generate action potentials increases (Middleton et al., 2023; Weir et al., 2017).

1.4 Molecular Strategies for Selective Expression

To achieve selective expression in specific sensory neuron subpopulations, precise control of GluCl expression patterns is required. Existing methods include utilising viral tropism, specific promoters, and Cre/LoxP technology.

Since most specific promoters are large, exceeding the packaging limit of adeno-associated viruses (AAV) of approximately 4.7 kb (Dong et al., 1996), the Cre/LoxP system has become the preferred method for directed expression. This system typically requires transgenic mice expressing Cre recombinase in specific cell types, followed by delivery of viral vectors containing LoxP sites.

Among the available Cre recombination strategies, the double-floxed inverted open reading frame (DIO) method offers the highest specificity and the lowest background expression. Compared to traditional LoxP-Stop-LoxP strategies, the DIO strategy places the transgene in an inverted orientation, flanked by pairs of heterotypic LoxP sites. In the presence of Cre, the transgene is flipped to the correct reading frame through a flip-excision process, enabling specific expression (Atasoy et al., 2008; Schnütgen et al., 2003). This method significantly reduces background leakage expression, making it particularly suitable for neural modulation applications requiring high specificity.

Our GluCl.CreON system employs this DIO strategy, placing the GluClα and GluClβ subunits in separate AAV vectors, each containing inverted subunit sequences flanked by heterologous loxP sites. This design ensures that functional GluCl channels are only expressed in Cre-expressing cells, providing cell-type specificity.

1.5 Targeting Nav1.8-Positive Afferents

The voltage-gated sodium channel Nav1.8, encoded by the SCN10A gene, is a key ion channel expressed in sensory neurons. Early work suggested that Nav1.8 was primarily

expressed in nociceptors, making it an important target for pain research (Djouhri et al., 2003). More recent studies refined this view, showing that Nav1.8 expression is not strictly limited to nociceptors and can also be found in some mechanoreceptors, such as C-low-threshold mechanoreceptors (C-LTMRs) (Shields et al., 2012). Approximately 60-70% of dorsal root ganglion (DRG) neurons express Nav1.8, encompassing peptidergic and non-peptidergic neurons (Y. Zheng et al., 2019). Such widespread expression makes Nav1.8-positive neurons a practical entry point to modulate pain-relevant circuits while still permitting analyses within defined subpopulations.

Nav1.8 has long been considered a compelling therapeutic target. Selective small-molecule blockers, such as the preclinical agent A-803467, have been shown to attenuate neuropathic and inflammatory pain in animal models (Jarvis et al., 2007). The clinical relevance of this strategy was recently highlighted. On January 30, 2025, the U.S. Food and Drug Administration (FDA) approved Journavx™ (suzetrigine), the first non-opioid analgesic in its class for moderate to severe acute pain in adults, by targeting peripheral sodium channels to block pain signals before they reach the brain (FDA, 2025).

Although suzetrigine is not a selective Nav1.8 inhibitor, its approval is a major milestone. It strengthens the clinical case for targeting peripheral sodium channels as a non-opioid analgesic strategy and aligns with decades of research placing Nav1.8-positive neurons at the centre of pain signalling.

In parallel with pharmacology, genetic tools provide a robust method for accessing this neuronal population. Nav1.8^Cre driver lines are widely used and well-characterised for the conditional manipulation of nociceptor function in vivo (Nassar et al., 2004; Stirling et al., 2005). Functionally, Nav1.8-positive neurons contribute to mechanical and thermal

nociception and undergo sensitisation in inflammatory states, a process thought to underlie key components of inflammatory pain (Gold & Gebhart, 2010).

For these reasons, Nav1.8-positive afferents represent an ideal proof-of-concept population for testing our GluCl.CreON chemogenetic system. Their selection is motivated by their wide yet pain-enriched expression pattern, the strong clinical validation for targeting peripheral sodium channels, and the availability of mature genetic tools.

1.6 Objectives

This chapter will systematically address these objectives, first detailing the molecular design and construction of the GluCl-CreON system, then assessing its expression and function in Nav1.8-positive DRG neurons, and finally evaluating its effectiveness in modulating acute and inflammatory pain responses. Through this research, we aim not only to provide a new neural modulation tool but also to gain new insights into the differential contributions of sensory neuron subpopulations in pain processing. Ultimately, this work will lay the foundation for developing more effective and specific pain treatment strategies.

2. Methods

2.1 Molecular Cloning and Plasmid Construction

2.1.1 GluCl.CreON Plasmid Design Strategy

The design of the GluCl.CreON construct uses a double-floxed inverted open reading frame (DIO) strategy to prevent GluCl expression in the absence of Cre recombinase while allowing expression in the presence of Cre. The construction is based on previously

optimised GluClv2.0 subunits (Frazier et al., 2013), which have been shown to provide effective neural silencing in vitro.

Our strategy involved the following key steps:

1. PCR amplification of GluClα and GluClβ subunits separately, using primers containing hanging restriction enzyme sites (5' NheI and 3' AscI)

2. Insertion of the amplified products into AAV backbone plasmids containing these restriction sites, with RFP driven by a short CAG promoter in an inverted orientation flanked by heterologous loxP sites

3. By replacing the RFP sequence, the GluCl subunits were placed in an inverted orientation, flanked by the same heterologous loxP sites, to ensure Cre-mediated recombination

This design ensures strict expression control: in cells lacking Cre, the GluCl subunits remain in an inverted orientation and cannot be transcribed, while in Nav1.8^Cre positive cells, Cre-mediated recombination flips the transgene to the correct reading frame, allowing GluCl channel expression.

2.1.2 Detailed Plasmid Cloning Process

GluClα and GluClβ subunits were amplified by PCR using the following primers:

GluClα-NheI forward primer: 5' CTAGTTGCTAGCATGGCCACGTGGATCGTG 3'

GluClα-AscI reverse primer: 5' TTGACTGGCGCGCCCTAGCTCAGAACAGAACGTTCTGC 3'

GluClβ-NheI forward primer: 5' CTAGAGGCTAGCCCACCATGGCCACCCCCT 3'

GluClβ-AscI reverse primer: 5' TGGATTGGCGCGCCCTACACCAGGGACTCGGGGGT 3'

PCR reactions used high-fidelity DNA polymerase (Phusion Hot Start II, Thermo Scientific), with cycling parameters as follows:

- Initial denaturation: 98°C for 30 seconds
- 30 cycles: 98°C for 10 seconds, 62°C for 20 seconds, 72°C for 2 minutes
- Final extension: 72°C for 5 minutes

PCR products were purified using the QIAquick PCR Purification Kit (Qiagen) and digested with NheI and AscI restriction enzymes at 37°C for 1 hour. The vector plasmid contained a short CAG promoter and RFP in an inverted orientation, flanked by heterologous loxP sites. The RFP sequence was removed using the same restriction enzymes, and the vector was separated by gel electrophoresis and extracted. The digested GluCl insert fragments and vector were incubated overnight at 16°C using T4 DNA ligase, and the ligation products were transformed into NEB 5-alpha competent E. coli. Successful clones were verified by restriction enzyme analysis and Sanger sequencing.

2.1.3 Virus Production and Packaging

Verified GluCl.CreON plasmids were packaged into AAV9 serotype vectors by the Viral Vector Facility (VVF) at the Neuroscience Centre Zurich (ZNZ), University of Zurich and ETH Zurich. Briefly, production was performed in HEK293T cells cultured in Dulbecco's Modified Eagle Medium (DMEM; Thermo Fisher Scientific) supplemented with 10% foetal calf serum (FBS). Cells were transfected using JetPEI (PolyPlus Transfection, France) with a triple-plasmid system comprising the AAV-GluCl.CreON transgene plasmid, AAV9 serotype helper plasmid, and adenoviral helper plasmid. Viral

particles were purified via caesium chloride (CsCl) gradient ultracentrifugation and dialysed. The final viral titers were: AAV9-GluCl.CreONα: 9.8×10^{12} vg/mL, and AAV9-GluCl.CreONβ: 1.6×10^{13} vg/mL.

2.2 Experimental Animals

This study used the following mouse lines: Nav1.8^Cre mice (a gift from John Wood from UCL, Nassar et al., 2004) and C57BL/6J wild-type mice. All mice were group-housed in a pathogen-free facility, kept in individually ventilated cages with free access to food and water, and maintained on a 12-hour light-dark cycle. All experiments were conducted on 8–12-week-old adult mice, with both sexes used. All experiments involving animals were conducted in compliance with the United Kingdom Home Office (Scientific Procedures) Act of 1986 and received ethical approval from the University of Oxford's local committees. The study design and reporting adhere to the ARRIVE 2.0 guidelines (Percie Du Sert et al., 2020).

2.3 Intrathecal Injection Surgery

2.3.1 Surgical Preparation and Anaesthesia

For intrathecal virus administration, heterozygous Nav1.8^Cre mice of both sexes (4–8 weeks old) were anaesthetised with 2% isoflurane. Following surgical preparation, which included shaving and sterilising the dorsal thoracic region, a 1–2 cm incision was made along the midline. The T10 and T11 vertebrae were located, and soft tissue was minimally dissected to expose the dura mater. After a brief application of topical lidocaine (1–2 minutes), the dura was carefully punctured with a 30-gauge needle, with successful entry into the subarachnoid space confirmed by a visible leak of cerebrospinal fluid (CSF). A custom-made cannula system, featuring a tip with an outer diameter of 0.008 inches, was then inserted and advanced approximately 1 cm caudally. Using a syringe pump, 8 μl of

the AAV solution was infused at a rate of 1 µl/min. Animals received either the functional heteromeric channel combination (AAV9-GluCl.CreONα + AAV9-GluCl.CreONβ) or the control vector (AAV9-GluCl.CreONβ alone). The beta-only condition was selected as the negative control because the beta subunit cannot form functional homomeric channels (Slimko et al., 2002). The cannula was left in place for 2 minutes post-injection to prevent backflow before being slowly withdrawn. The dural puncture site was sealed with a drop of dural gel. Finally, the incision was sutured, and animals received post-operative analgesia (2 mg/kg Marcain, local; 5 mg/kg Rimadyl, systemic). A minimum recovery period of three weeks was observed before any subsequent experiments were conducted.

2.4 Immunohistochemistry and In Situ Hybridisation

2.4.1 Tissue Preparation and Sectioning

Mice were deeply anaesthetised with pentobarbital, perfusion-fixed, and DRG (post-fixed for 1-2 hours), spinal cord (post-fixed for 24 hours), and skin (post-fixed for 1-2 hours) were collected. Tissues were cryoprotected in 30% sucrose, then sectioned: DRG (12µm), spinal cord (20µm), and skin (30µm).

2.4.2 Detailed Immunohistochemistry Protocol

After washing in PBS, tissue sections were permeabilised and blocked for 1 hour using a solution of 5% normal donkey serum and 0.3% Triton X-100 in PBS. The sections were then incubated overnight at room temperature with primary antibodies, including NeuN (1:500, Rabbit, Abcam Ab177487). The following day, sections were washed and incubated for 2 hours with appropriate Alexa Fluor 488-conjugated secondary antibodies

(1:500, Thermo Fisher Scientific). Finally, sections were mounted onto slides using Vectashield mounting medium, with or without DAPI for nuclear counterstaining.

2.4.3 RNAscope In Situ Hybridisation

The RNAscope 2.5 RED Chromogenic Kit (Advanced Cell Diagnostics) was used according to the manufacturer's protocol to detect viral transcripts. To maximise detection sensitivity, probes were designed to target the fluorescent protein tags (Cerulean for GluClα and YFP for GluClβ) rather than the channel subunits themselves. Specifically, an EGFP-specific probe was utilised, which recognises both YFP and Cerulean transcripts due to high sequence homology. Consequently, while this approach ensured robust detection of viral expression, it did not distinguish between individual subunits. Following tissue pretreatment with hydrogen peroxide and protease, sections were incubated with the probe for 2 hours at 40°C. The signal was amplified through a series of steps and visualised using Fast Red or TSA Vivid 520. For quantification, cellular mRNA signal intensity was measured using FIJI/ImageJ. A cell was classified as positive if its signal was at least two standard deviations above the mean background intensity, which was determined from negative control probe-stained tissues.

2.5 Behavioural Testing

All behavioural assays were conducted with both male and female mice during a consistent time of day within a standardised environment, following habituation to the testing apparatus. To prevent bias, the experimenter remained blinded to the animals' group assignments from the beginning of testing until the completion of data analysis. For tests requiring video scoring (e.g., pinprick, formalin), a second experimenter, who was also unaware of the experimental groups and study design, performed the analysis.

The experimental group consisted of mice that received an injection of AAV-GluCl.CreONαβ, while the control group was composed of mice injected with AAV-GluCl.CreONβ-only. The β-only construct was chosen as an appropriate control because it forms a non-functional, homomeric channel that does not respond to ivermectin, thereby isolating the effects of viral transduction and protein expression from the specific silencing activity of the complete αβ heteromeric channel. Behavioural testing commenced 4–6 weeks after the AAV injections. Unless specified otherwise, a stable baseline for each assay was established by averaging data from 2–3 independent test days. The tests were then repeated 24 hours following the administration of ivermectin (IVM; Noromectin 1.0% w/v, 0.5 μL/g, equivalent to 5 mg/kg). For all mechanical sensitivity assays, mice were randomly selected from their home cages and acclimatised for 30–60 minutes in individual transparent enclosures (5 x 5 x 10 cm) placed on an elevated wire mesh platform.

Von Frey Test

Mechanical sensitivity was quantified by determining the 50% paw withdrawal threshold (PWT) using calibrated von Frey filaments (Linton Instrumentation). The stimulus was applied to the plantar surface of the hind paw using the "up-down" method.

Brush/Cotton Swab Test

Responsiveness to light dynamic stimuli was assessed using a method adapted from previous studies. The plantar surface of the hind paw was stroked at approximately 1 cm/s with either a fine artist's paintbrush or a cotton swab that had been fluffed to about three times its original size. Each mouse received two series of five consecutive stimuli, applied to alternating hind paws with a 10-second interval. A positive response was defined as lifting, flicking, moving the paw, or walking away from the stimulus.

Pinprick Test

Sensitivity to noxious mechanical stimuli was evaluated using a sharp pin attached to a 1 g calibrated von Frey filament. The stimulus was applied to the plantar hind paw, and withdrawal latency was analysed from video recorded at 120 frames per second (8.33 ms/frame) using a smartphone.

Tape Test

The latency to detect a non-noxious tactile stimulus was measured by applying a small (1 x 1 cm) piece of tape to the mouse's hindlimb. The time taken for the mouse to notice the tape (sense time) was recorded.

Hot Plate Test

Thermal pain sensitivity was evaluated by placing mice in a Plexiglas enclosure on a hot plate apparatus (Ugo Basile) maintained at 53°C. The latency to exhibit a nocifensive response with the hind paws (i.e., lifting, flicking, or licking) was recorded. A 30-second cut-off time was imposed to prevent tissue damage.

Rotarod Test

Motor coordination and balance were evaluated using a rotarod apparatus (Ugo Basile, 47600). Following a brief acclimatisation period, mice were placed on the rod, which rotated at a constant speed of 32 rpm. The latency to fall was recorded.

Formalin Test

The formalin test was used to assess nocifensive responses to a persistent chemical irritant. Mice received a subcutaneous injection of 2% formalin into the plantar surface of the left hind paw. Immediately after injection, they were placed in a custom test chamber (5 x 5 x 10 cm) featuring a glass floor and mirrored walls, which was elevated above a camera

to allow for clear visualisation of the injected paw. The animals' behaviour was recorded for 60 minutes. Subsequent offline analysis quantified the cumulative duration of nocifensive behaviours—defined as lifting, licking, flinching, and shaking of the injected paw—within 5-minute bins across the entire hour.

2.6 Imaging and Quantitative Analysis

Imaging was performed using a Zeiss LSM 710 confocal microscope, with image analysis using FIJI/ImageJ software. For each animal, at least three DRG sections were analysed to ensure sample representativeness. Neurons were categorised by diameter into three classes: small (<25μm), medium (25-35μm), and large (>35μm). Fluorescence intensity was determined by measuring the average fluorescence intensity of individual cells and subtracting background fluorescence.

2.7 Statistical Analysis

Statistical analysis was performed using GraphPad Prism 9 software. Data distribution was first assessed using the D'Agostino-Pearson normality test, then appropriate statistical tests were chosen based on data nature. For single comparisons, t-tests or Mann-Whitney U tests were used, while for multiple comparisons, analysis of variance (ANOVA) with appropriate post-hoc tests was used. All data are presented as mean ± standard error (SEM), with statistical significance indicated as: * $P < 0.05$, ** $P < 0.01$, *** $P < 0.001$, **** $P < 0.0001$.

3. Results

3.1 GluCl.CreON System Shows Highly Specific Expression in Nav1.8-Positive Neurons

3.1.1 Molecular Design of GluCl.CreON

The design of the GluCl.CreON system employs a double-floxed inverted open reading frame (DIO) strategy to ensure Cre-dependent expression. Due to the limited packaging capacity of adeno-associated virus (AAV) vectors (~4.7 kb), the system was designed as a dual-vector approach rather than a single bicistronic vector. The large size of the *C. elegans* GluCl subunits fused with fluorescent reporters (GluClα-Cerulean and GluClβ-YFP), combined with the regulatory elements, necessitated separating the components into two distinct viral vectors: AAV9-sCAG-GluClα-Cerulean-DIO and AAV9-sCAG-GluClβ-YFP-DIO.

Consequently, the final injectate comprises a viral cocktail containing an equimolar mixture of the two independent AAVs. While this approach introduces a probability factor for the co-transduction of both vectors into the same neuron, the high viral titers used (see Methods) increase the likelihood of co-expression in the target population.

In this design, the coding sequences are placed in an inverted orientation flanked by heterotypic loxP sites (Figure 2.1). We utilised a shortened CAG (sCAG) promoter to drive strong, ubiquitous expression once the recombination event occurs. Although the CAG promoter is non-specific, the spatial restriction of expression to Nav1.8-positive neurons is achieved by requiring Cre recombinase to flip the gene into the correct sense orientation.

Upon successful co-transduction and Cre-mediated recombination, functional heteromeric GluClαβ channels are trafficked to the cell membrane. As illustrated in Figure 2.1, the administration of the specific ligand ivermectin (IVM) triggers the opening of these chloride channels, resulting in Cl^- influx and subsequent silencing of the Nav1.8-positive DRG neurons.

A

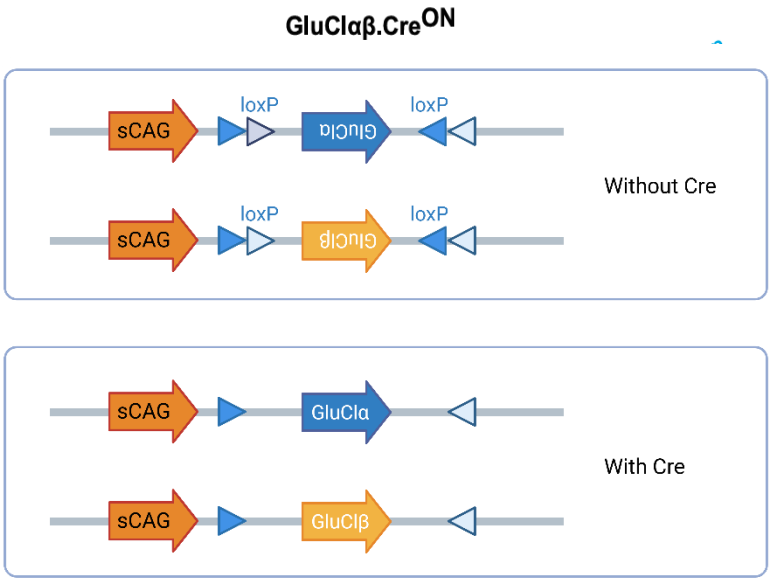

B

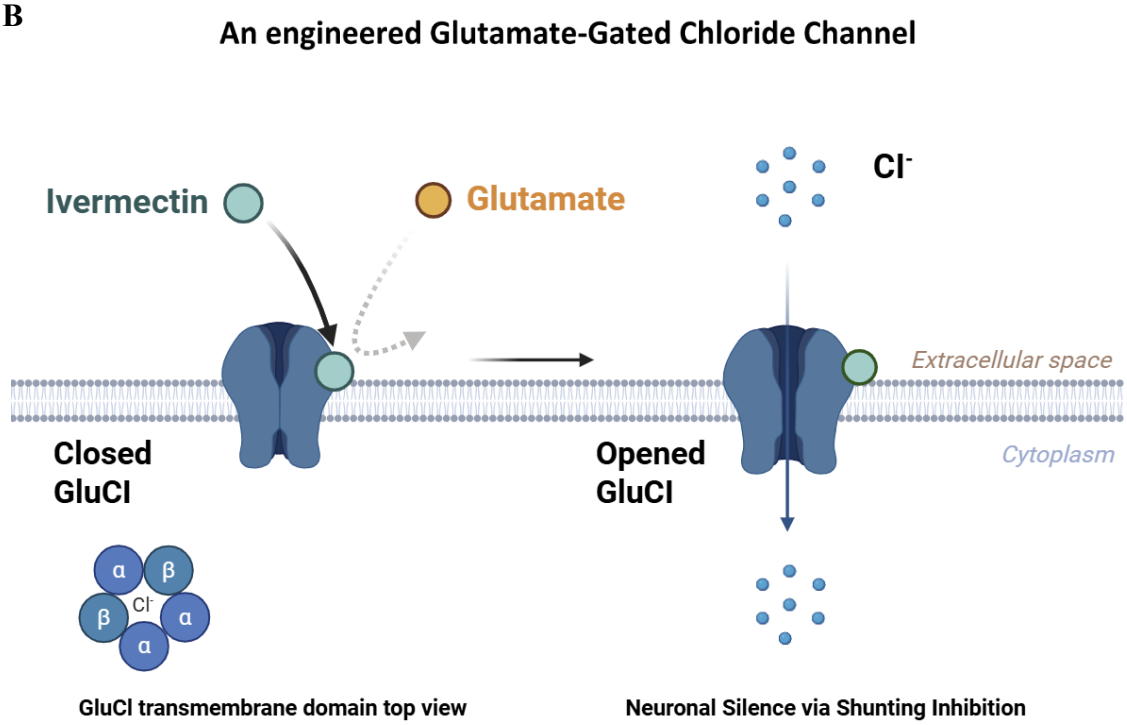

Figure 2.1. Mechanism of the GluCl.CreON system

A. Cre-dependent strategy for GluCl.CreON expression. In Cre-negative cells (Without Cre, top), the GluCl$\boldsymbol{\alpha}$ and GluCl$\boldsymbol{\beta}$ Subunit genes are oriented in an inverted manner relative to the sCAG promoter, preventing the transcription of functional GluCl subunits. In Cre-positive cells (With Cre, bottom), Cre recombinase mediates site-specific recombination at the loxP sites, irreversibly reorienting the coding sequences to enable the expression of both subunits.

B. Structural organisation and inhibitory mechanism of the engineered GluCl channel complex. The functional GluCl channel assembles as a heteropentameric structure incorporating both $\boldsymbol{\alpha}$and $\boldsymbol{\beta}$subunits (bottom left), forming a transmembrane chloride-permeable pore. Ivermectin (IVM) selectively binds to the transmembrane domain of the channel. This binding induces channel opening and a subsequent influx of chloride ions (Cl^-), while the engineered channel remains unresponsive to endogenous glutamate. The resulting Cl^-Influx leads to neuronal silence via shunting inhibition.

3.1.2 Expression Pattern of GluCl.CreON in DRG Neurons

To assess the expression characteristics of the GluCl.CreON system in Nav1.8-positive neurons, we delivered AAV9-GluCl.CreONα and AAV9-GluCl.CreONβ to Nav1.8Cre mice via intrathecal injection and analysed their expression pattern through immunohistochemistry and in situ hybridisation 3-4 weeks later (Figure 2.2).

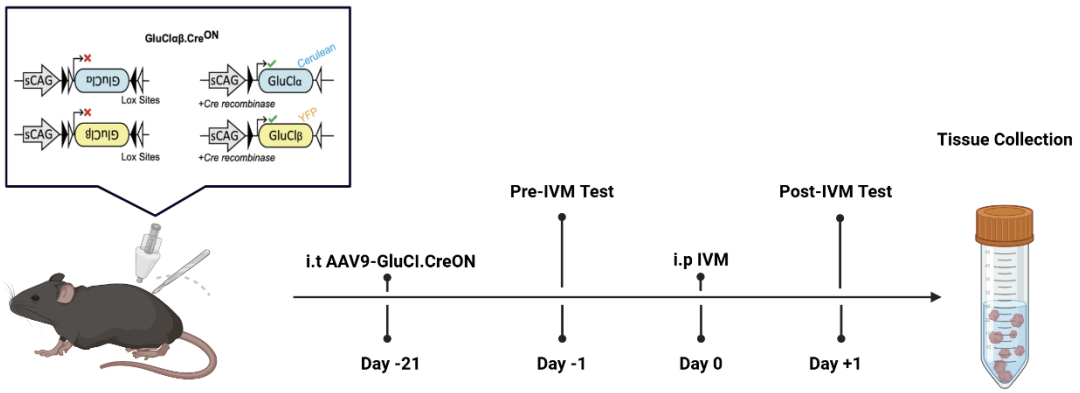

Figure 2.2. Experimental design and timeline for GluCl.CreON characterisation.

Schematic representation of the experimental protocol. AAV9-GluCl.CreON vectors were administered via intrathecal delivery to Nav1.8-Cre transgenic mice.
Experimental Groups: Mice received either the functional mix (AAV9-GluClα and AAV9-GluClβ) or the control vector (AAV9-GluClβ alone). The β-only group serves as a negative control because GluCl beta subunits cannot form functional homomeric channels in the absence of alpha subunits, ensuring any observed effects are due to the functional heteropentameric channel.
Timeline: following a 3-week incubation period for viral transduction, baseline behavioural assessments were conducted on Day -1. On Day 0, mice received systemic IVM (5 mg/kg, i.p.) to activate the channel. Post-silencing behavioural testing was performed 24 hours later (Day +1), immediately followed by tissue collection for histological and molecular analyses.

Initial attempts to quantify sensor expression using immunohistochemistry against its protein components yielded weak and inconsistent signals, a common challenge for overexpressed membrane proteins. Therefore, to obtain a more precise and sensitive measure of expression, we employed RNAscope in situ hybridisation, which is capable

of detecting low-level transcripts. Specifically, the probes were designed to recognise the mRNA sequences encoding the Yellow Fluorescent Protein (YFP) and Cerulean components of the GluCl.CreON sensor. As shown in Figure 2.3A, the analysis confirmed that GluCl.CreON transcripts co-localised with the neuronal marker NeuN, indicating that expression was restricted to neuronal cells rather than glial cells. Quantitative analysis of lumbar DRGs from injected Nav1.8 Cre mice revealed that, on average, 29.40 ± 5.35% of neurons expressed GluCl.CreON mRNA (Figure 2.3B, n = 8 mice, a total of 2,414 cells were analysed)

We further conducted cell morphological analysis of neurons expressing GluCl.CreON in Nav1.8-Cre mice (Figure 2.3C). The size distribution of GluCl-positive neurons closely mirrored that of the total neuronal population, indicating no preferential transduction based on cell size.

3.1.3 Verification of Cre Dependency and Expression Specificity

To verify the Cre dependency of the GluCl.In the CreON system, we injected the same AAV9-GluCl.CreON into wild-type mice and analysed mRNA expression. As shown in Figure 2.3D, in the absence of Cre recombinase, less than 10% of DRG neurons showed weak background expression (n = 3 mice, 1,181 cells), far lower than the expression level in Nav1.8Cre mice, demonstrating the system's Cre dependency.

Notably, our intrathecal injection method achieved good regional selectivity. As shown in Figure 2.3E, when examining spinal cord tissue sections, no GluCl.CreON mRNA expression signals were detected, indicating that the viral vectors primarily transduced DRG neurons without affecting the central nervous system, which is critical for specifically studying peripheral sensory neuron function.

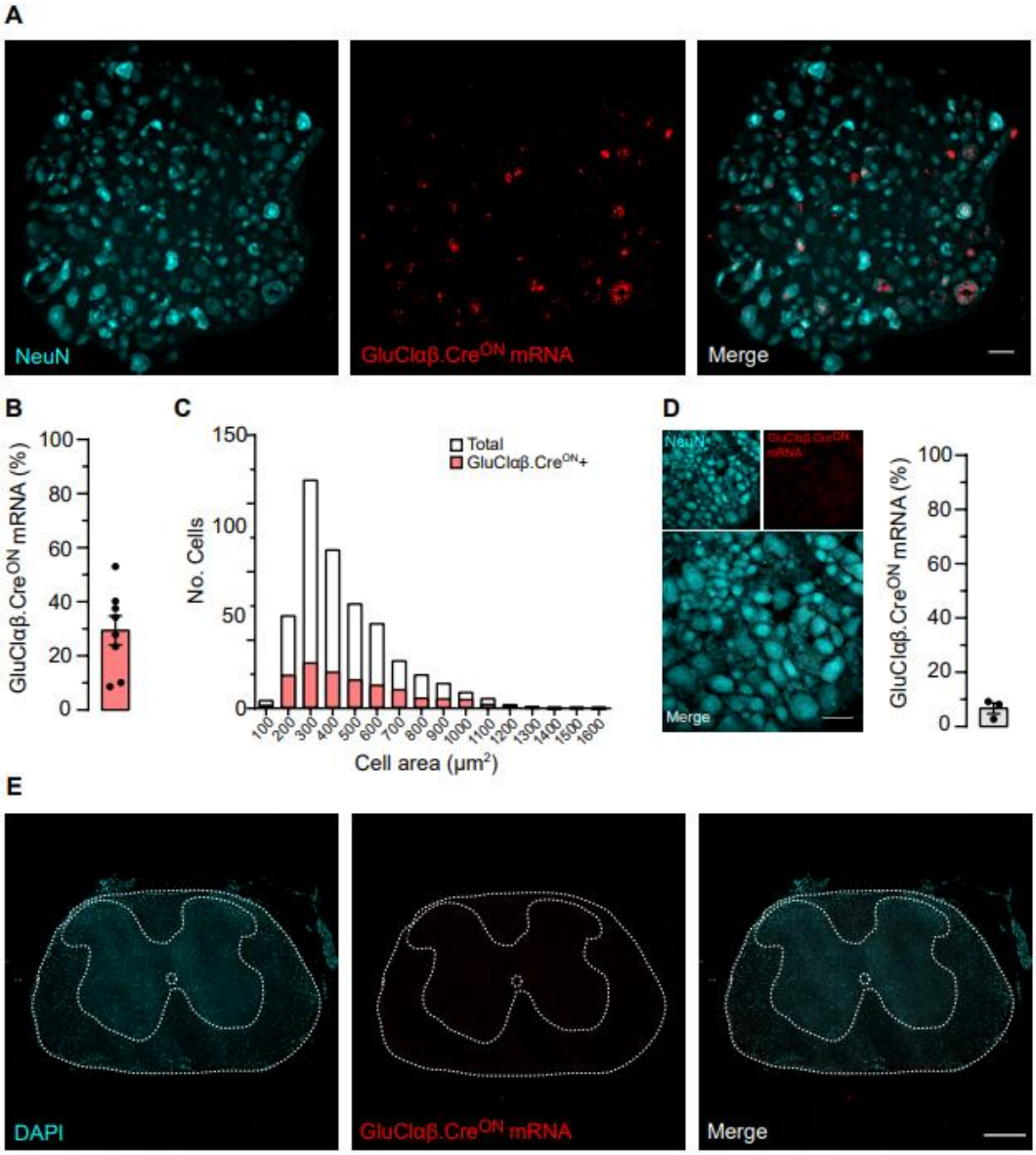

Figure 2.3. DRG-specific expression of AAV-GluClαβ.CreON following intrathecal administration.

A. Representative confocal images demonstrating GluClαβ.CreON mRNA expression in DRG L4 neurons from Nav1.8-Cre mice. Left: Neurons are identified by the marker NeuN (cyan). Middle: Viral transcripts are detected by in situ hybridisation (red). Right: The merged image confirms co-localisation. Scale bar: 50 μm.

B. Quantification of transduction efficiency. Analysis of 2,414 neurons from 8 Nav1.8^Cre mice revealed that 29.40 ± 5.35% of DRG neurons were positive for GluClαβ.CreON mRNA.

C. Cell size distribution analysis. The size distribution of transduced neurons followed the general size profile of the total neuronal population,

D. Assessment of Cre-dependency in wild-type mice from the littermate control group. In the absence of Cre recombinase, only minimal background (leakage) expression of the transcript was detected in fewer than 10% of neurons (analysed from 1,181 cells across 3 mice). Scale bar: 50 μm.

E. Regional specificity of viral transduction. Examination of the spinal cord from Nav1.8^Cre mice injected with the AAVs showed no detectable GluClαβ.CreON mRNA, indicating that expression was restricted to the DRG. Scale bar: 300 μm.

Data are presented as mean ± SEM. This figure is adapted from Middleton et al. (2023), published in *Pain* (Middleton et al., 2023).

3.2 Selective Modulation of Pain Perception by the GluCl-CreON System

3.2.1 Sensory Modality-Specific Regulation Performance

To evaluate the functional effects of the GluCl-CreON system in vivo, we conducted a series of behavioural experiments to study its impact on different sensory modalities. Three weeks after intrathecal injection of AAV9-GluCl-CreON virus in Nav1.8-Cre mice, we compared the behavioural differences between mice expressing complete GluClαβ channels and those expressing only the β subunit (control group) before and after IVM treatment (5 mg/kg, intraperitoneal injection) (Figure 2.4A). Prior to IVM administration, both groups exhibited similar baseline sensory thresholds.

We first tested the system's effect on non-noxious sensations. Behavioural tests showed that after IVM administration, both groups maintained similar levels of sensory thresholds to various light touch stimuli. There were no statistical differences between the groups in brush stimulation (Figure 2.4B), cotton swab touch response (Figure 2.4C), sticky tape test (Figure 2.4D), or von Frey filament threshold (Figure 2.4E). These results suggest that activation of the GluCl-CreON system does not affect mice's normal perception of non-noxious mechanical stimuli.

Equally important, activation of the GluCl system does not interfere with the motor coordination of mice. Rotarod test results showed no significant difference in the time mice stayed on the rotarod after IVM administration (Figure 2.4F).

3.2.2 Specific Inhibition of Noxious Sensations

In stark contrast to the intact non-noxious sensations, the GluCl-CreON system showed potent inhibitory effects on noxious sensation processing. In the pin-prick test, mice expressing GluClαβ exhibited significantly prolonged paw withdrawal latency after IVM administration (Figure 2.4G). This delayed response did not exist under baseline conditions, clearly indicating that activation of the GluCl system specifically inhibits the mechanical nociceptive process mediated by Nav1.8-positive neurons.

Heat pain testing further confirmed this modality-specific regulation. In the 53°C hot plate experiment, GluClαβ group mice showed significantly prolonged response latency after IVM treatment (Figure 2.4H), demonstrating that the system can effectively attenuate heat pain perception mediated by Nav1.8-positive neurons. This dual regulatory capability for heat pain and mechanical pain suggests that the GluCl-CreON system can influence the processing of multiple noxious sensations.

3.2.3 Long-lasting Inhibition of Inflammatory Pain

To explore the potential of the GluCl system in regulating persistent pain states, we used the formalin plantar injection model, a classic model that induces sustained inflammatory responses and central sensitisation. We recorded and analysed nociceptive behaviours (lifting, licking, shaking, etc.) exhibited by mice during the 60 minutes following formalin injection. Results showed that Nav1.8-Cre mice expressing GluClαβ, when pretreated with IVM 24 hours prior, exhibited significantly reduced pain behaviours (Figure 2.4I). This inhibitory effect was evident throughout the observation period but was particularly pronounced at later time points (35-40 minutes). When analysing the formalin response in the traditional two-phase manner, we found that the inhibitory effect of the GluCl system was mainly manifested in the second phase (15-60 minutes) (Figure 2.4J). Combining all behavioural data, our study shows that the GluCl-CreON system can achieve highly selective modulation of sensory functions: effectively inhibiting noxious sensory inputs of multiple modalities (mechanical pain, heat pain, and chemically induced inflammatory pain) while preserving the integrity of non-noxious sensations and motor functions.

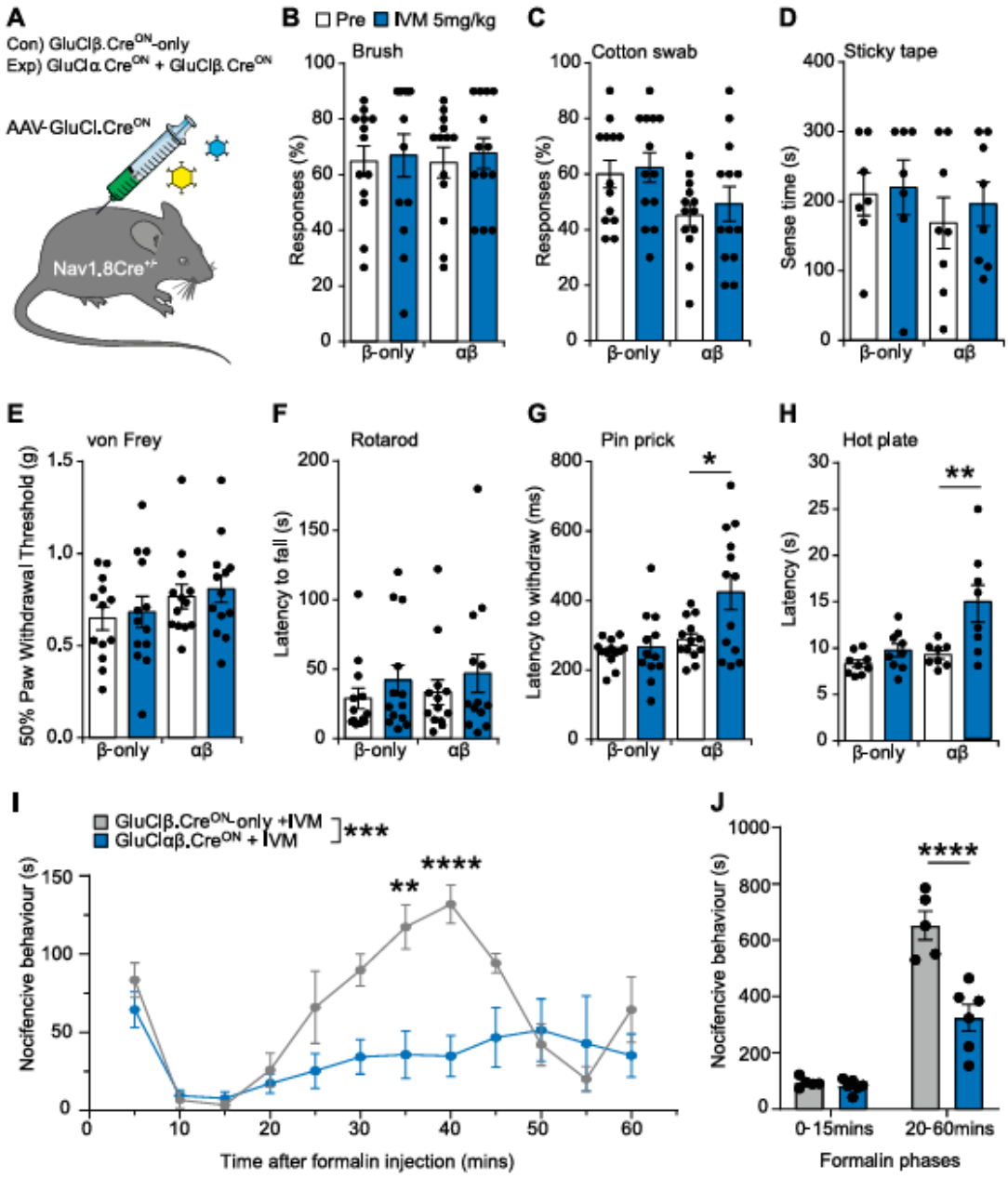

Figure 2.4. Selective silencing of Nav1.8-positive neurons attenuates nociceptive behaviours while sparing non-noxious sensation and motor function

A. Experimental design overview: Intrathecal delivery of AAV-GluCl.CreON (α+β or β-only) to Nav1.8^Cre mice followed by behavioural assessment before and after IVM administration.

B. IVM administration did not alter the response frequency to light brush stimuli in either the control (β-only) or experimental (αβ) group (β-only group, n = 13; αβ group, n = 13; p > 0.99 for both comparisons).

C. Cotton swab detection sensitivity was unaffected by IVM administration in either experimental or control group β-only, n = 13; αβ, n = 13; p > 0.99 and p = 0.655, respectively.

D. Adhesive tape detection capability showed no significant alterations after IVM treatment in both groups (β-only, n = 7; αβ, n = 8; p > 0.99 for both comparisons).

E. Mechanical thresholds assessed by von Frey filaments demonstrated no significant changes following IVM administration in either group (β-only, n = 13; αβ, n = 13; p > 0.99 for both comparisons).

F. Motor coordination assessed by rotarod performance remained intact after Nav1.8-positive neuron silencing: β-only, n = 13, p = 0.165; αβ, n = 13, p = 0.146).

G. In the pinprick test, IVM treatment significantly prolonged the withdrawal latency for the αβ group, while the control group showed no change. (β-only, n = 13, p = 0.517; αβ, n = 13, p = 0.016*).

H. Thermal pain sensitivity (at 53°C) was significantly reduced (longer latency to respond) in Nav1.8^Cre GluCl.CreON αβ mice after IVM administration (β-only, n = 9, p = 0.464; αβ, n = 8, p = 0.0017**).

I. Chemical-induced pain behaviour in the formalin test was markedly reduced in GluClαβ.CreON-expressing mice following IVM treatment compared to β-only controls (β-only, n = 5; αβ, n = 6; F (1,9) = 23.81, p = 0.0009***).

J. Analysis of the two phases of the formalin test showed that the anti-nociceptive effect of silencing was confined to the second (tonic) phase, with no effect observed in the initial acute phase (phase 1, p > 0.99; phase 2, p < 0.0001****).

B-J: two-way RM ANOVA with Bonferroni corrections. All data expressed as mean ± SEM. Statistical significance: *p < 0.05, **p < 0.01, ***p < 0.001, ****p < 0.0001. ANOVA: analysis of variance; IVM: ivermectin; RM: repeated measures.

This figure is adapted from Middleton et al. (2023), published in *Pain* (Middleton et al., 2023). I contributed the data presented in panels G, I, and J. The experimental design and

data for all other panels (A–F and H) were generated by the first author of the original publication, Steve Middleton.

4. Discussion

4.1 Performance of the GluCl.CreON System as a Selective Neural Modulation Tool

To selectively target and silence specific subpopulations of sensory neurons, we constructed a novel Cre recombinase-dependent GluCl construct, called GluCl.CreON, thereby expanding the chemogenetic toolbox (Atasoy et al., 2008; Schnütgen et al., 2003). In our designed and generated GluCl construct, the α and β subunits of GluCl are inverted, with their open reading frames (ORFs) surrounded by two pairs of heterotypic LoxP sites. In the presence of Cre, the target gene is restored to forward orientation, leading to GluCl expression. In Cre-negative neurons, the construct is designed to remain silent; however, consistent with our observations in wild-type mice, we detected a low level (<10%) of leaky mRNA expression, likely attributable to spontaneous recombination of the viral vectors. We selected the Nav1.8 Cre mouse line, which is known to express Cre recombinase in nociceptors and C-type low-threshold mechanoreceptors (Middleton et al., 2022; Nassar et al., 2004).

We performed intrathecal injection of AAV9.sCAG. GluCl.CreON into Nav1.8Cre mice and wild-type mice. After waiting 4-6 weeks for maximum transgene expression, we detected GluCl expression levels. Although we attempted to enhance the fluorescent signal using immunohistochemistry with an anti-GFP antibody, the detection sensitivity remained insufficient, and the observed positive rate was low. Therefore, we applied in situ hybridisation and used RNAscope to detect mRNA of the fluorescent tags (YFP/Cerulean) fused to GluCl subunits. Results showed that GluCl.CreON mRNA

expression in total DRG neurons was 29.40 ± 5.35%. Cell size analysis revealed that the distribution of GluCl.CreON-positive neurons were similar to those of the total neuronal population. Furthermore, when GluCl.CreON was injected into Cre-negative wild-type mice, a small amount of GluCl mRNA expression was observed, indicating a low level of leaky expression without Cre dependency.

Using immunohistochemical methods, we detected low levels of GluCl, with approximately 30% of sensory neurons expressing GluCl.CreON mRNA (Nav1.8 population accounts for 60-70% of DRG). Effective expression of GluCl may depend on multiple conditions, such as the need for Cre-mediated recombination of α and β subunits in GluCl.CreON, the strength of the Cre line, and the number of viral copies transduced into each neuron, plus the GluCl.CreON design using a shorter CAG promoter, which increases the uncertainty of success and may reduce expression efficiency.

Subsequently, to verify the functionality of GluCl.CreON, we administered AAV-GluCl.CreON αβ or β only (as a control group) to Nav1.8Cre mice and conducted a series of behavioural experiments before and after IVM administration. Behavioural tests clearly demonstrated the modality specificity of the GluCl-CreON system in sensory modulation. In Nav1.8-GluCl mice, IVM administration (5mg/kg, i.p.) significantly reduced sensitivity to noxious heat stimuli and sharp mechanical stimuli, while thoroughly preserving reaction capability to non-noxious tactile stimuli and motor coordination.

Particularly noteworthy is that activation of GluCl-CreON significantly inhibited nociceptive behaviours in the second phase (10-60 minutes) of the formalin test, a period closely associated with central sensitisation and sustained inflammatory responses. This finding emphasises the key role of sustained activity of Nav1.8-positive neurons in

maintaining inflammatory pain states and suggests the potential of therapeutic strategies targeting these neurons.

4.2 Comparison with Existing Methods

The GluCl.CreON system offers several significant advantages compared to existing methods, including genetic ablation, optogenetic intervention, and other chemogenetic tools.

4.2.1 Advantages Over Genetic Ablation Methods

Compared to methods that permanently ablate Nav1.8-positive neurons using the diphtheria toxin DTR/DTX system (Abrahamsen et al., 2008), the GluCl-CreON system demonstrates significant methodological advantages. As an innovative reversible chemogenetic tool, GluCl-CreON allows researchers to precisely control the time window of neuronal activity precisely, enabling repeated testing and longitudinal studies in the same animal. Unlike DTX-induced irreversible neuronal death, GluCl preserves intact neuronal structure, avoiding confounding factors such as secondary immune responses and synaptic reorganisation, thereby providing purer functional data. This feature is significant because permanent ablation often induces immune responses related to cell death and microglial recruitment (Passaro et al., 2021). There are strong interactions between the immune system and pathological pain. Notably, our heat pain test results differ from the ablation study by Abrahamsen et al. (2008)—they reported that ablation of Nav1.8-positive neurons primarily affects mechanical pain rather than heat pain, while we observed that the GluCl-CreON system has significant inhibitory effects on heat pain (Abrahamsen et al., 2008). This difference may reflect the fundamental distinction between acute reversible inhibition and compensatory changes after permanent ablation, indicating that the GluCl-CreON technique can reveal the direct

functional effects of these neurons without being masked by compensatory mechanisms in the nervous system.

4.2.2 Advantages Over Optogenetic Methods

In sensory neuron research, optogenetics and the GluCl system each have their characteristics and limitations. Optogenetic tools provide millisecond-level temporal resolution but face multiple technical challenges: light source requirements, limited light penetration depth, invasive implants, and light-induced thermal effects (Iyer et al., 2014; Walker & Kullmann, 2020; Wiegert et al., 2017). These challenges are particularly prominent in practical applications—tissue damage from fibre optic implantation can induce local inflammatory responses, especially in sensitive structures like DRGs; meanwhile, the need for continuous illumination limits experiment duration and the use of freely moving animals.

More critically, the mechanism of action of optogenetic tools themselves may introduce non-specific interfering factors. For example, Zeng et al. (2015) confirmed that heterologously expressed ASICs can be activated by Arch-mediated proton efflux (Zeng et al., 2015); while Daou et al. (2013) observed pain relief using optogenetic silencing of Nav1.8-positive afferents, their tool requires continuous proton efflux, and such changes in extracellular pH may activate acid-sensitive ion channels and other pH-sensitive proteins, interfering with the interpretation of experimental results (Daou et al., 2013).

In comparison, the GluCl system is activated by systemic IVM administration. It achieves neural inhibition through a chloride ion channel-mediated hyperpolarisation mechanism, fundamentally avoiding confounding factors such as tissue damage, local heating, and pH changes. More importantly, GluCl can maintain continuous inhibition for several days in freely moving animals without any invasive devices or continuous intervention, which

provides a unique advantage for studying the long-term dynamics of chronic pain states, making it a powerful tool for studying the function of sensory neurons.

The GluCl.CreON system appears to offer several potential advantages for circuit interrogation in pain research. One apparent benefit is its capacity for sustained inhibition through ivermectin (IVM), a clinically approved agonist with established pharmacokinetic properties. We infer that a single IVM administration may induce neuronal silencing persisting for several days (e.g., ~3-5 days), which could potentially simplify experimental protocols. This duration potentially simplifies experimental protocols compared to methods requiring repeated interventions. This characteristic might be beneficial for longitudinal behavioural assessments in chronic pain models.

The double-floxed inverted open reading frame design seems to provide compatibility with various Cre driver lines, potentially enabling targeted manipulation of specific sensory neuron subpopulations. As a silencing rather than ablative approach, it is theoretically expected to suppress neuronal excitability without destroying the cells, possibly reducing confounding tissue responses associated with ablation techniques.

4.2.3 Advantages Over Other Tools

Besides optogenetics and ablation, other widely used tools for neuronal inhibition include tetanus toxin (TeNT) and DREADDs (like hM4Di). TeNT blocks neurotransmitter release by cutting a protein called synaptobrevin (Schiavo et al., 1992). It is widely used to stop synaptic transmission (Sweeney et al., 1995). However, TeNT expression is usually permanent. It lacks the flexible timing of ligand-gated systems. Furthermore, TeNT only stops vesicle release at the synapse. It does not suppress the excitability of the neuronal soma.

In summary, existing tools have clear benefits. For example, optogenetics has great temporal precision. However, they also have limits for long-term pain research. Ablation and TeNT cause irreversible changes. Optogenetics requires invasive implants. The GluCl.CreON system solves these problems. It provides a non-invasive, long-lasting, and reversible way to silence neurons. It avoids implants, tissue damage, heat, and pH changes. Therefore, it is an ideal tool for studying chronic pain over time.

4.3 Technical Considerations and Limitations

Despite the significant advantages demonstrated by the GluCl.CreON system, several technical limitations and considerations need to be addressed in this study. Expression efficiency: Although the GluCl-CreON system performed well functionally in this study, we observed that expression efficiency was still low, which may be related to various factors, including technical challenges of intrathecal injection, differences in AAV9 transduction efficiency, and the characteristics of a dual-component system requiring co-expression of two subunits. To address this issue, future work could consider using a 2A self-cleaving peptide sequence to integrate the GluClα and GluClβ subunits into a single AAV vector, simplifying delivery and improving co-expression efficiency (Tang et al., 2009). Additionally, exploring new AAV serotypes such as AAV-PHP.S may further improve transduction efficiency for DRG neurons (Chan et al., 2017).

Complexity of DRG neuron specificity: While Nav1.8 primarily labels nociceptors, it is also expressed in some non-nociceptors, such as C-LTMRs and a few mechanoreceptors (Shields et al., 2012; Usoskin et al., 2015). Our observation that the GluCl-CreON system does not affect light touch perception may reflect that the contribution of these Nav1.8-

positive non-nociceptors to light touch perception is relatively limited or that functional redundancy exists. With the development of more refined Cre driver lines, the GluCl-CreON system can be applied to more specific neuronal subpopulations, further dissecting sensory circuit functions.

Temporal resolution: IVM-induced GluCl activation takes several hours to reach its maximum effect, a temporal characteristic that limits the study of neural events requiring millisecond precision but offers clear advantages for studying long-term processes such as chronic pain. In contrast, optogenetic methods provide millisecond-level control, making them more suitable for studying rapid neural events that require precise temporal control.

A critical parameter in our study design was the dosage of the ligand, ivermectin (IVM). We utilised a systemic dose of 5 mg/kg (i.p.), which aligns with established standards for GluCl-based chemogenetic silencing in rodents (Lerchner et al., 2007; Weir et al., 2017). We acknowledge that this dosage is significantly higher than the typical therapeutic dose used for antiparasitic treatment in humans (~0.2 mg/kg) (González Canga et al., 2008). This disparity is necessitated by the pharmacokinetics of IVM at the blood-brain barrier (BBB). IVM is a substrate for P-glycoprotein (P-gp) efflux pumps, which actively limit its accumulation in the mammalian CNS (Lespine et al., 2007). Consequently, higher systemic doses are required in murine models to achieve sufficient intracerebral concentrations for receptor activation compared to the nanomolar levels required for antiparasitic activity.

Regarding safety, it is important to note that the 5 mg/kg dose falls well within the safety margin for mice, remaining substantially below the reported LD50 of approximately 30 mg/kg (i.p.) (Crump & Omura, 2011). To control for potential off-target effects of this

high dosage, our study employed a beta-only control group. These animals received the full 5 mg/kg dose of IVM but lacked functional heteromeric channels. The absence of behavioural or motor abnormalities in this group confirms that IVM alone, at this specific dosage, does not induce confounding sedative or analgesic effects in our experimental context.

However, for future translational applications, the administration of 5 mg/kg to humans would likely present safety concerns. Bridging this translational gap will require the development of GluCl variants with higher sensitivity to allow for lower dosing, or the identification of novel ligands with superior BBB penetrance that can bypass P-gp efflux.

4.4 Potential Applications

Although the GluCl-CreON system is primarily used for basic research, its working principle provides a conceptual basis for developing new pain treatment strategies. The ability of the GluCl.The CreON system to target specific neuronal populations while preserving other sensory functions represents an ideal model of precision medicine in pain management. Compared to traditional analgesics such as opioids and local anaesthetics, this selective targeting has the potential to reduce side effects such as motor dysfunction, respiratory depression, and addiction risk (Obeng et al., 2021).

The modular design of the GluCl-CreON system allows it to be easily applied to other sensory neuron subpopulations with available Cre driver lines. Of particular interest are TrkA^Cre (peptidergic nociceptors), TrkB^Cre (Aδ-LTMR), MrgprD^Cre (non-peptidergic nociceptors), and TH^Cre (C-LTMR) lines (Cavanaugh et al., 2009).

AAV-mediated gene therapy has entered clinical trials for various neurological disorders (Hudry & Vandenberghe, 2019). Notably, many preclinical and clinical studies have

shown good safety and efficacy (Terashima et al., 2018). This provides a feasible path for the clinical application of the GluCl system.

5. Conclusion

GluCl-CreON is a new tool for studying the role of sensory neuron populations in pain processing. Our research demonstrates the effectiveness of this system in selective expression and functional modulation, achieving specific inhibition of heat pain, mechanical pain, and inflammatory pain mediated by Nav1.8-positive neurons, while preserving non-noxious sensations and motor functions. The key advantages of the GluCl-CreON system lie in its high selectivity, potent inhibitory effects, reversibility, and unique characteristics compared to other techniques. These features make it a new tool for studying sensory processing, pain mechanisms, and developing novel analgesic strategies. As sensory neurobiology and pain research continue to advance, the application range of the GluCl-CreON system will continue to expand, providing support for dissecting neural circuit functions, developing targeted therapeutic strategies, and achieving precision medicine goals in pain management.

6. Acknowledgements

In this study, I was primarily responsible for executing and analysing immunohistochemistry and in situ hybridisation experiments. Specifically, I conducted a histological analysis of the expression characteristics of the GluCl.CreON system in DRGs, including assessment of efficiency, cell type distribution, and specificity verification. I also participated in behavioural data collection and analysis.

Dr Steven Middleton, as the project's principal investigator, was responsible for the overall experimental design, construction of the GluCl.CreON plasmid, and the design and execution of behavioural tests.

The findings of this chapter have been published in the journal *Pain* (Middleton et al., 2023). I am one of the co-authors and have obtained permission from the main author, Dr Steven Middleton, and the corresponding author, Professor David Bennett, to include the relevant content in this chapter.

Chapter III A Neonatal Subcutaneous Injection Strategy: Achieving Efficient Gene Delivery to Dorsal Root Ganglia (DRG) and Trigeminal Ganglia (TG)

Abstract

In the previous chapter, we constructed and optimised GluCl.CreON to selectively silence Nav1.8-positive sensory neurons. However, chemogenetic delivery relies on adeno-associated virus (AAV) vectors and intrathecal delivery methods, which while effective, have challenges with restricted lumbar DRG expression and significant inter-individual surgical variability. The anatomical location of the trigeminal ganglia (TG) at the cranial base results in poor accessibility, limiting in vivo chemogenetic research in the trigeminal pathway. Based on systematic evaluation of various delivery routes, we propose and validate a neonatal subcutaneous injection strategy that likely exploits the immature /blood-nerve barrier in neonates to achieve efficient AAV9 transduction of the peripheral nervous system. This strategy yields approximately 50% transduction efficiency in adult DRG and TG. We successfully used this route to deliver a more clinically translatable chemogenetic tool, AAV9-PSAM^4-GlyR, to both DRG and TG. This chapter provides a scalable delivery method for chemogenetics and other genetic manipulations in the peripheral sensory nervous system.

1. Introduction

In the previous chapter, we successfully constructed and optimised the chemogenetic tool GluCl.CreON is designed to selectively silence Nav1.8-expressing nociceptive sensory neurons (Middleton et al., 2023). However, its in vivo application is limited by the delivery efficiency of its adeno-associated virus (AAV) vector. Although AAV9 shows some affinity for the peripheral nervous system (PNS), its transduction efficiency in cell bodies of the DRG in adult animals is variable and often depends on the route of delivery (O'Donnell et al., 2024; Schuster et al., 2014). The TG is more challenging, located within Meckel's cave at the cranial base, adjacent to critical cranial nerves and blood vessels, making surgical exposure extremely difficult. Its poor surgical accessibility and the numerous side effects of existing delivery methods (Messlinger & Russo, 2019) significantly restrict our ability to target this structure in vivo virally. This lack of access has prevented chemogenetic modulation or genetic manipulation studies in the trigeminal pathway.

To deliver genetic tools to sensory neurons, researchers have explored various administration routes using various viral serotypes and engineered capsids. However, each strategy has limitations. This section reviews existing AAV delivery strategies. A review of different AAV serotypes will be explored in Chapter Six.

1.1 Delivery Challenges for Dorsal Root Ganglia (DRG)

As first-order neurons in the spinal sensory pathway, DRG neurons are critical targets for studying somatic sensation and pathological states like chronic pain. Although anatomically more superficial than the trigeminal ganglion, achieving efficient, uniform, and minimally invasive gene delivery to DRG neurons still faces numerous challenges. Current AAV delivery strategies for DRGs can be categorised as follows:

Intrathecal Injection (i.t.):

It is one of the most widely used DRG delivery routes and was the method employed in Chapter 2. This method involves injecting AAV into the subarachnoid space, utilising cerebrospinal fluid (CSF) circulation to cover multiple DRG segments. However, its disadvantage lies in variability. Transduction efficiency and spatial distribution are easily affected by CSF hydrodynamics, injection technique (e.g., speed, needle position, cannula vs lumbar puncture), and operator experience, resulting in substantial differences in gene expression levels between batches and even between animals within the same batch, affecting experimental reproducibility (Rahman et al., 2023). Numerous studies have used i.t. AAV to target DRG neurons with overall neuronal transduction commonly ranging from 10–80% depending on serotype, dose and promoter choice. Notably, efficiency can be significantly enhanced by co-treatments that increase permeability, such as intravenous mannitol (Jacques et al., 2012; Schuster et al., 2014; Towne et al., 2009; Vulchanova et al., 2010).

Direct Intraganglionic Injection:

This method surgically exposes the DRG for microinjection, providing the most direct path to neuronal cell bodies. A key advantage of this approach is its exceptional specificity, which enables gene expression to be strictly confined to peripheral sensory neurons, thereby avoiding off-target effects in the central nervous system (CNS). The DRG's porous structure and its encapsulation by connective tissue make it an ideal target for injection. Furthermore, the procedure has been demonstrated to be well-tolerated in both rodents and humans, and in a clinical setting, it is considered a straightforward outpatient procedure (Yu et al., 2016). However, this process is highly invasive in rodents. In rats, exposing lumbar DRGs requires complex and time-consuming paravertebral surgery (approximately 30 minutes just to expose L4/L5 DRG, with an additional 8 minutes per

injection) (Fischer et al., 2011). The challenge is amplified in mice due to their smaller size and narrower anatomical windows, where a traditional complete laminectomy easily destabilises the spine. Even modified approaches present trade-offs: partial osteotomy may preclude repeated injections (Yuan et al., 2023), while partial laminectomy, though enabling reinjection, involves greater surgical trauma and imposes limitations on the operational angle (O'Donnell et al., 2024). Nevertheless, the method demonstrates considerable efficacy in mice. Direct injection with leading serotypes like AAV2-retro and AAV8 has resulted in the transduction of approximately 294 neurons per DRG in mice (O'Donnell et al., 2024).

Intraneural/Perineural Injection:

Injecting AAV into a peripheral nerve, such as the sciatic nerve, can specifically transduce DRG subgroups that it innervates. This route has some feasibility in large animals or clinical settings. A primary limitation is its targeting specificity. Intraneural injection into the sciatic nerve has demonstrated a preferential and more efficient transduction of motor neurons compared to sensory neurons, which restricts its effectiveness when the goal is to specifically target sensory pathways (Boulis et al., 2003). Secondly, the technique is sensitive to microsurgical manipulation and injection parameters. Slight impropriety can cause fascicular injury and neurologic deficits (Hadzic et al., 2004). Rodents, with their small size, are particularly sensitive to injection-induced internal pressure changes, increasing the risk. Finally, because this approach relies on retrograde axonal transport for the vector to travel from the axon terminals back to the cell body, the selection of the AAV serotype is critical.

Peripheral Retrograde Delivery:

This involves injecting into areas innervated by DRG neurons, such as skin, muscle, or joints, relying on AAV uptake by nerve terminals and retrograde transport to the cell body.

This method has the advantage of being minimally invasive but is limited by difficulties in achieving uniform, controllable multi-segment coverage. For example, with AAV8, injection into the tibialis anterior/gastrocnemius muscles in adult mice results in positive staining in the ipsilateral sciatic nerve, bilateral DRGs, and spinal cord white matter. Still, transduction in DRG neurons was higher on the injected side than on the contralateral side, and greater in the lower spinal cord region compared to the upper region (H. Zheng et al., 2010). This method has also been used in an intra-articular manner to effectively transduce sensory neurons innervating the knee joint, responsible for signalling joint inflammation (Perez-Sanchez et al., 2023).

Systemic Intravenous Injection (i.v.):

In adult animals, intravenously injected AAV is strictly limited by the blood-nerve barrier (BNB). Most viral particles are preferentially sequestered by peripheral organs such as the liver and heart, leaving a low proportion capable of penetrating the barrier to reach the DRG. For example, with AAV9, when administered intravenously in adult mice under equivalent conditions, DRG transduction efficiency is significantly lower (approximately 9% positive in L4 DRG) compared to the same dose administered intrathecally (i.t.), which can reach approximately 73% or higher (Schuster et al., 2014).

1.2 AAV Delivery Challenges for the Trigeminal Ganglion (TG)

The TG is the primary sensory centre for facial sensation (including pain, touch, and temperature), which is important in disease contexts such as migraine and trigeminal neuralgia. Gene delivery to the TG is far more challenging than to the DRG. Due to its anatomical position, the TG is encased within the dural sac (Meckel's cave) at the cranial base, adjacent to numerous critical cranial nerves and blood vessels, making it highly inaccessible (Messlinger & Russo, 2019). Therefore, delivery strategies for the TG present significantly different methodologies and challenges compared to those for DRG.

Direct Cranial/Intraganglionic Injection: This involves approaching Meckel's cave through craniotomy, microsurgery or transorbital/transtemporal microsurgical routes to inject directly into the TG or surrounding Meckel's cave. Whilst this method provides the most direct route, it involves extremely high surgical difficulty and invasiveness, resulting in significant surgical trauma, high complication risk, and animal mortality, severely impacting subsequent behavioural studies and lacking scalability and standardisation. A study reported that while a vector reached the trigeminal ganglion in approximately 80% of cases, only about 30% of these injections resulted in the transduction of the specific neuronal subpopulation that innervates the periocular region. The same study also noted significant variability in transduction efficiency, with an average of 280 ± 144 neurons transduced per ganglion (Whitehead et al., 2003).

Peripheral Retrograde Delivery: Injecting AAV into peripheral regions innervated by the TG (such as whisker pads or cornea). The AAV travels along axons via retrograde transport to reach the trigeminal ganglion. This method is minimally invasive and easy to implement, but its efficiency is affected by serotype (AAV1 superior to 5/7/8/9), promoter, dosage, and day post-injection. For example, at one dose, transduction increased from 3.5% (day 3) to 18.3% (day 28), while higher doses achieved up to 25.25% of total TG neurons (Dang et al., 2017).

Infraorbital Delivery: Guiding the needle tip to Meckel's cave or directly to the TG via the infraorbital foramen--infraorbital canal--foramen rotundum. This method causes less trauma than craniotomy, with shorter surgery time and higher success rates in experienced hands. However, its transduction range is typically limited to neurons associated with V2, making it difficult to achieve uniform, comprehensive coverage of the entire TG (including V1 and V3 regions) (Neubert et al., 2005). There are risks of adverse events related to the orbit, sinus, and vasculature

Preauricular Cranial-Base Approach with 3D Guides: Based on anatomical measurements and image reconstruction, this approach directs a needle containing virus towards the trigeminal fossa from the external auditory canal/preauricular fissure, passing through a small area of cartilaginous tissue between the tympanic bulla and cranial base to enter the target area (Long et al., 2017). This has been further developed with 3D-printed guides to improve bilateral hit rates (Z. Wu et al., 2024). The advantages include minimal trauma, repeatability, and high positioning precision, with guides facilitating standardisation. Disadvantages include the need for imaging and custom guides, which must be redesigned for different species or animals of different weights within the same species.

A key challenge in sensory ganglia targeting is that delivery routes effective for the DRG are often ineffective for the TG. Intrathecal (i.t.) injection serves as a prime example; due to cerebrospinal fluid (CSF) flow dynamics, AAV vectors are largely prevented from reaching the TG in its protected intracranial location within Meckel's cave, resulting in negligible transduction. This inefficiency is even more pronounced with systemic intravenous (i.v.) delivery in adulthood. Vectors administered this way face the dual hurdles of the restrictive blood-nerve barrier and a strong hepatic first-pass effect, leading to expression levels in the TG that are even lower than the modest rates observed in the DRG.

In summary, the delivery dilemma for the TG arises from a combination of its anatomical isolation and the systemic physiological barriers that impede viral vectors. To consolidate the preceding discussion and provide a clear overview of the current landscape, the advantages and disadvantages of each major delivery route are summarised in Table 3.1. This comparison highlights the significant limitations of existing techniques, particularly

in achieving simultaneous, widespread, and minimally invasive transduction of both DRG and TG, thereby underscoring the need for a novel approach.

1.3 Neonatal Subcutaneous AAV Injection Strategy

Based on the above challenges, this study presents an innovative gene delivery strategy, Neonatal Nape Subcutaneous Injection (nSC). A single subcutaneous injection of AAV9 virus into the nape of the neck of P5-P7 neonatal mice. The core objective of this strategy is to achieve synchronous, efficient, and widespread gene transduction in sensory neurons of bilateral DRG and TG through a minimally invasive, standardisable procedure. This strategy is based on understanding the unique physiological window period in neonatal animals. Literature indicates that the neonatal period represents a unique "window of opportunity" where systemic AAV administration can achieve efficient gene transduction in both the central and peripheral nervous systems, an advantage that significantly diminishes in adult animals.

Research comparing transduction efficiency between neonatal and adult intravenous injections has provided evidence. Neonatal intravenous (IV) injection of AAV9 can effectively cross the still-immature blood-brain barrier and blood-nerve barrier. This enables AAV9 to not only broadly transduce neurons in the cerebral cortex, hippocampus, and cerebellum, but also efficiently enter the spinal cord and transduce sensory neurons in DRG across all spinal segments. In contrast, when administered via the tail vein in adulthood, AAV9's neuronal transduction efficiency is greatly limited, highlighting the unique advantage of neonatal administration for trans-barrier delivery (Foust et al., 2009). As another systemic administration method, neonatal intraperitoneal (IP) injection has also been proven to achieve powerful transduction in DRG (Foust et al., 2008). The practicality and safety of this route have been further confirmed in functional studies; for example, IP injection of AAV9 vectors expressing shRNA successfully achieved effective

gene silencing in DRG without obvious cytotoxicity or behavioural abnormalities (Machida et al., 2013). Quantitative analysis showed that IP injection on postnatal day 3 (P3) can achieve a positive rate of up to 70-80% in DRG neurons, with viral marking primarily concentrated in the white matter region of the spinal cord and relatively fewer transduced neurons in the grey matter, suggesting that neonatal systemic administration may have a certain targeting preference for peripheral ganglia such as DRG (H. Zheng et al., 2010).

Despite the foundation laid by the above research for targeting DRG in the neonatal period, two key knowledge gaps remain. First is unknown transduction to TG: Currently, there are no direct quantitative reports on the efficiency of neonatal systemic administration for TG transduction. Second is the unexplored neonatal nape subcutaneous route: The feasibility and efficiency of neonatal subcutaneous (SC) injection as a potential administration route for gene delivery to the nervous system similarly lack literature support.

Based on a comprehensive analysis of existing evidence, we propose a dual hypothesis:

Firstly, based on the homology between DRG and TG in terms of anatomical physiology and barrier characteristics, we infer that neonatal systemic delivery of AAV has the potential to transduce TG as well efficiently.

Secondly, we believe that neonatal subcutaneous injection is a feasible and potentially more advantageous administration route. The rationality of this inference stems from the following pharmacokinetic and anatomical considerations:

The blood-nerve barrier of DRG and TG features a relatively loose structural characteristic, with its microvascular system exhibiting fenestrated structures and discontinuous tight junctions. Additionally, the expression of related proteins shows heterogeneity (Hirakawa et al., 2004). This natural barrier heterogeneity provides more

exposure and permeation opportunities for blood-borne AAV vectors, serving as the anatomical premise for their high transduction rates.

A key study points out that during the perinatal period, the primary factor affecting the in vivo biodistribution of AAV9 is age, not the administration route (Bostick et al., 2007). This suggests that, whether IV, IP, or SC, as long as the vector can enter the systemic circulation during this critical neonatal window, similar transduction efficiency may be achieved.

The nape's subcutaneous tissue is loose, with rich vascular and lymphatic networks. After injection, a local drug depot can form, allowing AAV vectors to enter the blood and lymphatic circulation in a more gradual and sustained manner. Unlike the rapid peak exposure of intravenous administration, subcutaneous administration features a more gradual and prolonged absorption process. Its typical pharmacokinetic characteristics include a delayed time to maximum concentration (Tmax) and reduced maximum plasma concentration (Cmax). However, the total exposure (Area Under the Curve, AUC) can be comparable to intravenous administration, presenting a more gradual absorption-dominated exposure curve (Bittner et al., 2018). This principle has been confirmed in studies of nanocarriers of comparable size to AAV: after subcutaneous injection, the formulation mainly enters the systemic circulation slowly along the draining lymphatic vessels, resulting in significantly delayed appearance in the blood (Tmax delayed to hours) and weakened peak concentration; once in the blood, its subsequent biodistribution and elimination kinetics tend to be consistent with the intravenous administration pattern (Allen et al., 1993).

Based on this, we infer that this extended effective contact time can synergistically enhance the still-immature physiological barriers of the neonatal period and the relatively high permeability of sensory ganglia themselves. This advantageous combination of

sustained release into blood and efficient penetration theoretically promises to maximise the cumulative exposure and transduction probability of AAV vectors in DRG and TG, potentially achieving better targeting efficiency than traditional rapid injection (such as IV).

1.4 Research Objectives

Given that the aforementioned theoretical inferences require direct experimental data support, the core task of this chapter is to comprehensively confirm the delivery feasibility, transduction efficiency, and targeting specificity of the nSC strategy through experimentation. To this end, we designed a logically progressive two-step validation process to evaluate the gene delivery and expression systematically.

The first step is anatomical characterisation. We try to verify the delivery efficiency, breadth, and specificity of the nSC strategy. This step aims to systematically address the basic delivery capabilities of the nSC strategy. We will use AAV9 vectors carrying the mCherry reporter gene (AAV9-CAG-mCherry) to conduct comprehensive quantitative assessments from the following three key dimensions: (1) Core target transduction efficiency: Verify whether the nSC strategy can efficiently transduce DRG and TG sensory neurons. (2) Systemic distribution breadth and uniformity: Evaluate the coverage range of the virus in the sensory nervous system throughout the body. We will systematically detect the transduction of DRG at various segments from cervical to lumbosacral (rostrocaudal axis). (3) Targeting specificity analysis: Evaluate whether the nSC strategy will transduce other components of the central nervous system (CNS) and PNS.

After confirming the basic vector delivery capability, the second step is to explore the application potential of the nSC strategy. This step addresses a more demanding question: whether it can support the effective expression of a structurally complex functional

protein that requires correct folding and transport within cells. For this purpose, we selected the AAV9 vector loaded with the large chemogenetic tool PSAM⁴-GlyR (AAV9-CAG-mCherry-PSAM⁴-GlyR) for verification. This system is a chimeric receptor composed of an engineered ligand-binding domain and an ion channel, which, when activated by its exclusive ligand (such as varenicline), can produce rapid, stable, and reversible inhibition of neurons through mediating chloride ion influx (Magnus et al., 2019). This successful verification at the expression level also constitutes a key molecular biological premise for in vivo functional manipulation studies in the next chapter.

2. Methods

2.1 Experimental Animals

This study primarily used C57BL/6J wild-type mice, with experimental procedures performed on postnatal day 5 (P5).

All animal procedures follow the UK Home Office (Scientific Procedures) Act (1986) and are carried out under a UK Home Office Project Licence. All animal experiments were carried out per the University of Oxford policy on using animals in scientific research. All experiments were conducted in line with the ARRIVE guidelines 2.0 (Percie Du Sert et al., 2020). In a pathogen-free facility, all mice are raised in groups in separately ventilated cages with free access to food and water in humidity and temperature-controlled rooms with a 12-hour light and dark cycle. All experiments were carried out on male and female mice and were carried out blind to genotype or treatment group until the end of the analysis.

2.2 Viral Vectors

This study used two viral vectors, all of which were commercially packaged, purified, and titrated by the Viral Vector Facility (VVF), ETH Zurich. AAV9-CAG-mCherry: Used

for systematic evaluation of the nSC strategy's delivery efficiency, tissue distribution, and targeting specificity. Final titre was 3.1×10^{13} vg/mL (vector genomes/millilitre). AAV9-CAG-mCherry-PSAM^4-GlyR: Used to verify the nSC strategy's capacity to carry and express structurally complex functional proteins. This vector co-expresses mCherry reporter protein and PSAM^4-GlyR chemogenetic receptor. Final titre was 1.2×10^{13} vg/mL.

2.3 Neonatal Nape Subcutaneous Injection (nSC)

On P5, neonatal mice were briefly removed from the dam's cage. We chose subcutaneous (SC) injection at the nape over intraperitoneal (IP) injection for safety reasons. At P5, the abdominal organs of pups are very fragile. IP injections carry a high risk of fatal internal injury. SC injection at the nape is much safer and less invasive.

Additionally, SC injection is faster. This reduces handling time and lowers the risk of maternal rejection. While SC uptake is generally slower than IP uptake, we performed histological analysis 4-6 weeks after the injection. Therefore, the slower initial uptake does not affect our long-term results.

Using a 0.3 mL BD Ultra-Fine™ insulin syringe, a single SC injection (10 µL) was performed at the nape of the pup's neck. After injection, bedding from the dam's cage was gently applied to the pup's body to re-scent it with its own and littermates' odours. This procedure aimed to eliminate odours left by researchers, preventing the dam from refusing to nurse or attacking the pup. The pup was then immediately returned to the dam's cage. Injected animals were used for subsequent histological analysis 4-6 weeks later.

2.4 Tissue Processing and Immunofluorescence Histochemistry (IHC)

Four to six weeks after virus injection, mice were deeply anaesthetised (pentobarbital, intraperitoneal injection), and the vascular system was perfused via the heart, first with saline to remove blood, followed by 4% paraformaldehyde (PFA, in PBS, pH 7.4) for fixation. After fixation, the required tissues were rapidly dissected and collected, including DRG, TG, spinal cord, brain, superior cervical ganglia (SCG), and hindpaw pad skin. Collected tissues were post-fixed in 4% PFA (DRG/TG: 1-2 hours; spinal cord/brain: 24 hours), followed by cryoprotection in 30% sucrose solution (at least 48 hours). Finally, tissues were embedded in OCT embedding medium and sectioned using a cryostat (DRG/TG: 12 μm; spinal cord: 15 μm).

A standard immunofluorescence staining protocol was employed for the tissue sections. Briefly, after washing with PBS, sections were blocked for 1 hour at room temperature in a solution containing 5% normal donkey serum and 0.3% Triton X-100 in PBS. Subsequently, sections were incubated overnight at room temperature with primary antibodies diluted in the blocking solution. Primary antibodies included: rabbit anti-NeuN (1:500, Abcam, ab177487), sheep anti-CGRP (1:250, Enzo Life Sciences, CA1137), rabbit anti-NF200 (1:1000, Sigma-Aldrich, ABN76), streptavidin-conjugated Isolectin B4 (IB4, 1:50), and antibodies against ChAT and PGP9.5. The following day, after thorough washing with PBS containing 0.3% Triton X-100, sections were incubated for 2 hours at room temperature under light-protected conditions with appropriate fluorescent secondary antibodies. Fluorophores used for secondary detection included Pacific Blue (1:100), Alexa Fluor 488 (1:500), and Alexa Fluor 546 (1:500), all from Thermo Fisher Scientific. Finally, after a final wash, sections were mounted using Vectashield mounting medium for analysis.

2.5 Image Acquisition and Quantitative Analysis

All fluorescence images were acquired using a Zeiss LSM-710 confocal microscope with 20× (air) and 63× (oil) objectives. Image acquisition software was Zeiss Zen 2012.

Image analysis was performed using Fiji/ImageJ (NIH) software. Transduction efficiency was quantified as follows: in each DRG or TG section, the number of mCherry-positive (red fluorescence) neurons was manually counted and divided by the total number of neurons marked by NeuN, expressed as a percentage. To ensure statistical reliability, at least three independent tissue sections were analysed for each animal, with each group containing at least three independent animals (biological replicates).

2.6 Statistical Analysis

The sample size was determined by the requirements of histological quantification from preliminary experiments. All analyses were performed in GraphPad Prism 10. This study reports descriptive statistics only; no inferential hypothesis testing was conducted. For each endpoint (e.g., transduction percentage), the experimental unit was the animal (n = number of animals). Multiple sections per animal were treated as technical replicates and averaged to yield a single value per animal. Data are presented as mean ± SEM across animals, with individual animal values shown in the figures.

3. Results

3.1 Neonatal Nape Subcutaneous Injection (nSC) Can Efficiently and Simultaneously Transduce Sensory Neurons in DRG and TG

To verify the feasibility and efficiency of nSC as a gene delivery strategy, we first performed a single subcutaneous injection of 10 μL AAV9-CAG-mCherry virus into the nape of P5 C57BL/6J neonatal mice (Figure 3.1A).

Four to six weeks after injection, once the mice reached adulthood, we conducted systematic histological analysis of mCherry expression in their peripheral and central nervous systems. The results showed abundant and strong mCherry fluorescence in both the DRG and TG, our primary targets (Figure 3.1B, C).

Quantitative analysis further confirmed the high efficiency of the nSC strategy. In lumbar DRG, the average transduction efficiency of mCherry-positive neurons reached 48.99 ± 3.61% (n = 5 mice, 29,531 cells counted in total). In TG, the transduction efficiency was notably high, averaging 55.97 ± 7.29% (n = 4 mice, 2,525 cells counted in total) (Figure 3.1D). These data demonstrate for the first time that nSC is a minimally invasive gene delivery method capable of simultaneously and efficiently transducing sensory neurons in both DRG and TG.

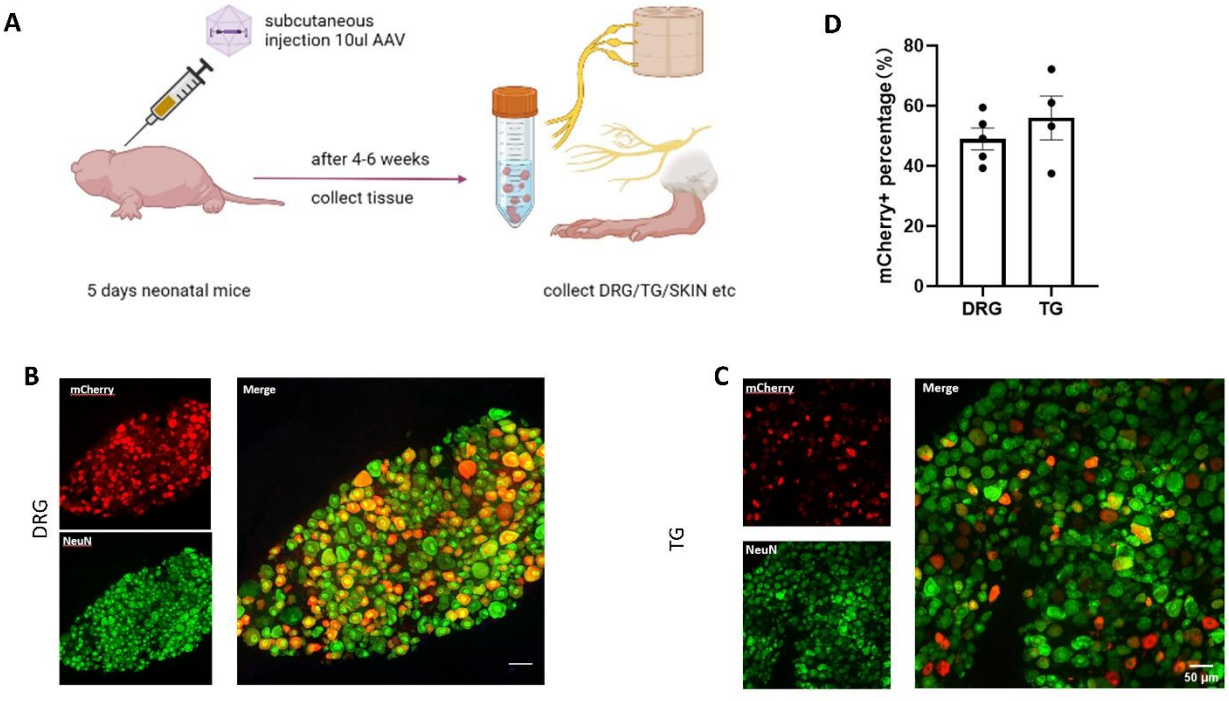

Figure 3.1: AAV9-mCherry effectively transduces DRG &TG neurons via neonatal nape subcutaneous injection *in vivo*

A. Schematic of the experimental design. C57/BL6 mice were nSC injected with AAV9-mCherry. After 6 weeks, samples were taken, and mCherry expression in the peripheral and central nervous system was analysed.
B. Immunohistology was used to identify mCherry expression in the DRG L4 following AAV injection. NeuN – pan neuronal marker.
C. Immunohistology was used to identify mCherry expression in the TG following AAV injection.
D. mCherry was detected in 48.99 ± 3.61% of DRG neurons (n = 5 mice, 29531 cells), and 55.97 ± 7.29% of TG neurons (n = 4 mice, 2525 cells) from C57/BL6 mice

All scale bars = 50 μm. All data mean ± SEM

3.2 The nSC strategy achieves widespread, efficient transduction of sensory ganglia

After confirming the efficient transduction of the nSC strategy in lumbar DRG and TG, we further evaluated its distribution breadth and uniformity across sensory ganglia throughout the body. Through systematic analysis of ganglia at cervical, thoracic, and lumbar/sacral segments, we found that AAV9-mCherry expression covered all neural segments of the body (Figure 3.2A, 3.2B).

Quantitative results indicated that in all detected segments from C2 to L5, neuronal transduction efficiency remained at relatively high levels, ranging from 35% to 64% (Figure 3.2B). Although there was some variation between segments, no obvious decreasing or increasing trend in transduction efficiency along the rostrocaudal axis was observed.

Next, we assessed the targeting specificity of this strategy, particularly its performance in different components of the CNS and PNS. First, we evaluated potential off-target expression of the virus in the spinal cord. In spinal cord cross-sections, we observed dense mCherry-positive fibre terminals in the superficial regions of the dorsal horn (Figure 3.2C). These fluorescence signals represent central axonal projections of successfully transduced DRG sensory neurons, confirming that virally expressed proteins can be normally transported to axonal terminals. Interestingly, despite the strong central projection fibre signals, we observed only a very small number of neuronal cell bodies expressing mCherry in the spinal cord grey matter (Figure 3.2D). Quantitative analysis showed that the proportion of cell bodies expressing mCherry was 0.31 ± 0.09% in dorsal horn neurons. It was a concern that we may inadvertently transduce motor neurons (retrograde) as their axons project into the PNS. However, only 0.28 ± 0.17% of Choline acetyltransferase (ChAT)-positive motor neurons in the ventral horn (Figure 3.2E) were mCherry positive. This observation suggests that the nSC delivery strategy primarily resulted in transduction of peripheral sensory neurons, whilst neuronal cell bodies within the spinal cord were largely not transduced.

We also examined the peripheral terminals of transduced neurons. In hindpaw skin samples, we observed numerous mCherry-positive peripheral nerve endings co-labelled with the pan-neuronal marker PGP9.5. As shown in our representative images, mCherry-positive fibres were present in the epidermis, upper dermis, and around hair follicles and We observed these fibres in both glabrous and hairy skin samples (Figure 3.3A). This finding indicates that transduced neurons, through the nSC strategy, are anatomically intact, and the viral cargo can be expressed and effectively transported anterogradely to neural terminals of innervation targets.

However, while we had focused on the peripheral sensory nervous system, we also wanted to examine other PNS structures, such as the Superior Cervical Ganglion (SCG), a key node of the sympathetic nervous system. We found significant viral transduction and mCherry expression in 43.71 ± 10.81% of neurons in the SCG. (Figure 3.3C). Demonstrating that our approach applies not only to sensory research but also to sympathetic research.

In summary, these data collectively depict the expression profile of the nSC strategy. This method can broadly and efficiently transduce multiple types of ganglia in the peripheral nervous system, including DRG and TG of the sensory system, as well as SCG of the sympathetic nervous system. Virally expressed proteins can be effectively transported to neural projection terminals located both centrally and peripherally. Meanwhile, neuronal cell bodies located in the central spinal cord largely do not express the viral vector cargo.

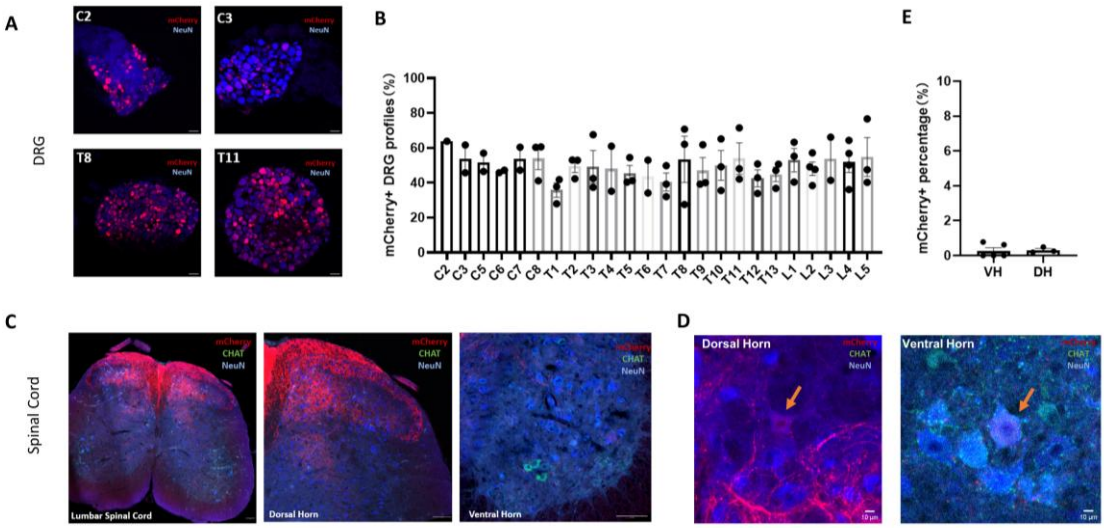

Figure 3.2: Immunolabeling of mCherry in cervical, thoracic, and lumbar levels of DRG and the dorsal horn and ventral horn of the Spinal Cord in C57/BL6 mice after subcutaneous injection *in vivo*

A. Mouse DRG sections at the C2, C3, T8, and T11 levels. mCherry is highly expressed in DRG neurons at different levels. Red: mCherry, Blue: NeuN. scale bars = 50 µm

B. Immunolabeling of mCherry at C2-L5 levels: C2 63.76 ± 0%, C3 53.67 ± 7.96%, C5 51.7 ± 5.23%, C6 46.47 ± 0.71%, C7 53.81 ± 6.59%, C8 53.98 ± 6.42%, T1 35.85 ± 4.13%, T2 49.42 ± 3.55%, T3 49.13 ± 9.31%, T4 48.04 ± 12.94%, T5 45.34 ± 4.57%, T6 43.56 ± 9.43%, T7 40.35 ± 5.17%, T8 53.42 ± 13.17%, T9 46.98 ± 7.39%, T10 49.91 ± 8.56%, T11 53.85 ± 8.96%, T12 42.51 ± 4.9%, T13 44.83 ± 4.16%, L1 52.94 ± 6.69%, L2 48.05 ± 3.84%, L3 53.74 ± 12.36%, L4 51.83 ± 5.98%, L5 54.77 ± 11.14%. (n = 5 mice, 29531 cells). All data mean ± SEM

C. mCherry-positive primary afferent terminals are visualised predominantly in the dorsal column, with projections extending into the dorsal horn region of the lumbar spinal cord. Red: mCherry, blue: NeuN, green: ChAT. Scale bar = 100 µm.

D. Higher magnification of spinal cord dorsal horn and ventral horn regions. Very few mCherry-positive cells can be seen, indicated by the orange squares. Red: mCherry, blue: NeuN, green: ChAT. scale bar = 10 µm

E. mCherry was detected 0.31 ± 0.09% in the dorsal horn (DH) sensory neurons of the spinal cord (n = 3, 3515 cells) and 0.28% ± 0.17% in the motor neurons of the ventral horn (VH) motor neurons of the spinal cord (n = 5, 360 cells).

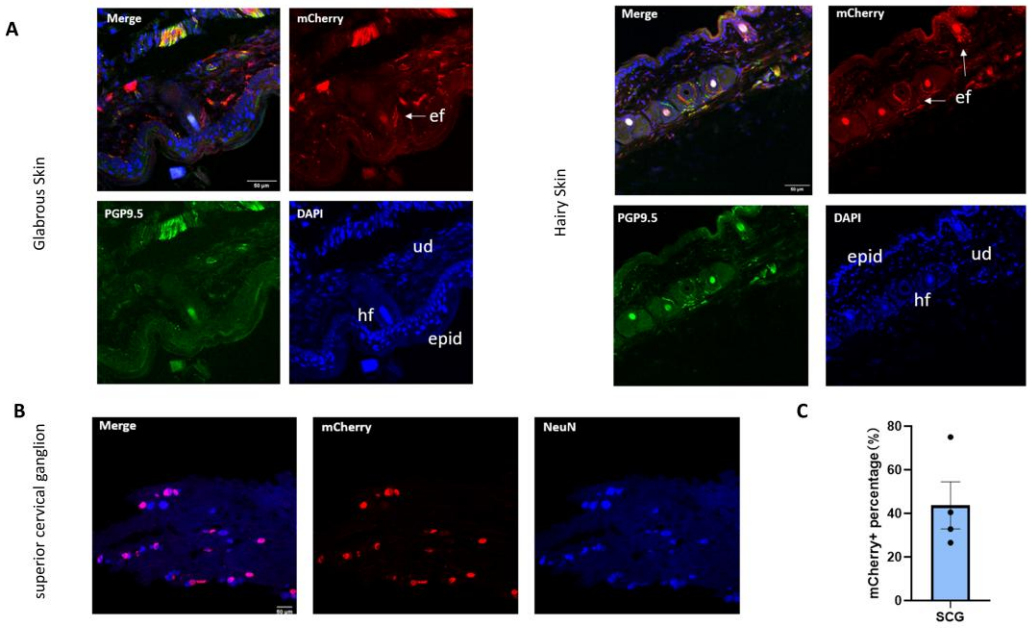

Figure 3.3: Immunolabeling of mCherry in PGP9.5-positive fibres of the hind paw skin and superior cervical ganglion in C57/BL6 mice after subcutaneous injection *in vivo*

A. mCherry expression in primary cutaneous afferents. Left- glabrous skin, Right- hairy skin. Red: mCherry, Blue: DAPI, Green: PGP9.5. epid, Epidermis; ud, upper dermis; hf, hair follicle; ef, epidermal fibres. scale bars = 50 μm.
B. mCherry expression in superior cervical ganglion (SCG) Red: mCherry, Blue: NeuN. scale bars = 50 μm Scale bar = 50 μm
C. mCherry was detected 43.71 ± 10.81% in the superior cervical ganglion (n = 4, 1020 cells).
D. All data mean ± SEM

3.3 Using the nSC AAV strategy to express the PSAM4-GlyR Chemogenetic System

After verifying that the nSC strategy could efficiently transduce AAV into DRG and TG neurons, we further explored its application to delivering more complex proteins that may offer gene therapeutic potential. Considering that GluCl is a non-human protein that might induce immune responses or other side effects during long-term expression, we opted to test a fully humanised chemogenetic system instead, which offers tremendous translational potential for reversible regulation of neuronal activity. I will review and introduce the PSAM/PSEM system in great detail in the next chapter. But briefly, PSAM4-GlyR is a potent chemogenetic system, formed of an engineered α7 nicotinic acetylcholine receptor ligand binding domain (LBD), and a Glycine receptor pore domain (PD). Mechanistically, PSAM4-GlyR is similar to GluCl in that it can be activated by highly selective agonists (Varenicline and uPSEM792) that lead to potent yet reversible neuronal inhibition (Figure 3.4A).

To visualise PSAM4-GlyR, our viral construct contained an mCherry reporter protein via a tandem linker sequence, termed mCherry-T-PSAM4-GlyR. Six weeks following nSC injection of AAV9-mCherry-T-PSAM4-GlyR, we observed strong mCherry expression in lumbar DRG neurons (Figure 3.4B). Similarly, we observed high levels of mCherry expression in TG neurons (Figure 3.4C and D). Immunohistochemical analysis showed that TG neurons expressing PSAM⁴-GlyR included both IB4-positive (non-peptidergic) and CGRP-positive (peptidergic) sensory neuron subgroups. Although a vehicle-only injection control was not imaged in parallel in this dataset to definitively rule out tissue autofluorescence, signal specificity was assessed based on cellular morphology. The distinct structural appearance of mCherry-positive neurons strongly suggests specific viral transduction rather than broad background signal. This result demonstrates that neonatal subcutaneous injection can deliver not only simple reporter genes (such as mCherry) to sensory ganglia but also effectively deliver functional chemogenetic tools (such as PSAM⁴-GlyR), covering different subtypes of sensory neurons.

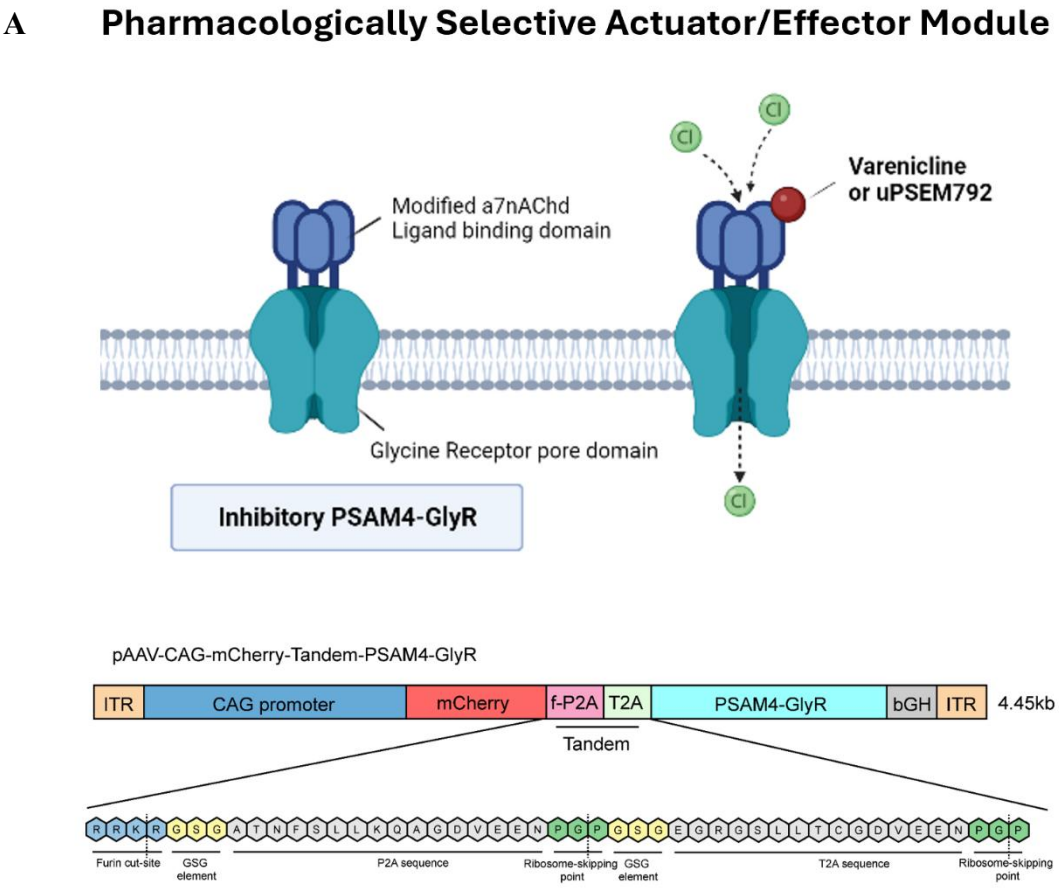

B

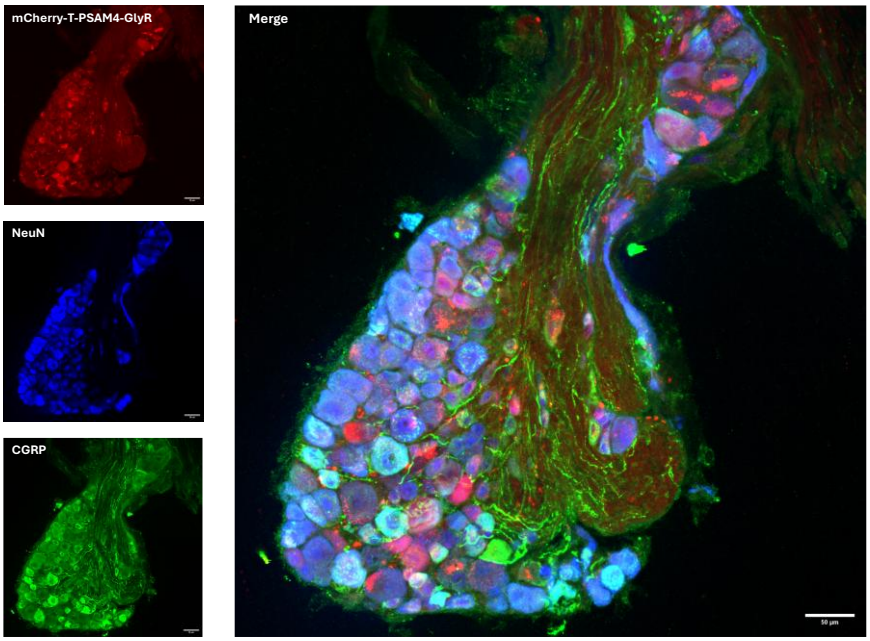
mCherry-T-PSAM4-GlyR
NeuN
CGRP
Merge

C

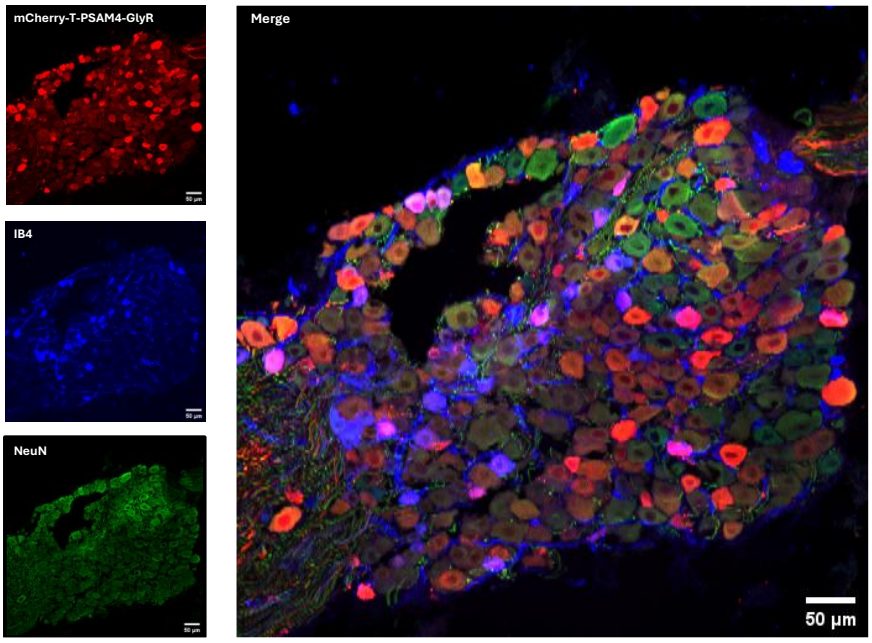
mCherry-T-PSAM4-GlyR
IB4
NeuN
Merge
50 µm

D

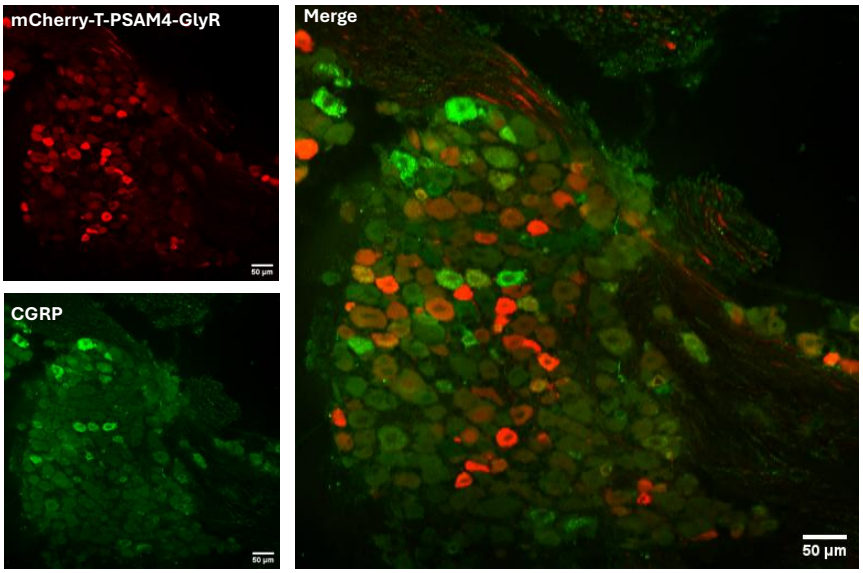
mCherry-T-PSAM4-GlyR
CGRP
Merge
50 µm

Figure 3.4: AAV9-mCherry-PSAM4-GlyR effectively transduces DRG &TG subpopulation neurons via neonatal subcutaneous injection *in vivo*

A. Schematic diagram of the PSAM/PSEM chemogenetic system and viral vector design. Top: Inhibitory PSAMs are formed by a mutant α7 nAChR ligand-binding domain with the anion-selective channel Glycine Receptor pore domain. The binding of PSEMs (Varenicline or uPSEM792) to inhibitory PSAMs results in chloride influx and inhibition of neuronal activity. Bottom: Schematic representation of the pAAV-CAG-mCherry-Tandem-PSAM4-GlyR viral vector construct. The expanded view details the amino acid sequence of the tandem cleavage elements (Furin cut-site, P2A, and T2A) linking mCherry and PSAM4-GlyR.

B. AAV9-mCherry-PSAM4-GlyR expression in DRG subpopulation via subcutaneous injection in vivo. Red: mCherry, Blue: NeuN, Green: CGRP.

C. AAV9-mCherry-PSAM4-GlyR expression in TG subpopulation via subcutaneous injection in vivo. Red: mCherry, Blue: IB4, Green: NeuN.

D. AAV9-mCherry-PSAM4-GlyR expression in TG subpopulation via subcutaneous injection in vivo. Red: mCherry, Green: CGRP.

Scale bars = 50 μm.

4. Discussion

This study proposes and validates a new gene delivery method, namely the nSC strategy. Through a single, minimally invasive AAV9 injection in P5 mice, we have for the first time achieved widespread and efficient gene transduction across the entire peripheral sensory system, including DRG at almost all segments and the traditionally difficult-to-access TG. We confirmed that this platform can stably carry and express the structurally complex chemogenetic tool PSAM^4-GlyR.

Notably, these transduction efficiencies not only reached levels close to or exceeding 50% in both major sensory ganglia, but also significantly outperformed various traditional methods reported in the literature, such as intravenous injection or direct intraganglionic injection in adult mice (efficiency typically between 10-30%), and overcame the limitations of traditional injection methods that are nearly ineffective for TG and have high variability in DRG. This efficient and uniform transduction pattern across all sensory ganglia represents a significant advantage of the nSC strategy. It greatly simplifies the experimental procedure by enabling researchers to simultaneously label or functionally manipulate sensory neurons distributed throughout the body, which innervate different target organs, with just a single simple subcutaneous injection.

The selection of the P5 injection time point was a critical component of this success, based on a comprehensive consideration of the neonatal physiological window. At this stage, the mouse's blood-nerve barrier (BNB) is not yet fully mature, and the immune system's ability to clear exogenous viruses is relatively weak, creating favourable conditions for AAV9's systemic distribution and long-term expression. At the same time, compared to earlier (P0-P3) neonatal mice, P5 mice are slightly larger, providing a more

spacious operational window for subcutaneous injection, thereby reducing technical difficulty and potential damage to the animals.

Current gene delivery methods targeting sensory neurons have long faced the irreconcilable contradiction between efficiency, coverage, and invasiveness. Adult-phase methods, whether intrathecal injection or direct intraganglionic injection, have significant defects due to their high invasiveness, strong technical dependence, and limited coverage range (especially ineffective access to TG) (Fischer et al., 2011; O'Donnell et al., 2024; Prabhakar et al., 2021; Rahman et al., 2023). Our nSC strategy circumvents these problems. It replaces complex surgeries with a simple, standardisable subcutaneous injection, not only minimising technical barriers and animal stress but also achieving widespread simultaneous coverage of DRG and TG that traditional methods cannot accomplish.

Compared to systemic administration (such as IV or IP) that also utilises the neonatal physiological window, the value of the nSC strategy is even more prominent. Although neonatal IV/IP has been proven to transduce DRG (Foust et al., 2008, 2009; H. Zheng et al., 2010), there has always been a lack of direct quantitative evidence of TG transduction efficiency, leaving bottlenecks in craniofacial sensory research. Our study fills this critical gap. Additionally, from an operational perspective, nSC avoids the high failure rate of venous puncture in neonatal mice and the potential risk of visceral injury from intraperitoneal injection, offering greater safety and reproducibility.

The core advantages of this method can be summarised as the unity of efficiency, simplicity, and cost-effectiveness. First, a single injection can achieve stable, efficient transduction in almost all segments of DRG and TG throughout the body, providing unprecedented convenience for exploring different sensory pathways simultaneously within the same animal. Second, the method is simple to operate and requires no special

equipment, greatly reducing technical barriers and facilitating promotion and standardisation across different laboratories. Finally, by covering the entire body with a single, small-dose injection, it significantly reduces costs associated with expensive viral vectors and experimental animals, and it implements the "3R" principles of animal experimentation through rapid, minimally invasive operations (Russell, 2005; Tannenbaum & Bennett, 2015).

During the systematic evaluation of the neonatal subcutaneous injection method, we unexpectedly discovered a noteworthy phenomenon: the mCherry-positive rate in the SCG was also relatively high, reaching 43.71 ± 10.81%. SCG is the largest of the three cervical ganglia and a key component of the sympathetic nervous system. It is located deep in the neck and is the uppermost ganglion of the cervical sympathetic chain. The SCG is an important part of the autonomic nervous system, innervating structures particularly in the head and neck. These include sympathetic innervation of numerous organs, glands, and the carotid arterial system. Functions include pupil dilation, salivary gland secretion, and carotid blood flow regulation (Maningat & Munakomi, 2023; Purves et al., 2018).

This high expression is an important potential issue that could interfere with normal sympathetic nerve function in animals, especially when delivering chemogenetic tools. For example, if inhibitory PSAM^4-GlyR is expressed in SCG neurons, it might inhibit the activity of these neurons in the presence of activators. This could lead to autonomic nervous system symptoms such as pupil constriction and changes in blood flow, thereby interfering with the interpretation of experimental results. However, direct evidence of this is currently lacking. In addition, research has identified a relationship between the sympathetic and sensory nervous systems, which can regulate sensory function, even in chronic pain states (McLachlan et al., 1993; Pertovaara, 2006). Untangling the

investigation of these two systems using our method might be challenging. However, one way to overcome this is by combining the Cre/LoxP recombinase system and nSC injections. For example, using Cre-dependent viral vectors in the Nav1.8-Cre mouse line would restrict transgene expression to Nav1.8+ sensory neurons, which are largely nociceptors. Since sympathetic neurons in SCG do not express Nav1.8, this method would achieve a more precise expression profile.

Besides the high expression in SCG, this method has other potential limitations. The 4-6 week waiting period from neonatal injection to functional analysis in adulthood limits the application of this method in acute experimental models requiring rapid intervention. Also, our understanding of the mechanism behind the nSC strategy's efficiency remains unclear, as it lacks direct pharmacokinetic/pharmacodynamic evidence and requires further systematic verification through future experiments.

In summary, the strategy of neonatal P5 nape subcutaneous injection of AAV represents a new paradigm for gene delivery in sensory nervous system research that combines efficiency, low invasiveness, and universality. It cleverly utilises the biological characteristics of neonatal animals, providing a concise and practical solution to the long-standing challenge of simultaneously targeting DRG and TG. This study not only paves the way for chemogenetics but also for future broader applications of tools such as gene editing and optogenetics across the entire peripheral sensory nervous system. These results demonstrate that neonatal subcutaneous injection is a feasible method for delivering chemogenetic tools such as PSAM^4-GlyR. In particular, the successful transduction of the TG, which is so difficult to target, is pivotal and lays the foundation for subsequent in vivo studies of peripheral afferent nerve function in oral-facial sensation and disorders such as migraine and trigeminal neuralgia.

5. Acknowledgements

I would like to thank Dr Steve Middleton for his guidance and initial injections and tissue acquisition. I was responsible for all subsequent histological processing, immunofluorescence staining, image acquisition, and data analysis work.

6. Appendices

Table 3.1: Summary of AAV Delivery Methods for DRG and TG

Delivery Route	Target Ganglion (s)	Advantages	Disadvantages	Typical Transduction Efficiency (Rodents)	Ref
Intrathecal (i.t.)	DRG	Broad. Relatively less invasive than direct surgery. Translational relevance Dose sparing	Highly variable. Risk of off-target transduction in the spinal cord. Post-Dural Puncture Headache Vector Dilution	10–80% in DRG	Rahman et al., 2023; Schuster et al., 2014; Vulchanova et al., 2010
Direct Intraganglionic	DRG, TG	The highest specificity confines expression to the targeted ganglion. Avoids CNS off-target effects.	Highly invasive and technically demanding. High risk of nerve damage and animal mortality Induces Inflammation Poor Scalability	DRG: ~294 neurons/ganglion	Fischer et al., 2011; O'Donnell et al., 2024; Whitehead et al., 2003

Delivery Route	Target Ganglion (s)	Advantages	Disadvantages	Typical Transduction Efficiency (Rodents)	Ref
Intraneural / Perineural	DRG	Targets specific DRG populations innervating a particular nerve.	Technically difficult Slow Transport Time Competition for Transport Machinery	Not specified in text, but the effectiveness for sensory neurons is limited.	Boulis et al., 2003; Hadzic et al., 2004
Peripheral Retrograde	DRG, TG	Minimally invasive (e.g., injection into skin, muscle).Targets neurons based on their innervation field.	Generally low and non-uniform efficiency.Highly dependent on AAV serotype, dose, and time post-injection.Coverage can be inconsistent and biased to the injection side.	DRG (muscle): Uneven distribution. TG (whisker pad): Up to 25% with high-dose AAV1.	Dang et al., 2017; H. Zheng et al., 2010
Systemic (i.v.) (Adult)	DRG, TG	Theoretically provides body-wide access. Procedurally Simple	Very low efficiency in adults due to the blood-nerve barrier (BNB). High sequestration by the liver and other organs. Requires very large vector doses for minimal effect. Dose-Dependent Toxicity	DRG: <10% TG: Negligible	Schuster et al., 2014
Infraorbital	TG	Less invasive than direct craniotomy for TG access.	Difficult to achieve comprehensive coverage of the entire ganglion.	Not specified quantitatively, but demonstrated to	Neubert et al., 2005

Delivery Route	Target Ganglion (s)	Advantages	Disadvantages	Typical Transduction Efficiency (Rodents)	Ref
			Risk of damage to orbital and vascular structures.	be a viable route.	
Neonatal Systemic (i.p. / i.v.)	DRG	High transduction efficiency by exploiting the immature BNB.	High failure rate (i.v.) or risk of organ injury (i.p.) in neonates Limited to a narrow neonatal window.	DRG: 70–80%	Foust et al., 2008; Machida et al., 2013; H. Zheng et al., 2010
Neonatal Subcutaneous (nSC)	DRG, TG, SCG	Minimally invasive, simple, and standardisable. Achieves widespread, simultaneous, and high-efficiency transduction of both DRG and TG. Safer than neonatal i.v. or i.p. injections. High Animal Welfare Potential for Broad PNS Targeting	Requires a 4-6 week waiting period for expression.Significant off-target transduction in the sympathetic system (e.g., SCG). Potential Developmental Effects	DRG: ~49% TG: ~56% SCG: ~44%	This Study

Chapter IV Using a humanised chemogenetic tool to silence the trigeminal ganglion (TG) and Dorsal Root Ganglion (DRG) in vitro and in vivo

Abstract

In Chapter 2, we successfully established a theoretical and experimental framework for analgesia using the inhibitory chloride channel, GluCl.CreON, systematically validating the feasibility of inducing analgesia by functionally silencing peripheral neurones via chloride influx. Subsequently, in Chapter 3, we developed and optimised a neonatal subcutaneous (nSC) viral delivery strategy, effectively overcoming the bottleneck of achieving synchronous, widespread, and long-term stable expression in the Dorsal Root Ganglia (DRG) and Trigeminal Ganglia (TG).

Building upon this foundation, the subsequent chapters employ the fully humanised PSAM4-GlyR as a core tool for systematic validation, from *in vitro* function to *in vivo* behaviour, within the DRG and TG. This chapter aims to determine whether PSAM4-GlyR, delivered via the nSC strategy, can be efficiently expressed and function within the sensory nervous system. It also seeks to evaluate its efficacy across different sensory pathways and disease models, focusing on mechanical allodynia, orofacial pain, and nitroglycerin (NTG)-induced sensitisation.

1. Introduction

The trigeminal ganglion (TG) serves as the critical gateway for orofacial sensation, housing the primary sensory neurones that relay mechanical, thermal, and chemical signals from the head and face to the trigeminal nucleus caudalis (TNC) within the brainstem (Fried et al., 2001; Messlinger & Russo, 2019). A substantial body of clinical and preclinical evidence indicates that aberrant neuronal excitability within the TG is a core driver in the pathophysiology of numerous pain disorders, including migraine, trigeminal neuralgia, and post-traumatic neuropathic pain (Bendtsen et al., 2020; Goadsby et al., 2017; Rappaport & Devor, 1994; Salter, 2014). This peripheral sensitisation, characterised by lowered neuronal firing thresholds, enhanced release of vasoactive neuropeptides such as calcitonin gene-related peptide (CGRP), and a pro-inflammatory microenvironment involving satellite glial and immune cells, collectively drives central amplification, manifesting as TNC activation and tactile-evoked mechanical allodynia (Gangadharan & Kuner, 2013; Goadsby et al., 2017; Iwata et al., 2017; Latremoliere & Woolf, 2009; Messlinger & Russo, 2019).

The core mechanism of many clinically effective therapies can be interpreted as reducing the signal gain of the trigeminal pathway (Woolf & Salter, 2000). For instance, first-line treatments for trigeminal neuralgia, such as the anticonvulsant carbamazepine, are associated with dizziness, sedation, and potential liver toxicity (Di Stefano et al., 2018), while surgical microvascular decompression carries inherent risks of invasive procedures and potential sensory loss. Similarly, for migraine, triptans and gepants acutely inhibit neuropeptide release from trigeminal terminals, whilst prophylactic anti-CGRP monoclonal antibodies produce a long-term downregulation of the peripheral CGRP axis. However, these regimens are often constrained by variable inter-individual efficacy,

central side-effects, wearing-off effects, and potential cardiovascular risks (Edvinsson, Haanes, et al., 2018; Gambeta et al., 2020; Goadsby et al., 2017). This highlights the need for a more targeted strategy: to downregulate the input gain of primary trigeminal afferents directly at the peripheral source in a reversible and programmable manner.

Chemogenetics provides an elegant solution, enabling the reversible and cell-type-specific control of neuronal activity through engineered receptors activated by dedicated small-molecule ligands (Atasoy & Sternson, 2018; Roth, 2016). Chemogenetic tools are broadly divided into two classes: metabotropic tools, such as DREADDs (Designer Receptors Exclusively Activated by Designer Drugs), which are based on G-protein coupled receptors (GPCRs) and modulate neuronal function indirectly via second messenger cascades; and ionotropic tools, based on ligand-gated ion channels (LGICs), which elicit rapid electrophysiological effects by directly altering membrane ion conductance (Atasoy & Sternson, 2018; Magnus et al., 2011).

While GPCR-based tools like DREADDs are widely used, their utility for silencing sensory neurones is hampered by several documented limitations. Beyond their reliance on indirect second messenger cascades, they have shown insufficient efficacy in some contexts, such as in mouse DRG neurones, due to a lack of key downstream effectors like G-protein-gated inwardly rectifying potassium channels (GIRKs). Furthermore, concerns exist regarding ligand off-target effects and metabolic conversion (Gomez et al., 2017; MacLaren et al., 2016; Nockemann et al., 2013). In contrast, ionotropic chemogenetic tools offer a more direct and robust approach. By directly altering membrane ion conductance, they bypass these complex intracellular networks, providing faster response kinetics, clearer mechanistic interpretability, and greater predictability. This makes them particularly well-suited for modulating the rapid signalling of sensory pathways (Atasoy & Sternson, 2018; Perez-Sanchez et al., 2023).

Among these ionotropic tools, we selected the PSAM⁴-GlyR/PSEM system, a fully humanised inhibitory chloride channel notable for its modular design and translational potential (Magnus et al., 2011, 2019). The system's actuator module (PSAM⁴, a Pharmacologically Selective Actuator Module) is engineered from the human α7 nicotinic receptor ligand-binding domain to be insensitive to endogenous ligands but potently activated by specific Pharmacologically Selective Effector Molecules (PSEMs). These include the FDA-approved drug varenicline and the ultra-potent ligand uPSEM792. For our inhibitory purpose, this PSAM⁴ module is fused to the chloride-permeable ion pore from the human glycine receptor (GlyR).

Critically, the effectiveness of PSAM⁴-GlyR in sensory neurones is amplified by their unique intracellular ionic environment. Both TG and dorsal root ganglia (DRG) neurones maintain a high intracellular chloride concentration due to high expression of the chloride importer NKCC1 and low expression of the exporter KCC2 (Rivera et al., 1999; Sung et al., 2000). This results in a relatively depolarised reversal potential for chloride (ECl). Consequently, activation of the PSAM⁴-GlyR chloride channel creates a powerful shunting inhibition. While this may cause a slight membrane depolarisation, the dominant effect is a massive increase in chloride conductance, which clamps the membrane potential, drastically increasing the threshold for action potential firing and thereby producing potent functional silencing—a phenomenon ideal for suppressing neuronal hyperexcitability (Prescott et al., 2006; Price et al., 2009).

The principle of silencing peripheral sensory ganglia for analgesia is well-established. Previous work has shown that chemogenetic inhibition of TG neurones using a Gi-coupled DREADD can attenuate facial hypersensitivity (Korczeniewska et al., 2022). Furthermore, our own laboratory has previously validated the potent analgesic effects of PSAM⁴-GlyR in DRG neurons and human induced pluripotent stem cell (hiPSC)-derived

sensory neurons in different disease models (Perez-Sanchez et al., 2023). However, the application of this more advanced, translationally relevant ionotropic system to the TG, a key hub for headache and craniofacial pain, remains unexplored. A major barrier has been the technical challenge of achieving efficient and widespread gene delivery to the TG, due to its deep and protected anatomical location. Our study overcomes this long-standing hurdle by employing a recently developed neonatal subcutaneous (nSC) AAV delivery method, which enables robust and widespread transgene expression throughout the TG (as detailed in Chapter 3), thus providing the first opportunity to interrogate the TG using the PSAM/PSEM system functionally.

To test our strategy in a clinically relevant context, we employed a chronic migraine model induced by repeated nitroglycerin (NTG) administration. This model reliably recapitulates key features of migraine pathophysiology, including TG neuronal activation, CGRP release, and central sensitisation, making it ideal for testing our hypothesis that peripheral TG inhibition can attenuate centrally mediated pain behaviours (Goadsby et al., 2017; Pradhan et al., 2014). To comprehensively assess facial pain sensitivity, this study employs both conventional von Frey filament testing for mechanical thresholds and the Orofacial Pain Score (OFPS). The OFPS, by quantifying defensive behaviours (e.g., grooming, avoidance) in response to non-noxious facial touch, sensitively captures mild-to-moderate allodynia, serving as a valuable complement to von Frey thresholds (Farkas et al., 2016).

Therefore, this study aims to address two core scientific questions. Firstly, can the PSAM/PSEM chemogenetic tool replicate and extend the paradigm of specific, reversible, and potent peripheral analgesia, previously observed in the DRG, to now include the TG? Secondly, does this strategy retain its efficacy in a migraine-like pathological context? We anticipate that this work will not only expand the methodological boundaries for

chemogenetics in the peripheral trigeminal pathway but also provide a robust preclinical evidence base and a clear translational rationale for precision interventions targeting craniofacial pain and migraine.

2. Materials and Methods

2.1 Animals

This study used C57BL/6J wild-type mice. Neonatal pups at postnatal day 5-7 (P5-P7) were used for viral injections. Adult mice were used for behavioural experiments and for preparing primary neuron cultures for *in vitro* transfection. All animal procedures were conducted in compliance with the UK Home Office (Scientific Procedures) Act (1986) under a UK Home Office Project Licence. The work adhered to the University of Oxford's policy on the use of animals in scientific research and the ARRIVE guidelines 2.0 (Percie Du Sert et al., 2020). Mice were housed in group-ventilated cages within a pathogen-free facility, with ad libitum access to food and water, under a 12-hour light/dark cycle in a temperature and humidity-controlled environment. Experiments were conducted on both male and female mice, and experimenters were blinded to the viral vector or treatment group until the completion of data analysis.

2.2 Viral and Plasmid Vectors

Viral Vectors: For *in vivo* and *in vitro* experiments, AAV vectors were commercially packaged and purified by the Viral Vector Facility (VVF), ETH Zurich. The study utilised AAV9-CAG-mCherry-T-PSAM4-GlyR (1.2×10^{13} vg/mL) and the control vector AAV9-CAG-mCherry (3.1×10^{13} vg/mL).

Plasmid Vectors: For *in vitro* electroporation, the pAAV-CAG-mCherry-T-PSAM plasmid and the control pAAV-mCherry plasmid were purified from bacterial cultures

using a Maxiprep Kit (Qiagen). Purity was confirmed by ensuring an A260/A280 ratio between 1.8 and 2.0 via UV spectrophotometry (NanoDrop).

2.3 Neonatal Subcutaneous (nSC) AAV Injection

On P5-P7, neonatal pups were removed from their home cage. A single 10 µL subcutaneous injection of the AAV vector was administered at the nape of the neck using a syringe. To prevent maternal rejection, bedding from the home cage was gently rubbed on the pup to reapply litter-specific scents before it was immediately returned to the cage. Mice were allowed a minimum of 6 weeks for viral expression before subsequent experiments.

2.4 Primary Neuron Culture

Adult mice were euthanised by a Schedule 1 method. Bilateral trigeminal ganglia or lumbar (L3-L5) dorsal root ganglia were dissected and placed in ice-cold HBSS. For TG, ganglia were first digested in papain (20 U/mL) for 30 minutes at 37°C, followed by a 30-minute incubation in a solution of collagenase (1 mg/mL) and Dispase II (2 mg/mL). For DRG, ganglia were digested in a solution of collagenase (1 mg/mL) and Dispase II (2 mg/mL) for 60-90 minutes at 37°C. Following digestion, a single-cell suspension was created by gentle mechanical trituration and passed through a 40 µm cell strainer. Neurons were immediately plated on glass-bottom dishes pre-coated with poly-D-lysine (0.1 mg/mL) and laminin (10 µg/mL) and cultured at 37°C in a 5% CO_2 incubator.

2.5 Electroporation

Following enzymatic digestion and filtration, the single-cell suspension was centrifuged at 300 g for 5 minutes. The supernatant was discarded, and the cell pellet was washed once with sterile PBS to remove residual enzymes. After a second centrifugation, the pellet was resuspended in Resuspension Buffer R (part of the Neon® Transfection System

kit). For transfection, the appropriate volume of plasmid DNA (1-2 µg per 10^6 cells) was mixed with the cell suspension in a microcentrifuge tube. Using a 100 µL Neon® tip, the cell/DNA mixture was carefully aspirated, avoiding bubbles. The electroporation was performed using the Neon® Transfection System (Thermo Fisher Scientific)

Immediately following electroporation, the transfected neurons were expelled from the tip directly into a culture dish containing pre-warmed culture medium. The cells were then gently plated onto glass-bottom dishes pre-coated with poly-D-lysine (0.1 mg/mL) and laminin (10 µg/mL) and transferred to a 37°C, 5% CO_2 incubator for subsequent experiments

2.6 Calcium Imaging

Cultured TG and DRG neurons were loaded with Fura-2 AM (5 µM, Thermo Fisher Scientific) for 45 minutes at 37°C. Imaging was performed on an inverted microscope system, acquiring fluorescence at 340/380 nm excitation wavelengths at a frequency of 2 Hz.

Inhibition Assay: The protocol began with establishing a stable baseline, followed by a 10-second application of 50 mM KCl to evoke an initial response (Pulse 1). Neurons were then incubated for approximately 15 minutes with either uPSEM792 (10 nM), varenicline (20 nM), or vehicle (ECF). A second KCl pulse (Pulse 2) was delivered in the continued presence of the compound to assess its inhibitory effect. Following Pulse 2, neurons were exposed to lidocaine (10 mM) for 3 minutes, and a subsequent KCl pulse was applied in the presence of lidocaine to serve as an internal positive control for maximal response blockade. Finally, reversibility was assessed with a third KCl pulse (Pulse 3) after an approximately 10-minute washout period with ECF. The ECF contained (in mM): 140 NaCl, 5 KCl, 2 $CaCl_2$, 1 $MgCl_2$, 10 HEPES, and 10 glucose, with pH adjusted to 7.4.

Sensory Agonist Screening: To assess broad sensory inhibition, neurons were continuously perfused with either uPSEM792 (10 nM) or varenicline (20 nM). During this perfusion, cells were sequentially challenged with brief (10-15 second) pulses of menthol (200 μM), ATP (100 μM), capsaicin (1 μM), and finally KCl (50 mM).

In vitro Validation: Following behavioural experiments, trigeminal (TG) or dorsal root ganglia (DRG) neurons were acutely isolated from mice. To confirm the long-term functional effects of the compounds, these neurons were subjected to a modified inhibition assay. Briefly, an initial response to 50 mM KCl (10 s) was recorded (Pulse 1), followed by an approximately 15-minute incubation with uPSEM792 (10 nM). A second KCl pulse was applied in the presence of the compound (Pulse 2), and a third pulse (Pulse 3) was delivered after an approximately 15-minute washout period. The lidocaine control step was omitted here, as functional specificity was rigorously confirmed by comparing responses in PSAM-expressing neurons to those in adjacent, non-expressing neurons (internal negative controls) within the same preparation.

Using ImageJ/Fiji, regions of interest (ROIs) were manually drawn around mCherry-positive (POS) and adjacent mCherry-negative (NEG) cells. The raw 340/380 nm fluorescence ratio data for each ROI were exported. The response magnitude was calculated as the change in fluorescence ratio over baseline ($\Delta F/F_0$), where F_0 is the average ratio during the pre-stimulus baseline period. For inhibition assays, the percentage of inhibition was calculated for each cell using the formula: Inhibition (%) = [1 – (Peak $\Delta F/F_0$ of Pulse 2 / Peak $\Delta F/F_0$ of Pulse 1)] × 100 For the sensory agonist screen, a cell was considered a responder if the agonist-evoked peak $\Delta F/F_0$ exceeded 0.2.

2.7 Behavioural Assessments

Paw Withdrawal Threshold (PWT): A stable baseline 50% paw withdrawal threshold (PWT) was determined using Dixon's up-down method. On the test day, after establishing the baseline, mice received an intraperitoneal (i.p.) injection of either uPSEM792 (3 or 5 mg/kg) or an equivalent volume of saline. The PWT was measured again at 2 hours and 24 hours post-administration.

Orofacial Mechanical Sensitivity: mice were acclimated for 10 minutes in a custom restrainer (Stoelting Co.) that allowed access to the head. Once the animal ceased exploratory behaviour, the periorbital region was stimulated three times on each side with a 0.40 g von Frey filament until it bent. Responses were scored on a scale where 0 indicated no response, 0.25 a mild head shake or forepaw swipe, 0.5 a vigorous head shake or aggression, and 1 indicated complete head withdrawal or facial grimacing. The scores from the three applications per side were summed, and these totals were averaged to produce a final orofacial pain score with a maximum of 3.

NTG-induced Chronic Pain and Intervention: A chronic migraine-like model was induced by intraperitoneal (i.p.) injections of nitroglycerin (NTG, Hameln,10 mg/kg) or saline on days 1, 3, 5, 7, and 9. Orofacial and paw sensitivity and vonfrey were measured 2 hours after each injection. On day 10, mice received an i.p. injection of uPSEM792 (5 mg/kg) to assess its analgesic effect.

2.8 Immunocytochemistry (ICC) and Immunofluorescence Histochemistry (IHC)

TG tissue and L3-L5 DRGs were dissected and fixed in 4% paraformaldehyde (PFA), followed by cryoprotection in 30% sucrose solution overnight. Tissues were embedded in Optimal Cutting Temperature (OCT) compound and sectioned into 12 μm cryosections.

Sections were processed for immunofluorescence staining using the following primary antibodies, including rabbit anti-NeuN (1:500, Abcam, ab177487), sheep anti-CGRP (1:250, Enzo Life Sciences, CA1137), streptavidin-conjugated Isolectin B4 (IB4, 1:50, sigma, L2140), and Tyrosine Hydroxylase (1:500, Millipore, Lot 3705678). The following day, after thorough washing with PBS containing 0.3% Triton X-100, sections were incubated for 2 hours at room temperature under light-protected conditions with appropriate fluorescent secondary antibodies. Fluorophores used for secondary detection included Pacific Blue (1:100), Alexa Fluor 488 (1:500), Alexa Fluor 546 (1:500), and Alexa Fluor 647 (1:500), all from Thermo Fisher Scientific. Finally, after a final wash, sections were mounted using Vectashield mounting medium for analysis.

All fluorescence images were acquired using a Zeiss LSM-710 confocal microscope with 20× objectives and Zeiss Zen 2012 software.

2.9 Statistical Analysis

All data were analysed and graphed using GraphPad Prism 10. Normality was assessed using the D'Agostino & Pearson or the Shapiro-Wilk test.

Behavioural Data Analysis: Data from the von Frey test and the Orofacial Pain Score (OFPS) were analysed using a two-way repeated-measures ANOVA, with treatment (e.g., uPSEM792 vs. vehicle) and time as factors. Bonferroni's post-hoc test was used for multiple comparisons where appropriate. Data are presented as mean ± standard error of the mean (SEM).

Calcium Imaging Data Analysis:

In vitro Inhibition Assays (Electroporation): Due to the relatively low and variable efficiency of electroporation for *in vitro* studies, there was often an imbalance in the

number of PSAM-positive and PSAM-negative neurones on each coverslip. Hence, analysis was performed at the coverslip level. Data from all responding cells on a single coverslip were averaged to represent one biological replicate (n = 1 coverslip). These averaged data were then analysed using one-way or two-way ANOVA followed by Bonferroni's *post-hoc* test. Data are presented as mean ± SEM.

In vitro Validation Assays (AAV Delivery): The high transduction efficiency achieved with neonatal subcutaneous (nSC) AAV delivery resulted in a substantial and more balanced population of PSAM-positive and PSAM-negative neurones within each ganglion preparation. This permitted a more granular analysis at the single-cell level (n = 1 neuron). Data often did not follow a normal distribution in this experiment. Non-parametric tests were employed. Comparisons were made using the Mann-Whitney U test (for two groups) or the Kruskal-Wallis test with Dunn's *post-hoc* test (for multiple groups). These data are presented as swarm plots displaying the median and interquartile ranges.

Proportional Data: The proportion of responding neurons was compared using Fisher's exact test.

All statistical tests were two-sided, and a P-value < 0.05 was considered significant. Significance is denoted as *P < 0.05, **P < 0.01, ***P < 0.001, and ****P < 0.0001.

3. Results

3.1 The PSAM/PSEM system can be effectively expressed in primary trigeminal neurons and specifically inhibits neuronal excitability *in vitro*

To express and validate the function of the PSAM/PSEM chemogenetic system in primary trigeminal ganglion (TG) neurons *in vitro*, we first established the experimental workflow shown in Figure 4.1A. We acutely isolated TGs from adult wild-type (WT) mice, prepared a single-cell suspension, and transfected the neurons with either the pAAV-CAG-mCherry-T-PSAM plasmid (experimental group) or the pAAV-mCherry plasmid (control group) via electroporation. Immunofluorescence staining confirmed the successful expression of the PSAM receptor in TG neurons. As shown in Figure 4.1B, PSAM-positive neurons (red) co-expressed the pan-neuronal marker βIII-tubulin (green) and peptidergic neuron marker CGRP (purple), indicating successful transfection.

A

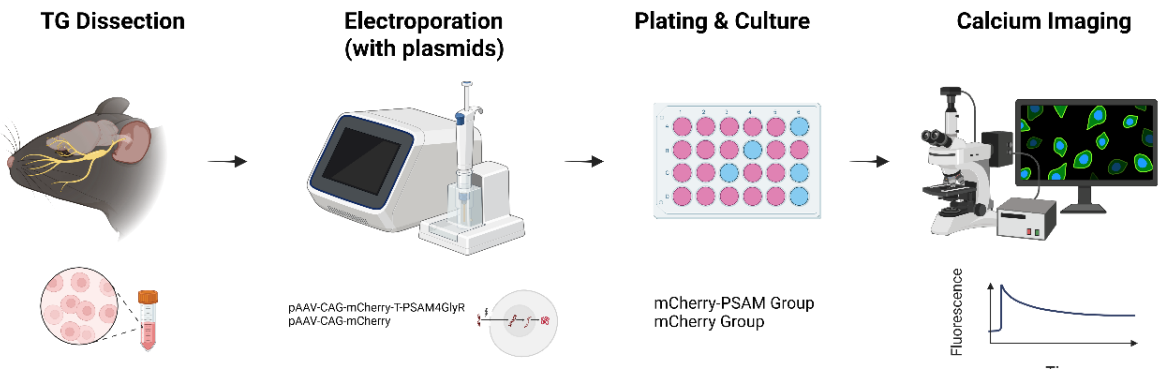

B

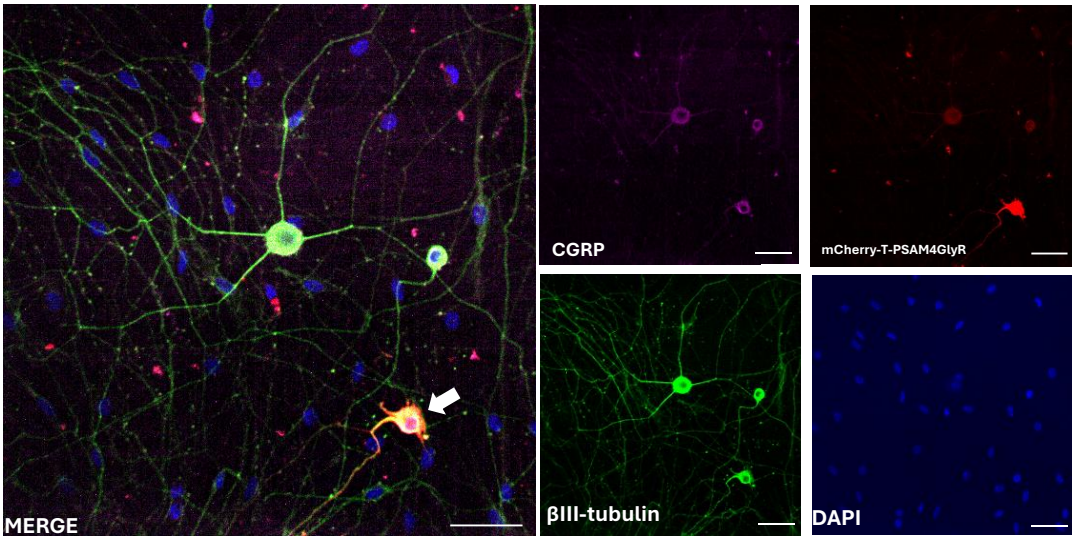

Figure 4.1. Workflow and expression of the PSAM/PSEM chemogenetic system in primary trigeminal ganglion neurons *in vitro*.

A. Schematic of the *in vitro* experimental workflow. Trigeminal ganglia (TG) were acutely dissociated from adult wild-type (WT) mice and prepared into a single-cell suspension. Neurons were then transfected with either the pAAV-CAG-mCherry-T-PSAM plasmid (experimental group) or the pAAV-mCherry plasmid (control group) via electroporation. Finally, the transfected neurons were plated on coverslips and cultured for subsequent functional experiments, such as calcium imaging.

B. Representative image of the transfected neuronal culture coverslip. The image displays PSAM positive neurons (red), which co-express with βIII-tubulin (green), CGRP (purple) and DAPI (blue). Scale bar: 50 µm.

Next, I assessed the efficacy of the PSAM/PSEM system in inhibiting neuronal excitability, using calcium flux as a proxy for neural activity. As shown in the representative calcium imaging traces in Figure 4.2A, Consecutive applications of potassium chloride (KCl) were used to stimulate the neurons and induce calcium influx. Applying uPSEM792 (10 nM) or varenicline (20 nM) before the second KCl stimulation

resulted in a selective reduction of the calcium peak in PSAM-positive neurons (dark blue, dark purple traces), indicating suppressed neuronal activity. This agonist treatment did not affect the adjacent PSAM-negative neurons (light blue, light purple traces). The inhibitory effect was also reversible. After a washout period, the response in PSAM-positive neurons recovered upon a final KCl stimulus, demonstrating the reversibility of our chemogenetic silencing system. As a positive control, the voltage-gated sodium channel blocker lidocaine (10 mM) was applied between the second and final pulses, suppressing responses in all neurons and establishing a benchmark for maximal inhibition.

During these initial experiments, we observed that raw calcium peak amplitudes (ΔF/F0) were subject to confounding variables. First, a universal response rundown was evident, as even vehicle-treated neurons showed a significant decrease in response amplitude between the first and second KCl pulse (Figure 4.2B, left panel). Second, there were significant differences in baseline excitability (1st KCl peak) between PSAM- and mCherry-expressing control populations (Figure 4.2B, right panel). These factors make direct comparison of raw amplitudes unreliable. Therefore, to isolate the specific pharmacological effect, we normalised the second peak to the first for each cell (Inhibition % = $[1 - Peak_2/Peak_1] \times 100\%$). This normalisation focuses the quantitative analysis on the initial inhibitory effect of the ligand, which is the primary measure of efficacy. While the response recovery after washout qualitatively demonstrates the reversibility of the system (Figure 4.2A), it was not subjected to quantitative analysis due to the confounding influence of the inherent response rundown, which makes it difficult to assess the true extent of recovery accurately.

This normalised analysis confirmed the specificity and efficacy of the system. Both uPSEM792 and varenicline induced significantly greater inhibition in PSAM+ neurons compared to their PSAM- counterparts ($p < 0.001$ and $p < 0.01$, respectively; Figure 4.2C).

The inhibition by uPSEM792 in PSAM+ neurons was also significantly greater than that seen in the vehicle control group ($p < 0.01$). Furthermore, we confirmed that this effect was receptor dependent. uPSEM792 produced profound inhibition in PSAM+ neurons, an effect significantly stronger than in adjacent PSAM- neurons ($p < 0.001$) and vastly greater than in mCherry-expressing control neurons ($p < 0.0001$; Figure 4.2D). No significant difference was observed between mCherry-positive and -negative cells, demonstrating that the inhibitory effect is mediated specifically by the PSAM receptor and not by non-specific consequences of protein overexpression.

A

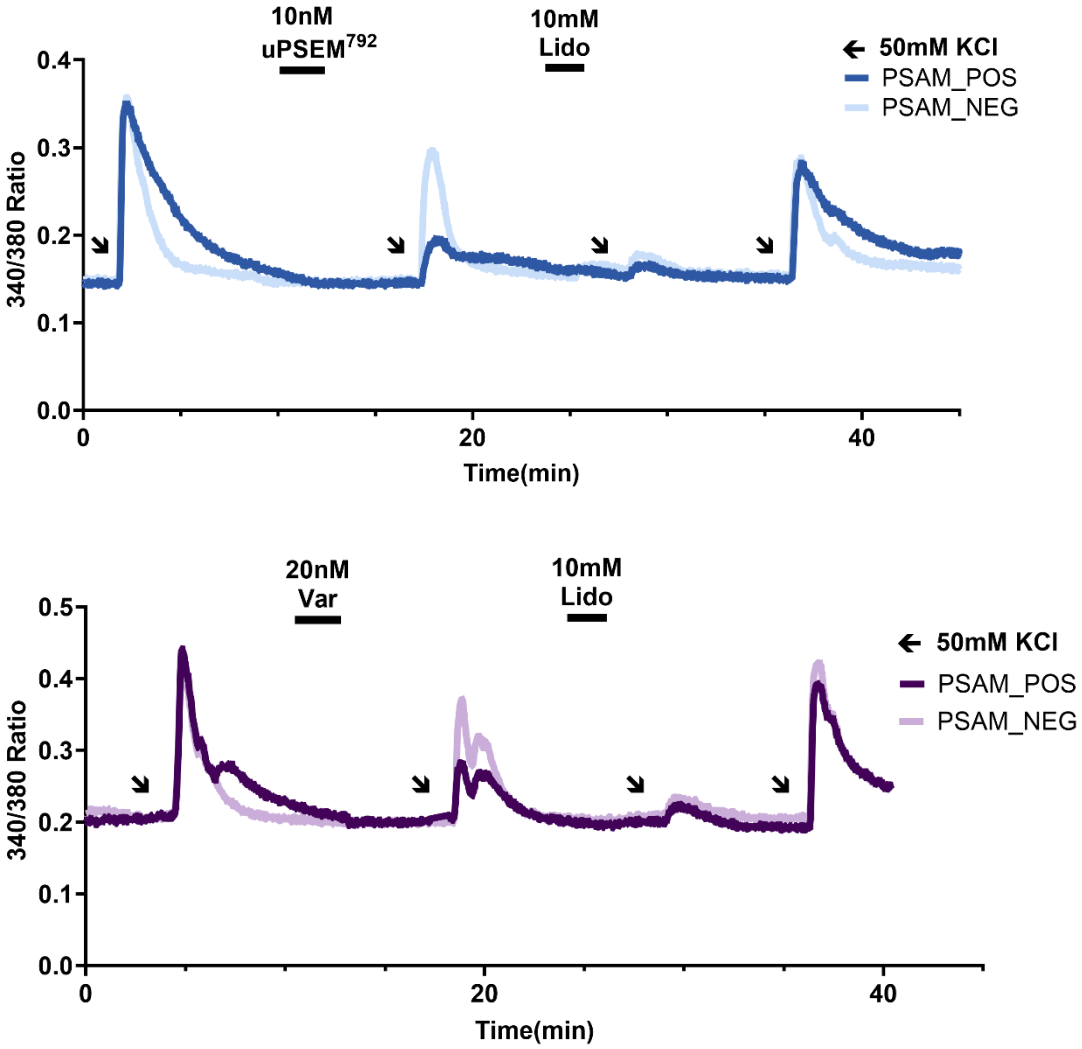
10nM
uPSEM792
10mM
Lido
50mM KCl
PSAM_POS
PSAM_NEG
340/380 Ratio
Time(min)
20nM
Var
10mM
Lido
50mM KCl
PSAM_POS
PSAM_NEG
340/380 Ratio
Time(min)

B

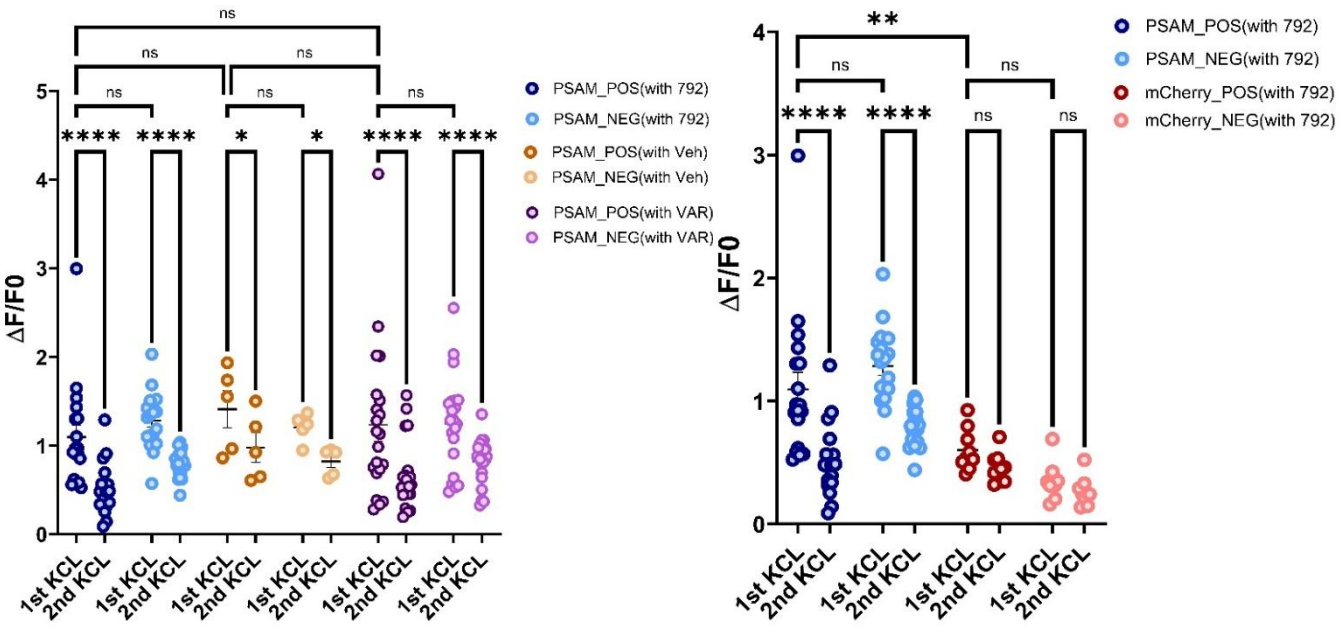
ΔF/F0
PSAM_POS(with 792)
PSAM_NEG(with 792)
PSAM_POS(with Veh)
PSAM_NEG(with Veh)
PSAM_POS(with VAR)
PSAM_NEG(with VAR)
1st KCL
2nd KCL
ΔF/F0
PSAM_POS(with 792)
PSAM_NEG(with 792)
mCherry_POS(with 792)
mCherry_NEG(with 792)

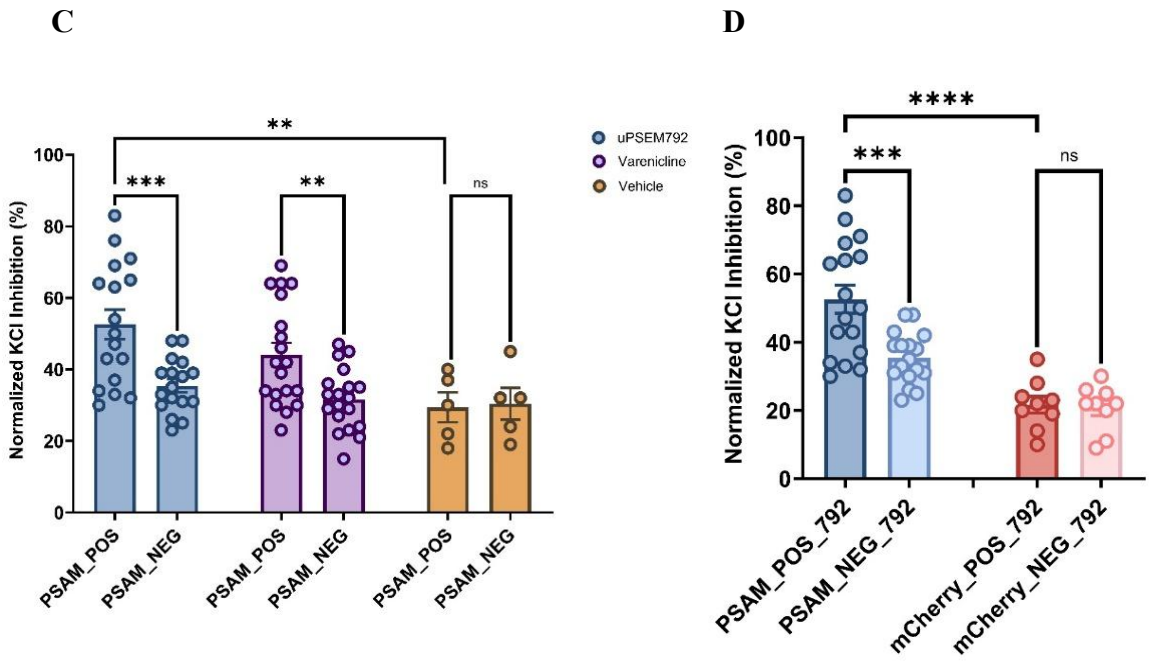

Figure 4.2. The PSAM/PSEM system specifically and effectively inhibits neuronal excitability in TG neurons ***in vitro*****.**

A. Representative traces of *in vitro* calcium imaging demonstrate the inhibitory effects of uPSEM792 and Varenicline. The traces show calcium responses (340/380 ratio) to four consecutive KCl stimulations in PSAM-positive neurons (dark blue, dark purple) and adjacent PSAM-negative neurons (light blue, light purple). The kinetic shape of the traces reflects rapid Calcium influx via voltage-gated calcium channels upon KCl-mediated depolarisation, followed by cytosolic clearance mechanisms. Direct comparison between groups is valid as PSAM-positive and -negative neurons were recorded simultaneously in the same field of view, ensuring identical exposure to solution exchanges.

Application of either uPSEM792 (10 nM) or Varenicline (20 nM) 15 min before the second stimulation selectively suppressed the subsequent calcium peak in PSAM-positive neurons, while having little influence on PSAM-negative neurons. As a positive control, Lidocaine (10 mM) suppressed all neuronal activity. After washout, the calcium response of PSAM-positive neurons recovered, indicating reversibility. Time is expressed in minutes.

B. Quantification of raw calcium peak amplitudes (ΔF/F0) for the first and second KCl stimulations, illustrating the confounding effects that necessitate data normalisation.

Left panel: Compares the effect of uPSEM792 (10 nM), Vehicle, and Varenicline (20 nM) on PSAM-expressing neurons. A significant decrease from the 1st to 2nd KCl peak is observed in all conditions, confirming a universal response rundown. Notably, the magnitude of this decrease is visually more pronounced in the agonist-treated groups (uPSEM792 and Varenicline) compared to the Vehicle control, hinting at a drug effect superimposed on the baseline rundown. Right panel: Compares the effect of uPSEM792 in PSAM-expressing neurons versus mCherry-expressing control neurons. A dramatic and significant drop in amplitude is seen in PSAM-expressing neurons, whereas mCherry-expressing control neurons exhibit only a minimal, non-significant decrease. Critically, this panel also reveals a significant difference in the initial baseline response (1st KCL peak) between the PSAM and mCherry groups. Taken together, these graphs demonstrate that analysing raw amplitude changes is unreliable due to the combined effects of a universal response rundown and significant differences in baseline excitability, thus necessitating data normalisation.

C. Normalised comparison of ligand specificity and efficacy. This graph quantifies the inhibition rate [$(1 - Peak_2/Peak_1) \times 100\%$] following application of Varenicline (20 nM), uPSEM792 (10 nM), or Vehicle. Both uPSEM792 and Varenicline induced significantly higher inhibition in PSAM-positive neurons compared to their negative counterparts (***$p < 0.001$ and **$p < 0.01$, respectively). Furthermore, inhibition in PSAM-positive neurons by uPSEM792 was significantly greater than in the Vehicle group (**$p < 0.01$). Data were derived from n = 19 (Varenicline), n = 17 (uPSEM792), and n = 5 (Vehicle) coverslips, comprising a total of 121 PSAM-positive and 2221 PSAM-negative cells.

D. Validation of receptor-specific inhibition using normalised data. This graph quantifies the inhibition rate in PSAM-transfected versus mCherry-transfected control neurons after application of uPSEM792 (10 nM). The inhibitory effect in PSAM-positive neurons was significantly more potent than in adjacent PSAM-negative neurons (***$p < 0.001$) and profoundly greater than in mCherry-expressing positive neurons (****$p < 0.0001$). No significant difference was observed between mCherry-positive and -negative cells, demonstrating that the inhibition is mediated explicitly by the PSAM receptor and not by non-specific effects of protein overexpression. The PSAM group included data from 17 coverslips (70 positive, 1269 negative cells), and

the mCherry control group included data from 9 coverslips (27 positive, 252 negative cells).

For all quantitative graphs (B-D), data were analysed at the coverslip level, where each dot represents the averaged value from all responding cells on a single coverslip. Data in B and C were analysed by two-way ANOVA, with a post-hoc Bonferroni test. Data in D were analysed by one-way ANOVA, followed by a post-hoc Bonferroni test. Bars indicate mean ± SEM. *$p < 0.05$, **$p < 0.01$, ***$p < 0.001$, ****$p < 0.0001$.

3.2 The PSAM/PSEM System Broadly Suppresses Responses to Diverse Sensory algogens

I next investigated whether the PSAM/PSEM system could suppress neuronal responses to a range of physiologically relevant sensory receptor agonists. I quantified the proportion of neurons responding to ATP (P2X agonist), menthol (TRPM8 agonist), capsaicin (TRPV1 agonist), and KCl while under continuous application of either uPSEM792 or varenicline (Figure 4.3A). In the presence of uPSEM792 (10 nM), the percentage of PSAM+ neurons that responded to ATP and KCl was significantly lower than the percentage of responding PSAM- neurons ($p = 0.017$ and $p = 0.0003$, respectively; Figure 4.3B). A similar pattern was observed with varenicline (20 nM), which also significantly reduced the proportion of PSAM+ neurons responding to ATP ($p = 0.018$) and KCl ($p = 0.011$) (Figure 4.3C). For menthol and capsaicin. However, although an inhibitory trend was observed, the difference in the proportion of responding neurons between positive and negative cells did not reach statistical significance. These results indicate that PSAM activation can significantly dampen excitability driven by general depolarisation (KCl) and purinergic signalling (ATP), while its efficacy against

specific TRP channel agonists (menthol, capsaicin) in this experimental setup was less pronounced.

A

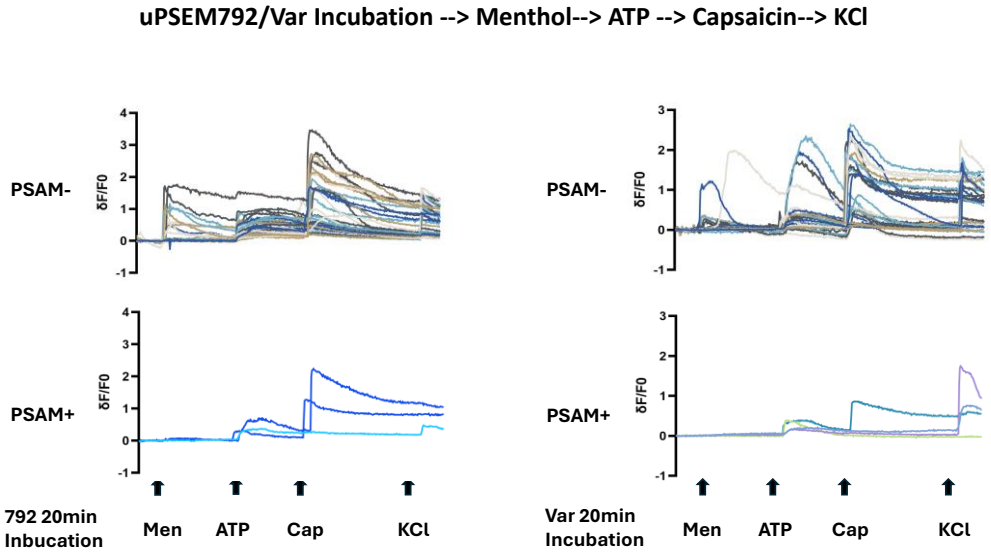

B

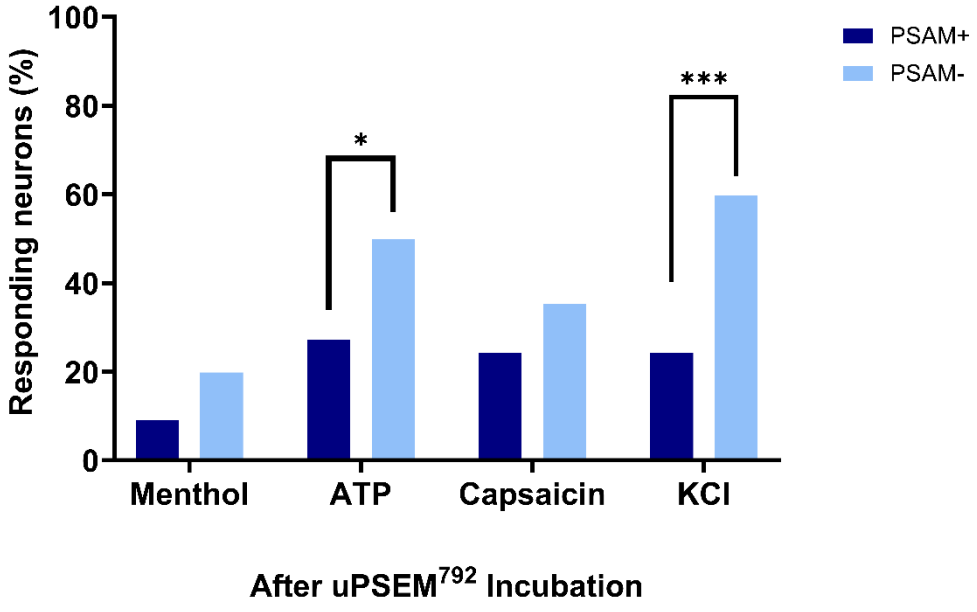

C

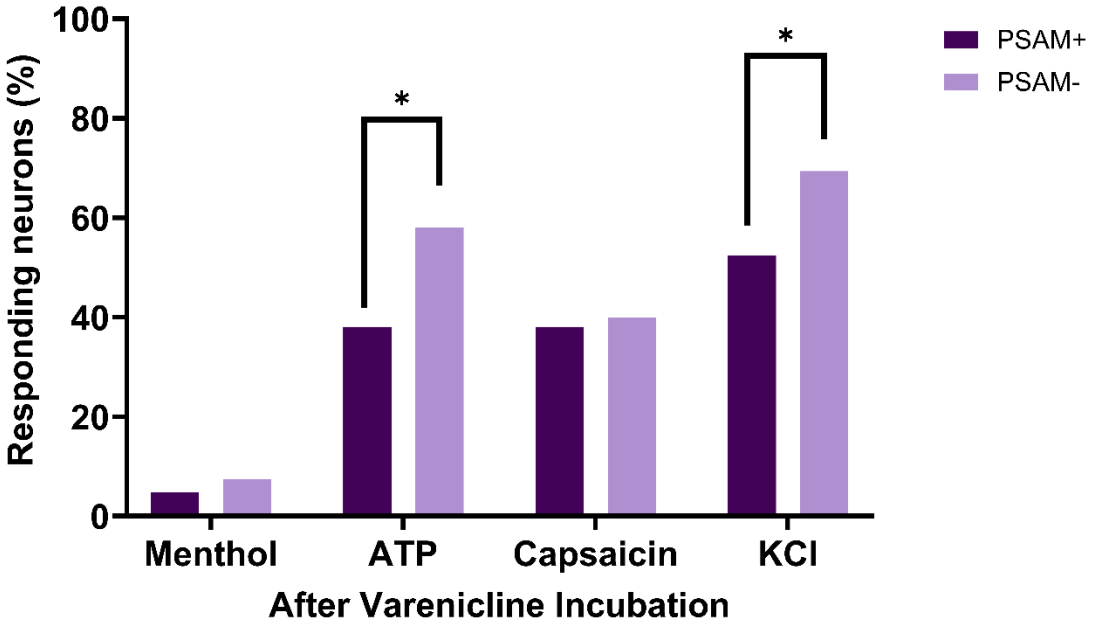

Figure 4.3. PSAM/PSEM system suppresses TG neuron responses to diverse sensory stimuli.

A. **Representative calcium imaging traces.** Prior to testing, the extracellular fluid (ECF) was replaced with either uPSEM792 (10 nM, left) or Varenicline (20 nM, right), followed by a 20-minute incubation in the incubator. The agonists were then applied under the continuous presence of the respective drug.

B. **Quantification of the inhibitory effect of uPSEM792 on the proportion of responding neurons.** This graph quantifies the percentage of PSAM-positive versus PSAM-negative neurons responding to different agonists in the presence of uPSEM792. Compared to PSAM-negative neurons, a significantly lower proportion of PSAM-positive neurons responded to ATP ($p = 0.017$) and KCl ($p = 0.0003$). No significant difference was observed for Menthol ($p = 0.118$) or Capsaicin ($p = 0.125$).

(C) **Quantification of the inhibitory effect of Varenicline on the proportion of responding neurons.** This graph quantifies the percentage of responding PSAM-positive versus PSAM-negative neurons in the presence of Varenicline. A significantly lower proportion of PSAM-positive neurons responded to ATP ($p = 0.018$) and KCl ($p = 0.011$) compared to PSAM-negative neurons. No significant difference was found for Menthol ($p = 0.697$) or Capsaicin ($p = 0.814$).

Proportions of responding neurons shown in (B) and (C) were compared between groups using Fisher's exact test. Contingency tables were constructed using the number of responding vs. non-responding cells in PSAM+ vs. PSAM- groups for each agonist. Significance is denoted on the graphs as: *$p < 0.05$, ***$p < 0.001$.

Data are derived from individual cells pooled from multiple coverslips. uPSEM792 group: n = 33 PSAM+ cells, n = 863 PSAM- cells. Varenicline group: PSAM+ cells, n = 73, PSAM- cells, n = 1565.

3.3 Proof-of-concept: silencing of DRG neurons using systemic AAV-PSAM4-GlyR

Before using PSAM4-GlyR to silence the TG *in vivo*, we first took a proof-of-principle approach to silence the DRG, a system we know is amenable to chemogenetic silencing. To establish our experimental model, we delivered AAV9-mCherry-T-PSAM4-GlyR viral vectors to neonatal mice (P5-P7) via nSC injection (Figure 4.4A). After maturation, we performed a histological examination of their DRG. Representative confocal micrographs demonstrated widespread and stable expression of the reporter gene mCherry in DRG neuronal cell bodies, co-localising with the neuronal marker NeuN (Figure 4.4B), consistent with Chapter 3.

Considering that previous research found nSC delivery might affect sympathetic ganglia (such as the SCG), we first conducted safety assessments on mice that had received viral

injections. The use of two different doses (3 mg/kg and 5 mg/kg) was intentional to evaluate the dose-dependent analgesic effect of uPSEM792. Following intraperitoneal injection of either 3 mg/kg or 5 mg/kg of uPSEM792, we continuously monitored the animals' body temperature, spontaneous activity, and general movement over a 1–6 hour observation period. No observable physiological disturbances or signs of discomfort were detected, indicating good safety within this dosage range.

We next evaluated the mechanical analgesic effect of uPSEM792 using the von Frey test of the hind paws. We observed that a 5 mg/kg dose of uPSEM792 induced a highly significant elevation in mechanical thresholds (compared to baseline and a saline group), two hours post-injection. After a 24-hour washout period, sensory thresholds largely returned to normal. In comparison, whilst the 3 mg/kg dose also produced some level of behavioural silencing compared to the saline group (*$P < 0.05$), its analgesic potency was significantly weaker than that of the 5 mg/kg dose (***$P < 0.001$), demonstrating a clear dose-dependent relationship in our system. Based on these results, which are consistent with our previous experience using PSAM4-GlyR and uPSEM792 to silence DRG sensory behaviours (Perez-Sanchez et al.), we chose 5 mg/kg to be the most appropriate *in vivo* dose for further experiments.

To confirm that our observed behavioural silencing was due to a functional expression of our PSAM/PSEM system, we took an *in vitro* approach to culture DRG from mice treated with AAV-PSAM4-GlyR. We undertook calcium imaging of PSAM transduced neurons and assessed their responses to KCL pre- and post-uPSEM792. Representative raw data curves clearly showed that after the application of uPSEM792, the calcium influx response of neurons expressing the PSAM receptor (PSAM+) to subsequent KCl stimulation was powerfully and selectively inhibited. Importantly, this inhibitory effect exhibited high cellular specificity, as the activity of adjacent neurons not expressing the

PSAM receptor (PSAM−) remained virtually unaffected (Figure 4.4D)**.** Analysis of the initial KCl response again revealed significant inherent variability in baseline excitability between PSAM+ and PSAM- neurons, and between PSAM and mCherry control neurons ($p < 0.0001$; Figure 4. 4E), reinforcing the necessity of data normalisation. The normalised analysis confirmed that the silencing effect was both ligand-specific (uPSEM792 vs. vehicle, $p < 0.0001$) and receptor-specific (PSAM vs. mCherry, $p < 0.01$) (Figure 4.4F). This demonstrates a direct link between the *in vivo* analgesic phenotype and the specific, reversible silencing of PSAM-expressing sensory neurons. All stimulation peaks are provided in the Appendix Figure 4.7.

A

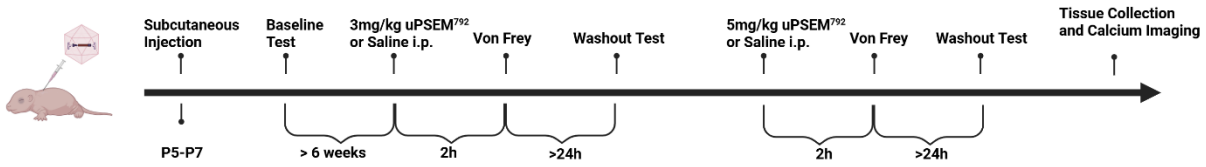

B

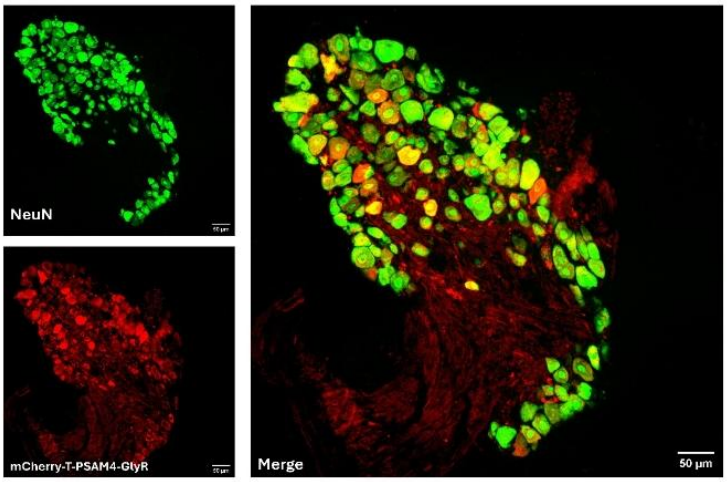

C

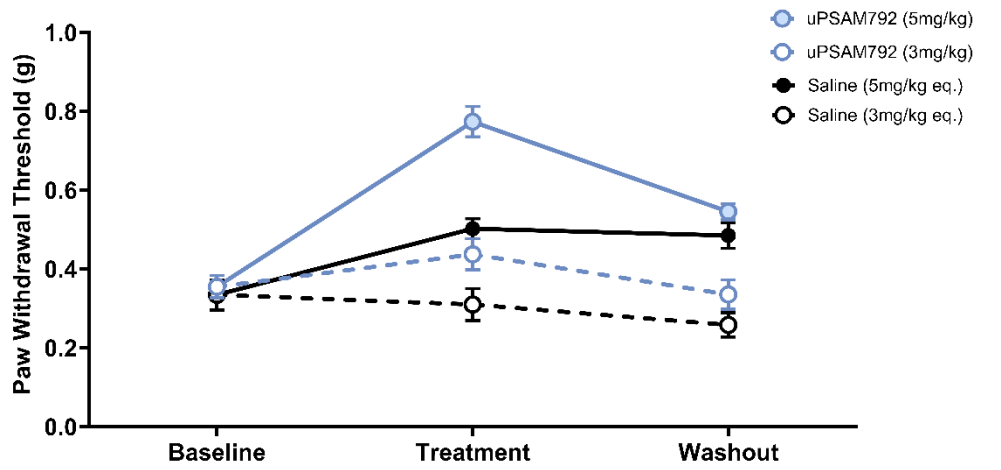
uPSAM792 (5mg/kg)
uPSAM792 (3mg/kg)
Saline (5mg/kg eq.)
Saline (3mg/kg eq.)
Paw Withdrawal Threshold (g)
1.0
0.8
0.6
0.4
0.2
0.0
Baseline
Treatment
Washout

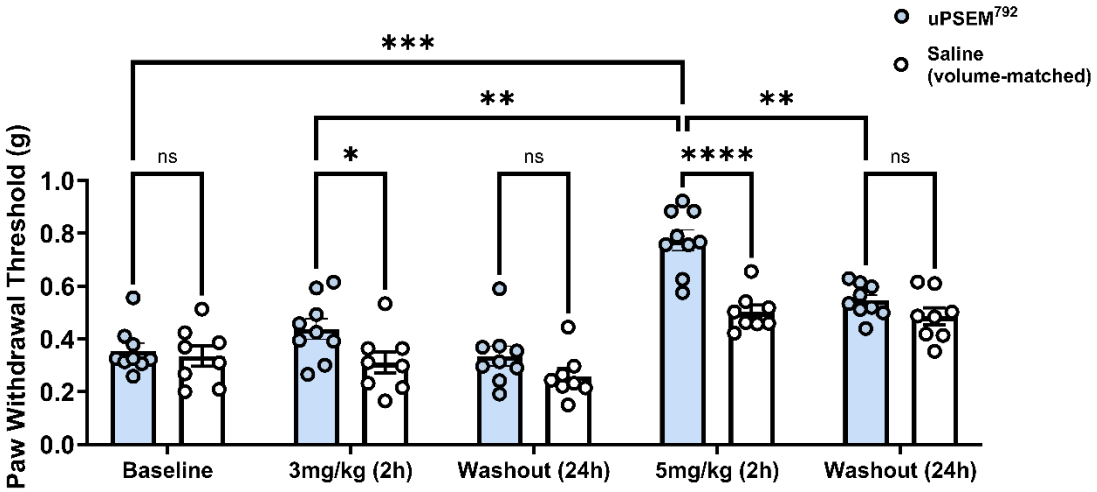
uPSEM792
Saline
(volume-matched)
***
**
**
ns
*
ns
****
ns
Paw Withdrawal Threshold (g)
1.0
0.8
0.6
0.4
0.2
0.0
Baseline
3mg/kg (2h)
Washout (24h)
5mg/kg (2h)
Washout (24h)

D

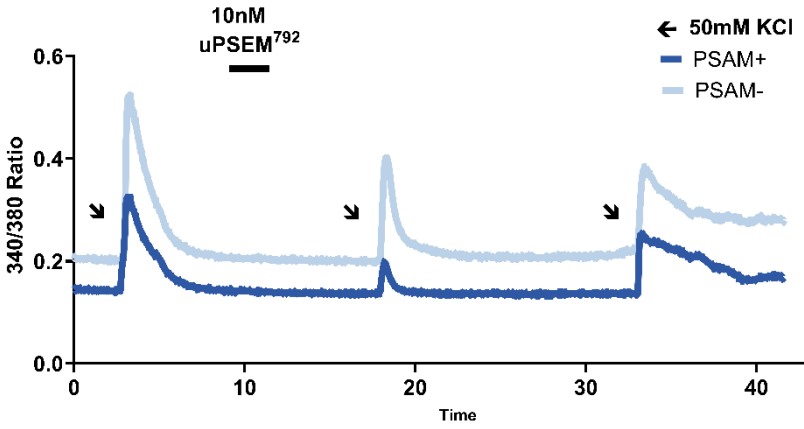
10nM
uPSEM792
50mM KCl
PSAM+
PSAM-
340/380 Ratio
0.6
0.4
0.2
0.0
0
10
20
30
40
Time

E

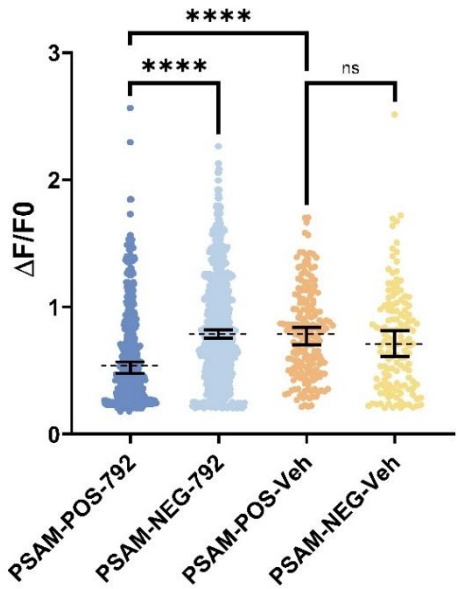
****
****
ns
ΔF/F0
3
2
1
0
PSAM-POS-792
PSAM-NEG-792
PSAM-POS-Veh
PSAM-NEG-Veh

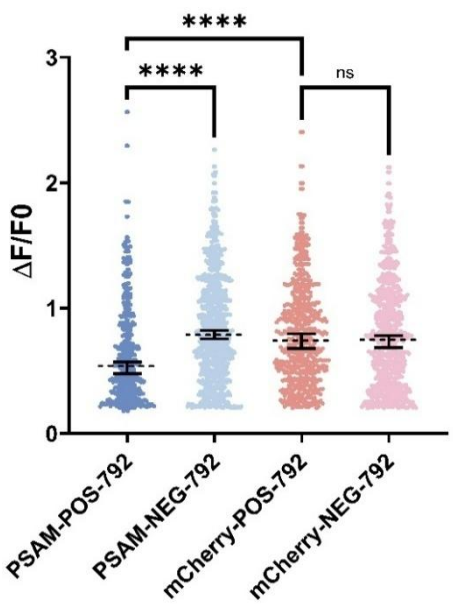
****
****
ns
ΔF/F0
3
2
1
0
PSAM-POS-792
PSAM-NEG-792
mCherry-POS-792
mCherry-NEG-792

F

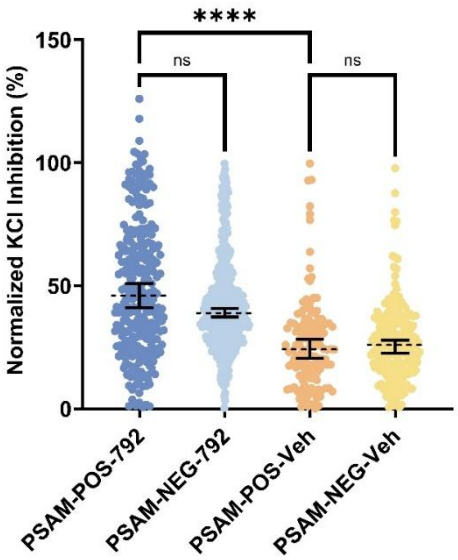
****
ns
ns
Normalized KCl Inhibition (%)
150
100
50
0
PSAM-POS-792
PSAM-NEG-792
PSAM-POS-Veh
PSAM-NEG-Veh

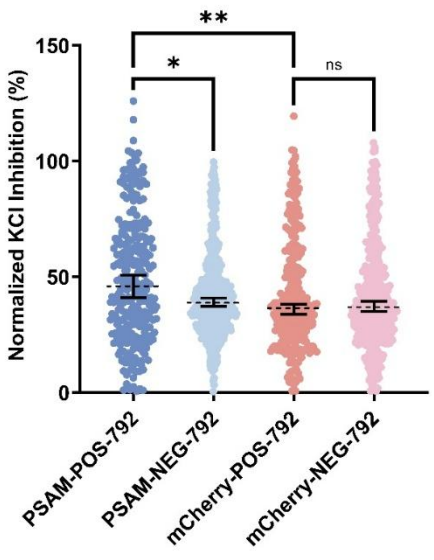
**
*
ns
Normalized KCl Inhibition (%)
150
100
50
0
PSAM-POS-792
PSAM-NEG-792
mCherry-POS-792
mCherry-NEG-792

Figure 4.4. Systemic administration of uPSEM792 produces reversible analgesia *in vivo* and functional silencing in dissociated DRG neurons *in vitro*.

A. Experimental timeline. Neonatal (P5-P7) mice received a subcutaneous injection of AAV9-mCherry-T-PSAM4-GlyR. After 6 weeks, adult mice underwent baseline Von Frey testing, followed by an intraperitoneal (i.p.) injection of uPSEM792 (3 or 5 mg/kg) or an equivalent volume saline. Behavioural testing was repeated at 2 hours post-injection, and tissues were collected for *in vitro* analysis after the final washout timepoint.

B. Representative confocal images of lumbar DRG sections. Left: Successful expression of the PSAM4 receptor (mCherry, red) in neurons, co-localising with the neuronal marker NeuN (green).

C. Systemic uPSEM792 administration produces dose-dependent and reversible analgesia. Top panel: A summary line graph illustrating the distinct pharmacodynamic profiles for all four experimental groups over time. Bottom panel: The 3 mg/kg dose produced a significant analgesic effect at 2 hours post-injection (*$P < 0.05$ vs. Saline control group), which was fully reversible by the 24-hour washout point. In contrast, the 5 mg/kg dose induced a more potent and long-lasting analgesia, showing a significantly stronger effect than the 3 mg/kg dose (*$P < 0.05$). At this peak time point, the 5 mg/kg effect was highly significant against both its baseline (**$P < 0.01$) and the saline control (****$P < 0.0001$). Saline groups received volume-matched injections corresponding to the 3 mg/kg or 5 mg/kg drug volumes, respectively.

D. Representative traces of intracellular calcium changes (Fura-2 340/380 ratio) in a mCherry-T-PSAM-GlyR-expressing neuron (PSAM+) and an adjacent non-expressing neuron (PSAM−) within the same field of view. Dissociated DRG neurons were repeatedly stimulated with brief pulses of KCl (50 mM, 10s) to evoke calcium influx. Bath application of uPSEM792 (10 nM) for 15 minutes between the first and second stimulation led to a selective suppression of the calcium response in the PSAM+ neuron, with minimal effect on the PSAM− neuron. The third stimulation, following a

washout period, shows partial recovery of the response, demonstrating the reversibility of the inhibition.

E. Intrinsic variability in baseline neuronal excitability necessitates data normalisation. These graphs plot the peak amplitude (ΔF/F0) to the first KCl stimulation across different experimental populations, before any drug or vehicle application. The left panel shows that the baseline response of PSAM-expressing neurons (PSAM-POS) is significantly lower than that of adjacent non-expressing neurons (PSAM-NEG) (****P < 0.0001). The right panel further illustrates this heterogeneity, revealing a significant difference in baseline excitability between neurons expressing the functional PSAM receptor and control neurons expressing only mCherry (****P < 0.0001). This inherent baseline heterogeneity renders direct comparisons of absolute post-treatment amplitudes unreliable. Therefore, to isolate the specific pharmacological effect from this biological variance, the analysis in Figure 4.4F utilises a normalised inhibition rate, where each neuron serves as its own pre-drug baseline. Inhibition (%) = $(1 - Peak_2/Peak_1) \times 100\%$.

F. Normalised inhibition analysis confirms the silencing effect is both ligand- and receptor-specific. Left Panel: The inhibitory effect is triggered explicitly by uPSEM792. Application of the vehicle (ECF) produced minimal inhibition in both PSAM-expressing (PSAM-POS-Veh) and non-expressing (PSAM-NEG-Veh) neurons. Consequently, the inhibition observed in the uPSEM792-treated group (PSAM-POS-792) was significantly greater than in the vehicle-treated group (****P < 0.0001). Right Panel: The silencing is mediated by the functional PSAM receptor. Inhibition by uPSEM792 was significantly greater in neurons expressing the PSAM receptor compared to control neurons expressing a non-functional mCherry protein (PSAM-POS-792 vs. mCherry-POS-792, **P < 0.01). Furthermore, within the PSAM group, expressing neurons showed significantly more inhibition than adjacent non-expressing neurons (P < 0.05), a difference not seen in the mCherry control group (ns). This confirms the effect is not due to non-specific consequences of protein overexpression.

Behavioural Data in (C) were analysed using a two-way ANOVA (mixed-effects model), post-hoc Bonferroni test. Data are presented as mean ± SEM. N = 8-9 animals per group. Y-axis represents the Paw Withdrawal Threshold (g), a measure of mechanical nociception.

In vitro Calcium image Data in (E, F) are presented as swarm plots where each dot represents an individual cell. Bars indicate the median and 95% confidence interval (CI). Statistical analysis was performed using a Kruskal-Wallis test with Dunn's multiple comparisons test.

The number of cells analysed was n = 287 (PSAM-POS-792), 488 (PSAM-NEG-792), 314 (mCherry-POS-792), 400 (mCherry-NEG-792), 136 (PSAM-POS-Veh), and 202 (PSAM-NEG-Veh).

Significance is denoted as: ns, not significant; *p < 0.05, **p < 0.01, ***p < 0.001, ****$p < 0.0001$.

3.4 PSAM/PSEM activation alleviates basal and chronic pain in both somatic and orofacial regions

After establishing an appropriate agonist dose and regimen that *works in DRG neurons,* we applied our principles to investigate the effect of chemogenetically silencing cutaneous facial neurons in the naïve state and in a model of chronic migraine-like pain. The experimental design is outlined in Figure 4.5A. We injected AAV9-mCherry-T-PSAM4-GlyR (PSAM group) or AAV9-mCherry (mCherry control group) subcutaneously into the nape of neonatal (P5-P7) mice. After a 6-week expression period, mice were behaviourally tested to assess both paw and facial mechanical sensitivity pre- and post uPSEM792. We then induced a chronic migraine-like pain model using intraperitoneal injections of nitroglycerin (NTG) and assessed the analgesic effect of uPSEM792/PSAM4-GlyR silencing.

Immunofluorescence of the trigeminal ganglia (TG) collected at the end of the experiment confirmed successful viral expression and targeting. As shown in Figures 4.5B and 4.5C, the virally expressed mCherry (red) co-localised with markers for the two

major nociceptive subpopulations, CGRP (green) and IB4 (green), as well as the marker for C-fibre low-threshold mechanoreceptors, TH (green). This indicates that PSAM4-GlyR was delivered to multiple types of sensory neurons involved in pain and touch within the TG. On a behavioural level, we first assessed the impact of PSAM4-GlyR activation on baseline nociception. As shown in Figures 4.5D and 4.5E, a single dose of uPSEM792 (5 mg/kg) significantly increased the paw withdrawal threshold (PWT) ($p < 0.05$). It decreased the orofacial mechanical sensitivity score ($p < 0.01$) in the PSAM group, with no significant change in the mCherry control group. This analgesic effect returned to baseline levels after 24 hours, demonstrating its reversibility.

To determine if chemogenetic activation could reverse an established chronic pain state, we subjected mice to intermittent NTG injections for 9 days. In PSAM-expressing mice, this regimen induced a progressive mechanical allodynia in the hind paw (Figure 4.5F). Compared to their saline-treated group (PSAM+Saline), the paw withdrawal thresholds (PWTs) of the PSAM+NTG group were significantly lower from Day 5 ($p = 0.0007$) and reached a maximal difference on Day 9 ($p = 0.0002$). On Day 10, a single administration of uPSEM792 (5 mg/kg, i.p.) produced a reversal of this allodynia after 2 hours. The PWT of the PSAM+NTG group was significantly elevated compared to its pre-drug state on Day 9 ($p = 0.0096$), confirming the drug's therapeutic efficacy. Following treatment, the paw withdrawal threshold returned to levels comparable to the original pre-NTG baseline ($p > 0.9999$). Furthermore, consistent with a reversal of the hypersensitive state, the PWT of the treated PSAM+NTG group was not significantly different from the PSAM+Saline control group ($p > 0.9999$).

Similarly, NTG exposure successfully induced cephalic hyperalgesia, evidenced by a significant increase in orofacial pain scores (Figure 4.5G). In PSAM-expressing mice, pain scores became significantly higher than in saline-treated controls as early as Day 3

($p = 0.0004$) and remained elevated throughout the 9 days. Application of uPSEM792 on Day 10 produced a complete reversal of this established pain state. The treatment significantly reduced pain scores compared to the peak hyperalgesia observed on Day 7 ($p = 0.0142$). More importantly, uPSEM792 restored the pain scores to a level that was not significantly different from both the animals' own pre-NTG baseline ($p > 0.9999$) and the saline-treated control group ($p > 0.9999$).

Following treatment, the PWT of the PSAM+NTG group was significantly higher than that of the mCherry+NTG control group ($p = 0.0052$). The orofacial pain scores in the PSAM+NTG mice were significantly lower than those in the mCherry+NTG control group ($p = 0.0022$), indicating the effect was PSAM-dependent. This comparison should be interpreted with caution due to the limited sample size of the mCherry control group ($n = 2$-3).

A

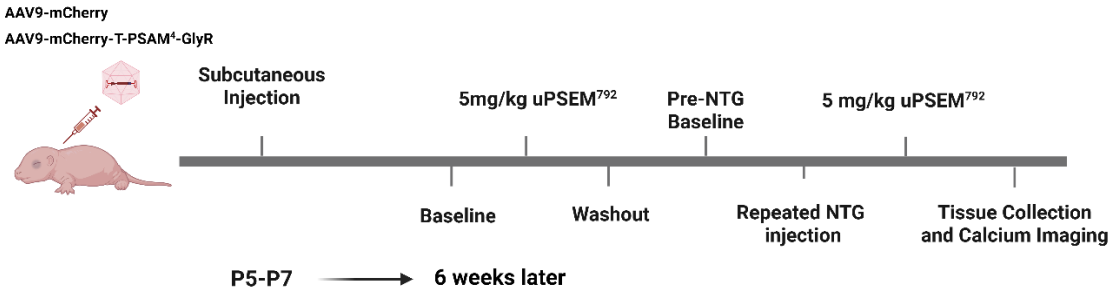
AAV9-mCherry
AAV9-mCherry-T-PSAM4-GlyR
Subcutaneous Injection
5mg/kg uPSEM792
Pre-NTG Baseline
5 mg/kg uPSEM792
Baseline
Washout
Repeated NTG injection
Tissue Collection and Calcium Imaging
P5-P7
6 weeks later

B

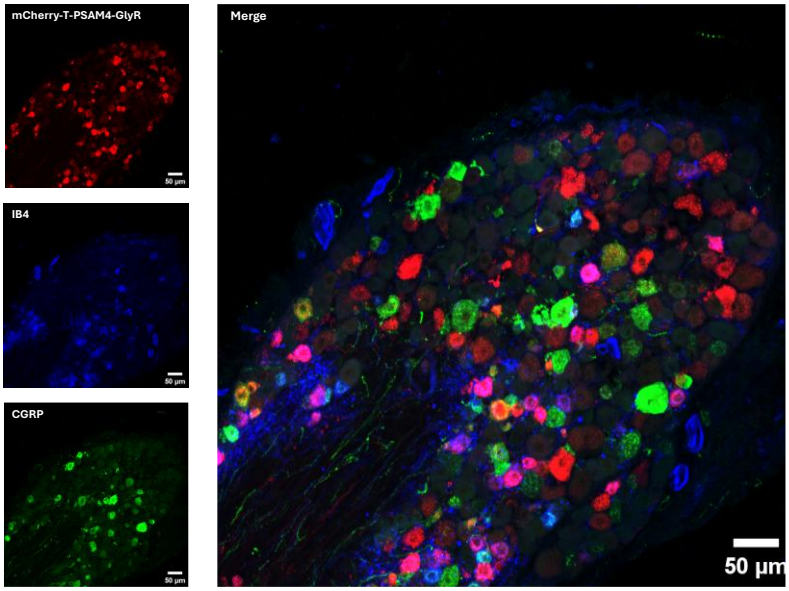
mCherry-T-PSAM4-GlyR
IB4
CGRP
Merge
50 µm

C

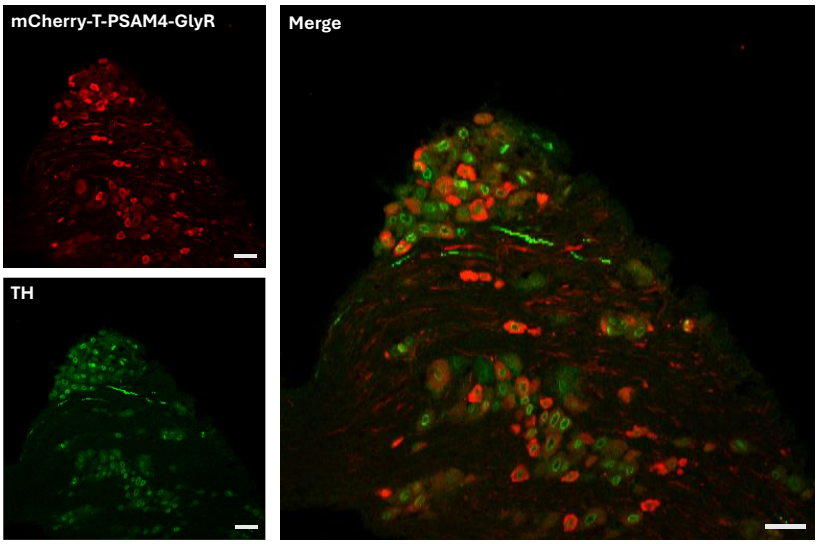
mCherry-T-PSAM4-GlyR
TH
Merge

D

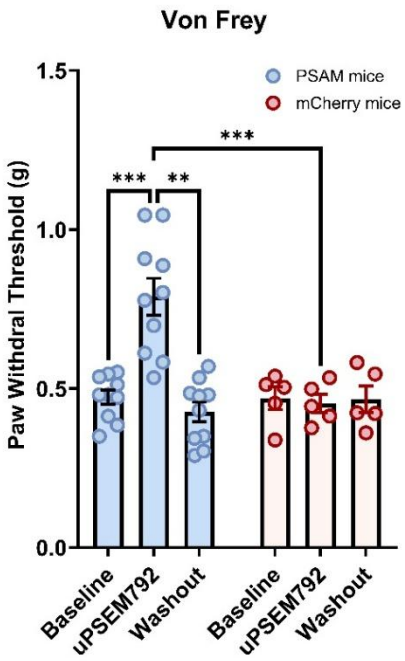
Von Frey
PSAM mice
mCherry mice
Paw Withdral Threshold (g)
1.5
1.0
0.5
0.0
***
***
**
Baseline
uPSEM792
Washout
Baseline
uPSEM792
Washout

E

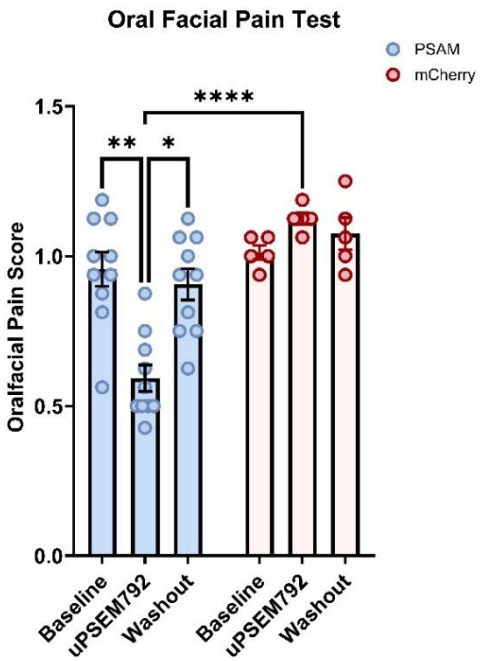
Oral Facial Pain Test
PSAM
mCherry
Oralfacial Pain Score
1.5
1.0
0.5
0.0
****
**
*
Baseline
uPSEM792
Washout
Baseline
uPSEM792
Washout

F

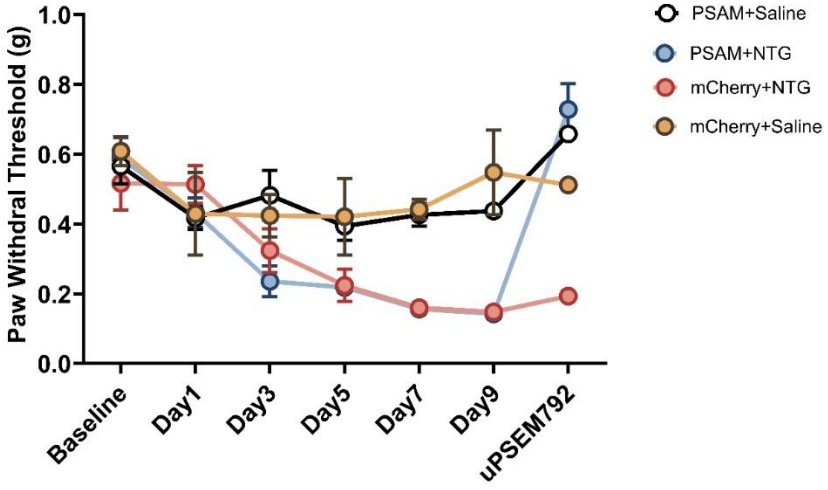
PSAM+Saline
PSAM+NTG
mCherry+NTG
mCherry+Saline
Paw Withdral Threshold (g)
1.0
0.8
0.6
0.4
0.2
0.0
Baseline
Day1
Day3
Day5
Day7
Day9
uPSEM792

G

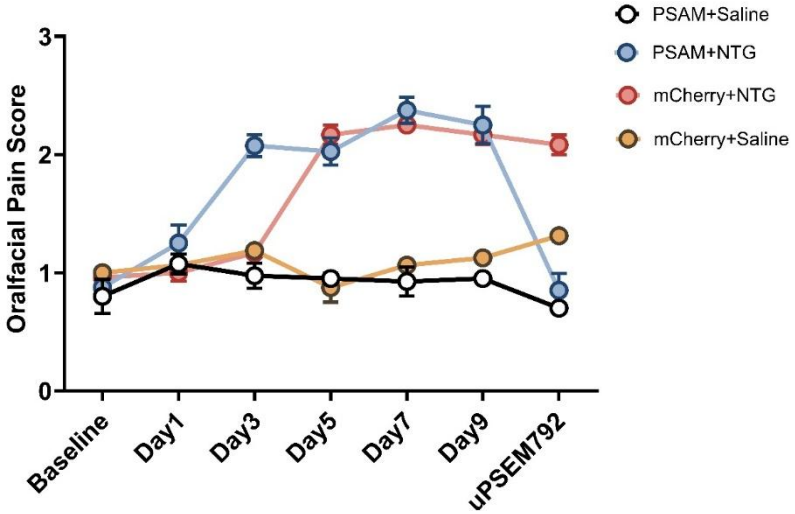
PSAM+Saline
PSAM+NTG
mCherry+NTG
mCherry+Saline
Oralfacial Pain Score
3
2
1
0
Baseline
Day1
Day3
Day5
Day7
Day9
uPSEM792

Figure 4.5. Activation of PSAM4-GlyR-expressing neurons reduces hind paw and orofacial mechanical sensitivity in naïve mice and following chronic NTG-induced allodynia.

A. **Schematic of the experimental design and timeline.** Neonatal (P5-P7) mice received subcutaneous injections of either AAV9-mCherry-T-PSAM4-GlyR (PSAM group) or AAV9-mCherry (mCherry control group). After a 6-week expression period, a series of behavioural assays were performed. First, baseline paw mechanical sensitivity (von Frey) and orofacial pain scores were assessed. Subsequently, mice were injected with uPSEM792 (5 mg/kg) to evaluate its effect on basal nociception, followed by a washout period. Later, A pre-NTG baseline was established before the induction of the chronic pain model. A chronic migraine-like state was then induced by repeated intraperitoneal (i.p.) injections of nitroglycerin (NTG, 10 mg/kg) or Saline on days 1, 3, 5, 7, and 9, creating four experimental groups. To test for analgesic efficacy, all groups received an injection of uPSEM792 (5 mg/kg) 24 hours after the final NTG/Saline administration. At the end of the experiment, trigeminal ganglia (TG) were collected for subsequent immunohistochemistry or calcium imaging.

B. **Viral expression in TG colocalises with nociceptive sensory neurons.** Representative immunofluorescence image of a TG section showing colocalization between virally expressed mCherry (red) and markers for two major nociceptive subpopulations, CGRP (Calcitonin Gene-Related Peptide, green) and IB4 (isolectin B4, green). Scale bar = 50 µm.

C. **Viral expression in TG colocalises with TH-positive neurons.** Representative immunofluorescence image of a TG section showing colocalization between virally expressed mCherry (red) and Tyrosine Hydroxylase (TH, green). TH is a marker for both a subset of sensory neurons, C-fibre low-threshold mechanoreceptors (C-LTMRs), and sympathetic neurons. Scale bar = 50 µm.

D. Paw withdrawal threshold (PWT) was measured using von Frey filaments in PSAM mice (n = 10) and mCherry controls (n = 5). Compared to baseline, administration of uPSEM792 led to a significant increase in PWT in the PSAM group at the 2-hour timepoint, an effect not observed in the mCherry group. This analgesic effect was reversible, with the PWT returning towards baseline after a 24-hour washout.

E. Orofacial mechanical sensitivity was scored in PSAM (n = 10) and mCherry (n = 5) mice at baseline, 2 hours post-uPSEM792, and after a 24-hour washout. In PSAM-expressing mice, uPSEM792 administration caused a significant reduction in the pain score compared to both their own baseline and to the mCherry control group at the same time point. This effect returned to baseline levels after washout.

F. PWT was measured in four groups of mice (PSAM+NTG,n = 5; PSAM+Saline, n = 5; mCherry+NTG, n = 3; mCherry+Saline, n = 2) over 9 days of intermittent nitroglycerin (NTG, 10 mg/kg, i.p.) or saline injections to induce a chronic migraine-like state. Repeated NTG administration induced a progressive and significant decrease in PWT in PSAM-expressing mice compared to saline controls, which was evident from Day 5 ($p = 0.0007$) and reached its maximum at Day 9 ($p = 0.0002$). On day 10, a single dose of uPSEM792 was administered to all groups. This treatment significantly reversed the established allodynia in the PSAM+NTG group, as demonstrated by a significant increase in PWT from Day 9 to the post-drug timepoint ($p = 0.0096$).

G. In the same chronic pain model, orofacial pain scores were quantified. NTG induced a significant increase in pain scores in both PSAM+NTG and mCherry+NTG mice, with an earlier onset in the PSAM+NTG group (Day 3, $p = 0.0004$ vs. saline). the analgesic effect of uPSEM792 was PSAM-dependent; it significantly reduced pain scores in the PSAM+NTG group (Day 7 vs. uPSEM792, $p = 0.0142$).

Both PWT and orofacial pain scores in the PSAM+NTG group were restored to levels statistically indistinguishable from their respective pre-NTG baselines and from the saline-treated control group ($p > 0.05$ for all)

All data are presented as mean ± SEM. Statistical analysis was conducted using a two-way ANOVA (mixed-effects model) and a post-hoc Bonferroni test. * $p < 0.05$, ** $p < 0.01$, *** $p < 0.001$. **** $p < 0.0001$.

3.5 The PSAM/PSEM System Remains Functional In vitro After Behavioural Experiments.

To provide direct cellular evidence of selective inhibition, we also acutely isolated TG neurons from mice that had completed behavioural testing and performed *in vitro* calcium imaging validation. Application of uPSEM792 selectively and reversibly silenced KCl-evoked responses in PSAM+ neurons with no effect on adjacent PSAM- neurons (Figure 4.6A). Once again, significant baseline variability necessitated data normalisation (Figure 4.6B). The normalised data confirmed that the silencing effect remained highly ligand-specific (uPSEM792 vs vehicle, $p < 0.0001$) and receptor-specific (PSAM vs mCherry, $p < 0.0001$) (Figure 4.6C). This result demonstrates the long-term stability and functional integrity of the PSAM/PSEM system, validating its use for modulating neuronal activity in chronic experimental models.

Upon closer inspection of the initial analysis, we noticed a noteworthy phenomenon. In Figure 4.6C, the PSAM-positive and PSAM-negative neurons in the TG did not reach statistical significance, although a difference in inhibition magnitude could be observed. Concurrently, for the DRG's PSAM-positive and PSAM-negative neurons in Figure 4.4E, the left panel showed no difference. In contrast, the right panel showed a significant difference, even though it was the same dataset. We hypothesised that this was likely a statistical artefact: the high variance between the highly responsive experimental groups (PSAM) and the non-responsive control groups (mCherry/Vehicle) reduces the statistical power of a post-hoc test to detect smaller, yet real, differences between subgroups. To address this and directly test our hypothesis, we performed a more targeted comparison using a Mann-Whitney U test exclusively between the PSAM-positive and PSAM-negative populations for both TG and DRG. This focused analysis, presented in Appendix

Figure 4.8, confirmed a statistically significant difference in the level of inhibition between these two cell populations in both ganglia (TG: $p < 0.05$; DRG: $p < 0.01$).

Overall, this result demonstrates the long-term stability and functional integrity of the PSAM/PSEM system, validating its use for modulating neuronal activity in chronic experimental models. All stimulation peaks are provided in the Appendix Figure 4.7.

A

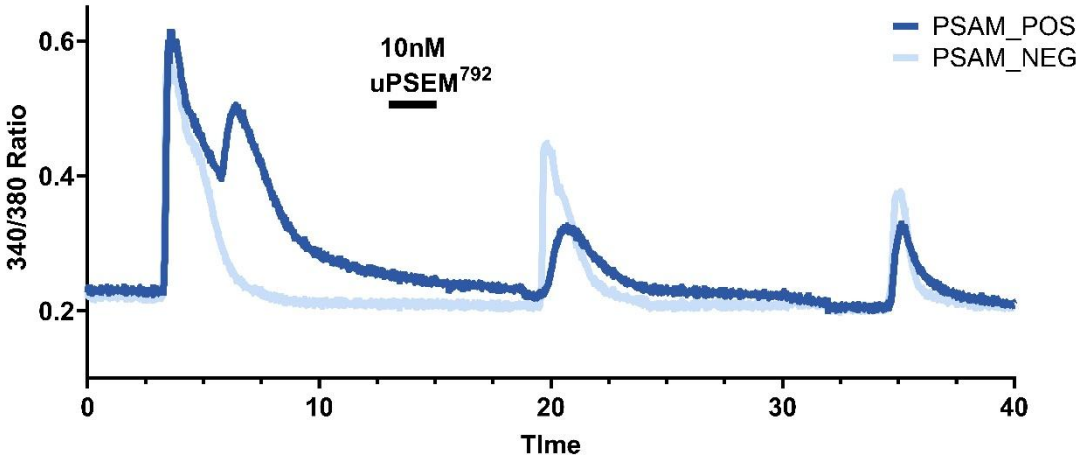
PSAM_POS
PSAM_NEG
10nM
uPSEM792
340/380 Ratio
0.6
0.4
0.2
0
10
20
30
40
TIme

B

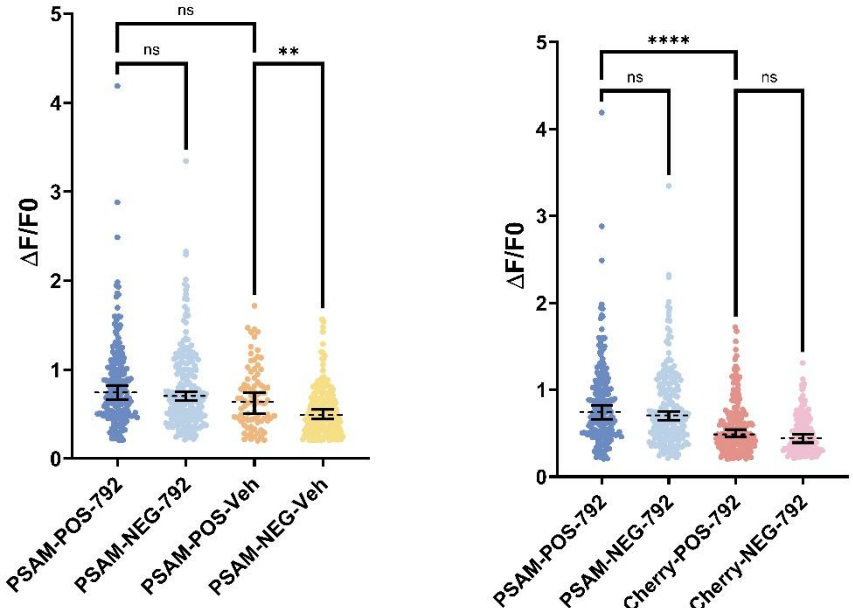
ΔF/F0
ns
ns
**
****
PSAM-POS-792
PSAM-NEG-792
PSAM-POS-Veh
PSAM-NEG-Veh
mCherry-POS-792
mCherry-NEG-792

C

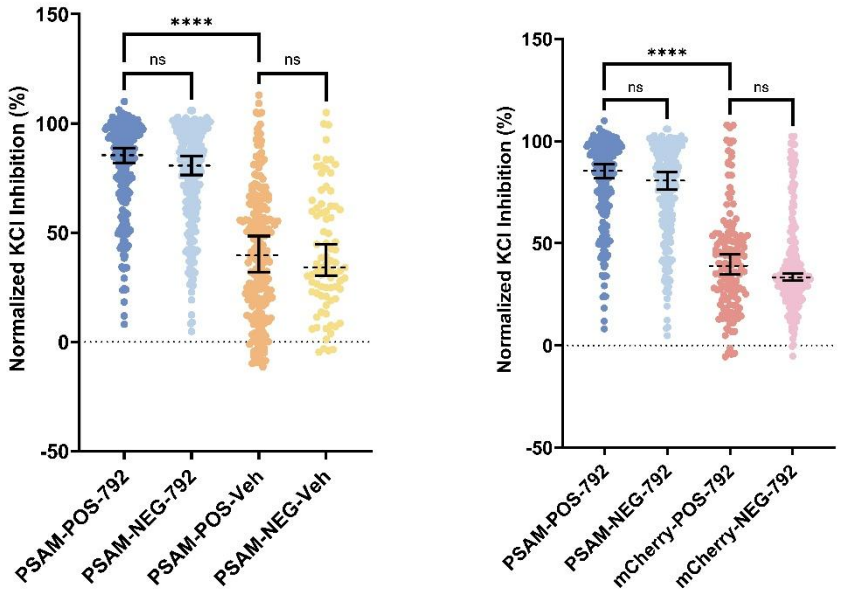
Normalized KCl Inhibition (%)
****
ns
ns
PSAM-POS-792
PSAM-NEG-792
PSAM-POS-Veh
PSAM-NEG-Veh
mCherry-POS-792
mCherry-NEG-792

Figure 4.6. The PSAM/PSEM chemogenetic system is functionally intact in acutely isolated trigeminal ganglion (TG) neurons *in vitro*

A. Representative traces of intracellular calcium changes (Fura-2 340/380 ratio) in a PSAM-expressing neuron (PSAM_POS, dark blue) and an adjacent non-expressing neuron (PSAM_NEG, light blue). Neurons were repeatedly stimulated with brief pulses of KCl to evoke calcium influx. The application of uPSEM792 (10 nM) between the first and second stimulations led to a selective and reversible suppression of the calcium response in the PSAM-positive neuron. In contrast, the adjacent PSAM-negative neuron remained unaffected, confirming that the receptor remains functional *in vitro*.

B. Intrinsic variability in baseline neuronal excitability necessitates data normalisation. These graphs plot the peak amplitude (ΔF/F0) to the first KCl stimulation across different experimental populations, before any drug or vehicle application. The left panel compares the baseline response between drug- and vehicle-assigned groups, revealing significant variability (e.g., PSAM-POS-Veh vs. PSAM-NEG-Veh, **P < 0.01). The right panel further highlights this heterogeneity, showing a profound difference in baseline excitability between neurons expressing the functional PSAM receptor and control neurons expressing only mCherry (****P < 0.0001). This inherent baseline heterogeneity confirms that direct comparison of raw amplitudes is unreliable, necessitating the use of a normalised inhibition rate for subsequent analysis: Inhibition (%) = (1 - $Peak_2/Peak_1$) × 100%.

C. Normalised inhibition analysis confirms the silencing effect is both ligand- and receptor-specific. Left Panel: Ligand Specificity. The inhibitory effect is specifically triggered by uPSEM792. Application of the vehicle (Veh) produced minimal inhibition in both PSAM-expressing (PSAM-POS-Veh) and non-expressing (PSAM-NEG-Veh) neurons. Consequently, the inhibition observed in the uPSEM792-treated group (PSAM-POS-792) was significantly greater than in the vehicle-treated control group (****P < 0.0001). Right Panel: Receptor Specificity. The functional PSAM receptor mediates the silencing. Inhibition by uPSEM792 was significantly greater in neurons expressing the PSAM receptor compared to control neurons expressing a non-functional mCherry protein (PSAM-POS-792 vs. mCherry-POS-792, ****P < 0.0001). This confirms the effect is not due to non-specific consequences of protein overexpression.

Data in (B) and (C) are presented as swarm plots where each dot represents an individual cell. Bars indicate the median and 95% confidence interval (CI). Statistical comparisons were performed using a Kruskal-Wallis test with Dunn's multiple comparisons test. The number of cells analysed was n = 203 (PSAM-POS-792), 224 (PSAM-NEG-792), 213 (mCherry-POS-792), 203 (mCherry-NEG-792), 83 (PSAM-POS-Veh), and 154 (PSAM-NEG-Veh). Significance is denoted as: * $p < 0.05$, ** $p < 0.01$, *** $p < 0.001$. **** $p < 0.0001$.

.

4. Discussion

This study demonstrates the feasibility and analgesic efficacy of the inhibitory chemogenetic tool, PSAM⁴-GlyR/uPSEM792, within the TG and DRG, establishing a robust evidence base spanning *in vitro*, *in vitro*, and *in vivo* analyses.

4.1 Successful Validation and Extension of the PSAM/PSEM System in the Trigeminal Ganglion

This study represents the first application and comprehensive functional validation of the human-derived inhibitory chemogenetic tool PSAM⁴-GlyR/PSEM in the trigeminal ganglion. Our *in vitro* calcium imaging results provide strong evidence for the system's efficacy: uPSEM792 and varenicline induced rapid and potent inhibition of PSAM-expressing TG neurons at nanomolar concentrations, while having no effect on adjacent non-expressing neurons or control neurons expressing only mCherry. This demonstrates high ligand specificity and receptor dependency. The observation that KCl-evoked responses were rapidly attenuated in the presence of the ligand and recovered upon washout confirms the tool's programmable on/off capability. This capacity for short-term, repeatable modulation is advantageous for potential on-demand clinical applications, minimising continuous interference with normal sensory function.

uPSEM792 demonstrated greater potency than varenicline in suppressing KCl-evoked responses in PSAM⁴-GlyR-positive neurons and was consequently selected for all subsequent behavioural experiments. This superior efficacy is rooted in the sophisticated pharmacological design of uPSEM792. Magnus et al. structurally optimised varenicline to mitigate its off-target effects on endogenous nicotinic receptors (particularly α4β2 and α7 nAChR). The resulting compound, uPSEM792, maintains sub-nanomolar affinity for

PSAM^4-GlyR ($K_i \approx 0.7$ nM) while enhancing agonist selectivity for this engineered receptor by several thousand-fold. In contrast, its activity at endogenous targets is substantially diminished. This cleaner pharmacological profile enables uPSEM792 to act with greater precision and potency on the introduced chemogenetic tool (Magnus et al., 2019).

Additionally, our research confirmed the system's broad inhibitory spectrum. Under uPSEM792 or varenicline, PSAM-positive neurons showed inhibited responses to various sensory agonists, including ATP and menthol. Although we were surprised that the inhibition of the capsaicin response was not more potent, the results were unexpected. This likely indicates that the capsaicin receptor TRPV1 is a non-selective cation channel that, upon activation, facilitates calcium influx. This Ca2+ influx will still occur when a neuron is chemogenetically silenced, reflecting a disadvantage of using Ca2+ imaging as a proxy for neuronal activity. However, a previous study using the GluCl chemogenetic silencer demonstrated, using patch-clamp recording, that capsaicin application was unable to excite silenced neurons (Weir et al., 2017). The broad applicability of PSAM/PSEM to a number of sensory stimuli has important translational implications. In the pathophysiology of complex pain conditions, peripheral sensitisation is a critical process driven not by a single mediator but by a concert of inflammatory and neurogenic molecules. For instance, ATP mediates nociceptive signalling via P2X3 receptors (Burnstock, 2016), the TRPV1 channel is central to heat and chemical pain (Caterina et al., 1997), whilst TRPM8 is associated with cold-evoked pain and sensory abnormalities (McKemy et al., 2002). Traditional drug development strategies typically focus on blocking a specific upstream receptor or channel, but these strategies often struggle to address the complex synergistic pathways. Our research demonstrates a fundamentally different interventional paradigm. This mechanism does not depend on any specific

sensory receptor but fundamentally reduces the neuron's excitability gain. Therefore, regardless of whether nociceptive signals originate from changes in P2X, TRPV1, or TRPM8 pathways, the PSAM system provides universal dampening at the primary sensory neuron itself. This broad-spectrum inhibitory capacity, independent of upstream stimulus source, presents an attractive therapeutic strategy for complex pain conditions like chronic migraine (Silberstein, 2004).

4.2 Interventional Potential of Chemogenetic Silencing of TG in Migraine Model

The nitroglycerin (NTG) migraine model is a popular model that replicates key migraine pathophysiology. For example, NTG facilitates the release of nitric oxide (NO) to activate TG neurons and promote CGRP release, demonstrating good translational validity in preclinical research (Edvinsson, 2017; Olesen et al., 1993; Pradhan et al., 2014; Sureda-Gibert et al., 2022). However, this model has some challenges, including systematic sensitisation of sensory pathways. NTG is not specific to affecting only trigeminal afferents and will also alter dorsal root afferents. We used this to our advantage to study the silencing capabilities of PSAM4-GlyR in both hindpaw and facial territories following NTG administration. We could use our strategy to directly interrogate trigeminal afferents that serve as the migraine signal source. Immunofluorescence results confirmed our viral delivery strategy targeted CGRP-positive neurons, an important population of nociceptors in migraine. Our observed analgesic effects likely operate partly through inhibiting the excitability of these critical peptidergic neurons and their CGRP release. This aligns with the broader objective of successful clinical migraine therapies (such as anti-CGRP monoclonal antibodies and gepants) to downregulate CGRP signalling pathways (Goadsby et al., 2017; T. W. Ho et al., 2010; Russo & Hay,

2023; Tepper, 2018). Our chemogenetic silencing mechanism acts upstream and directly to effectively turn down the volume at the first signal transmission station, rather than intercepting signals during transmission or at their destination. This study provides the first preclinical evidence for a fully humanised chemogenetic gene therapy approach to silence orofacial pain transmission as a potential treatment for chronic pain.

4.3 Clinical Translation Pathway and Challenges

Applying chemogenetic strategies to peripheral sensory ganglia, such as the trigeminal ganglion (TG), represents an attractive clinical translation pathway. Our strategy allows us to circumvent two fundamental obstacles present when using central nervous system interventions. Firstly, through minimally invasive techniques, we can achieve efficient viral vector delivery. Secondly, because the target is peripheral, the ligand does not need to cross the blood-brain barrier (BBB) to be effective, fundamentally avoiding potential CNS side effects and the higher doses required by traditional medications. Compared to irreversible neuro-ablative procedures and electrical stimulation therapies that depend on implanted hardware, this method offers a new, non-destructive, and reversible paradigm (J. S. Cheng et al., 2014; Miller et al., 2016; Tepper et al., 2009).

However, the journey from preclinical validation to clinical application still depends on carefully addressing several key translational challenges. Firstly, chemogenetic ligands must be validated for long-term administration safety and absence of endogenous off-target effects. Secondly, viral vectors require optimisation for tissue tropism, control of potential retrograde transport risks, and management of host immune responses. At a deeper level, achieving a qualitative leap in targeting precision is required. Future research needs to transition from current reliance on ubiquitous promoters driving pan-neuronal expression to utilising specific promoters that strictly limit chemogenetic tool expression to nociceptive neuron subpopulations, thereby effectively suppressing chronic

pain signals whilst maximally preserving protective pain and non-nociceptive sensory functions like touch, ultimately achieving truly precise peripheral neuromodulation (Espinosa-Juárez et al., 2023; Poth et al., 2021).

4.4 Study Limitations and Future Prospects

Despite the encouraging results, this study has several limitations that warrant discussion and guide future research. Firstly, the *in vivo* behavioural experiments included a small sample size for the mCherry control group (n = 2-3), resulting in large standard error measurements. Therefore, statistical comparisons with the PSAM group should be interpreted cautiously. Future studies must include larger control groups for more robust statistical validation.

Secondly, a core limitation stems from the use of the ubiquitous CAG promoter and nSC delivery method. This led to off-target expression in non-sensory tissue, notably the superior cervical ganglion (SCG), introducing uncertainty regarding the interpretation of the observed analgesic effect. In the PSAM+NTG group, the PWT threshold not only returned to baseline but also showed a trend of exceeding that of healthy controls. While potentially indicating profound efficacy, this effect could also be partially confounded by subtle, subclinical sedation arising from the inhibition of sympathetic tone in the SCG. Such an effect, while not producing overt abnormalities like lethargy or ataxia, could still be sufficient to delay motor responses in a sensitive behavioural assay like the von Frey test. The lack of overt side effects is likely due to robust homeostatic compensation and low basal sympathetic activity (Esler et al., 2010; La Rovere et al., 2008). Therefore, to formally dissociate true analgesia from potential motor or sedative confounds in studies using this broad approach, future work must incorporate dedicated control experiments, such as the open-field and rotarod tests.

Finally, the scope of our assessment was limited. This study primarily focused on mechanical sensitisation, using PWT and Orofacial pain scores, and did not investigate other key migraine-related phenotypes such as photophobia, phonophobia, or activity avoidance. Furthermore, we did not obtain direct readouts of central sensitisation at the trigeminal nucleus caudalis (TNC), for instance, through c-Fos or other immediate early gene (IEG) labelling, or via *in vivo* electrophysiological recordings. These omissions mean our understanding of the causal link between peripheral inhibition and the suppression of central pain processing remains inferential and requires more direct investigation.

Looking forward, a more refined genetic strategy offers a comprehensive solution to the specificity issues. Employing a cell-type-specific promoter, such as Nav1.8 or Advillin, which preferentially targets nociceptors. This approach would resolve two key issues simultaneously: it would prevent problematic off-target expression in autonomic tissues like the SCG, thereby avoiding sedative confounds, and it would confine expression to specific neuronal subtypes within the trigeminal ganglion. Furthermore, optimising the viral vector capsid (e.g., using engineered AAV serotypes with high tropism for peripheral sensory neurons) could further restrict transduction to the target tissue. Achieving this level of precision is essential to dissect which sensory neurons are critical for alleviating orofacial pain and to develop a safe, side-effect-free gene therapy for patients.

5. Conclusion

In summary, this study provides the first comprehensive validation of the PSAM/PSEM chemogenetic system's functionality in the trigeminal ganglion. It demonstrates its therapeutic potential in a clinically relevant chronic migraine model. Through a

minimally invasive viral delivery strategy, we achieved inhibition of TG neuronal activity and successfully alleviated chronic pain behaviours. This work not only provides a powerful new tool for studying the physiological and pathological mechanisms of the trigeminal sensory pathway but also delivers preclinical evidence and a translational pathway for developing precise, controllable gene therapy strategies for migraine and other intractable orofacial pain conditions.

6. Acknowledgements

I would like to thank Dr Steve Middleton and Dr Tina Wei for their guidance on these experiments.

7. Appendix

A

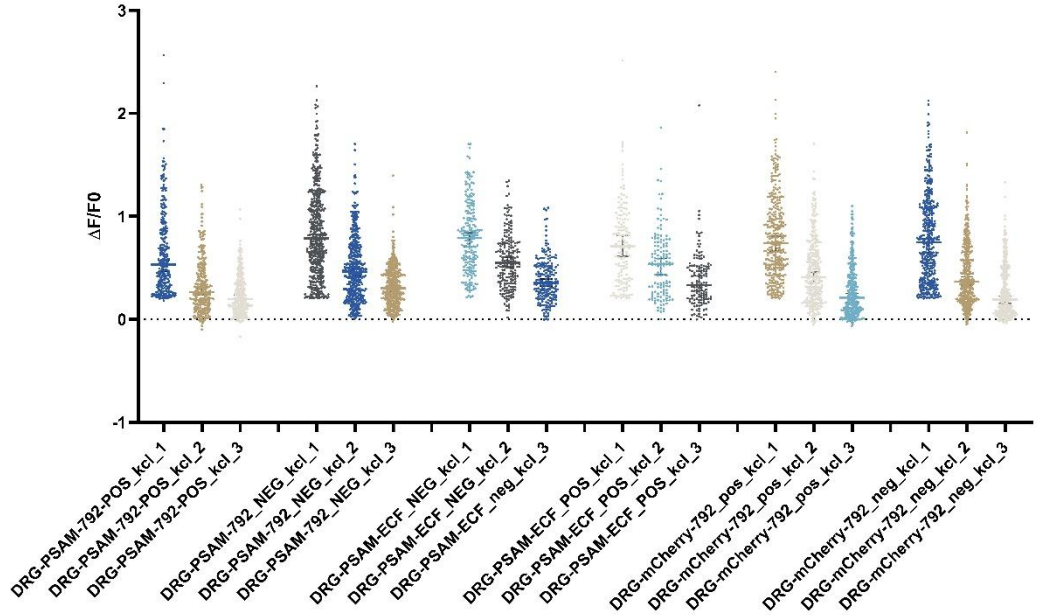

B

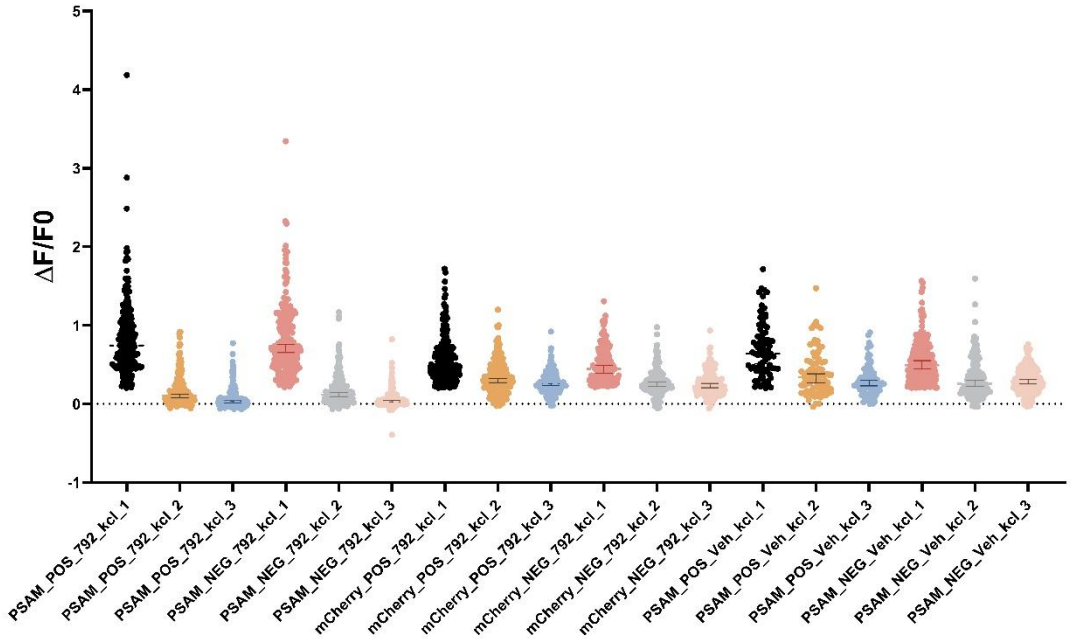

Appendix Figure 4.7: Raw peak amplitude data from *in vitro* functional validation experiments.

Raw peak ΔF/F0 responses from cultured dorsal root ganglion (DRG, A) and trigeminal ganglion (TG, B) neurons. Neurons were acutely isolated from animals that had completed behavioural testing following subcutaneous injection of either AAV9-PSAM4-GlyR or AAV9-mCherry. The plots display the raw peak amplitudes for sequential KCl stimulations, illustrating the cellular responses before and after the application of uPSEM792. These data represent the unnormalized source data corresponding to the quantitative analyses presented in the main text (Figs. 4 and 6), qualitatively illustrating the trend of reduced neuronal activity in PSAM-expressing neurons following agonist application.

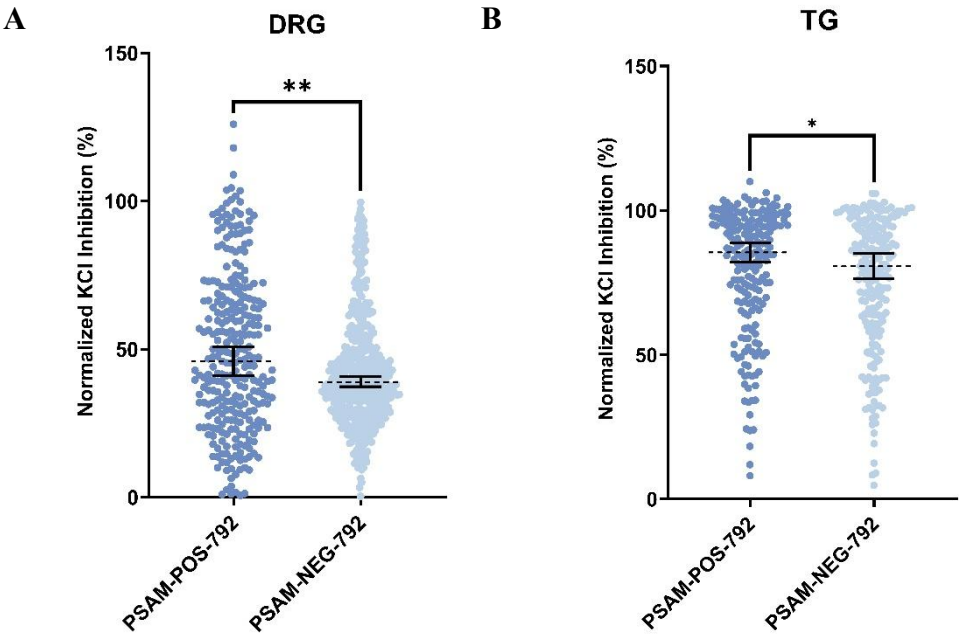

Appendix Figure 4.8: Direct comparison of inhibition between PSAM-positive and PSAM-negative neurons.

Quantification of uPSEM792-mediated inhibition in PSAM-positive (PSAM-POS) versus PSAM-negative (PSAM-NEG) neurons from **(A)** DRG and **(B)** TG. Data are presented as swarm plots where each dot represents an individual cell. Bars indicate the median and 95% confidence interval (CI). Statistical significance was determined using a Mann-Whitney U test. Asterisks indicate statistical significance: *p < 0.05, **p < 0.01. The number of cells analysed was for DRG n = 287 (PSAM-POS), 488 (PSAM-NEG). TG n = 203 (PSAM-POS), 224 (PSAM-NEG)

Chapter V Systematic Evaluation of AAV Vector Performance in Human iPSC-Derived Sensory Neurons

Abstract

Translating adeno-associated virus (AAV) gene therapies from animal models to human applications is often complicated by species-dependent vector performance, a key challenge for developing treatments for sensory neuropathies. To help address this translational issue, we evaluated thirteen natural and engineered AAV serotypes within a human iPSC-derived sensory neuron (iPSC-SN) model. Our assessment, which included metrics for transduction efficiency alongside indicators of axonal integrity and cytotoxicity, suggests a notable trade-off between vector potency and neuronal safety. Specifically, the engineered capsid AAV-PHP.S exhibited high transduction efficiency but was also associated with significant, dose-dependent neurotoxicity in our system. In contrast, the natural serotype AAV9 demonstrated a more favourable safety profile, maintaining good neuronal biocompatibility at the tested concentrations, which may indicate a wider therapeutic window. The poor performance of AAV5, a highly efficient vector in rodents, further highlights the importance of using human-specific models for preclinical validation. This study provides experimental data intended to inform AAV vector selection. It proposes a multi-parameter safety framework that may contribute to the safer and more effective clinical translation of gene therapies for neurological disorders.

1. Introduction

In previous chapters, I successfully verified the effectiveness of GluCl.CreON and PSAM/PSEM chemogenetic tools in regulating pain signals in mouse sensory neurons. This provided proof of concept for sensory neuron-targeted chemogenetics as a potential gene therapy for chronic pain.

Moving from animal research toward clinical applications, the cross-species adaptability of viral vectors presents the greatest challenge. While AAV-9 shows excellent performance in mice, this advantage may not necessarily translate to humans. Various AAV serotypes used in clinical trials exhibit species differences in receptor binding and intracellular transport, potentially leading to variations in transduction efficiency, cellular preference, and safety profiles (Hordeaux et al., 2018; Mingozzi & High, 2013).

To address this, our research advances on two fronts. Firstly, we have transitioned from mouse models to human iPSC-derived sensory neurons to establish a translation model closer to clinical conditions. Secondly, we have expanded from a single serotype AAV-9 to evaluating multiple serotypes, including natural and engineered capsids, systematically comparing their performance in human sensory neurons. These evaluations will provide a foundation for selecting vectors best suited for human systems, support the transfer of chemogenetic tools to human applications, and establish methodological foundations for preclinical pain gene therapy.

1.1 Adeno-Associated Viruses (AAVs)

Adeno-associated virus (AAV) is a small virus containing single-stranded DNA. Research on AAV began in the 1960s, initially focused on understanding its basic biological properties. Today, it has evolved into a sophisticated gene therapy tool (Atchison et al., 1965; Berns & Linden, 1995; Issa et al., 2023; Kuzmin et al., 2021).

Clinically, more than three hundred trials using AAV have been conducted worldwide. Many of these focus on treating neurological disorders, including both single-gene diseases and more complex multigenic conditions. This demonstrates AAV's broad feasibility as an in vivo therapeutic delivery strategy (High & Roncarolo, 2019; Ling et al., 2023).

1.1.1 AAV Biology and Vector Engineering

AAV belongs to the Parvoviridae family, with an icosahedral capsid approximately 26 nanometers in diameter that encapsulates a single-stranded DNA genome of about 4.7 kb. The genome features inverted terminal repeat (ITR) sequences at both ends, with rep genes encoding replication proteins and cap genes encoding three capsid proteins (VP1, VP2, VP3) in the middle (Daya & Berns, 2008; Samulski & Muzyczka, 2014). The viral capsid comprises 60 protein subunits, with variable regions on its surface determining the tissue tropism of different serotypes. Using this characteristic, researchers have discovered numerous novel AAV vectors with excellent properties from nature (G. Gao et al., 2002, 2003; Xie et al., 2002).

Wild-type AAV (wtAAV) is a "defective" virus that requires helper viruses such as adenovirus for efficient replication. Without helper viruses, wtAAV typically establishes latent transduction in host cells as an extrachromosomal episome. Notably, the wtAAV2 genome can integrate at low frequency into a specific site (AAVS1) on human chromosome 19, previously considered one of its latency mechanisms (Buller et al., 1981; Kotin et al., 1990, 1992). Though AAV has long been considered non-pathogenic, recent studies suggest AAV2 may be associated with some cases of unexplained acute hepatitis in children. The exact mechanism remains under investigation but might involve abnormal host immune responses (A. Ho et al., 2023; Servellita et al., 2023).

To safely apply AAV in gene therapy, scientists developed recombinant AAV (rAAV) vectors. In rAAV, only the functionally essential ITR sequences are retained. At the same time, viral genes (rep and cap) responsible for replication and immunogenicity are entirely removed and replaced with therapeutic gene expression cassettes. This modification serves two purposes: it creates space for therapeutic genes and eliminates the virus's replication capability and most immunogenicity caused by viral proteins, greatly enhancing its safety in vivo (Samulski et al., 1989; Samulski & Muzyczka, 2014).

1.1.2 Cell Entry Mechanism

The transduction of cells by adeno-associated virus (AAV) is a multi-step process, commencing with the interaction between the virus and the host cell surface. Initially, the AAV capsid proteins facilitate binding to specific receptors on the cell surface, such as heparan sulfate proteoglycans (HSPG) and terminal galactose. Recent research has identified a transmembrane protein called AAVR (AAV receptor) as a key receptor for multiple AAV serotypes to enter cells. Additionally, the G protein-coupled receptor GPR108 has been identified as a factor necessary for various AAVs to enter cells. (Dudek et al., 2020; Pillay et al., 2016; Summerford & Samulski, 1998).

Following this binding event, the virus is internalised into the cell through receptor-mediated endocytosis, entering endosomes. In the acidic environment of endosomes, the AAV capsid undergoes conformational changes, enabling it to escape into the cytoplasm and avoid degradation (Bartlett et al., 2000; Riyad & Weber, 2021).

Once in the cytoplasm, AAV particles are transported to the nucleus and enter the nucleus through nuclear pore complexes. In or near the nucleus, the capsid is removed, releasing the single-stranded DNA genome (Nicolson & Samulski, 2014; Riyad & Weber, 2021). For the therapeutic gene to be expressed, the viral ssDNA genome must first be converted

into a transcribable double-stranded DNA molecule by the host cell's own DNA polymerase. This process of second-strand synthesis constitutes the principal rate-limiting step for the transduction efficiency of conventional AAV vectors (Ferrari et al., 1996; McCarty et al., 2001). It is only after the formation of this double-stranded DNA that transcription and translation can occur, leading to the expression of the therapeutic protein.

1.1.3 Serotype Diversity, Tissue Targeting, and Engineering Strategies

Another feature of the AAV system is its rich serotype diversity. Multiple AAV serotypes (AAV1 to AAV13, sequentially) and variants exist in nature. The exploration of this natural diversity extends beyond human isolates, with researchers investigating AAVs from other species, such as non-human primates like macaques (e.g., MacAAVs), for their potential to efficiently transduce human cells (G. Gao et al., 2002). Different AAV serotypes exhibit targeting specificity (tropism) for different tissues and cells due to differences in their capsid proteins (Pillay et al., 2016; Summerford & Samulski, 1998; Vandenberghe et al., 2009). In practical research, scientists select the most appropriate serotype based on the target tissue. For example, AAV9 can cross the blood-brain barrier, making it suitable for treating neurological disorders (Foust et al., 2009); AAV1 and AAV6 work well in skeletal and cardiac muscle (Towne et al., 2009); AAV8 efficiently transduces the liver (G. Gao et al., 2002); while AAV2 has been successfully used in retinal gene therapy (Bennett et al., 2016).

When natural serotypes do not perform adequately or may cause immune issues, researchers employ capsid engineering strategies to modify AAV. One approach uses DNA recombination technology to combine the advantages of different serotypes, creating "chimeric capsids." For instance, AAV-DJ fuses the benefits of AAV2, AAV8,

and AAV9 to enhance its versatility and production titre (Grimm et al., 2008). Another powerful method is "in vivo directed evolution," which involves constructing vast libraries of AAV capsid mutations and screening them in specific cells or animal models to obtain new capsids with desired properties (such as enhanced targeting or immune evasion). The Cre recombinase-based AAV Targeted Evolution (CREATE) technology is one such powerful screening method that has successfully developed variants like AAV-PHP.B, AAV-PHP.eB, and AAV-PHP.S, which demonstrate superior performance in targeting the nervous system (Chan et al., 2017; Deverman et al., 2016). Additionally, rational design based on protein structure uses an understanding of AAV capsid structure and function to make site-directed mutations at specific amino acid positions, improving targeting ability or reducing immunogenicity (Asuri et al., 2012; Murlidharan et al., 2016). In recent years, using AI and machine learning models to predict relationships between capsid sequences and functions has become a cutting-edge approach to accelerate the development of new AAV vectors. These computational tools efficiently screen candidate capsids with specific functions from massive datasets, significantly improving research and development efficiency (Bryant et al., 2021; Tan et al., 2025).

1.2 Comparative Delivery Characteristics of Various Serotypes in Sensory Neurons

AAV applications in sensory neurons date back to the early 21st century. Glatzel et al. established the feasibility of AAV for sensory system delivery by achieving stable, persistent expression in sensory neurons through local injection into dorsal root ganglia (Glatzel et al., 2000). Subsequently, with the development of different serotypes and engineered capsids, AAV delivery to neurons has evolved from initial local injections to achieving broader, more efficient systemic coverage (Bedbrook et al., 2018).

Different serotypes exhibit significant variations in tissue tropism, overall efficiency, and cellular preference, which are highly dependent on the administration route, dosage, evaluation timepoint, and species (Issa et al., 2023). Therefore, understanding the transduction characteristics of existing and new AAV vectors in sensory neurons provides the theoretical foundation for subsequent experimental design and vector selection.

To better understand the potential applications of these AAV vectors in the peripheral nervous system (PNS), the following reviews evidence for natural serotypes AAV1-9 and engineered capsids like AAV-PHP.eB, AAV-PHP.S, AAV-retro, and AAV-DJ in sensory neurons. The summary table can be found in the Appendix.

AAV1

AAV1 supports axonal transport and can mediate anterograde transsynaptic tagging under defined experimental conditions (Zingg et al., 2017, 2022). Its overall expression is inferior to AAV5 when directly injected into DRG (Mason et al., 2010). However, in a mouse trigeminal ganglion (TG) peripheral retrograde model, AAV1 achieved the highest TG neuron expression levels (approximately 20-25% positive at 6 weeks) following intradermal whisker pad injection, significantly outperforming AAV7, AAV8, and AAV9, making it the clear preference for this specific application paradigm (Dang et al., 2017).

AAV2

As one of the earliest and most extensively studied serotypes, AAV2 often serves as a benchmark control in contemporary capsid evaluations. In sensory neurons, although early research demonstrated its "feasibility" for delivery, AAV2's overall efficiency is low to moderate, inferior to AAV1, AAV5, and AAV6 (Glatzel et al., 2000; Mason et al., 2010). Consequently, its application in current high-efficiency functional studies is relatively limited.

AAV3, AAV4

In systematic comparisons of direct DRG injection for sensory neurons, both AAV3 and AAV4 exhibit low transduction efficiency, which is significantly inferior to that of AAV1, AAV5, and AAV6 (Mason et al., 2010). Due to their lack of efficiency advantage, evidence, and reports of their application in sensory neuron research are very limited.

AAV5

AAV5 performs extremely efficiently in DRG. Whether via direct DRG injection or intrathecal delivery, its overall efficiency is very high, outperforming AAV8 in direct intrathecal delivery comparisons, with strong coverage of CGRP+ neurons (Mason et al., 2010; Vulchanova et al., 2010; Yu et al., 2016). However, in the whisker pad-to-TG peripheral retrograde model, although the viral genome reaches TG, protein expression in neurons is nearly zero. This suggests potential post-entry expression bottlenecks, such as nuclear import or uncoating in specific pathways (Dang et al., 2017).

AAV6

AAV6 is recognised as a highly efficient vector targeting nociceptive neurons, with effectiveness demonstrated across multiple administration routes. Via intrathecal injection, it transduces DRG neurons with approximately 60% efficiency, preferentially targeting medium and small-diameter nociceptive subgroups, providing precise targeting for pain research (Towne et al., 2009). Similarly, through direct DRG injection, AAV6 achieves efficient and persistent gene expression, further confirming its solid position as an efficient vector for sensory neurons (Yu et al., 2016).

AAV7

Systematic comparative data on AAV7 in sensory neurons are limited. In the available TG peripheral retrograde model, the expression level is generally lower than that of AAV1 (Dang et al., 2017).

AAV8

AAV8's transduction efficiency in sensory neurons varies across different scenarios. When delivered intrathecally to DRG, its efficiency is slightly lower than AAV5 and shows a preference for large-diameter neurons (Vulchanova et al., 2010). Although direct DRG injection confirms its ability to mediate stable expression (Yu et al., 2016), in the TG peripheral retrograde model, its protein expression levels are significantly lower than those of AAV1, despite effective viral genome entry into neurons. This reveals a post-entry expression problem for AAV8 in TG neurons, possibly due to inefficient transcription or translation (Dang et al., 2017).

AAV9

AAV9 is a commonly used and efficient tool for gene delivery to sensory neurons, particularly excelling in direct or regional delivery. It can achieve widespread coverage of dorsal root ganglia (DRG) across multiple spinal segments through intrathecal injection and mediate efficient local gene expression via direct ganglionic injection (Yu et al., 2016).

However, its relative efficiency is not optimal in all situations. For instance, in the trigeminal ganglion (TG) model, although AAV9 effectively drives gene expression, its efficiency is inferior to AAV1, highlighting performance differences between serotypes in specific neural pathways (Dang et al., 2017). Efficiency also depends on the administration method. In adult mice via intrathecal injection, AAV9's DRG transduction

rate significantly exceeds rAAV2-retro (Skorput et al., 2022). However, when administration changes to systemic injection in neonatal rats, AAV9 and rAAV2-retro show comparable efficiency (O. J. Yang et al., 2023).

AAV-PHP Series

The AAV-PHP series consists of novel capsids developed through an in vivo directed evolution strategy in mouse models, specifically using the CREATE (Cre recombinase-based AAV Targeted Evolution) platform. This technology was designed to select for variants with an enhanced ability to cross biological barriers (Deverman et al., 2016). Among them, AAV-PHP.eB primarily enhances crossing the blood-brain barrier (BBB) into the central nervous system, while PHP.s has reduced BBB penetration, making it more suited to the PNS. AAV-PHP.S, when administered intravenously in specific mouse strains (like C57BL/6J), achieves DRG transduction efficiency far exceeding AAV9. However, its advantage is strain and species-dependent, making it difficult to effectively reproduce in non-human primates, which constitutes a major obstacle to its clinical translation (Asencor et al., 2022; Chan et al., 2017; Deverman et al., 2016).

AAV-Retro

AAV-Retro was created through the innovative method of "in vivo directed evolution." Researchers conducted multiple rounds of screening in live animal models from a vast library of AAV2 capsid mutations, ultimately selecting this variant with superior retrograde transport capability. Its core mechanism is that when injected into areas with nerve terminal distribution, it can be efficiently taken up by axons and retrogradely transported to neuronal cell bodies, thereby achieving labelling of specific projection neuron populations (Tervo et al., 2016). Beyond its use as a local tracing tool, rAAV2-retro also demonstrates unique cellular targeting in systemic administration. A study in

neonatal rats found that after systemic delivery via intraperitoneal injection, AAV-Retro's overall transduction efficiency in dorsal root ganglia (DRG) was comparable to AAV9 and PHP.S. More importantly, it showed a distinct preference for large-diameter, myelinated sensory neurons (NF200-positive) (O. J. Yang et al., 2023).

AAV-DJ

AAV-DJ was created through DNA family shuffling technology, randomly recombining capsid genes from 8 different natural serotypes. This design endows AAV-DJ with extremely broad tissue tropism, particularly in in vitro cell experiments, where its transduction efficiency for various cell lines far exceeds traditional serotypes like AAV2 (Grimm et al., 2008). Currently, literature on AAV-DJ directly and quantitatively targeting DRG/TG sensory neurons is sparse; DJ's highlights are more in olfactory sensory neurons, while its effectiveness in PNS sensory neurons still requires independent verification.

1.3 Human iPSC-derived sensory neurons.

The emergence of human-induced pluripotent stem cell (iPSC) technology has reshaped the paradigm of neurological disease modelling and gene delivery assessment (Takahashi et al., 2007). By reprogramming somatic cells into a pluripotent state and directing their differentiation into specific neuronal cell types, the iPSC platform circumvents ethical and quantitative limitations in obtaining human neurons while preserving patient-specific genetic backgrounds. This facilitates scalable and standardised operations, significantly enhancing the comparability between in vitro models and clinical contexts.

In peripheral sensory system research, small molecule differentiation strategies based on dual SMAD inhibition can efficiently generate iPSC-derived sensory neurons (iPSC SNs), which demonstrate high consistency with in vivo human neurons at transcriptional, marker, and electrophysiological levels (Chambers et al., 2012; Clark et al., 2017).

Compared to traditional rodent or primate animal models, iPSC SNs exhibit greater clinical relevance and have been successfully applied in research areas such as neurotoxicity screening and neurodegenerative diseases (Engle et al., 2018; Tukker et al., 2018; Xiong et al., 2021). For gene delivery research, AAV entry exhibits significant cross-species differences, affecting transduction efficiency and cell type preferences of different serotypes and engineered capsids (Hordeaux et al., 2018). Human-derived models are expected to enhance better the extrapolation of in vitro results to clinical applications. Additionally, with the expanding gene therapy toolkit and continuous emergence of new variants, it is necessary to reassess the relative advantages of traditional gold standards like AAV9 in sensory neurons within an authentic human context.

1.4 Research Objectives

Evaluating rAAV transduction efficiency and safety in model systems more closely resembling human physiology serves as a crucial “bridge” connecting animal experiments to clinical applications. These considerations drive the core objective of this study: to systematically compare the transduction efficiency and safety of different rAAV serotypes and variants in sensory neurons derived from human iPSCs. This aims to identify AAV tools suitable for the nervous system with greater clinical translation potential. This research not only addresses performance differences of AAV vectors across species but also reassesses AAV9's dominant position in sensory neuron transduction amid the emergence of new variants. We have established two research objectives. The systematic evaluation of the transduction efficiency of 13 AAV serotypes in human iPSC-derived sensory neurons, and examination of the impact of different serotypes and doses on neuronal health status, including assessment of axonal morphology and cell survival.

2. Methods

2.1 Human iPSC-derived Sensory Neuron Differentiation and AAV Transduction

This study utilised the control human iPSC cell line (AD3) (Clark et al., 2017). Cells were maintained and expanded in mTeSR1 medium (STEMCELL Technologies, 85850) until reaching approximately 70-80% confluence. The medium was then changed to mouse embryonic fibroblast conditioned medium (MEF conditioned medium; R&D Systems, AR005) supplemented with FGF2 (10 ng/ml) for 24 hours to stabilise cell density and state to approximately 50% confluence before initiating differentiation. Subsequently, following a modified 11-day Chambers differentiation, which is established to generate a population enriched in nociceptor-like sensory neurons as previously characterized by the expression of typical peripheral sensory markers and nociceptor-specific channels. protocol (Chambers et al., 2012; Clark et al., 2017). Differentiation was initiated on Day 0 with KSR medium containing dual SMAD inhibitors SB431542 (10 μM) and LDN193189 (100 nM); Day 1 maintained the same formulation; Days 2-3 continued with dual SMAD inhibition, with the addition of a three-inhibitor combination (3i) of CHIR99021 (3 μM), SU5402 (10 μM), and DAPT (10 μM) on Day 3.

From Day 4, the medium gradually transitioned from KSR to N2: Days 4-5 used 75% KSR/25% N2, Days 6-7 used 50% KSR/50% N2, Days 8-9 used 25% KSR/75% N2, and Day 10 used 100% N2; 3i (CHIR99021 3 μM, SU5402 10 μM, DAPT 10 μM) was continuously used from Day 5. On Day 11, immature neurons were gently dissociated using TrypLE and reseeded onto Matrigel-precoated coverslips or culture plates. After adhesion, ROCK inhibitor Y27632 (10 μM) was briefly added (approximately 24 hours),

and low-dose CHIR99021 (3 μM) was maintained until Day 14 to promote early neurite growth and survival.

After reseeding, the medium was changed to N2 supplemented with NGF, BDNF, GDNF, and NT3 (each at 25 ng/ml) to promote maturation. To enhance purity, cells were briefly treated with one μM AraC (24-48 hours, depending on cell condition) during the early stage. Mature and stable sensory neuron populations were typically obtained approximately 4 weeks after reseeding and used for AAV transduction experiments.

Four weeks after neuronal maturation, transduction experiments were conducted using AAV vectors carrying the EGFP reporter gene (provided by VVF ETH Zurich). The tested serotypes included AAV1-9, AAV-DJ, and AAV-PHP.eB, AAV-PHP.S, and AAV-Retro, with multiplicities of transduction (MOI) of 1K, 10K, and 100K. All AAV vectors carried the pAAV-CAG-EGFP-WPRE-SV40p(A) expression cassette, provided by the Viral Vector Facility, ETH Zurich.

2.2 Immunocytochemistry

Immunocytochemistry experiments were performed two weeks after viral treatment, primarily analysing transduction efficiency through NF200 and EGFP double labelling. Specifically, cells were fixed in 4% paraformaldehyde, washed with PBS, and permeabilised and blocked with PBS containing 0.1% Triton X-100 and 5% normal goat serum. Subsequently, samples were incubated overnight at 4°C with primary antibody (mouse anti-NF200, 1:400). The following day, after PBS washing, samples were incubated with Alexa Fluor-labelled secondary antibody (anti-mouse Alexa 546, 1:500 dilution) at room temperature for 1 hour. Slides were mounted and analysed by confocal microscopy.

For direct assessment of cell viability status (direct toxicity and bystander toxicity), Live/Dead cell staining was added before the above procedure: Two weeks after AAV treatment, live cells were co-incubated with Live/Dead dye working solution (1:2000 dilution in buffer) at 37°C for 20 min, with gentle washing once with pre-warmed PBS before and after incubation to remove serum and free dye, minimizing background while maintaining cell condition. Immediately after completing live cell staining, cells were fixed and subsequently stained for NF200 and DAPI following standard immunostaining protocols.

2.3 Image Acquisition

All images in this study were acquired using a Leica LSM 710 confocal microscope with Zeiss 2012 imaging software and a 20× objective. For each experimental condition, we analysed at least three independent coverslips (as biological replicates). On each coverslip, a 4×4 tile scan was performed to obtain large-area images, ensuring representativeness of the field of view. To ensure objectivity and comparability of analysis between different AAV serotype treatment groups, all images were acquired under identical laser power, gain, and offset settings.

2.4 Analysis Methods

2.4.1 Transduction efficiency quantification

Transduction Efficiency (%) = number of EGFP+/NF200+ neurons divided by total NF200+ neurons × 100%. NF200 immunofluorescence was used to identify sensory neurons. The EGFP signal defined transduced cells. For each condition, ⩾ five random fields per well and ⩾ three technical replicates were analysed in Fiji/ImageJ (NIH).

2.4.2 Axonal integrity assessment

NF200-stained images were used. Fields were randomly selected from axon-only regions (no somata) to avoid soma-derived signal bias.

Beading Index (early axonal stress). To quantify early axonal stress, we established a beading index based on the established pathological feature of axonal swelling (Kneynsberg et al., 2016). Total axonal area was segmented by global thresholding. Beaded segments were identified as contiguous axonal regions with a local diameter ⩾ 1.5× the median axonal diameter within the same field. Beading Index = area of beaded axons / total axonal area.

Degeneration Index (late structural damage). To measure late-stage structural damage, we adapted a degeneration index based on the quantification of axonal fragmentation (Arrázola et al., 2019). Fragmented axonal elements were segmented using Fiji "Analyse Particles" after binarisation and skeleton exclusion, with size and circularity ranges pre-registered before analysis. Degeneration Index = area of fragmented axons / total axonal area.

2.4.3 Cytotoxicity Assessment

Cytotoxicity was evaluated using two complementary methods.

First, a Transduction-Associated Death Index (TADI) was calculated from fixed samples as a high-throughput proxy for toxicity. We classified EGFP+/NF200− circular bodies as apoptotic remnants of transduced cells (TD) and morphologically intact EGFP+/NF200+ neurons as transduced-alive (TA). The index was calculated as: TADI (%) = TD / (TA + TD) × 100%

Second, to more accurately quantify and distinguish toxicity mechanisms, a Live/Dead assay was performed on representative serotypes before fixation. This enabled cell classification into four groups based on viability dye uptake and EGFP expression: Transduced-Alive (TA: EGFP+, Live), Transduced-Dead (TD: EGFP+, Dead), Untransduced-Alive (UA: EGFP−, Live), and Untransduced-Dead (UD: EGFP−, Dead). This classification was used to calculate two distinct metrics:

Direct Toxicity Rate (%): TD / (TA + TD) × 100%

Bystander Toxicity Rate (%): UD / (UA + UD) × 100%

2.5 Statistical Analysis

Sample size was determined a priori from pilot data to detect a 20% difference in transduction efficiency at $\alpha = 0.05$ with > 80% power.

Data were analysed in GraphPad Prism 10 and are reported as mean ± SEM. For each MOI, group differences were assessed by ordinary one-way ANOVA. Model assumptions were checked in Prism (normality of residuals; homogeneity of variances via Brown–Forsythe). If variances were unequal, Welch's ANOVA was used. When the omnibus test was significant, Dunnett's multiple comparisons test compared each AAV group to the control, and multiplicity-adjusted two-sided P values were reported. Significance thresholds: *p < 0.05, **p < 0.01, ***p < 0.001, ****p < 0.0001.

3. Results

3.1 Generation of hiPSC-derived Sensory Neurons

To systematically evaluate the performance of different AAV serotypes in human iPSC-derived sensory neurons, we established and followed a standardised experimental protocol (Figure 5.1). Based on a modified Chambers differentiation protocol, we

successfully obtained sensory neuron populations from human iPSCs. Immunofluorescence revealed robust expression of the sensory neuron marker NF200 and formation of dense axonal networks, indicating morphological and phenotypic maturation, which provided a reliable in vitro platform for subsequent AAV evaluation. The study included 13,772 cells, over a hundred coverslip images, and more than 400 axon images, providing a robust statistical foundation for our conclusions.

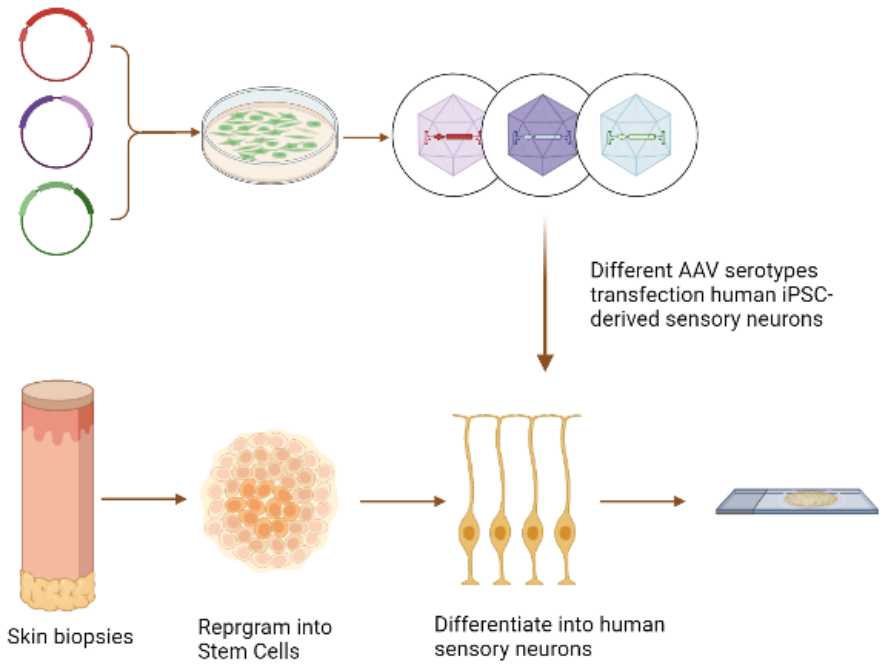

Figure 5.1: Experimental workflow for evaluating AAV in human iPSC-derived sensory neurons.

Skin biopsies were reprogrammed to iPSCs, differentiated to sensory neurons using a modified Chambers protocol (Day 0–10), replated on Day 11 and matured for ~4 weeks. Neurons were transduced with a CAG-EGFP reporter packaged in AAV1–AAV9, AAV-PHP.eB, AAV-PHP.S, AAV-DJ, or AAV-Retro at MOIs of 100k,10k,1k. Readouts included transduction efficiency, axonal integrity indices, and cytotoxicity.

3.2 Comparison of Transduction Efficiency Among AAV Serotypes

We systematically compared the transduction efficiency of multiple AAV serotypes in human iPSC-derived sensory neurons, testing each serotype at three different multiplicities of infection (MOI: 1k, 10k, 100k). Results are summarised in Table 5.1 and Figure 5.2.

At the lowest tested concentration (1k MOI), most serotypes showed low transduction activity, but some already demonstrated high performance. AAV-PHP.S was most outstanding, achieving a transduction efficiency of up to 72.0 ± 0.3%, significantly higher than other serotypes. AAV-3 (54.5 ± 5.4%), AAV-DJ (46.8 ± 2.5%), and AAV-2 (45.0 ± 5.7%) also showed considerable transduction capability. In contrast, AAV-7, AAV-5, and AAV-8 had very low efficiency, all below 4%. This finding suggests that AAV-PHP.S has a high intrinsic affinity for human sensory neurons even at low viral loads.

As viral concentration increased to 10k MOI, most serotypes showed significant improvement in transduction efficiency. For example, AAV-PHP.eB's transduction efficiency soared to 98.6 ± 0.4%, approaching saturation. AAV-2 (94.0 ± 0.9%), AAV-3 (93.6 ± 1.1%), and AAV-PHP.S (92.9 ± 0.8%) all exceeded 90% efficiency. In stark contrast, AAV-4 (12.4 ± 1.1%), AAV-5 (11.0 ± 0.5%), and AAV-7 (11.5 ± 0.9%) remained limited at this concentration, suggesting these serotypes have relatively low transduction efficiency for target cells.

At the highest tested concentration (100k MOI), multiple serotypes reached near-saturated levels. AAV-3 (99.7 ± 0.3%), AAV-6 (99.6 ± 0.2%), and AAV-PHP.S (99.4 ± 0.3%) approached 100% efficiency, demonstrating a very high transduction ceiling. Additionally, several other serotypes, including AAV-DJ, AAV-2, and AAV-9, also approached saturation, with efficiencies generally exceeding 90%. Notably, AAV-4 and

AAV-5 still performed poorly at this high concentration, at 38.0 ± 4.1% and 55.9 ± 12.5%, respectively. Especially for AAV5, despite an increased mean value, the large standard deviation (±12.5%) suggests potential instability in its transduction performance at this concentration.

Based on these dose-response characteristics, we categorized the tested serotypes into three functional classes: 1) High-Efficiency/Potency, represented by AAV-PHP.S, which shows excellent transduction even at low MOI; 2) Dose-Responsive, typified by AAV9, whose efficiency increases dramatically with increased dosage; and 3) Low-Efficiency, such as AAV-4 and AAV-5, which show poor transduction efficiency at all tested concentrations. To illustrate these differences, Figure 5.3 presents fluorescence micrographs of these three representative vectors (AAV-PHP.S, AAV9, AAV4) at 100k MOI.

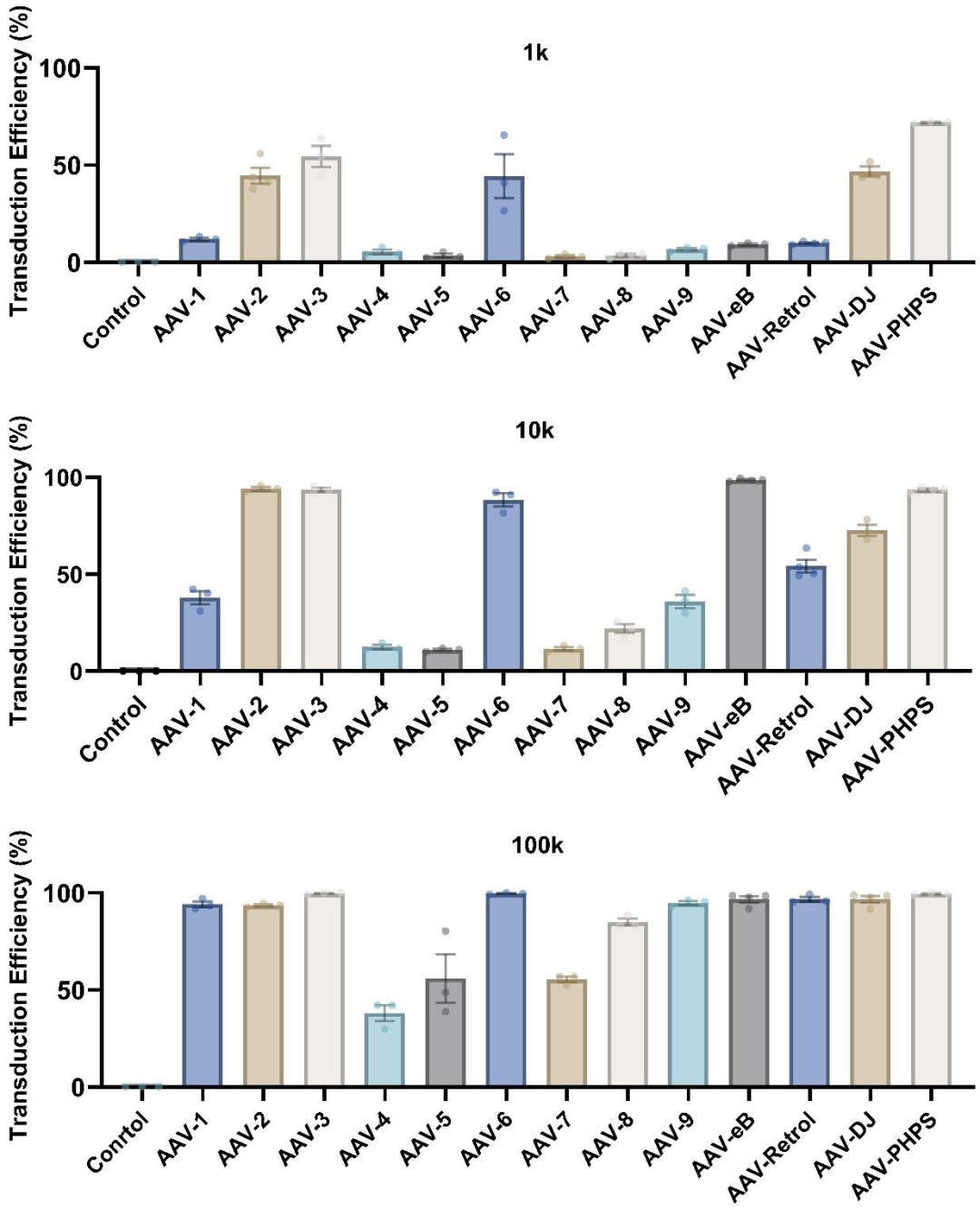

Figure 5.2. Quantification of Transduction Efficiency across AAV serotypes at 1k, 10k, and 100k MOI.

Human iPSC-derived sensory neurons were transduced with 13 different AAV serotypes at three multiplicities of infection (MOI): 1,000 (1k), 10,000 (10k), and 100,000 (100k). Transduction efficiency was quantified two weeks later as the percentage of NF200-positive neurons co-expressing the EGFP reporter gene. Data are presented as mean ± SEM from three independent replicates ($n \geq 3$).

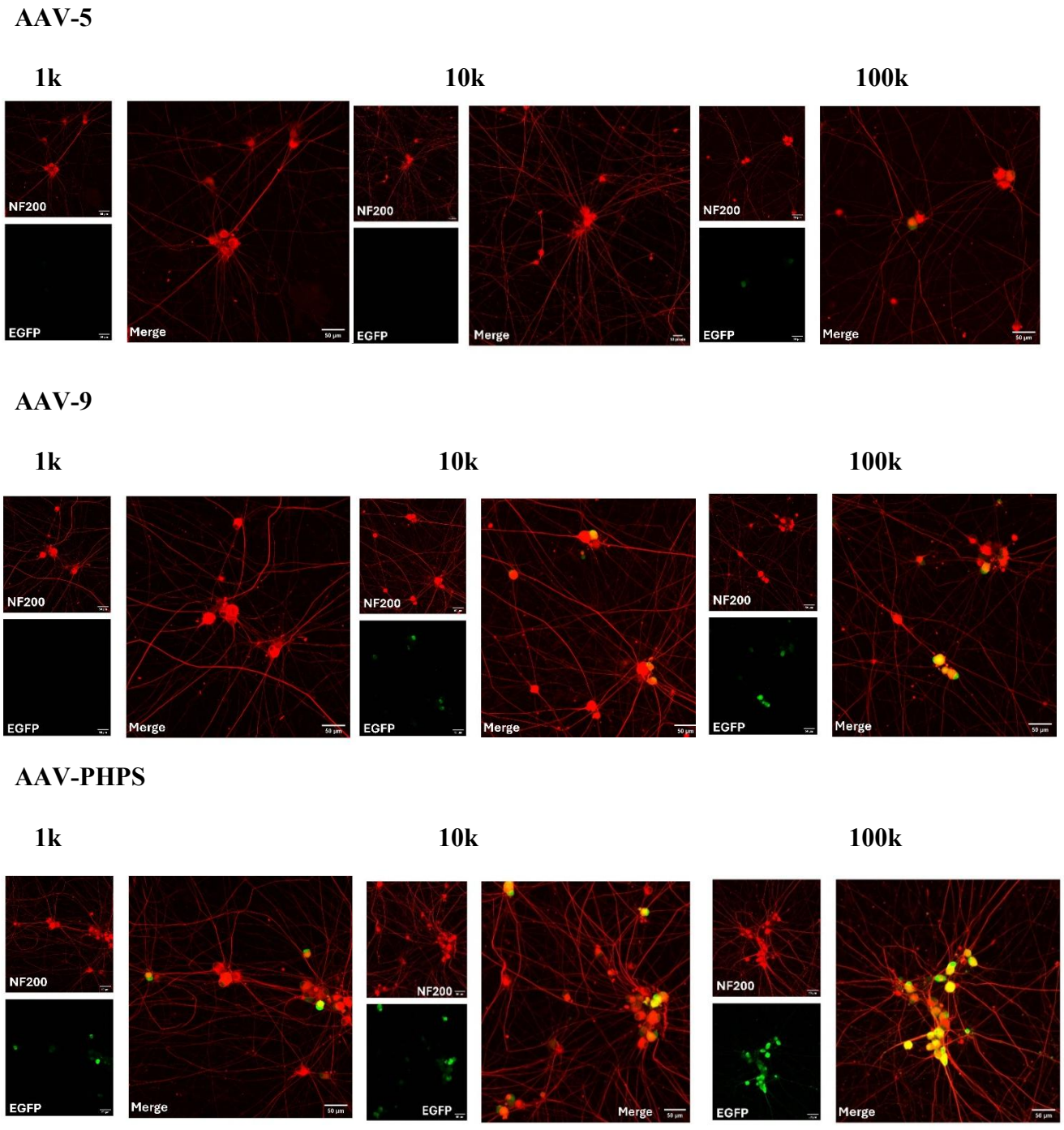

Figure 5.3: Representative images of AAV-5, AAV-9 and AAV-PHP.S showing transduction patterns at different MOIs (1k, 10k, 100k).

This panel array illustrates the transduction efficiency of three different AAV serotypes on primary neuronal cultures at three graded concentrations. Neurons were identified by immunofluorescence staining for NF200 (**red**), while cells successfully transduced by the eGFP-expressing AAVs are visualised by their green fluorescence (**green**).

3.3 Assessment of Axonal Integrity

An ideal gene delivery vector requires not only high transduction efficiency but also equivalent safety. To assess the potential impact of AAV transduction on the health status of human sensory neuron axons, we conducted quantitative analysis at two levels: examining early axonal stress responses through a Beading Index and evaluating late structural damage through a Degeneration Index.

We first focused on beading, considered an early sign of axonal dysfunction (Table 5.2 and Figure 5.4). At low viral concentration (1k MOI), axons in all treatment groups remained healthy, with beading indices showing no significant difference compared to untreated controls. However, when the concentration increased to moderate levels (10k MOI), early effects began to emerge for some serotypes. Neurons treated with AAV-PHP.S showed increasing beading indices. This dose-dependent effect became evident at the highest concentration (100k MOI), where AAV-PHP.S caused the most severe beading, followed by AAV-Retro.

We next asked whether this early functional stress response would eventually evolve into irreversible structural damage. For this, we used the Degeneration Index (DI) to quantify axonal fragmentation (Table 5.3 and Figure 5.5). A notable observation was that, despite observable early beading at moderate viral concentrations, this did not translate into statistically significant axonal degeneration. At high concentrations, 100k MOI, serotypes that caused early stress, such as AAV-PHP.S, now also caused statistically significant axonal degeneration. (Figure 5.6)

Taken together, these findings suggest a potential progression from early stress to late damage. At high viral loads, some AAV serotypes initially induce functional beading in axons, and if the dose is sufficient, this change can progress to irreversible structural

degeneration. This finding indicates that when using high viral doses to achieve high transduction efficiency, viral load must be carefully evaluated and controlled to avoid damage to the long-term structural integrity of neurons.

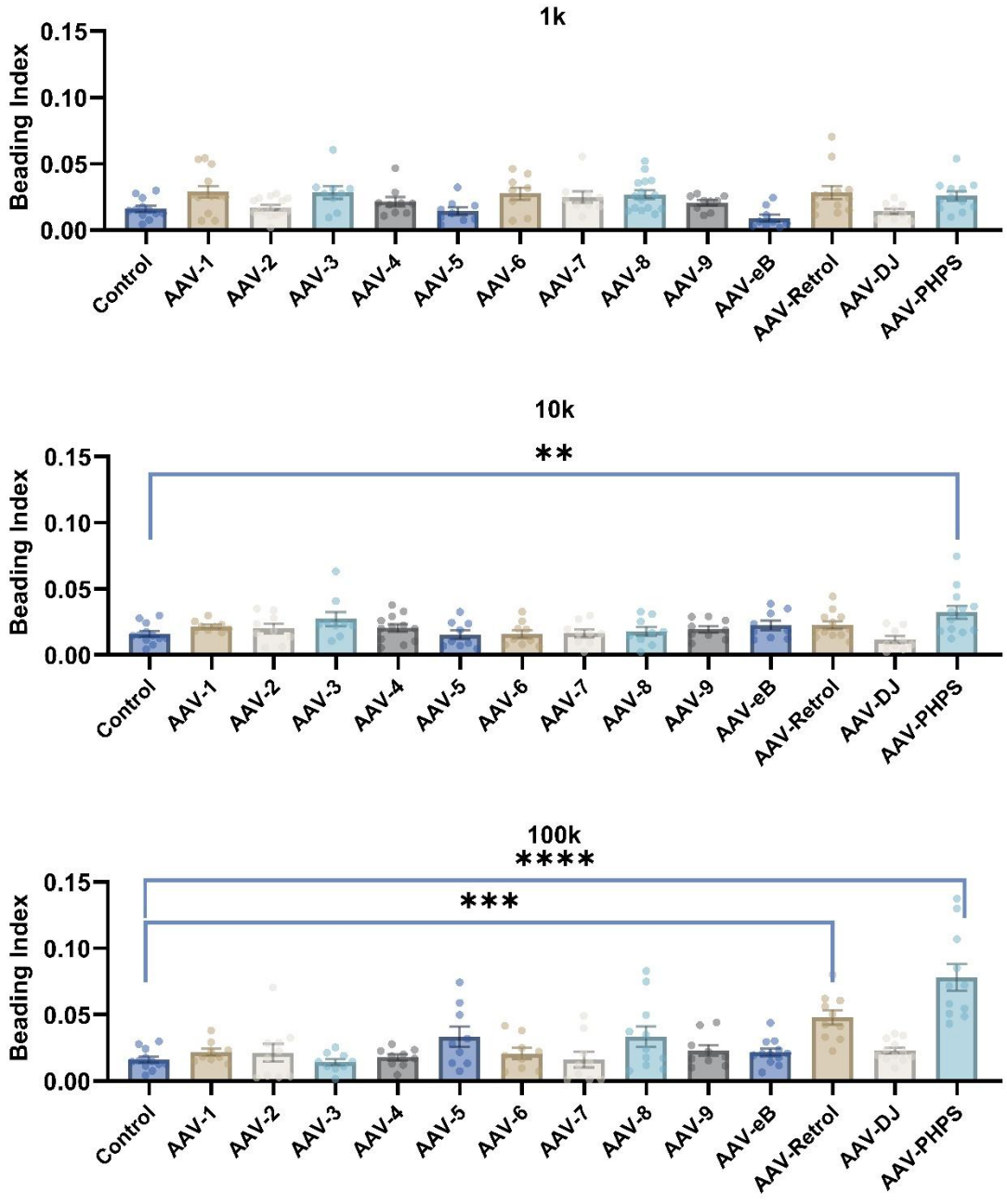

Figure 5.4. Quantitative assessment of beading index variations among AAV serotypes at 1k, 10k, and 100k MOI.

The Beading Index, a measure of early axonal stress, was quantified from NF200-stained axons two weeks after transducing human iPSC-derived sensory neurons with

AAVs at 1k, 10k, and 100k MOI. Each bar represents the mean ± SEM (n ≥ 3). Asterisks indicate significant differences from the untreated control group, determined by one-way ANOVA with Dunnett's multiple comparisons test (*p < 0.05, **p < 0.01, ***p < 0.001, ****p < 0.0001).

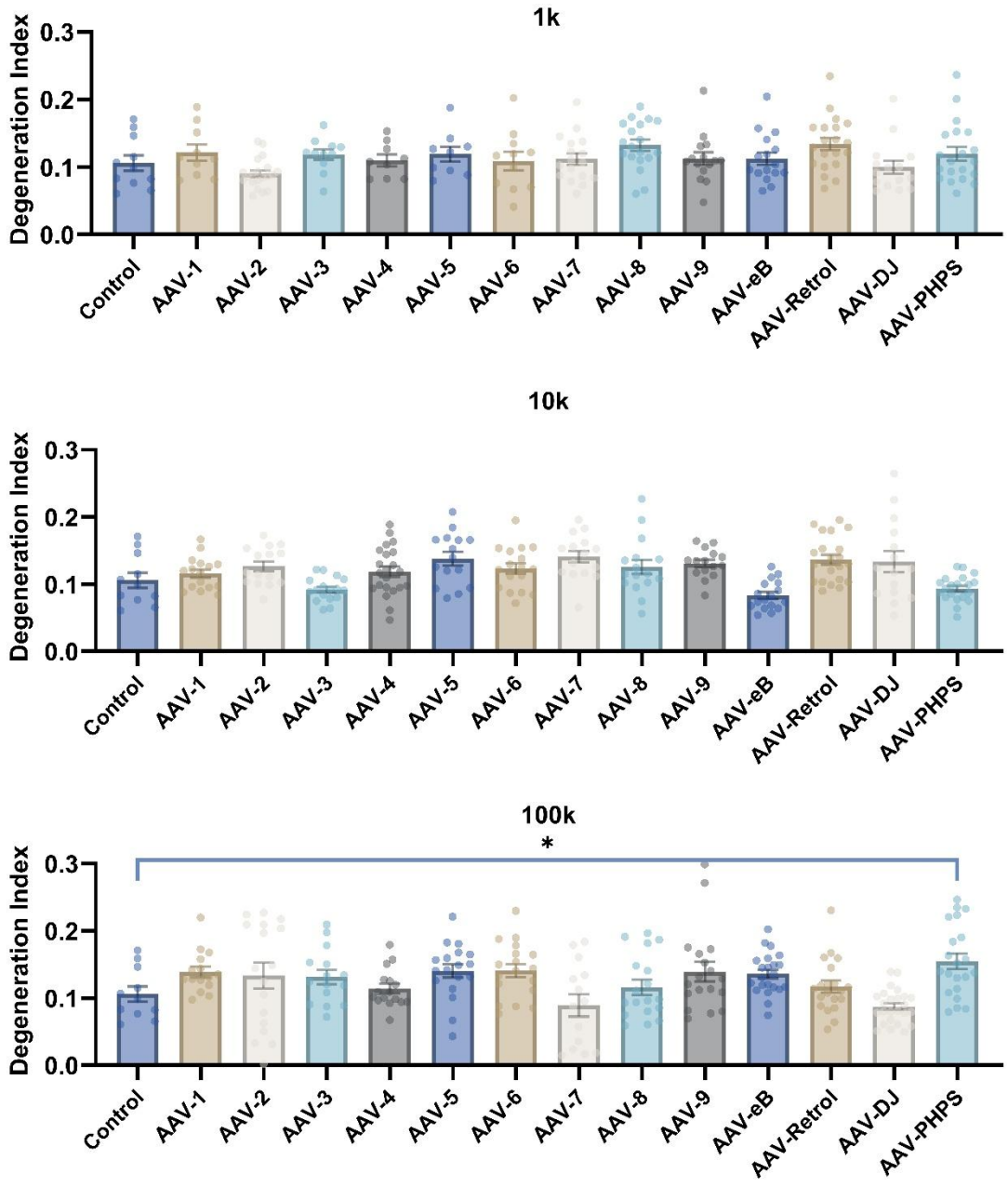

Figure 5.5. Analysis of axonal degeneration index across serotypes at 1k, 10k, and 100k MOI.

The Degeneration Index, a measure of late-stage structural damage (axonal fragmentation), was quantified from NF200-stained axons two weeks after treating human iPSC-derived sensory neurons with AAVs at 1k, 10k, and 100k MOI. Each bar represents the mean ± SEM ($n \geq 3$). Asterisks indicate significant differences from the untreated control group, determined by one-way ANOVA with Dunnett's multiple comparisons test (*$p < 0.05$, **$p < 0.01$, ***$p < 0.001$, ****$p < 0.0001$).

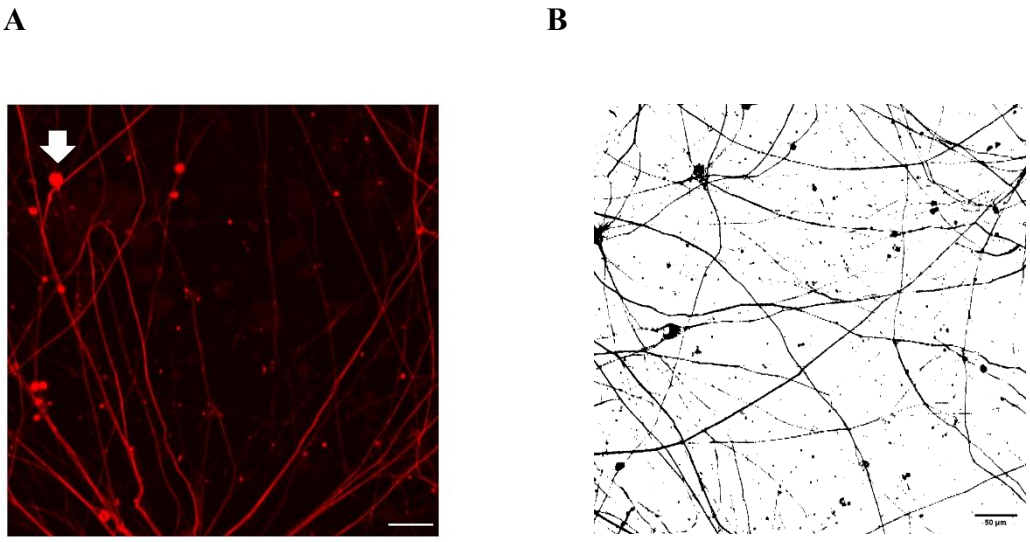

Figure 5.6: Morphological evidence of dose-dependent axonopathy following AAV-PHP.S transduction.

To visualise the cytopathological effects of high-dose AAV-PHP.S, human iPSC-derived sensory neurons were treated with 100k MOI and assessed for axonal integrity two weeks later via NF200 immunocytochemistry (red). Images depict damage occurring in a cell-autonomous fashion, as the affected neurons were confirmed to be EGFP-positive.

A. An example of moderate axonopathy, presenting as prominent axonal beading (arrow), an indicator of disrupted cytoskeletal structure and transport.

B. An example of axonopathy degeneration. Scale bars = 50um

3.4 Cell Death

While axonal morphological integrity is an important indicator of neuronal health, the ultimate safety assessment remains cell survival and death. To systematically evaluate the final impact of different AAV serotypes on neuronal survival, we adopted two complementary strategies. First, an endpoint morphological assessment was conducted to count "EGFP-positive cell bodies" that were not NF200 immunoreactive in fixed samples. This criterion followed the assumption that cells were transduced, expressed the EGFP transgene, but subsequently died. This allowed us to complete a broad-spectrum toxicity screen. While a good proxy for cell death, we also complemented these methods with an independent, more accurate, real-time live/dead assay using representative AAV serotypes.

3.4.1 Broad Cell Toxicity Screening

In the aforementioned coverslips, besides morphologically healthy EGFP-positive neurons, we also observed numerous rounds of EGFP-positive but neurofilament protein NF200-negative structures. We inferred these structures to be apoptotic bodies originating from neurons that died after transduction. The formation mechanism may be that when a successfully transduced neuron initiates apoptosis due to vector-associated intrinsic toxicity, its cytoskeleton (including NF200) disintegrates. The cell then shrinks and rounds up, eventually fragmenting into multiple membrane-bound bodies containing stably expressed EGFP protein.

Based on this observation, we classified EGFP-positive populations into two categories. Successfully transduced and surviving neurons (Transduced-Alive, TA) appeared as EGFP+/NF200+, and residues of neurons that died after transduction (Transduced-Dead, TD) appeared as round EGFP+/NF200- bodies. Accordingly, we established a

Transduction-Associated Death Index (TADI) aimed at directly evaluating AAV-mediated post-transduction cell death. This index reflects the proportion of successfully transduced cells that ultimately died.

Table 5.4 and Figure 5.8 show the Transduction-Associated Death Index (TADI) for different AAV serotypes at different concentrations, presenting a complex, non-linear dose-toxicity relationship. The representative picture is shown in Figure 5.7A.

At low doses (1k MOI), most vectors showed no detectable toxicity, but AAV2, AAV3, AAV6, and AAV-PHP.S already exhibited initial toxicity of about 5-7%.

When the dose increased to moderate levels (10k MOI), toxicity patterns among serotypes showed significant divergence. TADI values for AAV2 and AAV-PHP.eB steadily increased to about 16%. Notably, a group of vectors (including AAV-PHP.S, AAV-DJ, AAV6, AAV-Retro) reached peak toxicity at this dose, with the range being 15% to 19%, and AAV-PHP.S showing the highest (19.31 ± 1.26%).

At the highest tested dose (100k MOI), toxicity patterns further evolved. AAV2's toxicity rose sharply to the highest point among all vectors (31.35 ± 1.68%), while AAV1's toxicity also significantly emerged at this high dose (20.86 ± 3.07%). In stark contrast, serotypes that showed high toxicity at medium doses, such as AAV6, AAV-DJ, and AAV-PHP.S, saw their TADI values significantly decrease at the highest dose. Meanwhile, AAV4, AAV5, and AAV7 maintained extremely low toxicity levels across all tested doses.

3.4.2 Direct Toxicity and Bystander Toxicity Based on Live/Dead Cell Staining

Our earlier TADI assessment relied on counting predicted apoptotic bodies in fixed samples. However, this endpoint assessment method, while effective, may be affected by inconsistent degradation rates after cell death or potential influences from the fixation

process itself. For more direct and accurate capture of cell survival status, we performed live/dead double staining on iPSCs after viral transduction but before cell fixation.

Based on transduction efficiency (Table 5.1) and cell toxicity (Table 5.4) data, we selected three representative serotypes: AAV-2 (high efficiency/high toxicity), AAV-9 (high efficiency/low toxicity), and AAV-PHP.eB (high efficiency/moderate toxicity). This combination not only covers different toxicity gradients but also includes both natural serotypes (AAV-2, AAV-9) and engineered serotypes (AAV-PHP.eB). We deliberately excluded AAV-PHP.S. Despite its significant toxicity characteristics, its known axonal toxicity is a key confounding variable. Since axonal damage can induce cell death, it is difficult to clearly distinguish whether cell death results from direct intrinsic viral toxicity or is secondary to axonal degeneration, thus complicating mechanistic analysis. This is something to be untangled and explored further in the future.

Two weeks after transduction at 100K MOI, we first performed live/dead cell staining, followed by fixation and imaging. This methodological improvement not only enhanced the immediacy and accuracy of assessment but, more importantly, provided a new interpretive dimension. By combining cell survival status (live/dead) with transduction status (EGFP positive/negative), we were able to distinguish and quantify two potential sources of toxicity in our study system: direct viral toxicity to transduced cells and possible bystander toxicity to non-cell-autonomous effects on untransduced cells.

Specifically, we categorised cells into four types (see methods for criteria): TA (Transduced-Alive), TD (Transduced-Dead), UA (Untransduced-Alive), UD (Untransduced-Dead). Based on this classification, we established two indices to describe AAV toxicity patterns: Direct Toxicity Rate, which aims to quantify the proportion of dead cells among all transduced cells, reflecting the intrinsic cellular toxicity of the virus,

and Bystander Toxicity Rate, used to measure the death proportion in untransduced cell populations to examine the indirect toxic effects caused by viral transduction. Detailed analysis of these parameters is shown in Table 5.5, Figure 5.9, and a representative picture in Figure 5.7B.

First, at the high doses tested, the final overall cell survival rates for all virus treatment groups were the same as those of the control group. Specifically, the neuronal survival rates after treatment with AAV2 (72.64%), AAV9 (74.00%), and AAV-PHP.eB (73.59%) showed no statistically significant differences compared to the control group's survival rate (75.14%). In terms of direct toxicity, there were no significant differences between serotypes. The mean direct toxicity rates for AAV2, AAV9, and AAV-PHP.eB were 9.73%, 8.83%, and 9.33%, respectively. Considering the large standard deviations in each group, these small differences lack statistical significance. This result suggests that the direct killing effects of these viral vectors on transduced cells are quite limited and similar. A more significant phenomenon appeared in bystander toxicity: all virus treatment groups showed higher bystander toxicity rates than the control group (24.83%), with values ranging from 44% to 54%. This strongly suggests that non-cell-autonomous toxic effects triggered by viral transduction may be a common and major toxicity feature of these AAV vectors when acting on sensory neurons at high doses.

Overall, when integrating all evidence chains, although preliminary TADI screening marked AAV-2 as "high risk," more reliable overall survival rate data negated this concern. Under current experimental conditions, the three high-efficiency serotypes AAV2, AAV9, and AAV-PHP.eB did not show clearly distinguishable advantages or disadvantages in safety. In the sensory neuron model, these candidate vectors may all have acceptable safety windows.

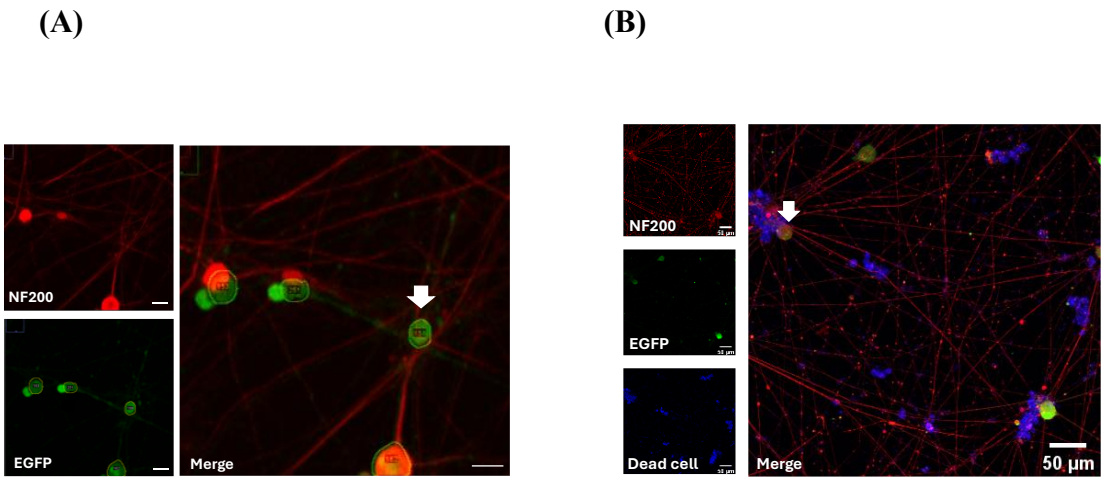

Figure 5.7: AAV-mediated transduction induces cytotoxicity

(A) Representative high-magnification images showing a neuron (NF200, red) successfully transduced with an eGFP-expressing AAV (EGFP, green). The arrow indicates a shrunken, EGFP-positive cell that has lost its NF200 immunoreactivity, consistent with an apoptotic body counted in the TADI analysis. Scale bars = 50 µm.

(B) Representative images from live/dead cell analysis. Neurons were identified by NF200 staining (red), transduced cells by eGFP expression (green), and dead cells were labelled with a viability dye (blue). This assay utilises a membrane-impermeable dye that only enters cells with compromised membranes (dead/dying), whereas NF200 (red) stains the internal cytoskeletal structure regardless of viability. The merged image clearly shows a cell that is triple-positive for NF200, eGFP, and the dead cell marker (indicated by the arrow), providing direct evidence of transduction-associated death in a target neuron. Scale bars = 50 µm.

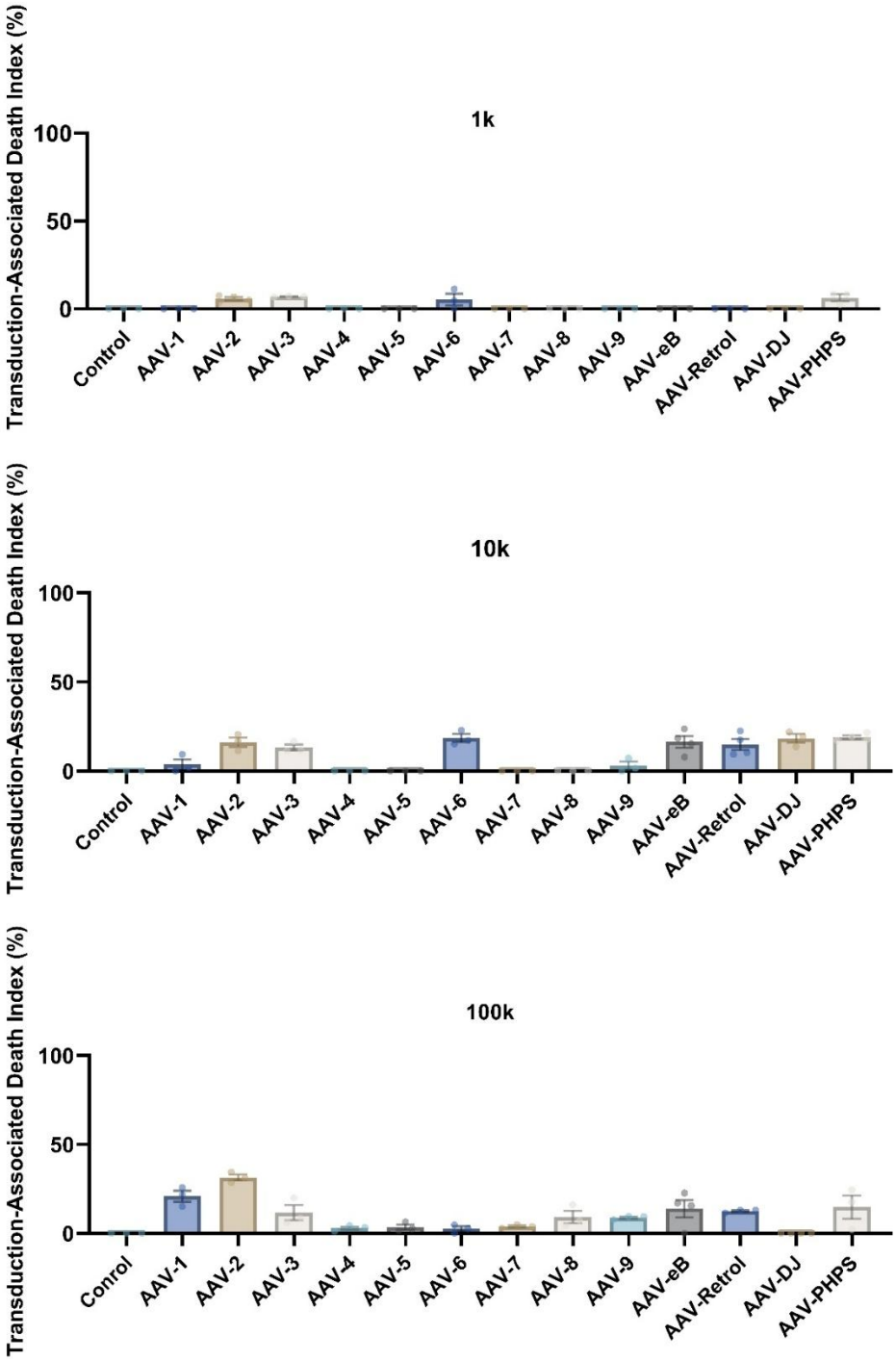

Figure 5.8. Analysis of transduction-associated death index across serotypes at 1k, 10k, and 100k MOI

The TADI was calculated two weeks post-transduction by quantifying the percentage of dead cells (identified as EGFP+/NF200− apoptotic bodies) relative to the total population of transduced cells. Each bar represents the mean ± SEM from three independent experiments ($n \geq 3$). Significance relative to the untreated **control was**

assessed via one-way ANOVA with Dunnett's multiple comparisons test (*p < 0.05, **p < 0.01, ***p < 0.001, ****p < 0.0001

A

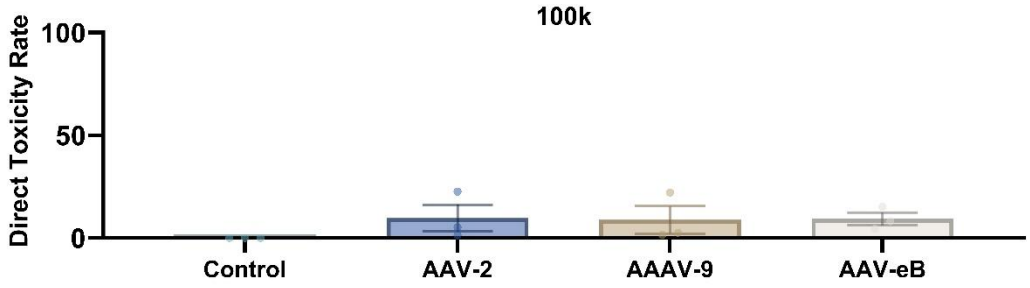

B

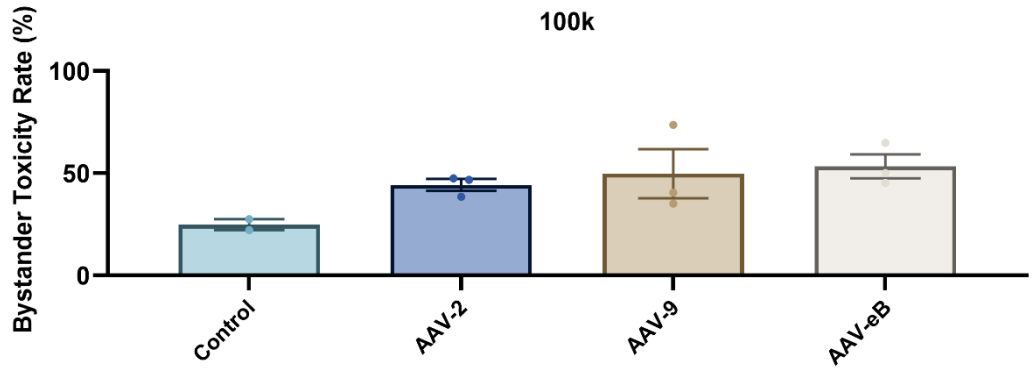

C

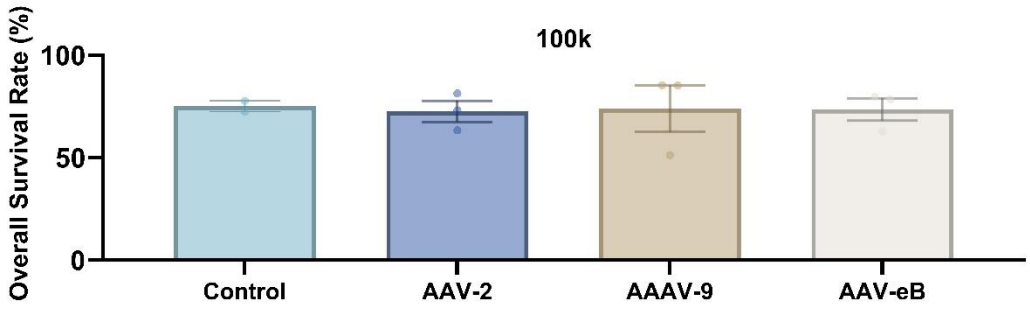

Figure 5.9. Quantification of direct toxicity, bystander toxicity, and overall survival using a Live/Dead assay at 100k MOI.

Human iPSC-derived sensory neurons were transduced with AAV-2, AAV-9, and AAV-eB at a multiplicity of infection (MOI) of 100,000. Cell viability was assessed

two weeks post-transduction using a Live/Dead assay to differentiate between toxicity mechanisms.

A. The Direct Toxicity Rate was calculated as the percentage of dead cells within the transduced (EGFP-positive) population.
B. The Bystander Toxicity Rate was calculated as the percentage of dead cells within the untransduced (EGFP-negative) population.
C. The Overall Survival Rate represents the total percentage of live cells in the culture. All bar charts display the mean ± SEM (control group n = 2, other group n = 3).

4. Discussion

This study systematically evaluated the performance of multiple AAV serotypes in human iPSC-derived sensory neurons, aiming to provide a data-driven basis for vector selection in sensory system gene therapy. Methodologically, this study established a multi-parameter safety assessment framework, quantifying axonal health as a more sensitive, early sub-lethal toxicity indicator than cell death. This approach provides a deeper, more comprehensive perspective for the preclinical evaluation of gene therapy vectors.

The performance of AAV-5 particularly highlights the necessity of this study. It is considered one of the most efficient serotypes in mouse models, but it was one of the worst performers in our human cell model (Vulchanova et al., 2010; Yu et al., 2016). This significant cross-species difference warns us that we cannot directly extrapolate the performance of viral vectors from animal models to human clinical applications.

A critical aspect of this framework involved reconciling data from different assessment methods, as a notable discrepancy arose when comparing our TADI (Total Apoptotic Debris Index) analysis with direct live/dead staining. The TADI analysis, based on apoptotic body counting, suggested extremely high toxicity for AAV-2 (~31%), while

live/dead staining indicated its toxicity was much lower (~9%), similar to AAV9 and AAV-PHP.eB. We attribute this significant difference not to more potent intrinsic cytotoxicity of AAV-2, but to the inherent biases of TADI as an endpoint morphological detection method. There are two likely reasons for this. First is the cumulative effect: TADI counts apoptotic bodies accumulated throughout the entire culture cycle. As this debris is difficult to clear completely in vitro, the readings reflect a cumulative total. Second is the signal amplification effect: a single dead cell may fragment into multiple apoptotic bodies, disproportionately amplifying the TADI reading. Hence, TADI likely overestimates per-cell death rates relative to instantaneous live/dead readouts and should be interpreted with caution.

Furthermore, the TADI analysis revealed a counterintuitive, non-linear dose-toxicity relationship for certain serotypes (e.g., AAV-6, AAV-DJ, AAV-PHP.S), where toxicity peaked at the 10k MOI and then unexpectedly decreased at the 100k MOI. A plausible explanation is that at extremely high viral loads (100k MOI), the toxic effects are so rapid that cells die and disintegrate before they can express detectable levels of EGFP. Consequently, these early-death cells would not be counted in the EGFP-positive Transduced-Dead (TD) population, artificially lowering the TADI score. Additionally, while the in vitro system lacks immune cells, neighbouring cells (such as other neurons or residual glia) may possess some capacity for debris clearance. It is possible that the moderate dose induced a wave of apoptosis that was readily detectable, whereas the highest dose triggered different death pathways or overwhelmed the system, altering the morphology or clearance efficiency of the resulting debris.

4.1 Balance Between Transduction Efficiency and Neuronal Safety

The core conclusion of this study is that AAV serotype selection is essentially about finding a balance between transduction efficiency and neuronal health. This trade-off is

particularly evident in the comparison between the engineered variant AAV-PHP.S and the natural serotype AAV9.

AAV-PHP.S's "high gain" comes with "high risk." AAV-PHP.S demonstrated excellent transduction efficiency at all tested doses, continuing its advantage seen in rodents (Chan et al., 2017). However, this "gain" coexists with risk. Our data show that high-dose AAV-PHP.S can induce severe axonal beading and cell death, indicating a relatively narrow safety window. It should be emphasised that this observation comes from an *in vitro* model of human iPSC-derived sensory neurons and cannot be directly equated to *in vivo* pathology. Studies have also pointed out that after high-dose AAV administration, most animals show no clinical symptoms, but autopsy reveals axonal degeneration and neuronal damage (Hinderer et al., 2018). In non-human primate models, blocking DRG toxicity by delivering miRNA-138 to reduce transgene expression suggests this adverse reaction is more likely related to the direct toxicity or expression burden of the transgene product, rather than being solely mediated by adaptive immunity (Ertl, 2022; Hordeaux et al., 2020).

AAV9's "robustness" stems from its "mild" biological characteristics. Natural serotype AAV9 demonstrated better safety, with minimal impact on neuronal survival and axonal health even at high doses. Evidence suggests AAV9 can achieve stable and manageable transgene expression within a reasonable dose range (Mendell et al., 2017). However, studies also suggest that dose-dependent dorsal root ganglion (DRG) toxicity remains a recognised risk, requiring mitigation through careful dose selection and delivery strategies (Hawley et al., 2025; Hinderer et al., 2018).

Unexpectedly, we observed bystander cell toxicity. A possible explanation for this is microenvironmental stress or viral infection-induced toxicity before transgene expression.

In the Live/Dead analysis, the AAV-PHP.eB group showed an overall survival rate similar to controls but a significantly higher proportion of bystander toxicity. We thus speculate that at high doses, efficient capsids can more easily trigger apoptotic mechanisms, perhaps related to microenvironmental stress or viral particle-induced stress, thereby increasing the risk to neighbouring untransduced cells. Alternatively, it is possible that these cells were indeed transduced but succumbed to a rapid, pre-expression toxicity before detectable levels of eGFP could be produced. This explanation remains a mechanistic inference awaiting further verification. Therefore, this indicates that although different serotypes may contribute differently to direct and bystander toxicity, their effects ultimately "converge to the same end," leading to similar overall survival outcomes.

It is important to note that serotype rankings in this iPSC model may differ from in vivo contexts due to the absence of systemic barriers. For example, while AAV-PHP.S ranks highest here due to superior cell entry, its performance in vivo depends heavily on crossing the BNB. Therefore, selecting a best serotype requires combining datasets: using iPSC data to screen for intrinsic capsid-receptor compatibility (cellular entry), and in vivo animal data to verify biodistribution and barrier penetration.

4.2 Axonal Pathology: From Early Reversible Stress to Late Irreversible Damage

By introducing axonal beading index and axonal degeneration index, this study not only observed but also quantified AAV-related neurotoxicity. Data show that AAV-PHP.S induces only beading at medium doses but causes both beading and axonal fragmentation at high doses. This toxicity manifests as a cascade process from early functional stress to

late structural collapse, consistent with classical axonal pathology theory (Misgeld & Schwarz, 2017; Waxman et al., 1995).

Axonal beading is a sensitive, reversible early warning. At moderate doses, some serotypes already induce significant axonal beading, while axons have not yet undergone large-scale breakage. The core mechanism is believed to be related to "traffic jams" caused by obstructed axonal transport and energy crises triggered by mitochondrial stagnation (Spillane et al., 2013; Waxman et al., 1995). If stress persists, axons will initiate a SARM1-mediated active self-destruction program. Interrupted axonal transport leads to the depletion of the protective molecule NMNAT2, which activates SARM1. SARM1 then destructively consumes NAD+, ultimately leading to cytoskeletal collapse and axonal fragmentation (Coleman & Höke, 2020; Essuman et al., 2017; Gilley et al., 2015).

4.3 Clinical Translation Implications and Strategies

The findings of this study provide strategic guidance for clinical translation of sensory system gene therapy.

First, for chronic diseases requiring long-term, stable expression with paramount safety (such as hereditary neuropathies), AAV-9 may be suitable. Its wide safety window is consistent with validated clinical experience in SMA treatment (Mendell et al., 2017), but its dose-related DRG toxicity should still be monitored. For efficiency-priority scenarios (such as short-term functional studies), low to medium doses of AAV-PHP.S are a powerful option, with the key being to define appropriate doses that keep axonal damage in the reversible stage.

Second, the pathological process of axonal damage suggests that monitoring markers such as neurofilament light chain (NfL) in cerebrospinal fluid or blood during clinical

trials may warn of dose-related toxicity earlier than clinical symptoms, providing a time window for dose adjustment (Khalil et al., 2018).

4.4 Research Limitations and Future Directions

As an *in vitro* study, this research has inherent limitations. The current model simplifies the complex physiological microenvironment, omitting key components like satellite glial cells, immune cells, and blood vessels. Crucially, this in vitro monolayer culture lacks the Blood-Nerve Barrier (BNB). Therefore, the high transduction efficiency observed here reflects cellular tropism (capsid-receptor binding) rather than the vector's ability to cross biological barriers from the systemic circulation. Future work should therefore employ more representative systems, such as DRG organoids, co-culture models, or organ-on-a-chip technology (Koyanagi et al., 2024; Lu et al., 2024).

The brief observation period also limits our understanding of long-term gene expression durability and potential delayed toxicity. This necessitates the development of improved long-term culture techniques and *in vitro-in vivo* bridging models, like transplanting human DRGs into immunodeficient mice (Zerboni & Arvin, 2011). Critically, validating these findings in human sensory neurons from organ donors and expanding to iPSC cohorts from diverse genetic backgrounds are essential next steps to address model fidelity and genetic influence.

Ultimately, future capsid engineering should integrate safety metrics, such as axonal health, directly into screening pipelines. This will enable the creation of next-generation vectors that optimally balance high efficiency with low toxicity, leveraging advanced design strategies like machine learning and structure-guided evolution (Bryant et al., 2021; Deverman et al., 2016; Zhu et al., 2024).

5. Conclusion

This study systematically compared multiple AAV serotypes in human sensory neurons, clearly revealing a critical trade-off between transduction efficiency and neurotoxicity. Our findings demonstrate that while AAV-PHP.S exhibits the highest transduction efficiency, it also induces significant, dose-dependent axonal degeneration and cytotoxicity. In stark contrast, AAV9 displays a superior safety profile, maintaining excellent neuronal biocompatibility across all tested concentrations, thereby offering a wider therapeutic window despite its more moderate efficiency. Consequently, our results establish AAV9 as the preferred serotype for long-term therapeutic applications demanding high safety, whereas AAV-PHP.S is the standout choice for short-term, efficiency-driven research scenarios. Serotypes AAV4, AAV7, and AAV8 are not recommended for this system due to poor performance.

Beyond these specific recommendations, our work introduces a multi-parameter assessment framework that serves as a more sensitive and mechanistically insightful tool for evaluating AAV vector performance. These findings provide a solid experimental basis for optimising gene therapy strategies for the sensory nervous system. Ultimately, this research lays the foundation to accelerate the translation of basic research to clinical applications, particularly for the development of novel treatments like chemogenetic silencing therapies for chronic pain.

6. Acknowledgements

Thanks to Dr Alex Clark and Dr Pao Sheng Chang for providing the iPSC cell line. The experiments in this section were completed under the guidance of Dr Steve Middleton.

7. Appendices

Summary Table of AAV Serotype Performance in Sensory Neurons

Serotype	Key Characteristics & Strengths	Performance in Sensory Neurons (DRG/TG)	Limitations & Weaknesses	Key References
AAV1	Supports axonal transport. Anterograde transsynaptic tagging.	High efficiency in TG peripheral retrograde model (~20-25%). Inferior to AAV5 for direct DRG injection.	Overall expression is not the highest in all paradigms.	Dang et al., 2017; Mason et al., 2010; Zingg et al., 2017, 2022
AAV2	Most widely studied serotype, often a benchmark.	Transduces DRG neurons *in vitro* and *in vivo*. Low to moderate overall efficiency, inferior to AAV5, 6, and 8.	Limited utility for modern high-efficiency studies due to lower comparative efficiency.	Glatzel et al., 2000; Mason et al., 2010
AAV3, AAV4	N/A	Low transduction efficiency in direct DRG injection.	Significantly inferior to other serotypes. Minimal reports or applications.	Mason et al., 2010
AAV5	Highly efficient to DRG transduction. Higher gene transfer efficiency than AAV2 in the CNS.	Very high efficiency via direct DRG or intrathecal injection. Preferentially targets large-diameter neurons. Strong coverage of CGRP+ neurons.	Near-zero protein expression in the TG peripheral retrograde model.	Dang et al., 2017; Mason et al., 2010; Vulchanova et al., 2010; Yu et al., 2016
AAV6	Highly efficient for nociceptive neurons.	High efficiency (~60%) in DRG via the intrathecal route. Preferentially targets small- and medium-diameter nociceptors.	Specificity for nociceptors may be a limitation if broad targeting is desired.	Towne et al., 2009; Vulchanova et al., 2010; Yu et al., 2016
AAV7	N/A	Moderate efficiency. Lower than AAV1 in	Limited systematic	Dang et al., 2017

Serotype	Key Characteristics & Strengths	Performance in Sensory Neurons (DRG/TG)	Limitations & Weaknesses	Key References
		the TG peripheral retrograde model.	comparative data available	
AAV8	Effective via multiple routes (direct, IT, IM, IV). Self-complementary (scAAV) versions used to enhance expression.	Efficiently transduces DRG neurons. Preferentially targets large-diameter neurons	Inefficient protein expression in the TG retrograde model.	Dang et al., 2017; Fischer et al., 2011; Storek et al., 2008; Vulchanova et al., 2010
AAV9	Common tool for sensory neurons. Widespread coverage via intrathecal injection.	High efficiency via direct or intrathecal routes. Inferior to AAV1 in TG retrograde model. Efficiency varies with delivery method and age.	Not always the optimal serotype; performance is context dependent.	Dang et al., 2017; Skorput et al., 2022; Yang et al., 2023; Yu et al., 2016
AAV-PHP Series (e.g., PHP.S)	Engineered to cross biological barriers. PHP.S is optimised for the PNS.	Far exceeds AAV9 for DRG transduction via IV route in C57BL/6J mice.	Advantage is strain and species-dependent; fails to translate to non-human primates	Asencor et al., 2022; Chan et al., 2017; Deverman et al., 2016
AAV-Retro (rAAV2-retro)	Engineered for superior retrograde transport. Excellent for tracing projection neurons.	Systemic delivery in neonates shows a preference for large-diameter, myelinated (NF200+) sensory neurons.	Primarily a retrograde tool; systemic use has a particular tropism.	Tervo et al., 2016; Yang et al., 2023
AAV-DJ	Chimeric capsid with very broad tropism, especially *in vitro*.	Highlights are in olfactory sensory neurons.	Sparse data for direct targeting of DRG/TG sensory neurons.	Grimm et al., 2008

Table 5.1. Transduction efficiency of different AAV serotypes across MOIs

AAV	MOI 100k	MOI 10k	MOI 1k
Control	2.6 ± 0.4	2.6 ± 0.4	2.6 ± 0.4
AAV-1	94.1 ± 1.5	37.8 ± 3.5	11.9 ± 0.8
AAV-2	93.6 ± 0.5	94.0 ± 0.9	44.7 ± 4.0
AAV-3	99.7 ± 0.3	93.6 ± 1.1	54.5 ± 5.4
AAV-4	38.0 ± 4.1	12.4 ± 1.1	5.5 ± 1.1
AAV-5	55.9 ± 12.5	11.0 ± 0.5	3.6 ± 0.9
AAV-6	99.6 ± 0.2	88.3 ± 3.3	44.38 ± 11.4
AAV-7	55.3 ± 1.5	11.5 ± 0.9	3.0 ± 0.7
AAV-8	85.0 ± 1.8	21.9 ± 2.3	3.7 ± 0.6
AAV-9	94.8 ± 1.0	35.9 ± 3.3	6.7 ± 0.6
AAV-eB	96.7 ± 1.6	98.6 ± 0.4	9.3 ± 0.5
AAV-Retro	96.9 ± 1.2	54.2 ± 3.2	10.0 ± 0.3
AAV-DJ	96.8 ± 1.7	72.6 ± 2.9	46.8 ± 2.5
AAV-PHPS	99.4 ± 0.3	93.4 ± 0.7	72.0 ± 0.3

Table 5.2. Effects of AAV serotype and dose on the axonal Beading Index

AAV	MOI 100k (Beading Index)	MOI 10k (Beading Index)	MOI 1k (Beading Index)
Control	0.0160 ± 0.0022	0.0160 ± 0.0022	0.0160 ± 0.0022
AAV-1	0.0215 ± 0.0026	0.0215 ± 0.0014	0.0288 ± 0.0044

AAV	MOI 100k (Beading Index)	MOI 10k (Beading Index)	MOI 1k (Beading Index)
AAV-2	0.0213 ± 0.0067	0.0201 ± 0.0036	0.0170 ± 0.0018
AAV-3	0.0141 ± 0.0024	0.0272 ± 0.0053	0.0284 ± 0.0048
AAV-4	0.0176 ± 0.0023	0.0204 ± 0.0029	0.0213 ± 0.0036
AAV-5	0.0332 ± 0.0077	0.0152 ± 0.0033	0.0142 ± 0.0029
AAV-6	0.0207 ± 0.0042	0.0158 ± 0.0030	0.0276 ± 0.0045
AAV-7	0.0160 ± 0.0059	0.0163 ± 0.0029	0.0249 ± 0.0043
AAV-8	0.0333 ± 0.0079	0.0177 ± 0.0034	0.0268 ± 0.0032
AAV-9	0.0230 ± 0.0042	0.0194 ± 0.0025	0.0206 ± 0.0019
AAV-eB	0.0215 ± 0.0028	0.0223 ± 0.0035	0.0090 ± 0.0026
AAV-Retro	0.0479 ± 0.0054	0.0225 ± 0.0029	0.0282 ± 0.0051
AAV-DJ	0.0228 ± 0.0023	0.0117 ± 0.0027	0.0140 ± 0.0021
AAV-PHPS	0.0780 ± 0.0100	0.0322 ± 0.0048	0.0258 ± 0.0034

Table 5.3. Effects of AAV serotype and dose on the axonal Degeneration Index

AAV	MOI 100k (Deg. Index)	MOI 10k (Deg. Index)	MOI 1k (Deg. Index)
Control	0.1057 ± 0.0115	0.1057 ± 0.0115	0.1057 ± 0.0115
AAV-1	0.1387 ± 0.0081	0.1159 ± 0.0061	0.1213 ± 0.0118
AAV-2	0.1334 ± 0.0190	0.1266 ± 0.0073	0.0901 ± 0.0049
AAV-3	0.1310 ± 0.0105	0.0920 ± 0.0043	0.1182 ± 0.0077
AAV-4	0.1138 ± 0.0071	0.1187 ± 0.0078	0.1099 ± 0.0087
AAV-5	0.1404 ± 0.0098	0.1379 ± 0.0101	0.1189 ± 0.0111
AAV-6	0.1406 ± 0.0099	0.1230 ± 0.0079	0.1089 ± 0.0136
AAV-7	0.0890 ± 0.0166	0.1406 ± 0.0087	0.1119 ± 0.0084
AAV-8	0.1157 ± 0.0111	0.1255 ± 0.0107	0.1323 ± 0.0081

AAV	MOI 100k (Deg. Index)	MOI 10k (Deg. Index)	MOI 1k (Deg. Index)
AAV-9	0.1392 ± 0.0147	0.1309 ± 0.0056	0.1124 ± 0.0094
AAV-eB	0.1358 ± 0.0065	0.0829 ± 0.0052	0.1124 ± 0.0091
AAV-Retro	0.1171 ± 0.0090	0.1365 ± 0.0074	0.1340 ± 0.0089
AAV-DJ	0.0870 ± 0.0050	0.1334 ± 0.0156	0.0998 ± 0.0096
AAV-PHPS	0.1547 ± 0.0116	0.0934 ± 0.0043	0.1195 ± 0.0100

Table 5.4. Effects of AAV serotype and dose on the Transduction-Associated Death Index (TADI)

AAV	MOI 100k	MOI 10k	MOI 1k
Control	0.00 ± 0.00	0.00 ± 0.00	0.00 ± 0.00
AAV-1	20.86 ± 3.07	3.79 ± 2.82	0.00 ± 0.00
AAV-2	31.35 ± 1.68	16.18 ± 2.66	5.73 ± 0.92
AAV-3	11.61 ± 4.18	13.22 ± 1.67	7.09 ± 0.18
AAV-4	2.88 ± 0.91	0.00 ± 0.00	0.00 ± 0.00
AAV-5	3.51 ± 1.43	0.00 ± 0.00	0.00 ± 0.00
AAV-6	2.45 ± 1.36	18.40 ± 2.28	4.96 ± 2.96
AAV-7	3.87 ± 0.56	0.00 ± 0.00	0.00 ± 0.00
AAV-8	9.23 ± 3.47	0.00 ± 0.00	0.00 ± 0.00
AAV-9	8.82 ± 0.61	2.92 ± 2.21	0.00 ± 0.00
AAV-eB	13.79 ± 5.44	16.34 ± 4.55	0.00 ± 0.00
AAV-Retro	12.54 ± 0.50	14.85 ± 3.11	0.00 ± 0.00
AAV-DJ	0.00 ± 0.00	18.29 ± 2.44	0.00 ± 0.00
AAV-PHPS	14.69 ± 6.59	19.31 ± 1.26	6.34 ± 1.96

Table 5.5. Direct and bystander toxicity at 100k MOI for representative AAV serotypes

AAV	Direct toxicity rate (%)	Bystander toxicity rate (%)	Overall survival rate (%)
Control	0	24.83 ± 2.64	75.14 ± 2.64
AAV2	9.73 ± 6.53	44.25 ± 2.9	72.64 ± 5.22
AAV9	8.83 ± 6.70	49.79 ± 12.05	74.00 ± 11.32
AAV-eB	9.33 ± 3.13	53.37 ± 5.91	73.59 ± 5.48

Chapter VI General Discussion

This thesis investigates and establishes a chemogenetic technology platform for the cell-type specific and reversible modulation of the peripheral sensory system. The core objective of this research is to address the dysregulation of signal input caused by the hyperexcitability of peripheral neurones in sensory disorders such as chronic pain. This chapter will discuss the contributions and limitations of this work, position it within the broader field of neuromodulation, and explore the future directions for both basic research and clinical translation, following the specific framework provided.

1. Contributions to Theoretical and Methodological Frameworks

The theoretical innovation of this study lies in its departure from traditional approaches of ion channel blockade or receptor antagonism. Instead, we have leveraged the unique chloride ion homeostasis of peripheral sensory neurones to transform the electrophysiological concept of shunting inhibition into a viable therapeutic strategy. The central thesis of this work is that this inhibitory model, which acts on the common input pathway, can effectively bypass the complexity and heterogeneity of upstream pathophysiological processes (such as persistent stimulation by multiple inflammatory factors or the dysfunction of various ion channels). Our findings support the hypothesis that such a strategy holds the potential for greater robustness and broader applicability in managing pathological pain driven by complex aetiologies.

To put this into practice, this thesis details a series of experiments, each designed to overcome key challenges. The first step was tool iteration and humanisation. We began by validating the feasibility of the GluCl.CreON tool in the Nav1.8+ subpopulation,

providing an initial proof-of-concept for subpopulation-targeted analgesia. However, we recognised that the immunogenicity of its non-human proteins, the complexity of dual-virus delivery, and the widespread prevalence of pre-existing neutralising antibodies against various AAV serotypes in the human population (Boutin et al., 2010) were fundamental obstacles to its clinical translation. Consequently, we introduced and comprehensively validated the fully humanised PSAM⁴-GlyR system (Magnus et al., 2019). Through its use of a single viral vector, a humanised protein sequence, and a nanomolar-potency ligand (either uPSEM792 or the FDA-approved drug varenicline), this system represents an ideal therapeutic approach with low immunogenic risk, high pharmacological specificity, and clinical tractability. We established a complete chain of evidence from the cellular and tissue levels to whole-organism behaviour, confirming the strategy's efficacy at different scales through calcium imaging and in vivo behavioural experiments. The successful application in a chronic migraine model induced by NTG provided the first direct causal evidence for this technology's use in craniofacial pain, a major clinical challenge.

The second step involved innovation and scalability of delivery. We developed a subcutaneous injection strategy in neonatal mice. This method exploits the permeability window of the neonatal blood-nerve barrier to achieve efficient and stable transduction of multiple DRG and TG segments throughout the body with a single, minimally invasive injection. This has substantially improved experimental reproducibility and reduced injury to the animal models.

The final step, and the most forward-looking aspect of this study's methodological framework, was the humanisation and safety assessment. Confronting the species translation gap in AAV gene therapy, we established an evaluation platform based on human induced pluripotent stem cell (hiPSC)-derived sensory neurones to assess

transduction efficiency, axonal health, and cytotoxicity. We argue that during AAV capsid screening, one should not solely pursue the highest transduction efficiency. Instead, neuronal health must be a primary and mandatory safety consideration, especially given that some studies have reported that certain AAV serotypes can induce dorsal root ganglion pathology at high doses (Hawley et al., 2025; Hinderer et al., 2018). Based on this framework, we propose that AAV9, with its wider safety window, may be a more robust clinical candidate than high-efficiency capsids like AAV-PHP.S, which have shown poor translational efficacy in non-rodent species. This research challenges the efficiency-first paradigm traditionally adopted in AAV screening.

2. Targeting Sensory Neuron Subpopulations – What is Next?

This study successfully silenced the broad Nav1.8+ nociceptor population, providing robust proof-of-concept for the chemogenetic analgesia of DRG subpopulations. However, this is merely the first step towards precision neuromodulation. To fully realise the potential of this technological platform, the next crucial step is to leverage its precision, moving beyond broad inhibition towards the reversible modulation of other specific sensory neuron subpopulations.

Single-cell transcriptomics has unveiled the molecular heterogeneity of sensory neurons, providing a clear molecular address map for precision targeting (Qi et al., 2024; Sharma et al., 2020; Usoskin et al., 2015; Zeisel et al., 2018). Based on this map, we can advance two core targeting strategies:

First, targeting classical functional subpopulations. For example, we can separately validate peptidergic nociceptors (PEP), considered drivers of thermal hyperalgesia and neurogenic inflammation (Basbaum et al., 2009); non-peptidergic nociceptors (NP)

associated with mechanical pain (Cavanaugh et al., 2009); TRPM8+ neurons, which play a central role in cold allodynia (Knowlton et al., 2013); and PIEZO2+ low-threshold mechanoreceptors (LTMRs), which are implicated in tactile allodynia following nerve injury. Targeting the latter holds the promise of precisely alleviating symptoms without affecting protective pain sensation (Szczot et al., 2018).

Second, targeting dynamic, pathological-state subpopulations. This is a more advanced strategy, aiming to target neurons induced by injury or inflammation into a specific sensitised state. By identifying and utilising the regulatory elements of genes specifically upregulated in these pathological states (e.g., ATF3), we may be able to achieve the ultimate goal of silencing only pathological neural activity while completely preserving normal physiological functions (Renthal et al., 2020).

However, targeting these specific subpopulations is not without its challenges. The core issue lies in achieving a delicate balance between effective analgesia and the preservation of necessary physiological functions. For instance, inhibiting PEP or TRPM8 neurons requires avoiding damage to protective pain and temperature sensation, while targeting PIEZO2 must be done with caution regarding its potential impact on normal touch and proprioception (McKemy, 2005; Woo et al., 2015). For strategies targeting injury states, we must also consider the dynamic nature of their molecular markers over time, which directly relates to the durability of the therapeutic effect.

To translate these concepts into clinical reality, we must also overcome the significant gulf between basic research reliant on Cre-driver mice and non-Cre-dependent applications in humans. We can leverage the growing wealth of human sensory neuron single-cell omics data (Nguyen et al., 2021; Tavares-Ferreira et al., 2022) to discover compact promoter or enhancer sequences that can drive gene expression specifically in human sensory neuron subpopulations. This can be combined with logic-gate designs,

such as using dual-specificity promoters or recombinase systems, to enhance specificity further (Nissim et al., 2014). Furthermore, we can further optimise delivery tools, such as engineered AAV capsids. A promising example is the recently developed AAV-MaCPNS1/2 capsid, created through in vivo directed evolution. Following intravenous injection, it efficiently targets peripheral sensory neurons while significantly reducing transduction in non-target organs like the liver, offering the possibility of non-invasive, systemic administration (Chen et al., 2022). The efficacy and safety of these constructed non-Cre-dependent gene therapy vectors must ultimately be confirmed through a rigorous pipeline, from screening in hiPSC-derived cells, to simulation in more biomimetic organoids/organ-on-a-chip models, and finally to validation in large animal models (Clark et al., 2017; Hordeaux et al., 2020; Lu et al., 2024).

In summary, having established the feasibility of broad inhibition, the next phase of research will be a systematic undertaking driven by our understanding of heterogeneity. By using the chemogenetic tools validated in this study, and under the premise of clearly managing risks related to specificity, safety, dosage, and manufacturability, we can achieve precise modulation of specific functional or pathological-state neuronal subpopulations. This will propel the field from mechanistic dissection towards the development of gene therapy prototypes with clinical translation potential for specific indications.

3. Chemogenetics vs other neuromodulation technology

The chemogenetic platform developed in this thesis is not positioned to replace existing neuromodulation technologies, but rather to occupy a unique and complementary niche within the current technological landscape. Its value proposition becomes clear when

compared with the three major paradigms: optogenetics, electrical stimulation therapies, and traditional pharmacology. As a gene therapy, chemogenetics integrates features from these fields, aiming to overcome their respective core limitations.

3.1 Comparison with Optogenetics: Trading Temporal Precision for Therapeutic Scalability

Chemogenetics and optogenetics are both revolutionary, gene-based tools capable of achieving excellent cell-type specificity. However, they are optimised for different objectives. Optogenetics offers millisecond-scale temporal control, making it an indispensable research tool for dissecting rapid neural coding mechanisms such as sensory processing and synaptic transmission (Boyden, 2011; Deisseroth, 2015; Fenno et al., 2011). The response speed of chemogenetics, in contrast, is limited by ligand pharmacokinetics (minutes to hours), making it unsuitable for investigating such high-frequency signalling (Atasoy & Sternson, 2018). However, optogenetics requires surgically implanted hardware (e.g., optical fibres, LEDs) to deliver light signals, which carries risks of infection and tissue damage, and confines its application to localised brain regions (Han, 2012; Warden et al., 2014). In contrast, chemogenetics enables non-invasive, repeatable, and scalable modulation of deep and widely distributed targets (such as the entire dorsal root ganglion or trigeminal ganglion populations) through systemic or local administration of small-molecule ligands. This non-invasive nature gives it far greater clinical acceptability and practicality for chronic conditions than optogenetics.

3.2 Comparison with Electrical Stimulation Therapies (SCS/PNS): Trading Molecular-Level Precision for Real-Time Adjustability

Electrical stimulation therapies, such as Spinal Cord Stimulation (SCS) or Peripheral Nerve Stimulation (PNS), are established, device-based treatments. As a gene therapy, chemogenetics represents a fundamental shift from regional targeting to molecular

targeting. Electrical stimulation is anatomically targeted but biologically non-specific. The applied electric field indiscriminately modulates all neural components within its range, including target neurons, non-target neurons, and fibres of passage, which often leads to off-target side effects like paraesthesia (Deer et al., 2014; Holsheimer, 2002; Jeon, 2012). Chemogenetics, however, achieves true cell-type-level precision. By using subpopulation-specific regulatory elements, it can selectively silence only the nociceptors causing pain while sparing adjacent mechanosensory neurons, a feat unattainable with electrical fields (Middleton et al., 2023). While electrical stimulation can be adjusted in real-time by the patient or clinician, providing immediate control, the effects of chemogenetics are governed by ligand pharmacology and cannot be instantly reversed. Nevertheless, by using engineered ion channels to achieve definitive shunting inhibition, chemogenetics is generally more predictable and physiologically targeted than the complex and sometimes poorly understood effects of electrical fields, as it acts directly on a defined ion channel to produce hyperpolarisation or shunting inhibition, rather than the complex, mixed effects of an electric field (Weir et al., 2017).

3.3 Comparison with Traditional Pharmacology: Trading Delivery Complexity for Unprecedented Target Engagement

At first glance, chemogenetics appears similar to traditional pharmacology, as both use systemically administered drugs. However, the difference in their target engagement is fundamental. Traditional small-molecule drugs target endogenous receptors and channels that are widely expressed throughout the body, leading to narrow therapeutic windows and significant side effects (Finnerup et al., 2015; Kingwell, 2019). Chemogenetics solves this problem by introducing an engineered, exogenous receptor exclusively into the target cells. Its activating ligand is pharmacologically inert at its effective dose, meaning its effects are strictly confined to the cells expressing the artificial receptor,

thereby dramatically widening the therapeutic window (Perez-Sanchez et al., 2023). Furthermore, the efficacy of traditional drugs is often limited because the complex aetiology of chronic pain means that targeting a single endogenous receptor may be insufficient. Chemogenetics offers a more potent solution by acting as a switch. Regardless of the diversity of upstream excitatory inputs, it can effectively silence a neuronal population, potentially leading to more durable and profound therapeutic effects. In conclusion, the chemogenetic strategy represents a third path, situated between systemic drug therapies and invasive device implantations. As a gene therapy, it combines the molecular precision of modern genetics with the non-invasive delivery model of pharmacology to address intractable neurological disorders.

4. Clinical Translation for Trigeminal Pain: A Feasible Path for PSAM4-GlyR

The preclinical data in this thesis demonstrate the efficacy of the PSAM4-GlyR/uPSEM792 system in a migraine-related model induced by nitroglycerin (NTG). Although the path to clinical translation is still in its early stages, we can evaluate its potential applications.

4.1 Application Strategies for Chronic Migraine

In migraine therapy, targeting the peripheral trigeminal system has a solid theoretical basis and has been clinically validated. The trigeminovascular system is widely recognised for its pivotal role in the pathophysiology of migraine pain initiation. The recent immense clinical success of monoclonal antibodies and gepants targeting the calcitonin gene-related peptide (CGRP) pathway, which revolutionised prophylactic migraine treatment by blocking peripheral nociceptive transmission, confirms this

principle. However, a significant proportion of patients exhibit an inadequate response to these treatments, and others may experience tolerability issues, highlighting a persistent unmet clinical need. Therefore, developing alternative or complementary strategies that effectively inhibit the activity of peripheral trigeminal afferent fibres remains a highly relevant and efficient approach for migraine prevention. (Edvinsson, Haanes, et al., 2018; Negro & Martelletti, 2019).

Based on this, we propose two potential scenarios. The primary application for this gene therapy would be as a Prophylactic Treatment. The core mechanism involves the long-term, stable expression of an inhibitory ion channel to raise the activation threshold of nociceptors, thereby reducing the frequency and severity of migraine attacks. Following a one-time delivery of the gene vector, a daily low-dose oral ligand would maintain sustained inhibition of the trigeminal neurons. The main considerations for this regimen are the long-term safety profile of the ligand and patient adherence. An alternative is an On-demand Prophylaxis regimen, which is a more attractive and innovative model. In this scenario, the patient would only take the ligand when they anticipate a migraine trigger (e.g., specific stressful situations, hormonal cycle changes). This model could significantly reduce total drug exposure, lower potential side effects, and grant patients greater autonomy over their treatment. In contrast, this system is likely unsuitable for Abortive Treatment. Its main limitation is the pharmacokinetic profile of the oral ligand, namely its relatively slow onset of action, which cannot meet the clinical need for rapid termination of an acute migraine attack.

4.2 Prospects for Trigeminal Neuralgia (TN): A Highly Promising Focal Target

Although the model in this thesis is for migraine, applying the PSAM4-GlyR system to Trigeminal Neuralgia (TN) is a logical and promising next step. TN serves as an ideal

indication to validate the efficacy of this technology for focal neuropathic pain. The primary pathology of classical TN involves demyelination followed by ectopic, high-frequency firing of afferent neurons (Ashina et al., 2024). This pathological mechanism is an almost perfect match for the mechanism of action of PSAM4-GlyR, which is specifically designed to suppress neuronal hyperexcitability potently. The therapeutic goal is not to block all sensation, but to quell the abnormal, pathological discharges, which is precisely the strength of this system.

Moreover, current treatments are all suboptimal. Systemic anticonvulsants (e.g., carbamazepine) have significant side effects; the more invasive microvascular decompression surgery carries surgical risks; and ablative procedures (e.g., radiofrequency thermocoagulation, glycerol rhizotomy) lack specificity, are destructive, and can lead to permanent sensory loss (anaesthesia dolorosa) (Andersen et al., 2022; Krzemińska et al., 2025; Maarbjerg et al., 2015; Worm et al., 2025; Zakrzewska & Linskey, 2014). A PSAM4-GlyR therapy could offer an alternative: it is non-ablative, reversible (controlled by ligand administration), and has the potential for cell-type specificity, enabling long-term pain control without permanently damaging the nerve.

4.3 Long-Term Vision: Towards Autonomous Gene Therapies Regulated by Endogenous Signals

Looking to the future, the ultimate goal of chemogenetic technology is to build smart therapies that can respond autonomously to endogenous pathological signals. Drawing inspiration from the design philosophy in the paper "Cocaine chemogenetics blunts drug-seeking" by Gomez et al., 2025 (Gomez et al., 2025). We can envision a more sophisticated, next-generation gene therapy: a closed-loop therapeutic system directly activated by key endogenous molecules. The working principle would be to express an engineered biosensor-effector fusion protein in trigeminal neurons. When the

concentration of a biomarker associated with a migraine attack rises in the local microenvironment, the system would be autonomously activated, inhibiting neuronal excitability and achieving automated self-suppression without external ligand intervention, before the pain signal can fully escalate.

The success of this system design depends on two key factors: the choice of an endogenous trigger signal and the feasibility of sensor-effector engineering. An ideal trigger signal should have high disease specificity (only significantly elevated in a pathological state) and a high signal-to-noise ratio (indicating a large change in concentration). In contrast, the ideal engineering path should be simple and efficient. Below are several potential candidate molecules:

CGRP (Calcitonin Gene-Related Peptide): As a core molecule in migraine pathophysiology, it is released explicitly from trigeminal neurons during an attack, and its clinical relevance has been thoroughly validated by CGRP-targeting drugs (Russo & Hay, 2023). This makes it an ideal trigger signal with the highest specificity. However, its receptor is a GPCR, and engineering it to directly drive an ion channel or couple to its gating function presents a significant protein engineering challenge.

PACAP (Pituitary Adenylate Cyclase-Activating Polypeptide): Similar to CGRP, this is another key migraine molecule; infusion of PACAP into migraine patients can induce a delayed migraine-like headache (Edvinsson, Tajti, et al., 2018). Its specific receptor, PAC1, is highly expressed in the trigeminal ganglion. PAC1 is also a GPCR, facing the same complex GPCR-ion channel coupling engineering problem.

A possible solution is to replace the engineered ion channel effector with a DREADD. The extracellular ligand-binding domain of the endogenous receptor could be chimerised with the transmembrane and intracellular domains of hM4Di (which is also a GPCR).

This is equivalent to swapping modules between two structurally similar proteins and is a mature strategy in synthetic biology.

ATP (Adenosine Triphosphate): As a danger signal in neurogenic inflammation, its P2X receptor is itself an ion channel (Jarvis & Khakh, 2009). This makes fusing a sensing domain with an inhibitory channel more straightforward from an engineering perspective, representing an attractive technical route. However, its relatively low specificity and the risk of spurious activation would need to be addressed.

Protons (H^+ / low pH): As a universal signal of inflammation and tissue stress, its sensors (such as ASIC channels) are the simplest to design (Wemmie et al., 2002). However, its extremely low specificity limits its application, as it could lead to frequent non-specific activation.

A potential strategy is to move beyond the search for a single, perfect biomarker and instead, through engineering design, create a system that recognises a pathological state signature composed of multiple non-specific signals. This is essentially constructing a biological AND-gate, where the therapeutic system is activated only when multiple conditions are met simultaneously. For example, while an increase in ATP or a decrease in pH might occur during normal physiological activities (like exercise), the simultaneous occurrence of high-concentration ATP and significant local acidosis (low pH) is a much more reliable composite signature of neurogenic inflammation.

5. Limitations of the Study

Whilst this study has yielded positive results, it is imperative to acknowledge its limitations to evaluate its scientific value and guide future research objectively. First, there are limitations of the model systems. This research was primarily validated in mouse models. Although we incorporated human iPSC-derived neurones for in vitro

assessment, significant differences remain between mice and humans in pain perception pathways, immune responses, and neuroanatomy. Furthermore, the transduction tropism and efficiency of AAV vectors can be inconsistent across species (Hordeaux et al., 2018), suggesting that re-evaluation will be necessary when translating to higher-order animal models, such as non-human primates. Moreover, the pain models used in this study (e.g., NTG-induced migraine) can only simulate specific aspects of chronic migraine, which in humans can arise due to many mechanisms. Therefore, further validation is required to determine if the conclusions can be generalised.

Second, there are unresolved technical challenges. The chemogenetic strategy relies on the long-term expression of an exogenous protein and periodic administration of a ligand. This study has not systematically evaluated the potential effects of ultra-long-term (>1 year) expression of PSAM^4-GlyR on neuronal physiological function and survival, nor the potential for unknown off-target effects or tolerance issues arising from long-term, localised use of ligands like varenicline. Additionally, whilst the highly efficient neonatal delivery strategy is an excellent research tool, it might not be best suited to treating the adult population. In particular, the amount of virus required would be extensive, and as discussed in Chapter 3, our approach will likely transduce the sympathetic system.

Finally, there is an insufficient depth of mechanistic exploration. This study focused on directly silencing neuronal output via shunting inhibition. The potential adaptive remodelling within neuronal networks and neuro-glial interactions following long-term inhibition, along with the potential long-term effects of this strategy on non-nociceptive sensory modalities such as touch and temperature sensation, have not been explored in depth.

6. General Conclusions

In summary, this thesis has successfully designed, constructed, and validated a complete technology platform, from the optimisation of chemogenetic tools to a humanised preclinical evaluation pipeline, for the targeted and reversible inhibition of the peripheral sensory system. We first demonstrated the feasibility of targeting specific neuronal subpopulations with the GluCl.CreON tool. We then developed and validated the fully humanised PSAM^4-GlyR system, which, when combined with an innovative neonatal systemic delivery strategy, produces robust and reversible analgesic effects in mouse models of pain. More importantly, this study directly confronts the translational challenges of AAV gene therapy by establishing a dual efficiency-safety evaluation system based on human iPSC-derived sensory neurones. In doing so, it challenges the efficiency-first paradigm and provides critical data and methodological guidance for the rational selection of future clinical AAV vectors. This research lays a solid foundation for the development of an entirely new class of gene therapy targeting the peripheral nervous system.

Reference

Abrahamsen, B., Zhao, J., Asante, C. O., Cendan, C. M., Marsh, S., Martinez-Barbera, J. P., Nassar, M. A., Dickenson, A. H., & Wood, J. N. (2008). The Cell and Molecular Basis of Mechanical, Cold, and Inflammatory Pain. *Science*, *321*(5889), 702–705. https://doi.org/10.1126/science.1156916

Alexander, G. M., Rogan, S. C., Abbas, A. I., Armbruster, B. N., Pei, Y., Allen, J. A., Nonneman, R. J., Hartmann, J., Moy, S. S., Nicolelis, M. A., McNamara, J. O., & Roth, B. L. (2009). Remote Control of Neuronal Activity in Transgenic Mice Expressing Evolved G Protein-Coupled Receptors. *Neuron*, *63*(1), 27–39. https://doi.org/10.1016/j.neuron.2009.06.014

Allen, T. M., Hansen, C. B., & Guo, L. S. S. (1993). Subcutaneous administration of liposomes: A comparison with the intravenous and intraperitoneal routes of injection. *Biochimica et Biophysica Acta (BBA) - Biomembranes*, *1150*(1), 9–16. https://doi.org/10.1016/0005-2736(93)90115-G

Almeida, T. F., Roizenblatt, S., & Tufik, S. (2004). Afferent pain pathways: A neuroanatomical review. *Brain Research*, *1000*(1–2), 40–56. https://doi.org/10.1016/j.brainres.2003.10.073

Andersen, A. S. S., Heinskou, T. B., Rochat, P., Springborg, J. B., Noory, N., Smilkov, E. A., Bendtsen, L., & Maarbjerg, S. (2022). Microvascular decompression in trigeminal neuralgia—A prospective study of 115 patients. *The Journal of Headache and Pain*, *23*(1), 145. https://doi.org/10.1186/s10194-022-01520-x

Armbruster, B. N., Li, X., Pausch, M. H., Herlitze, S., & Roth, B. L. (2007). Evolving the lock to fit the key to create a family of G protein-coupled receptors potently

activated by an inert ligand. *Proceedings of the National Academy of Sciences*, *104*(12), 5163–5168. https://doi.org/10.1073/pnas.0700293104

Arrázola, M. S., Saquel, C., Catalán, R. J., Barrientos, S. A., Hernandez, D. E., Martínez, N. W., Catenaccio, A., & Court, F. A. (2019). Axonal Degeneration Is Mediated by Necroptosis Activation. *The Journal of Neuroscience*, *39*(20), 3832–3844. https://doi.org/10.1523/JNEUROSCI.0881-18.2019

Asencor, A. I., Dvoryanchikov, G., Makhoul, V., Tsoulfas, P., & Chaudhari, N. (2022). Selectively Imaging Cranial Sensory Ganglion Neurons Using AAV-PHP.S. *Eneuro*, *9*(3), ENEURO.0373-21.2022. https://doi.org/10.1523/ENEURO.0373-21.2022

Ashina, S., Robertson, C. E., Srikiatkhachorn, A., Di Stefano, G., Donnet, A., Hodaie, M., Obermann, M., Romero-Reyes, M., Park, Y. S., Cruccu, G., & Bendtsen, L. (2024). Trigeminal neuralgia. *Nature Reviews Disease Primers*, *10*(1), 39. https://doi.org/10.1038/s41572-024-00523-z

Asuri, P., Bartel, M. A., Vazin, T., Jang, J.-H., Wong, T. B., & Schaffer, D. V. (2012). Directed Evolution of Adeno-associated Virus for Enhanced Gene Delivery and Gene Targeting in Human Pluripotent Stem Cells. *Molecular Therapy*, *20*(2), 329–338. https://doi.org/10.1038/mt.2011.255

Atasoy, D., Aponte, Y., Su, H. H., & Sternson, S. M. (2008). A FLEX Switch Targets Channelrhodopsin-2 to Multiple Cell Types for Imaging and Long-Range Circuit Mapping. *The Journal of Neuroscience*, *28*(28), 7025–7030. https://doi.org/10.1523/JNEUROSCI.1954-08.2008

Atasoy, D., & Sternson, S. M. (2018). Chemogenetic Tools for Causal Cellular and Neuronal Biology. *Physiological Reviews*, *98*(1), 391–418. https://doi.org/10.1152/physrev.00009.2017

Atchison, R. W., Casto, B. C., & Hammon, W. McD. (1965). Adenovirus-Associated Defective Virus Particles. *Science*, *149*(3685), 754–756. https://doi.org/10.1126/science.149.3685.754

Baron, R., Binder, A., & Wasner, G. (2010). Neuropathic pain: Diagnosis, pathophysiological mechanisms, and treatment. *The Lancet Neurology*, *9*(8), 807–819. https://doi.org/10.1016/S1474-4422(10)70143-5

Bartlett, J. S., Wilcher, R., & Samulski, R. J. (2000). Infectious Entry Pathway of Adeno-Associated Virus and Adeno-Associated Virus Vectors. *Journal of Virology*, *74*(6), 2777–2785. https://doi.org/10.1128/JVI.74.6.2777-2785.2000

Basbaum, A. I., Bautista, D. M., Scherrer, G., & Julius, D. (2009). Cellular and Molecular Mechanisms of Pain. *Cell*, *139*(2), 267–284. https://doi.org/10.1016/j.cell.2009.09.028

Baskozos, G., Hébert, H. L., Pascal, M. M. V., Themistocleous, A. C., Macfarlane, G. J., Wynick, D., Bennett, D. L. H., & Smith, B. H. (2023). Epidemiology of neuropathic pain: An analysis of prevalence and associated factors in UK Biobank. *PAIN Reports*, *8*(2), e1066. https://doi.org/10.1097/PR9.0000000000001066

Bedbrook, C. N., Deverman, B. E., & Gradinaru, V. (2018). Viral Strategies for Targeting the Central and Peripheral Nervous Systems. *Annual Review of Neuroscience*, *41*(1), 323–348. https://doi.org/10.1146/annurev-neuro-080317-062048

Bell, P., Wang, L., Lebherz, C., Flieder, D. B., Bove, M. S., Wu, D., Gao, G. P., Wilson, J. M., & Wivel, N. A. (2005). No Evidence for Tumorigenesis of AAV Vectors in a Large-Scale Study in Mice. *Molecular Therapy*, *12*(2), 299–306. https://doi.org/10.1016/j.ymthe.2005.03.020

Bendtsen, L., Zakrzewska, J. M., Heinskou, T. B., Hodaie, M., Leal, P. R. L., Nurmikko, T., Obermann, M., Cruccu, G., & Maarbjerg, S. (2020). Advances in diagnosis,

classification, pathophysiology, and management of trigeminal neuralgia. *The Lancet Neurology*, *19*(9), 784–796. https://doi.org/10.1016/S1474-4422(20)30233-7

Bennett, J., Wellman, J., Marshall, K. A., McCague, S., Ashtari, M., DiStefano-Pappas, J., Elci, O. U., Chung, D. C., Sun, J., Wright, J. F., Cross, D. R., Aravand, P., Cyckowski, L. L., Bennicelli, J. L., Mingozzi, F., Auricchio, A., Pierce, E. A., Ruggiero, J., Leroy, B. P., … Maguire, A. M. (2016). Safety and durability of effect of contralateral-eye administration of AAV2 gene therapy in patients with childhood-onset blindness caused by RPE65 mutations: A follow-on phase 1 trial. *The Lancet*, *388*(10045), 661–672. https://doi.org/10.1016/S0140-6736(16)30371-3

Berns, K. I., & Linden, R. M. (1995). The cryptic life style of adenoassociated virus. *BioEssays*, *17*(3), 237–245. https://doi.org/10.1002/bies.950170310

Bittner, B., Richter, W., & Schmidt, J. (2018). Subcutaneous Administration of Biotherapeutics: An Overview of Current Challenges and Opportunities. *BioDrugs*, *32*(5), 425–440. https://doi.org/10.1007/s40259-018-0295-0

Bostick, B., Ghosh, A., Yue, Y., Long, C., & Duan, D. (2007). Systemic AAV-9 transduction in mice is influenced by animal age but not by the route of administration. *Gene Therapy*, *14*(22), 1605–1609. https://doi.org/10.1038/sj.gt.3303029

Boulis, N. M., Noordmans, A. J., Song, D. K., Imperiale, M. J., Rubin, A., Leone, P., During, M., & Feldman, E. L. (2003). Adeno-associated viral vector gene expression in the adult rat spinal cord following remote vector delivery. *Neurobiology of Disease*, *14*(3), 535–541. https://doi.org/10.1016/j.nbd.2003.08.025

Boutin, S., Monteilhet, V., Veron, P., Leborgne, C., Benveniste, O., Montus, M. F., & Masurier, C. (2010). Prevalence of Serum IgG and Neutralizing Factors Against Adeno-Associated Virus (AAV) Types 1, 2, 5, 6, 8, and 9 in the Healthy Population: Implications for Gene Therapy Using AAV Vectors. *Human Gene Therapy*, *21*(6), 704–712. https://doi.org/10.1089/hum.2009.182

Boyden, E. S. (2011). A history of optogenetics: The development of tools for controlling brain circuits with light. *F1000 Biology Reports*, *3*. https://doi.org/10.3410/B3-11

Breivik, H., Collett, B., Ventafridda, V., Cohen, R., & Gallacher, D. (2006). Survey of chronic pain in Europe: Prevalence, impact on daily life, and treatment. *European Journal of Pain*, *10*(4), 287–287. https://doi.org/10.1016/j.ejpain.2005.06.009

Bryant, D. H., Bashir, A., Sinai, S., Jain, N. K., Ogden, P. J., Riley, P. F., Church, G. M., Colwell, L. J., & Kelsic, E. D. (2021). Deep diversification of an AAV capsid protein by machine learning. *Nature Biotechnology*, *39*(6), 691–696. https://doi.org/10.1038/s41587-020-00793-4

Buller, R. M. L., Janik, J. E., Sebring, E. D., & Rose, J. A. (1981). Herpes Simplex Virus Types 1 and 2 Completely Help Adenovirus-Associated Virus Replication. *Journal of Virology*, *40*(1), 241–247. https://doi.org/10.1128/jvi.40.1.241-247.1981

Burnstock, G. (2016). Purinergic Mechanisms and Pain. In *Advances in Pharmacology* (Vol. 75, pp. 91–137). Elsevier. https://doi.org/10.1016/bs.apha.2015.09.001

Busse, J. W., Wang, L., Kamaleldin, M., Craigie, S., Riva, J. J., Montoya, L., Mulla, S. M., Lopes, L. C., Vogel, N., Chen, E., Kirmayr, K., De Oliveira, K., Olivieri, L., Kaushal, A., Chaparro, L. E., Oyberman, I., Agarwal, A., Couban, R., Tsoi, L., … Guyatt, G. H. (2018). Opioids for Chronic Noncancer Pain: A Systematic Review

and Meta-analysis. *JAMA*, *320*(23), 2448. https://doi.org/10.1001/jama.2018.18472

Calcedo, R., & Wilson, J. M. (2013). Humoral Immune Response to AAV. *Frontiers in Immunology*, *4*. https://doi.org/10.3389/fimmu.2013.00341

Caterina, M. J., Schumacher, M. A., Tominaga, M., Rosen, T. A., Levine, J. D., & Julius, D. (1997). The capsaicin receptor: A heat-activated ion channel in the pain pathway. *Nature*, *389*(6653), 816–824. https://doi.org/10.1038/39807

Cavanaugh, D. J., Lee, H., Lo, L., Shields, S. D., Zylka, M. J., Basbaum, A. I., & Anderson, D. J. (2009). Distinct subsets of unmyelinated primary sensory fibers mediate behavioral responses to noxious thermal and mechanical stimuli. *Proceedings of the National Academy of Sciences*, *106*(22), 9075–9080. https://doi.org/10.1073/pnas.0901507106

Chambers, S. M., Qi, Y., Mica, Y., Lee, G., Zhang, X.-J., Niu, L., Bilsland, J., Cao, L., Stevens, E., Whiting, P., Shi, S.-H., & Studer, L. (2012). Combined small-molecule inhibition accelerates developmental timing and converts human pluripotent stem cells into nociceptors. *Nature Biotechnology*, *30*(7), 715–720. https://doi.org/10.1038/nbt.2249

Chan, K. Y., Jang, M. J., Yoo, B. B., Greenbaum, A., Ravi, N., Wu, W.-L., Sánchez-Guardado, L., Lois, C., Mazmanian, S. K., Deverman, B. E., & Gradinaru, V. (2017). Engineered AAVs for efficient noninvasive gene delivery to the central and peripheral nervous systems. *Nature Neuroscience*, *20*(8), 1172–1179. https://doi.org/10.1038/nn.4593

Chen, X., Choo, H., Huang, X.-P., Yang, X., Stone, O., Roth, B. L., & Jin, J. (2015). The First Structure–Activity Relationship Studies for Designer Receptors Exclusively

Activated by Designer Drugs. *ACS Chemical Neuroscience*, *6*(3), 476–484. https://doi.org/10.1021/cn500325v

Chen, X., Ravindra Kumar, S., Adams, C. D., Yang, D., Wang, T., Wolfe, D. A., Arokiaraj, C. M., Ngo, V., Campos, L. J., Griffiths, J. A., Ichiki, T., Mazmanian, S. K., Osborne, P. B., Keast, J. R., Miller, C. T., Fox, A. S., Chiu, I. M., & Gradinaru, V. (2022). Engineered AAVs for non-invasive gene delivery to rodent and non-human primate nervous systems. *Neuron*, *110*(14), 2242-2257.e6. https://doi.org/10.1016/j.neuron.2022.05.003

Cheng, J. S., Lim, D. A., Chang, E. F., & Barbaro, N. M. (2014). A Review of Percutaneous Treatments for Trigeminal Neuralgia. *Operative Neurosurgery*, *10*(1), 25–33. https://doi.org/10.1227/NEU.00000000000001687

Cheng, J.-K., & Ji, R.-R. (2008). Intracellular Signaling in Primary Sensory Neurons and Persistent Pain. *Neurochemical Research*, *33*(10), 1970–1978. https://doi.org/10.1007/s11064-008-9711-z

Clark, A. J., Kaller, M. S., Galino, J., Willison, H. J., Rinaldi, S., & Bennett, D. L. H. (2017). Co-cultures with stem cell-derived human sensory neurons reveal regulators of peripheral myelination. *Brain*, *140*(4), 898–913. https://doi.org/10.1093/brain/awx012

Coleman, M. P., & Höke, A. (2020). Programmed axon degeneration: From mouse to mechanism to medicine. *Nature Reviews Neuroscience*, *21*(4), 183–196. https://doi.org/10.1038/s41583-020-0269-3

Colloca, L., Ludman, T., Bouhassira, D., Baron, R., Dickenson, A. H., Yarnitsky, D., Freeman, R., Truini, A., Attal, N., Finnerup, N. B., Eccleston, C., Kalso, E., Bennett, D. L., Dworkin, R. H., & Raja, S. N. (2017). Neuropathic pain. *Nature Reviews Disease Primers*, *3*(1), 17002. https://doi.org/10.1038/nrdp.2017.2

Cooper, A. H., Barry, A. M., Chrysostomidou, P., Lolignier, R., Wang, J., Redondo Canales, M., Titterton, H. F., Bennett, D. L., & Weir, G. A. (2024). Peripheral nerve injury results in a biased loss of sensory neuron subpopulations. *Pain*, *165*(12), 2863–2876. https://doi.org/10.1097/j.pain.0000000000003321

Costigan, M., Scholz, J., & Woolf, C. J. (2009). Neuropathic Pain: A Maladaptive Response of the Nervous System to Damage. *Annual Review of Neuroscience*, *32*(1), 1–32. https://doi.org/10.1146/annurev.neuro.051508.135531

Cox, J. J., Reimann, F., Nicholas, A. K., Thornton, G., Roberts, E., Springell, K., Karbani, G., Jafri, H., Mannan, J., Raashid, Y., Al-Gazali, L., Hamamy, H., Valente, E. M., Gorman, S., Williams, R., McHale, D. P., Wood, J. N., Gribble, F. M., & Woods, C. G. (2006). An SCN9A channelopathy causes congenital inability to experience pain. *Nature*, *444*(7121), 894–898. https://doi.org/10.1038/nature05413

Crump, A., & Omura, S. (2011). Ivermectin, 'Wonder drug' from Japan: The human use perspective. *Proceedings of the Japan Academy, Series B*, *87*(2), 13–28. https://doi.org/10.2183/pjab.87.13

Dang, C. H., Aubert, M., De Silva Feelixge, H. S., Diem, K., Loprieno, M. A., Roychoudhury, P., Stone, D., & Jerome, K. R. (2017). In vivo dynamics of AAV-mediated gene delivery to sensory neurons of the trigeminal ganglia. *Scientific Reports*, *7*(1), 927. https://doi.org/10.1038/s41598-017-01004-y

Daou, I., Tuttle, A. H., Longo, G., Wieskopf, J. S., Bonin, R. P., Ase, A. R., Wood, J. N., De Koninck, Y., Ribeiro-da-Silva, A., Mogil, J. S., & Séguéla, P. (2013). Remote Optogenetic Activation and Sensitization of Pain Pathways in Freely Moving Mice. *The Journal of Neuroscience*, *33*(47), 18631–18640. https://doi.org/10.1523/JNEUROSCI.2424-13.2013

Darrow, J. J. (2019). Luxturna: FDA documents reveal the value of a costly gene therapy. *Drug Discovery Today*, *24*(4), 949–954. https://doi.org/10.1016/j.drudis.2019.01.019

Day, J. W., Finkel, R. S., Chiriboga, C. A., Connolly, A. M., Crawford, T. O., Darras, B. T., Iannaccone, S. T., Kuntz, N. L., Peña, L. D. M., Shieh, P. B., Smith, E. C., Kwon, J. M., Zaidman, C. M., Schultz, M., Feltner, D. E., Tauscher-Wisniewski, S., Ouyang, H., Chand, D. H., Sproule, D. M., … Mendell, J. R. (2021). Onasemnogene abeparvovec gene therapy for symptomatic infantile-onset spinal muscular atrophy in patients with two copies of SMN2 (STR1VE): An open-label, single-arm, multicentre, phase 3 trial. *The Lancet Neurology*, *20*(4), 284–293. https://doi.org/10.1016/S1474-4422(21)00001-6

Daya, S., & Berns, K. I. (2008). Gene Therapy Using Adeno-Associated Virus Vectors. *Clinical Microbiology Reviews*, *21*(4), 583–593. https://doi.org/10.1128/CMR.00008-08

Deer, T. R., Mekhail, N., Provenzano, D., Pope, J., Krames, E., Leong, M., Levy, R. M., Abejon, D., Buchser, E., Burton, A., Buvanendran, A., Candido, K., Caraway, D., Cousins, M., DeJongste, M., Diwan, S., Eldabe, S., Gatzinsky, K., Foreman, R. D., … North, R. (2014). The Appropriate Use of Neurostimulation of the Spinal Cord and Peripheral Nervous System for the Treatment of Chronic Pain and Ischemic Diseases: The Neuromodulation Appropriateness Consensus Committee. *Neuromodulation: Technology at the Neural Interface*, *17*(6), 515–550. https://doi.org/10.1111/ner.12208

Deisseroth, K. (2015). Optogenetics: 10 years of microbial opsins in neuroscience. *Nature Neuroscience*, *18*(9), 1213–1225. https://doi.org/10.1038/nn.4091

Denk, F., & McMahon, S. B. (2012). Chronic Pain: Emerging Evidence for the Involvement of Epigenetics. *Neuron*, *73*(3), 435–444. https://doi.org/10.1016/j.neuron.2012.01.012

Derry, S., Bell, R. F., Straube, S., Wiffen, P. J., Aldington, D., & Moore, R. A. (2019). Pregabalin for neuropathic pain in adults. *Cochrane Database of Systematic Reviews*, *2019*(5). https://doi.org/10.1002/14651858.CD007076.pub3

Descalzi, G., Mitsi, V., Purushothaman, I., Gaspari, S., Avrampou, K., Loh, Y.-H. E., Shen, L., & Zachariou, V. (2017). Neuropathic pain promotes adaptive changes in gene expression in brain networks involved in stress and depression. *Science Signaling*, *10*(471), eaaj1549. https://doi.org/10.1126/scisignal.aaj1549

Deval, E., & Lingueglia, E. (2015). Acid-Sensing Ion Channels and nociception in the peripheral and central nervous systems. *Neuropharmacology*, *94*, 49–57. https://doi.org/10.1016/j.neuropharm.2015.02.009

Deverman, B. E., Pravdo, P. L., Simpson, B. P., Kumar, S. R., Chan, K. Y., Banerjee, A., Wu, W.-L., Yang, B., Huber, N., Pasca, S. P., & Gradinaru, V. (2016). Cre-dependent selection yields AAV variants for widespread gene transfer to the adult brain. *Nature Biotechnology*, *34*(2), 204–209. https://doi.org/10.1038/nbt.3440

Devor, M. (2009). Ectopic discharge in Aβ afferents as a source of neuropathic pain. *Experimental Brain Research*, *196*(1), 115–128. https://doi.org/10.1007/s00221-009-1724-6

Dewey, J. (1896). The reflex arc concept in psychology. *Psychological Review*, *3*(4), 357–370. https://doi.org/10.1037/h0070405

Di Stefano, G., Truini, A., & Cruccu, G. (2018). Current and Innovative Pharmacological Options to Treat Typical and Atypical Trigeminal Neuralgia. *Drugs*, *78*(14), 1433–1442. https://doi.org/10.1007/s40265-018-0964-9

Dib-Hajj, S. D., Cummins, T. R., Black, J. A., & Waxman, S. G. (2010). Sodium Channels in Normal and Pathological Pain. *Annual Review of Neuroscience*, *33*(1), 325–347. https://doi.org/10.1146/annurev-neuro-060909-153234

Djouhri, L., Fang, X., Okuse, K., Wood, J. N., Berry, C. M., & Lawson, S. N. (2003). The TTX-Resistant Sodium Channel Na_v 1.8 (SNS/PN3): Expression and Correlation with Membrane Properties in Rat Nociceptive Primary Afferent Neurons. *The Journal of Physiology*, *550*(3), 739–752. https://doi.org/10.1113/jphysiol.2003.042127

Dong, J.-Y., Fan, P.-D., & Frizzell, R. A. (1996). Quantitative Analysis of the Packaging Capacity of Recombinant Adeno-Associated Virus. *Human Gene Therapy*, *7*(17), 2101–2112. https://doi.org/10.1089/hum.1996.7.17-2101

Dudek, A. M., Zabaleta, N., Zinn, E., Pillay, S., Zengel, J., Porter, C., Franceschini, J. S., Estelien, R., Carette, J. E., Zhou, G. L., & Vandenberghe, L. H. (2020). GPR108 Is a Highly Conserved AAV Entry Factor. *Molecular Therapy*, *28*(2), 367–381. https://doi.org/10.1016/j.ymthe.2019.11.005

Eagles, D. A., Chow, C. Y., & King, G. F. (2022). Fifteen years of Na_V 1.7 channels as an analgesic target: Why has excellent in vitro pharmacology not translated into in vivo analgesic efficacy? *British Journal of Pharmacology*, *179*(14), 3592–3611. https://doi.org/10.1111/bph.15327

Edvinsson, L. (2017). The Trigeminovascular Pathway: Role of CGRP and CGRP Receptors in Migraine. *Headache: The Journal of Head and Face Pain*, *57*(S2), 47–55. https://doi.org/10.1111/head.13081

Edvinsson, L., Haanes, K. A., Warfvinge, K., & Krause, D. N. (2018). CGRP as the target of new migraine therapies—Successful translation from bench to clinic. *Nature Reviews Neurology*, *14*(6), 338–350. https://doi.org/10.1038/s41582-018-0003-1

Edvinsson, L., Tajti, J., Szalárdy, L., & Vécsei, L. (2018). PACAP and its role in primary headaches. *The Journal of Headache and Pain*, *19*(1), 21. https://doi.org/10.1186/s10194-018-0852-4

Engle, S. J., Blaha, L., & Kleiman, R. J. (2018). Best Practices for Translational Disease Modeling Using Human iPSC-Derived Neurons. *Neuron*, *100*(4), 783–797. https://doi.org/10.1016/j.neuron.2018.10.033

Ertl, H. C. J. (2022). Immunogenicity and toxicity of AAV gene therapy. *Frontiers in Immunology*, *13*, 975803. https://doi.org/10.3389/fimmu.2022.975803

Esler, M., Lambert, E., & Schlaich, M. (2010). Point: Chronic Activation of the Sympathetic Nervous System is the Dominant Contributor to Systemic Hypertension. *Journal of Applied Physiology*, *109*(6), 1996–1998. https://doi.org/10.1152/japplphysiol.00182.2010

Espinosa-Juárez, J. V., Chiquete, E., Estañol, B., & Aceves, J. D. J. (2023). Optogenetic and Chemogenic Control of Pain Signaling: Molecular Markers. *International Journal of Molecular Sciences*, *24*(12), 10220. https://doi.org/10.3390/ijms241210220

Essuman, K., Summers, D. W., Sasaki, Y., Mao, X., DiAntonio, A., & Milbrandt, J. (2017). The SARM1 Toll/Interleukin-1 Receptor Domain Possesses Intrinsic NAD+ Cleavage Activity that Promotes Pathological Axonal Degeneration. *Neuron*, *93*(6), 1334-1343.e5. https://doi.org/10.1016/j.neuron.2017.02.022

Fang, K., Yang, X., Liu, Y., Xia, J., Wu, R., Yang, F., Feng, C., Liu, X., Shi, L., Geng, G., & Yang, H. (2025). A comprehensive study of AAV tropism across C57BL/6 mice, BALB/c mice, and crab-eating macaques. *Molecular Therapy Methods & Clinical Development*, *33*(1), 101434. https://doi.org/10.1016/j.omtm.2025.101434

Farkas, S., Bölcskei, K., Markovics, A., Varga, A., Kis-Varga, Á., Kormos, V., Gaszner, B., Horváth, C., Tuka, B., Tajti, J., & Helyes, Z. (2016). Utility of different outcome measures for the nitroglycerin model of migraine in mice. *Journal of Pharmacological and Toxicological Methods*, *77*, 33–44. https://doi.org/10.1016/j.vascn.2015.09.006

FDA. (2025, January 30). *FDA Approves Novel Non-Opioid Treatment for Moderate to Severe Acute Pain*. FDA. FDA. https://www.fda.gov/news-events/press-announcements/fda-approves-novel-non-opioid-treatment-moderate-severe-acute-pain

Fenno, L., Yizhar, O., & Deisseroth, K. (2011). The Development and Application of Optogenetics. *Annual Review of Neuroscience*, *34*(1), 389–412. https://doi.org/10.1146/annurev-neuro-061010-113817

Ferrari, F. K., Samulski, T., Shenk, T., & Samulski, R. J. (1996). Second-strand synthesis is a rate-limiting step for efficient transduction by recombinant adeno-associated virus vectors. *Journal of Virology*, *70*(5), 3227–3234. https://doi.org/10.1128/jvi.70.5.3227-3234.1996

Finnerup, N. B., Attal, N., Haroutounian, S., McNicol, E., Baron, R., Dworkin, R. H., Gilron, I., Haanpää, M., Hansson, P., Jensen, T. S., Kamerman, P. R., Lund, K., Moore, A., Raja, S. N., Rice, A. S. C., Rowbotham, M., Sena, E., Siddall, P., Smith, B. H., & Wallace, M. (2015). Pharmacotherapy for neuropathic pain in adults: A systematic review and meta-analysis. *The Lancet Neurology*, *14*(2), 162–173. https://doi.org/10.1016/S1474-4422(14)70251-0

Finnerup, N. B., Kuner, R., & Jensen, T. S. (2021). Neuropathic Pain: From Mechanisms to Treatment. *Physiological Reviews*, *101*(1), 259–301. https://doi.org/10.1152/physrev.00045.2019

Finnerup, N. B., Otto, M., McQuay, H. J., Jensen, T. S., & Sindrup, S. H. (2005). Algorithm for neuropathic pain treatment: An evidence based proposal. *Pain*, *118*(3), 289–305. https://doi.org/10.1016/j.pain.2005.08.013

Fischer, G., Kostic, S., Nakai, H., Park, F., Sapunar, D., Yu, H., & Hogan, Q. (2011). Direct injection into the dorsal root ganglion: Technical, behavioral, and histological observations. *Journal of Neuroscience Methods*, *199*(1), 43–55. https://doi.org/10.1016/j.jneumeth.2011.04.021

Flor, H., Elbert, T., Knecht, S., Wienbruch, C., Pantev, C., Birbaumers, N., Larbig, W., & Taub, E. (1995). Phantom-limb pain as a perceptual correlate of cortical reorganization following arm amputation. *Nature*, *375*(6531), 482–484. https://doi.org/10.1038/375482a0

Foust, K. D., Nurre, E., Montgomery, C. L., Hernandez, A., Chan, C. M., & Kaspar, B. K. (2009). Intravascular AAV9 preferentially targets neonatal neurons and adult astrocytes. *Nature Biotechnology*, *27*(1), 59–65. https://doi.org/10.1038/nbt.1515

Foust, K. D., Poirier, A., Pacak, C. A., Mandel, R. J., & Flotte, T. R. (2008). Neonatal Intraperitoneal or Intravenous Injections of Recombinant Adeno-Associated Virus Type 8 Transduce Dorsal Root Ganglia and Lower Motor Neurons. *Human Gene Therapy*, *19*(1), 61–70. https://doi.org/10.1089/hum.2007.093

Frazier, S. J., Cohen, B. N., & Lester, H. A. (2013). An Engineered Glutamate-gated Chloride (GluCl) Channel for Sensitive, Consistent Neuronal Silencing by Ivermectin. *Journal of Biological Chemistry*, *288*(29), 21029–21042. https://doi.org/10.1074/jbc.M112.423921

Fried, K., Bongenhielm, U., Boissonade, F. M., & Robinson, P. P. (2001). Nerve Injury-!Induced Pain in the Trigeminal System. *The Neuroscientist*, *7*(2), 155–165. https://doi.org/10.1177/107385840100700210

Funk, K., Woitecki, A., Franjic-Würtz, C., Gensch, T., Möhrlen, F., & Frings, S. (2008). Modulation of Chloride Homeostasis by Inflammatory Mediators in Dorsal Root Ganglion Neurons. *Molecular Pain*, *4*, 1744-8069-4–32. https://doi.org/10.1186/1744-8069-4-32

Gamba, G. (2005). Molecular Physiology and Pathophysiology of Electroneutral Cation-Chloride Cotransporters. *Physiological Reviews*, *85*(2), 423–493. https://doi.org/10.1152/physrev.00011.2004

Gambeta, E., Chichorro, J. G., & Zamponi, G. W. (2020). Trigeminal neuralgia: An overview from pathophysiology to pharmacological treatments. *Molecular Pain*, *16*, 1744806920901890. https://doi.org/10.1177/1744806920901890

Gangadharan, V., & Kuner, R. (2013). Pain hypersensitivity mechanisms at a glance. *Disease Models & Mechanisms*, *6*(4), 889–895. https://doi.org/10.1242/dmm.011502

Gao, G., Alvira, M. R., Somanathan, S., Lu, Y., Vandenberghe, L. H., Rux, J. J., Calcedo, R., Sanmiguel, J., Abbas, Z., & Wilson, J. M. (2003). Adeno-associated viruses undergo substantial evolution in primates during natural infections. *Proceedings of the National Academy of Sciences*, *100*(10), 6081–6086. https://doi.org/10.1073/pnas.0937739100

Gao, G., Alvira, M. R., Wang, L., Calcedo, R., Johnston, J., & Wilson, J. M. (2002). Novel adeno-associated viruses from rhesus monkeys as vectors for human gene therapy. *Proceedings of the National Academy of Sciences*, *99*(18), 11854–11859. https://doi.org/10.1073/pnas.182412299

Gao, N., Li, M., Wang, W., Liu, Z., & Guo, Y. (2024). The dual role of TRPV1 in peripheral neuropathic pain: Pain switches caused by its sensitization or

desensitization. *Frontiers in Molecular Neuroscience*, *17*, 1400118. https://doi.org/10.3389/fnmol.2024.1400118

Ghosh, K., & Pan, H.-L. (2022). Epigenetic Mechanisms of Neural Plasticity in Chronic Neuropathic Pain. *ACS Chemical Neuroscience*, *13*(4), 432–441. https://doi.org/10.1021/acschemneuro.1c00841

Gilley, J., Orsomando, G., Nascimento-Ferreira, I., & Coleman, M. P. (2015). Absence of SARM1 Rescues Development and Survival of NMNAT2-Deficient Axons. *Cell Reports*, *10*(12), 1974–1981. https://doi.org/10.1016/j.celrep.2015.02.060

Giorgi, S., Nikolaeva-Koleva, M., Alarcón-Alarcón, D., Butrón, L., & González-Rodríguez, S. (2019). Is TRPA1 Burning Down TRPV1 as Druggable Target for the Treatment of Chronic Pain? *International Journal of Molecular Sciences*, *20*(12), 2906. https://doi.org/10.3390/ijms20122906

Glatzel, M., Flechsig, E., Navarro, B., Klein, M. A., Paterna, J. C., Büeler, H., & Aguzzi, A. (2000). Adenoviral and adeno-associated viral transfer of genes to the peripheral nervous system. *Proceedings of the National Academy of Sciences*, *97*(1), 442–447. https://doi.org/10.1073/pnas.97.1.442

Goadsby, P. J., Holland, P. R., Martins-Oliveira, M., Hoffmann, J., Schankin, C., & Akerman, S. (2017). Pathophysiology of Migraine: A Disorder of Sensory Processing. *Physiological Reviews*, *97*(2), 553–622. https://doi.org/10.1152/physrev.00034.2015

Gold, M. S., & Gebhart, G. F. (2010). Nociceptor sensitization in pain pathogenesis. *Nature Medicine*, *16*(11), 1248–1257. https://doi.org/10.1038/nm.2235

Gomez, J. L., Bonaventura, J., Lesniak, W., Mathews, W. B., Sysa-Shah, P., Rodriguez, L. A., Ellis, R. J., Richie, C. T., Harvey, B. K., Dannals, R. F., Pomper, M. G., Bonci, A., & Michaelides, M. (2017). Chemogenetics revealed: DREADD

occupancy and activation via converted clozapine. *Science*, *357*(6350), 503–507. https://doi.org/10.1126/science.aan2475

Gomez, J. L., Magnus, C. J., Bonaventura, J., Solis, O., Curry, F. P., Levinstein, M. R., Budinich, R. C., Carlton, M. L., Ventriglia, E. N., Lam, S., Wang, L., Schoenborn, I., Dunne, W., Michaelides, M., & Sternson, S. M. (2025). Cocaine chemogenetics blunts drug-seeking by synthetic physiology. *Nature*, *646*(8085), 746–753. https://doi.org/10.1038/s41586-025-09427-8

González Canga, A., Sahagún Prieto, A. M., Diez Liébana, M. J., Fernández Martínez, N., Sierra Vega, M., & García Vieitez, J. J. (2008). The Pharmacokinetics and Interactions of Ivermectin in Humans—A Mini-review. *The AAPS Journal*, *10*(1), 42–46. https://doi.org/10.1208/s12248-007-9000-9

Grieger, J. C., Soltys, S. M., & Samulski, R. J. (2016). Production of Recombinant Adeno-associated Virus Vectors Using Suspension HEK293 Cells and Continuous Harvest of Vector From the Culture Media for GMP FIX and FLT1 Clinical Vector. *Molecular Therapy*, *24*(2), 287–297. https://doi.org/10.1038/mt.2015.187

Grimm, D., Lee, J. S., Wang, L., Desai, T., Akache, B., Storm, T. A., & Kay, M. A. (2008). In Vitro and In Vivo Gene Therapy Vector Evolution via Multispecies Interbreeding and Retargeting of Adeno-Associated Viruses. *Journal of Virology*, *82*(12), 5887–5911. https://doi.org/10.1128/JVI.00254-08

Haberberger, R. V., Barry, C., Dominguez, N., & Matusica, D. (2019). Human Dorsal Root Ganglia. *Frontiers in Cellular Neuroscience*, *13*, 271. https://doi.org/10.3389/fncel.2019.00271

Hackett, N. R., & Crystal, R. G. (2025). Four decades of adenovirus gene transfer vectors: History and current use. *Molecular Therapy*, *33*(5), 2192–2204. https://doi.org/10.1016/j.ymthe.2025.03.062

Hadzic, A., Dilberovic, F., Shah, S., Kulenovic, A., Kapur, E., Zaciragic, A., Cosovic, E., Vuckovic, I., Divanovic, K., & Mornjakovic, Z. (2004). Combination of intraneural injection and high injection pressure leads to fascicular injury and neurologic deficits in dogs. *Regional Anesthesia and Pain Medicine*, *29*(5), 417–423. https://doi.org/10.1016/j.rapm.2004.06.002

Han, X. (2012). In Vivo Application of Optogenetics for Neural Circuit Analysis. *ACS Chemical Neuroscience*, *3*(8), 577–584. https://doi.org/10.1021/cn300065j

Hanani, M. (2005). Satellite glial cells in sensory ganglia: From form to function. *Brain Research Reviews*, *48*(3), 457–476. https://doi.org/10.1016/j.brainresrev.2004.09.001

Hanani, M., & Spray, D. C. (2020). Emerging importance of satellite glia in nervous system function and dysfunction. *Nature Reviews Neuroscience*, *21*(9), 485–498. https://doi.org/10.1038/s41583-020-0333-z

Hawley, Z. C. E., Pardo, I. D., Cao, S., Zavodszky, M. I., Casey, F., Ferber, K., Luo, Y., Hana, S., Chen, S. K., Doherty, J., Costa, R., Cullen, P., Liu, Y., Carlile, T. M., Chowdhury, T., Doyle, B., Clarner, P., Mangaudis, K., Guilmette, E., … Lo, S.-C. (2025). Dorsal root ganglion toxicity after AAV intra-CSF delivery of a RNAi expression construct into non-human primates and mice. *Molecular Therapy*, *33*(1), 215–234. https://doi.org/10.1016/j.ymthe.2024.11.029

He, J.-T., Li, X.-Y., Zhao, X., & Liu, X. (2019). Hyperpolarization-activated and cyclic nucleotide-gated channel proteins as emerging new targets in neuropathic pain.

Reviews in the Neurosciences, *30*(6), 639–649. https://doi.org/10.1515/revneuro-2018-0094

High, K. A., & Roncarolo, M. G. (2019). Gene Therapy. *New England Journal of Medicine*, *381*(5), 455–464. https://doi.org/10.1056/NEJMra1706910

Hill, R. (2000). NK1 (substance P) receptor antagonists – why are they not analgesic in humans? *Trends in Pharmacological Sciences*, *21*(7), 244–246. https://doi.org/10.1016/S0165-6147(00)01502-9

Hinderer, C., Katz, N., Buza, E. L., Dyer, C., Goode, T., Bell, P., Richman, L. K., & Wilson, J. M. (2018). Severe Toxicity in Nonhuman Primates and Piglets Following High-Dose Intravenous Administration of an Adeno-Associated Virus Vector Expressing Human SMN. *Human Gene Therapy*, *29*(3), 285–298. https://doi.org/10.1089/hum.2018.015

Hirakawa, H., Okajima, S., Nagaoka, T., Kubo, T., Takamatsu, T., & Oyamada, M. (2004). Regional differences in blood–nerve barrier function and tight-junction protein expression within the rat dorsal root ganglion: *NeuroReport*, *15*(3), 405–408. https://doi.org/10.1097/00001756-200403010-00004

Ho, A., Orton, R., Tayler, R., Asamaphan, P., Herder, V., Davis, C., Tong, L., Smollett, K., Manali, M., Allan, J., Rawlik, K., McDonald, S. E., Vink, E., Pollock, L., Gannon, L., Evans, C., McMenamin, J., Roy, K., Marsh, K., … Thomson, E. C. (2023). Adeno-associated virus 2 infection in children with non-A–E hepatitis. *Nature*, *617*(7961), 555–563. https://doi.org/10.1038/s41586-023-05948-2

Ho, T. W., Edvinsson, L., & Goadsby, P. J. (2010). CGRP and its receptors provide new insights into migraine pathophysiology. *Nature Reviews Neurology*, *6*(10), 573–582. https://doi.org/10.1038/nrneurol.2010.127

Holsheimer, J. (2002). Which Neuronal Elements are Activated Directly by Spinal Cord Stimulation. *Neuromodulation: Technology at the Neural Interface*, *5*(1), 25–31. https://doi.org/10.1046/j.1525-1403.2002._2005.x

Hordeaux, J., Buza, E. L., Jeffrey, B., Song, C., Jahan, T., Yuan, Y., Zhu, Y., Bell, P., Li, M., Chichester, J. A., Calcedo, R., & Wilson, J. M. (2020). MicroRNA-mediated inhibition of transgene expression reduces dorsal root ganglion toxicity by AAV vectors in primates. *Science Translational Medicine*, *12*(569), eaba9188. https://doi.org/10.1126/scitranslmed.aba9188

Hordeaux, J., Wang, Q., Katz, N., Buza, E. L., Bell, P., & Wilson, J. M. (2018). The Neurotropic Properties of AAV-PHP.B Are Limited to C57BL/6J Mice. *Molecular Therapy*, *26*(3), 664–668. https://doi.org/10.1016/j.ymthe.2018.01.018

Hou, X., Zaks, T., Langer, R., & Dong, Y. (2021). Lipid nanoparticles for mRNA delivery. *Nature Reviews Materials*, *6*(12), 1078–1094. https://doi.org/10.1038/s41578-021-00358-0

Hudry, E., & Vandenberghe, L. H. (2019). Therapeutic AAV Gene Transfer to the Nervous System: A Clinical Reality. *Neuron*, *102*(1), 263. https://doi.org/10.1016/j.neuron.2019.03.020

Huygen, F. J. P. M., Kallewaard, J. W., Nijhuis, H., Liem, L., Vesper, J., Fahey, M. E., Blomme, B., Morgalla, M. H., Deer, T. R., & Capobianco, R. A. (2020). Effectiveness and Safety of Dorsal Root Ganglion Stimulation for the Treatment of Chronic Pain: A Pooled Analysis. *Neuromodulation: Technology at the Neural Interface*, *23*(2), 213–221. https://doi.org/10.1111/ner.13074

Huygen, F. J. P. M., Soulanis, K., Rtveladze, K., Kamra, S., & Schlueter, M. (2024). Spinal Cord Stimulation vs Medical Management for Chronic Back and Leg Pain:

A Systematic Review and Network Meta-Analysis. *JAMA Network Open*, *7*(11), e2444608. https://doi.org/10.1001/jamanetworkopen.2024.44608

Issa, S. S., Shaimardanova, A. A., Solovyeva, V. V., & Rizvanov, A. A. (2023). Various AAV Serotypes and Their Applications in Gene Therapy: An Overview. *Cells*, *12*(5), 785. https://doi.org/10.3390/cells12050785

Iwata, K., Katagiri, A., & Shinoda, M. (2017). Neuron-glia interaction is a key mechanism underlying persistent orofacial pain. *Journal of Oral Science*, *59*(2), 173–175. https://doi.org/10.2334/josnusd.16-0858

Iyer, S. M., Montgomery, K. L., Towne, C., Lee, S. Y., Ramakrishnan, C., Deisseroth, K., & Delp, S. L. (2014). Virally mediated optogenetic excitation and inhibition of pain in freely moving nontransgenic mice. *Nature Biotechnology*, *32*(3), 274–278. https://doi.org/10.1038/nbt.2834

Jacques, S. J., Ahmed, Z., Forbes, A., Douglas, M. R., Vigenswara, V., Berry, M., & Logan, A. (2012). AAV8gfp preferentially targets large diameter dorsal root ganglion neurones after both intra-dorsal root ganglion and intrathecal injection. *Molecular and Cellular Neuroscience*, *49*(4), 464–474. https://doi.org/10.1016/j.mcn.2012.03.002

Jarvis, M. F., Honore, P., Shieh, C.-C., Chapman, M., Joshi, S., Zhang, X.-F., Kort, M., Carroll, W., Marron, B., Atkinson, R., Thomas, J., Liu, D., Krambis, M., Liu, Y., McGaraughty, S., Chu, K., Roeloffs, R., Zhong, C., Mikusa, J. P., … Krafte, D. S. (2007). A-803467, a potent and selective Na_v 1.8 sodium channel blocker, attenuates neuropathic and inflammatory pain in the rat. *Proceedings of the National Academy of Sciences*, *104*(20), 8520–8525. https://doi.org/10.1073/pnas.0611364104

Jarvis, M. F., & Khakh, B. S. (2009). ATP-gated P2X cation-channels. *Neuropharmacology*, *56*(1), 208–215. https://doi.org/10.1016/j.neuropharm.2008.06.067

Jeon, Y. H. (2012). Spinal Cord Stimulation in Pain Management: A Review. *The Korean Journal of Pain*, *25*(3), 143–150. https://doi.org/10.3344/kjp.2012.25.3.143

Ji, R.-R., Chamessian, A., & Zhang, Y.-Q. (2016). Pain regulation by non-neuronal cells and inflammation. *Science*, *354*(6312), 572–577. https://doi.org/10.1126/science.aaf8924

Ji, R.-R., Nackley, A., Huh, Y., Terrando, N., & Maixner, W. (2018). Neuroinflammation and Central Sensitization in Chronic and Widespread Pain. *Anesthesiology*, *129*(2), 343–366. https://doi.org/10.1097/ALN.0000000000002130

Ji, Y., Shi, W., Yang, J., Ma, B., Jin, T., Cao, B., Liu, X., & Ma, K. (2022). Effect of sympathetic sprouting on the excitability of dorsal root ganglion neurons and afferents in a rat model of neuropathic pain. *Biochemical and Biophysical Research Communications*, *587*, 49–57. https://doi.org/10.1016/j.bbrc.2021.11.096

Kang, H. J., Krumm, B. E., Tassou, A., Geron, M., DiBerto, J. F., Kapolka, N. J., Gumpper, R. H., Sakamoto, K., Dewran Kocak, D., Olsen, R. H. J., Huang, X.-P., Zhang, S., Huang, K. L., Zaidi, S. A., Nguyen, MyV. T., Jo, M. J., Katritch, V., Fay, J. F., Scherrer, G., & Roth, B. L. (2024). Structure-guided design of a peripherally restricted chemogenetic system. *Cell*, *187*(26), 7433-7449.e20. https://doi.org/10.1016/j.cell.2024.11.001

Kaur, R., Sidhu, P., & Singh, S. (2016). What failed BIA 10–2474 Phase I clinical trial? Global speculations and recommendations for future Phase I trials. *Journal of*

Pharmacology and Pharmacotherapeutics, *7*(3), 120–126. https://doi.org/10.4103/0976-500X.189661

Khalil, M., Teunissen, C. E., Otto, M., Piehl, F., Sormani, M. P., Gattringer, T., Barro, C., Kappos, L., Comabella, M., Fazekas, F., Petzold, A., Blennow, K., Zetterberg, H., & Kuhle, J. (2018). Neurofilaments as biomarkers in neurological disorders. *Nature Reviews Neurology*, *14*(10), 577–589. https://doi.org/10.1038/s41582-018-0058-z

Khare, P., Dave, K. M., Kamte, Y. S., Manoharan, M. A., O'Donnell, L. A., & Manickam, D. S. (2021). Development of Lipidoid Nanoparticles for siRNA Delivery to Neural Cells. *The AAPS Journal*, *24*(1), 8. https://doi.org/10.1208/s12248-021-00653-2

Kim, J. S., Meeker, S., Ru, F., Tran, M., Zabka, T. S., Hackos, D., & Undem, B. J. (2024). Role of Na_V 1.7 in postganglionic sympathetic nerve function in human and guinea-pig arteries. *The Journal of Physiology*, *602*(14), 3505–3518. https://doi.org/10.1113/JP286538

Kingwell, K. (2019). Nav1.7 withholds its pain potential. *Nature Reviews Drug Discovery*, *18*(5), 321–323. https://doi.org/10.1038/d41573-019-00065-0

Klein, P. M., Nguyen, Q., Homidan, J., & Soltesz, I. (2021). *Controlling focal seizures using novel chemogenetic tools*. https://aesnet.org/abstractslisting/controlling-focal-seizures-using-novel-chemogenetic-tools

Kneynsberg, A., Collier, T. J., Manfredsson, F. P., & Kanaan, N. M. (2016). Quantitative and semi-quantitative measurements of axonal degeneration in tissue and primary neuron cultures. *Journal of Neuroscience Methods*, *266*, 32–41. https://doi.org/10.1016/j.jneumeth.2016.03.004

Knowlton, W. M., Palkar, R., Lippoldt, E. K., McCoy, D. D., Baluch, F., Chen, J., & McKemy, D. D. (2013). A Sensory-Labeled Line for Cold: TRPM8-Expressing Sensory Neurons Define the Cellular Basis for Cold, Cold Pain, and Cooling-Mediated Analgesia. *The Journal of Neuroscience*, *33*(7), 2837–2848. https://doi.org/10.1523/JNEUROSCI.1943-12.2013

Koivisto, A.-P., Voets, T., Iadarola, M. J., & Szallasi, A. (2024). Targeting TRP channels for pain relief: A review of current evidence from bench to bedside. *Current Opinion in Pharmacology*, *75*, 102447. https://doi.org/10.1016/j.coph.2024.102447

Korczeniewska, O. A., James, M. H., Eliav, T., Katzmann Rider, G., Mehr, J. B., Affendi, H., Aston-Jones, G., & Benoliel, R. (2022). Chemogenetic inhibition of trigeminal ganglion neurons attenuates behavioural and neural pain responses in a model of trigeminal neuropathic pain. *European Journal of Pain*, *26*(3), 634–647. https://doi.org/10.1002/ejp.1887

Kotin, R. M., Linden, R. M., & Berns, K. I. (1992). Characterization of a preferred site on human chromosome 19q for integration of adeno-associated virus DNA by non-homologous recombination. *The EMBO Journal*, *11*(13), 5071–5078. https://doi.org/10.1002/j.1460-2075.1992.tb05614.x

Kotin, R. M., Siniscalco, M., Samulski, R. J., Zhu, X. D., Hunter, L., Laughlin, C. A., McLaughlin, S., Muzyczka, N., Rocchi, M., & Berns, K. I. (1990). Site-specific integration by adeno-associated virus. *Proceedings of the National Academy of Sciences*, *87*(6), 2211–2215. https://doi.org/10.1073/pnas.87.6.2211

Koyanagi, M., Ogido, R., Moriya, A., Saigo, M., Ihida, S., Teranishi, T., Kawada, J., Katsuno, T., Matsubara, K., Terada, T., Yamashita, A., & Imai, S. (2024). Development of a 3-dimensional organotypic model with characteristics of

peripheral sensory nerves. *Cell Reports Methods*, *4*(8), 100835. https://doi.org/10.1016/j.crmeth.2024.100835

Krames, E. S. (2014). The Role of the Dorsal Root Ganglion in the Development of Neuropathic Pain. *Pain Medicine*, *15*(10), 1669–1685. https://doi.org/10.1111/pme.12413

Kriya Therapeutics. (2022, November 16). *Kriya Acquires Redpin Therapeutics, Adding Neurology Pipeline to Gene Therapy Portfolio*. https://kriyatherapeutics.com/news/kriya-acquires-redpin-therapeutics-adding-neurology-pipeline-to-gene-therapy-portfolio/

Krzemińska, A., Koźba-Gosztyła, M., Bladowska, J., & Czapiga, B. (2025). Efficacy of microvascular decompression in the treatment of trigeminal neuralgia: A retrospective Single-Center study of 28 cases. *Neurosurgical Review*, *48*(1), 614. https://doi.org/10.1007/s10143-025-03772-y

Kuner, R., & Kuner, T. (2021). Cellular Circuits in the Brain and Their Modulation in Acute and Chronic Pain. *Physiological Reviews*, *101*(1), 213–258. https://doi.org/10.1152/physrev.00040.2019

Kuzmin, D. A., Shutova, M. V., Johnston, N. R., Smith, O. P., Fedorin, V. V., Kukushkin, Y. S., Van Der Loo, J. C. M., & Johnstone, E. C. (2021). The clinical landscape for AAV gene therapies. *Nature Reviews Drug Discovery*, *20*(3), 173–174. https://doi.org/10.1038/d41573-021-00017-7

La Rovere, M. T., Pinna, G. D., & Raczak, G. (2008). Baroreflex Sensitivity: Measurement and Clinical Implications. *Annals of Noninvasive Electrocardiology*, *13*(2), 191–207. https://doi.org/10.1111/j.1542-474X.2008.00219.x

Latremoliere, A., & Woolf, C. J. (2009). Central Sensitization: A Generator of Pain Hypersensitivity by Central Neural Plasticity. *The Journal of Pain*, *10*(9), 895–926. https://doi.org/10.1016/j.jpain.2009.06.012

Lee, P. R., Kim, J., Rossi, H. L., Chung, S., Han, S. Y., Kim, J., & Oh, S. B. (2023). Transcriptional profiling of dental sensory and proprioceptive trigeminal neurons using single-cell RNA sequencing. *International Journal of Oral Science*, *15*(1), 45. https://doi.org/10.1038/s41368-023-00246-z

Lerchner, W., Xiao, C., Nashmi, R., Slimko, E. M., Van Trigt, L., Lester, H. A., & Anderson, D. J. (2007). Reversible Silencing of Neuronal Excitability in Behaving Mice by a Genetically Targeted, Ivermectin-Gated Cl− Channel. *Neuron*, *54*(1), 35–49. https://doi.org/10.1016/j.neuron.2007.02.030

Lespine, A., Martin, S., Dupuy, J., Roulet, A., Pineau, T., Orlowski, S., & Alvinerie, M. (2007). Interaction of macrocyclic lactones with P-glycoprotein: Structure–affinity relationship. *European Journal of Pharmaceutical Sciences*, *30*(1), 84–94. https://doi.org/10.1016/j.ejps.2006.10.004

Li, C., & Samulski, R. J. (2020). Engineering adeno-associated virus vectors for gene therapy. *Nature Reviews Genetics*, *21*(4), 255–272. https://doi.org/10.1038/s41576-019-0205-4

Lieb, A., Qiu, Y., Dixon, C. L., Heller, J. P., Walker, M. C., Schorge, S., & Kullmann, D. M. (2018). Biochemical autoregulatory gene therapy for focal epilepsy. *Nature Medicine*, *24*(9), 1324–1329. https://doi.org/10.1038/s41591-018-0103-x

Lieb, A., Weston, M., & Kullmann, D. M. (2019). Designer receptor technology for the treatment of epilepsy. *EBioMedicine*, *43*, 641–649. https://doi.org/10.1016/j.ebiom.2019.04.059

Ling, Q., Herstine, J. A., Bradbury, A., & Gray, S. J. (2023). AAV-based in vivo gene therapy for neurological disorders. *Nature Reviews Drug Discovery*, *22*(10), 789–806. https://doi.org/10.1038/s41573-023-00766-7

Long, H., Liao, L., Zhou, Y., Shan, D., Gao, M., Huang, R., Yang, X., & Lai, W. (2017). A novel technique of delivering viral vectors to trigeminal ganglia in rats. *European Journal of Oral Sciences*, *125*(1), 1–7. https://doi.org/10.1111/eos.12326

Love, S., & Coakham, H. B. (2001). Trigeminal neuralgia: Pathology and pathogenesis. *Brain*, *124*(12), 2347–2360. https://doi.org/10.1093/brain/124.12.2347

Lu, T., Wang, M., Zhou, W., Ni, Q., Yue, Y., Wang, W., Shi, Y., Liu, Z., Li, C., Hong, B., Zhou, X., Zhong, S., Wang, K., Zeng, B., Zhang, J., Wang, W., Zhang, X., Wu, Q., & Wang, X. (2024). Decoding transcriptional identity in developing human sensory neurons and organoid modeling. *Cell*, *187*(26), 7374-7393.e28. https://doi.org/10.1016/j.cell.2024.10.023

Ma, Q. (2012). Population coding of somatic sensations. *Neuroscience Bulletin*, *28*(2), 91–99. https://doi.org/10.1007/s12264-012-1201-2

Maarbjerg, S., Wolfram, F., Gozalov, A., Olesen, J., & Bendtsen, L. (2015). Significance of neurovascular contact in classical trigeminal neuralgia. *Brain*, *138*(2), 311–319. https://doi.org/10.1093/brain/awu349

Machida, A., Kuwahara, H., Mayra, A., Kubodera, T., Hirai, T., Sunaga, F., Tajiri, M., Hirai, Y., Shimada, T., Mizusawa, H., & Yokota, T. (2013). Intraperitoneal Administration of AAV9-shRNA Inhibits Target Gene Expression in the Dorsal Root Ganglia of Neonatal Mice. *Molecular Pain*, *9*, 1744-8069-9–36. https://doi.org/10.1186/1744-8069-9-36

MacLaren, D. A. A., Browne, R. W., Shaw, J. K., Krishnan Radhakrishnan, S., Khare, P., España, R. A., & Clark, S. D. (2016). Clozapine N-Oxide Administration Produces Behavioral Effects in Long–Evans Rats: Implications for Designing DREADD Experiments. *Eneuro*, *3*(5), ENEURO.0219-16.2016. https://doi.org/10.1523/ENEURO.0219-16.2016

Magnus, C. J., Lee, P. H., Atasoy, D., Su, H. H., Looger, L. L., & Sternson, S. M. (2011). Chemical and Genetic Engineering of Selective Ion Channel–Ligand Interactions. *Science*, *333*(6047), 1292–1296. https://doi.org/10.1126/science.1206606

Magnus, C. J., Lee, P. H., Bonaventura, J., Zemla, R., Gomez, J. L., Ramirez, M. H., Hu, X., Galvan, A., Basu, J., Michaelides, M., & Sternson, S. M. (2019). Ultrapotent chemogenetics for research and potential clinical applications. *Science*, *364*(6436), eaav5282. https://doi.org/10.1126/science.aav5282

Maningat, A. L., & Munakomi, S. (2023). Neuroanatomy, Superior Cervical Ganglion. In *StatPearls*. StatPearls Publishing. http://www.ncbi.nlm.nih.gov/books/NBK544331/

Mason, M. R., Ehlert, E. M., Eggers, R., Pool, C. W., Hermening, S., Huseinovic, A., Timmermans, E., Blits, B., & Verhaagen, J. (2010). Comparison of AAV Serotypes for Gene Delivery to Dorsal Root Ganglion Neurons. *Molecular Therapy*, *18*(4), 715–724. https://doi.org/10.1038/mt.2010.19

McCarty, D., Monahan, P., & Samulski, R. (2001). Self-complementary recombinant adeno-associated virus (scAAV) vectors promote efficient transduction independently of DNA synthesis. *Gene Therapy*, *8*(16), 1248–1254. https://doi.org/10.1038/sj.gt.3301514

McGinnis, A., & Ji, R.-R. (2023). The Similar and Distinct Roles of Satellite Glial Cells and Spinal Astrocytes in Neuropathic Pain. *Cells*, *12*(6), 965. https://doi.org/10.3390/cells12060965

McKemy, D. D. (2005). How Cold is It? TRPM8 and TRPA1 in the Molecular Logic of Cold Sensation. *Molecular Pain*, *1*, 1744-8069-1–16. https://doi.org/10.1186/1744-8069-1-16

McKemy, D. D., Neuhausser, W. M., & Julius, D. (2002). Identification of a cold receptor reveals a general role for TRP channels in thermosensation. *Nature*, *416*(6876), 52–58. https://doi.org/10.1038/nature719

McLachlan, E. M., Jänig, W., Devor, M., & Michaelis, M. (1993). Peripheral nerve injury triggers noradrenergic sprouting within dorsal root ganglia. *Nature*, *363*(6429), 543–546. https://doi.org/10.1038/363543a0

Meacham, K., Shepherd, A., Mohapatra, D. P., & Haroutounian, S. (2017). Neuropathic Pain: Central vs. Peripheral Mechanisms. *Current Pain and Headache Reports*, *21*(6), 28. https://doi.org/10.1007/s11916-017-0629-5

Mendell, J. R., Al-Zaidy, S., Shell, R., Arnold, W. D., Rodino-Klapac, L. R., Prior, T. W., Lowes, L., Alfano, L., Berry, K., Church, K., Kissel, J. T., Nagendran, S., L'Italien, J., Sproule, D. M., Wells, C., Cardenas, J. A., Heitzer, M. D., Kaspar, A., Corcoran, S., … Kaspar, B. K. (2017). Single-Dose Gene-Replacement Therapy for Spinal Muscular Atrophy. *New England Journal of Medicine*, *377*(18), 1713–1722. https://doi.org/10.1056/NEJMoa1706198

Messlinger, K., & Russo, A. F. (2019). Current understanding of trigeminal ganglion structure and function in headache. *Cephalalgia*, *39*(13), 1661–1674. https://doi.org/10.1177/0333102418786261

Middleton, S. J., Hu, H., Perez-Sanchez, J., Zuberi, S., McGrath Williams, J., Weir, G. A., & Bennett, D. L. (2023). GluCl.CreON enables selective inhibition of molecularly defined pain circuits. *Pain*, *164*(12), 2780–2791. https://doi.org/10.1097/j.pain.0000000000002976

Middleton, S. J., Perini, I., Themistocleous, A. C., Weir, G. A., McCann, K., Barry, A. M., Marshall, A., Lee, M., Mayo, L. M., Bohic, M., Baskozos, G., Morrison, I., Löken, L. S., McIntyre, S., Nagi, S. S., Staud, R., Sehlstedt, I., Johnson, R. D., Wessberg, J., … Bennett, D. L. (2022). Nav1.7 is required for normal C-low threshold mechanoreceptor function in humans and mice. *Brain*, *145*(10), 3637–3653. https://doi.org/10.1093/brain/awab482

Miller, S., Sinclair, A. J., Davies, B., & Matharu, M. (2016). Neurostimulation in the treatment of primary headaches. *Practical Neurology*, *16*(5), 362–375. https://doi.org/10.1136/practneurol-2015-001298

Mills, S. E. E., Nicolson, K. P., & Smith, B. H. (2019). Chronic pain: A review of its epidemiology and associated factors in population-based studies. *British Journal of Anaesthesia*, *123*(2), e273–e283. https://doi.org/10.1016/j.bja.2019.03.023

Milone, M. C., & O'Doherty, U. (2018). Clinical use of lentiviral vectors. *Leukemia*, *32*(7), 1529–1541. https://doi.org/10.1038/s41375-018-0106-0

Mingozzi, F., & High, K. A. (2013). Immune responses to AAV vectors: Overcoming barriers to successful gene therapy. *Blood*, *122*(1), 23–36. https://doi.org/10.1182/blood-2013-01-306647

Misgeld, T., & Schwarz, T. L. (2017). Mitostasis in Neurons: Maintaining Mitochondria in an Extended Cellular Architecture. *Neuron*, *96*(3), 651–666. https://doi.org/10.1016/j.neuron.2017.09.055

Morchio, M., Sankaranarayanan, I., Tavares-Ferreira, D., Wong, N., Atkins, S., Sher, E., Price, T. J., Lambert, D. W., & Boissonade, F. M. (2024). *Investigation of cellular and molecular changes linked with neuropathic pain in healthy and injured human trigeminal nerves* (p. 2024.10.05.616798). bioRxiv. https://doi.org/10.1101/2024.10.05.616798

Muhuri, M., Maeda, Y., Ma, H., Ram, S., Fitzgerald, K. A., Tai, P. W. L., & Gao, G. (2021). Overcoming innate immune barriers that impede AAV gene therapy vectors. *Journal of Clinical Investigation*, *131*(1), e143780. https://doi.org/10.1172/JCI143780

Murlidharan, G., Sakamoto, K., Rao, L., Corriher, T., Wang, D., Gao, G., Sullivan, P., & Asokan, A. (2016). CNS-restricted Transduction and CRISPR/Cas9-mediated Gene Deletion with an Engineered AAV Vector. *Molecular Therapy - Nucleic Acids*, *5*, e338. https://doi.org/10.1038/mtna.2016.49

Nagai, Y., Miyakawa, N., Takuwa, H., Hori, Y., Oyama, K., Ji, B., Takahashi, M., Huang, X.-P., Slocum, S. T., DiBerto, J. F., Xiong, Y., Urushihata, T., Hirabayashi, T., Fujimoto, A., Mimura, K., English, J. G., Liu, J., Inoue, K., Kumata, K., … Minamimoto, T. (2020). Deschloroclozapine, a potent and selective chemogenetic actuator enables rapid neuronal and behavioral modulations in mice and monkeys. *Nature Neuroscience*, *23*(9), 1157–1167. https://doi.org/10.1038/s41593-020-0661-3

Naldini, L. (2015). Gene therapy returns to centre stage. *Nature*, *526*(7573), 351–360. https://doi.org/10.1038/nature15818

Naso, M. F., Tomkowicz, B., Perry, W. L., & Strohl, W. R. (2017). Adeno-Associated Virus (AAV) as a Vector for Gene Therapy. *BioDrugs*, *31*(4), 317–334. https://doi.org/10.1007/s40259-017-0234-5

Nassar, M. A., Stirling, L. C., Forlani, G., Baker, M. D., Matthews, E. A., Dickenson, A. H., & Wood, J. N. (2004). Nociceptor-specific gene deletion reveals a major role for Na_v 1.7 (PN1) in acute and inflammatory pain. *Proceedings of the National Academy of Sciences*, *101*(34), 12706–12711. https://doi.org/10.1073/pnas.0404915101

Nault, J.-C., Datta, S., Imbeaud, S., Franconi, A., Mallet, M., Couchy, G., Letouzé, E., Pilati, C., Verret, B., Blanc, J.-F., Balabaud, C., Calderaro, J., Laurent, A., Letexier, M., Bioulac-Sage, P., Calvo, F., & Zucman-Rossi, J. (2015). Recurrent AAV2-related insertional mutagenesis in human hepatocellular carcinomas. *Nature Genetics*, *47*(10), 1187–1193. https://doi.org/10.1038/ng.3389

Negro, A., & Martelletti, P. (2019). Gepants for the treatment of migraine. *Expert Opinion on Investigational Drugs*, *28*(6), 555–567. https://doi.org/10.1080/13543784.2019.1618830

Neubert, J. K., Mannes, A. J., Keller, J., Wexel, M., Iadarola, M. J., & Caudle, R. M. (2005). Peripheral targeting of the trigeminal ganglion via the infraorbital foramen as a therapeutic strategy. *Brain Research Protocols*, *15*(3), 119–126. https://doi.org/10.1016/j.brainresprot.2005.05.003

Nguyen, M. Q., Von Buchholtz, L. J., Reker, A. N., Ryba, N. J., & Davidson, S. (2021). Single-nucleus transcriptomic analysis of human dorsal root ganglion neurons. *eLife*, *10*, e71752. https://doi.org/10.7554/eLife.71752

Nguyen, M. Q., Wu, Y., Bonilla, L. S., Von Buchholtz, L. J., & Ryba, N. J. P. (2017). Diversity amongst trigeminal neurons revealed by high throughput single cell sequencing. *PLOS ONE*, *12*(9), e0185543. https://doi.org/10.1371/journal.pone.0185543

NICE. (2020, September 22). *Overview | Neuropathic pain in adults: Pharmacological management in non-specialist settings | Guidance | NICE*. NICE. https://www.nice.org.uk/guidance/cg173

Nicolson, S. C., & Samulski, R. J. (2014). Recombinant Adeno-Associated Virus Utilizes Host Cell Nuclear Import Machinery To Enter the Nucleus. *Journal of Virology*, *88*(8), 4132–4144. https://doi.org/10.1128/JVI.02660-13

Nissim, L., Perli, S. D., Fridkin, A., Perez-Pinera, P., & Lu, T. K. (2014). Multiplexed and Programmable Regulation of Gene Networks with an Integrated RNA and CRISPR/Cas Toolkit in Human Cells. *Molecular Cell*, *54*(4), 698–710. https://doi.org/10.1016/j.molcel.2014.04.022

Nockemann, D., Rouault, M., Labuz, D., Hublitz, P., McKnelly, K., Reis, F. C., Stein, C., & Heppenstall, P. A. (2013). The K^+ channel GIRK2 is both necessary and sufficient for peripheral opioid-mediated analgesia. *EMBO Molecular Medicine*, *5*(8), 1263–1277. https://doi.org/10.1002/emmm.201201980

Obeng, S., Hiranita, T., León, F., McMahon, L. R., & McCurdy, C. R. (2021). Novel Approaches, Drug Candidates, and Targets in Pain Drug Discovery. *Journal of Medicinal Chemistry*, *64*(10), 6523–6548. https://doi.org/10.1021/acs.jmedchem.1c00028

O'Donnell, M., Fontaine, A., Caldwell, J., & Weir, R. (2024). Direct dorsal root ganglia (DRG) injection in mice for analysis of adeno-associated viral (AAV) gene transfer to peripheral somatosensory neurons. *Journal of Neuroscience Methods*, *411*, 110268. https://doi.org/10.1016/j.jneumeth.2024.110268

Olesen, J., Iversen, H. K., & Thomsen, L. L. (1993). Nitric oxide supersensitivity: A possible molecular mechanism of migraine pain: *NeuroReport*, *4*(8), 1027–1030. https://doi.org/10.1097/00001756-199308000-00008

Ozelo, M. C., Mahlangu, J., Pasi, K. J., Giermasz, A., Leavitt, A. D., Laffan, M., Symington, E., Quon, D. V., Wang, J.-D., Peerlinck, K., Pipe, S. W., Madan, B., Key, N. S., Pierce, G. F., O'Mahony, B., Kaczmarek, R., Henshaw, J., Lawal, A., Jayaram, K., … Kim, B. (2022). Valoctocogene Roxaparvovec Gene Therapy for Hemophilia A. *New England Journal of Medicine*, *386*(11), 1013–1025. https://doi.org/10.1056/NEJMoa2113708

Pasi, K. J., Rangarajan, S., Mitchell, N., Lester, W., Symington, E., Madan, B., Laffan, M., Russell, C. B., Li, M., Pierce, G. F., & Wong, W. Y. (2020). Multiyear Follow-up of AAV5-hFVIII-SQ Gene Therapy for Hemophilia A. *New England Journal of Medicine*, *382*(1), 29–40. https://doi.org/10.1056/NEJMoa1908490

Passaro, A. P., Lebos, A. L., Yao, Y., & Stice, S. L. (2021). Immune Response in Neurological Pathology: Emerging Role of Central and Peripheral Immune Crosstalk. *Frontiers in Immunology*, *12*, 676621. https://doi.org/10.3389/fimmu.2021.676621

Percie Du Sert, N., Ahluwalia, A., Alam, S., Avey, M. T., Baker, M., Browne, W. J., Clark, A., Cuthill, I. C., Dirnagl, U., Emerson, M., Garner, P., Holgate, S. T., Howells, D. W., Hurst, V., Karp, N. A., Lazic, S. E., Lidster, K., MacCallum, C. J., Macleod, M., … Würbel, H. (2020). Reporting animal research: Explanation and elaboration for the ARRIVE guidelines 2.0. *PLOS Biology*, *18*(7), e3000411. https://doi.org/10.1371/journal.pbio.3000411

Perez-Sanchez, J., Middleton, S. J., Pattison, L. A., Hilton, H., Ali Awadelkareem, M., Zuberi, S. R., Renke, M. B., Hu, H., Yang, X., Clark, A. J., St. John Smith, E., & Bennett, D. L. (2023). A humanized chemogenetic system inhibits murine pain-related behavior and hyperactivity in human sensory neurons. *Science*

Translational Medicine, *15*(716), eadh3839. https://doi.org/10.1126/scitranslmed.adh3839

Pertovaara, A. (2006). Noradrenergic pain modulation. *Progress in Neurobiology*, *80*(2), 53–83. https://doi.org/10.1016/j.pneurobio.2006.08.001

Pfeffer, C. K., Stein, V., Keating, D. J., Maier, H., Rinke, I., Rudhard, Y., Hentschke, M., Rune, G. M., Jentsch, T. J., & Hübner, C. A. (2009). NKCC1-Dependent GABAergic Excitation Drives Synaptic Network Maturation during Early Hippocampal Development. *The Journal of Neuroscience*, *29*(11), 3419–3430. https://doi.org/10.1523/JNEUROSCI.1377-08.2009

Pillay, S., Meyer, N. L., Puschnik, A. S., Davulcu, O., Diep, J., Ishikawa, Y., Jae, L. T., Wosen, J. E., Nagamine, C. M., Chapman, M. S., & Carette, J. E. (2016). An essential receptor for adeno-associated virus infection. *Nature*, *530*(7588), 108–112. https://doi.org/10.1038/nature16465

Poth, K. M., Texakalidis, P., & Boulis, N. M. (2021). Chemogenetics: Beyond Lesions and Electrodes. *Neurosurgery*, *89*(2), 185–195. https://doi.org/10.1093/neuros/nyab147

Prabhakar, S., Lule, S., Da Hora, C. C., Breakefield, X. O., & Cheah, P. S. (2021). AAV9 transduction mediated by systemic delivery of vector via retro-orbital injection in newborn, neonatal and juvenile mice. *Experimental Animals*, *70*(4), 450–458. https://doi.org/10.1538/expanim.20-0186

Pradhan, A. A., Smith, M. L., McGuire, B., Tarash, I., Evans, C. J., & Charles, A. (2014). Characterization of a novel model of chronic migraine. *Pain*, *155*(2), 269–274. https://doi.org/10.1016/j.pain.2013.10.004

Prescott, S. A., Sejnowski, T. J., & De Koninck, Y. (2006). Reduction of Anion Reversal Potential Subverts the Inhibitory Control of Firing Rate in Spinal Lamina I

Neurons: Towards a Biophysical Basis for Neuropathic pain. *Molecular Pain*, *2*, 1744-8069-2–32. https://doi.org/10.1186/1744-8069-2-32

Price, T. J., Cervero, F., Gold, M. S., Hammond, D. L., & Prescott, S. A. (2009). Chloride regulation in the pain pathway. *Brain Research Reviews*, *60*(1), 149–170. https://doi.org/10.1016/j.brainresrev.2008.12.015

Purves, D., Augustine, G. J., Fitzpatrick, D., Hall, W. C., LaMantia, A.-S., Mooney, R. D., Platt, M. L., & White, L. E. (Eds). (2018). *Neuroscience*. OUP USA.

Qi, L., Iskols, M., Shi, D., Reddy, P., Walker, C., Lezgiyeva, K., Voisin, T., Pawlak, M., Kuchroo, V. K., Chiu, I. M., Ginty, D. D., & Sharma, N. (2024). A mouse DRG genetic toolkit reveals morphological and physiological diversity of somatosensory neuron subtypes. *Cell*, *187*(6), 1508-1526.e16. https://doi.org/10.1016/j.cell.2024.02.006

Rahman, Md., Lee, J., Kim, Y., & Park, C.-K. (2023). Epidural and Intrathecal Drug Delivery in Rats and Mice for Experimental Research: Fundamental Concepts, Techniques, Precaution, and Application. *Biomedicines*, *11*(5), 1413. https://doi.org/10.3390/biomedicines11051413

Raper, J., Morrison, R. D., Daniels, J. S., Howell, L., Bachevalier, J., Wichmann, T., & Galvan, A. (2017). Metabolism and Distribution of Clozapine-N-oxide: Implications for Nonhuman Primate Chemogenetics. *ACS Chemical Neuroscience*, *8*(7), 1570–1576. https://doi.org/10.1021/acschemneuro.7b00079

Rappaport, H. Z., & Devor, M. (1994). Trigeminal neuralgia: The role of self-sustaining discharge in the trigeminal ganglion. *Pain*, *56*(2), 127–138. https://doi.org/10.1016/0304-3959(94)90086-8

Rapti, K., Louis-Jeune, V., Kohlbrenner, E., Ishikawa, K., Ladage, D., Zolotukhin, S., Hajjar, R. J., & Weber, T. (2012). Neutralizing Antibodies Against AAV Serotypes

1, 2, 6, and 9 in Sera of Commonly Used Animal Models. *Molecular Therapy*, *20*(1), 73–83. https://doi.org/10.1038/mt.2011.177

Reinhold, A. K., & Rittner, H. L. (2020). Characteristics of the nerve barrier and the blood dorsal root ganglion barrier in health and disease. *Experimental Neurology*, *327*, 113244. https://doi.org/10.1016/j.expneurol.2020.113244

Ren, K., & Dubner, R. (2010). Interactions between the immune and nervous systems in pain. *Nature Medicine*, *16*(11), 1267–1276. https://doi.org/10.1038/nm.2234

Renthal, W., Tochitsky, I., Yang, L., Cheng, Y.-C., Li, E., Kawaguchi, R., Geschwind, D. H., & Woolf, C. J. (2020). Transcriptional Reprogramming of Distinct Peripheral Sensory Neuron Subtypes after Axonal Injury. *Neuron*, *108*(1), 128-144.e9. https://doi.org/10.1016/j.neuron.2020.07.026

Rivera, C., Voipio, J., Payne, J. A., Ruusuvuori, E., Lahtinen, H., Lamsa, K., Pirvola, U., Saarma, M., & Kaila, K. (1999). The K+/Cl− co-transporter KCC2 renders GABA hyperpolarizing during neuronal maturation. *Nature*, *397*(6716), 251–255. https://doi.org/10.1038/16697

Riyad, J. M., & Weber, T. (2021). Intracellular trafficking of adeno-associated virus (AAV) vectors: Challenges and future directions. *Gene Therapy*, *28*(12), 683–696. https://doi.org/10.1038/s41434-021-00243-z

Roth, B. L. (2016). DREADDs for Neuroscientists. *Neuron*, *89*(4), 683–694. https://doi.org/10.1016/j.neuron.2016.01.040

Rupniak, N. M. J., & Kramer, M. S. (2017). NK1 receptor antagonists for depression: Why a validated concept was abandoned. *Journal of Affective Disorders*, *223*, 121–125. https://doi.org/10.1016/j.jad.2017.07.042

Russell, W. (2005). The Three Rs: Past, present and future. *Animal Welfare*, *14*(4), 279–286. https://doi.org/10.1017/S0962728600029596

Russo, A. F., & Hay, D. L. (2023). CGRP physiology, pharmacology, and therapeutic targets: Migraine and beyond. *Physiological Reviews*, *103*(2), 1565–1644. https://doi.org/10.1152/physrev.00059.2021

Saloman, J. L., Scheff, N. N., Snyder, L. M., Ross, S. E., Davis, B. M., & Gold, M. S. (2016). Gi-DREADD Expression in Peripheral Nerves Produces Ligand-Dependent Analgesia, as well as Ligand-Independent Functional Changes in Sensory Neurons. *The Journal of Neuroscience*, *36*(42), 10769–10781. https://doi.org/10.1523/JNEUROSCI.3480-15.2016

Salter, M. W. (2014). Deepening understanding of the neural substrates of chronic pain. *Brain*, *137*(3), 651–653. https://doi.org/10.1093/brain/awu028

Samulski, R. J., Chang, L. S., & Shenk, T. (1989). Helper-free stocks of recombinant adeno-associated viruses: Normal integration does not require viral gene expression. *Journal of Virology*, *63*(9), 3822–3828. https://doi.org/10.1128/jvi.63.9.3822-3828.1989

Samulski, R. J., & Muzyczka, N. (2014). AAV-Mediated Gene Therapy for Research and Therapeutic Purposes. *Annual Review of Virology*, *1*(1), 427–451. https://doi.org/10.1146/annurev-virology-031413-085355

Sapunar, D., Sandra Kostic, Adriana Banozic, & Livia Puljak. (2012). Dorsal root ganglion – a potential new therapeutic target for neuropathic pain. *Journal of Pain Research*, 31. https://doi.org/10.2147/JPR.S26603

Schiavo, G. G., Benfenati, F., Poulain, B., Rossetto, O., De Laureto, P. P., DasGupta, B. R., & Montecucco, C. (1992). Tetanus and botulinum-B neurotoxins block neurotransmitter release by proteolytic cleavage of synaptobrevin. *Nature*, *359*(6398), 832–835. https://doi.org/10.1038/359832a0

Schnütgen, F., Doerflinger, N., Calléja, C., Wendling, O., Chambon, P., & Ghyselinck, N. B. (2003). A directional strategy for monitoring Cre-mediated recombination at the cellular level in the mouse. *Nature Biotechnology*, *21*(5), 562–565. https://doi.org/10.1038/nbt811

Schuster, D. J., Dykstra, J. A., Riedl, M. S., Kitto, K. F., Belur, L. R., McIvor, R. S., Elde, R. P., Fairbanks, C. A., & Vulchanova, L. (2014). Biodistribution of adeno-associated virus serotype 9 (AAV9) vector after intrathecal and intravenous delivery in mouse. *Frontiers in Neuroanatomy*, *8*. https://doi.org/10.3389/fnana.2014.00042

Servellita, V., Sotomayor Gonzalez, A., Lamson, D. M., Foresythe, A., Huh, H. J., Bazinet, A. L., Bergman, N. H., Bull, R. L., Garcia, K. Y., Goodrich, J. S., Lovett, S. P., Parker, K., Radune, D., Hatada, A., Pan, C.-Y., Rizzo, K., Bertumen, J. B., Morales, C., Oluniyi, P. E., … Chiu, C. Y. (2023). Adeno-associated virus type 2 in US children with acute severe hepatitis. *Nature*, *617*(7961), 574–580. https://doi.org/10.1038/s41586-023-05949-1

Sharma, N., Flaherty, K., Lezgiyeva, K., Wagner, D. E., Klein, A. M., & Ginty, D. D. (2020). The emergence of transcriptional identity in somatosensory neurons. *Nature*, *577*(7790), 392–398. https://doi.org/10.1038/s41586-019-1900-1

Shields, S. D., Ahn, H.-S., Yang, Y., Han, C., Seal, R. P., Wood, J. N., Waxman, S. G., & Dib-Hajj, S. D. (2012). Nav1.8 expression is not restricted to nociceptors in mouse peripheral nervous system. *Pain*, *153*(10), 2017–2030. https://doi.org/10.1016/j.pain.2012.04.022

Silberstein, S. (2004). Migraine Pathophysiology and its Clinical Implications. *Cephalalgia*, *24*(2_suppl), 2–7. https://doi.org/10.1111/j.1468-2982.2004.00892.x

Skorput, A. G. J., Gore, R., Schorn, R., Riedl, M. S., Marron Fernandez De Velasco, E., Hadlich, B., Kitto, K. F., Fairbanks, C. A., & Vulchanova, L. (2022). Targeting the somatosensory system with AAV9 and AAV2retro viral vectors. *PLOS ONE*, *17*(3), e0264938. https://doi.org/10.1371/journal.pone.0264938

Slimko, E. M., McKinney, S., Anderson, D. J., Davidson, N., & Lester, H. A. (2002). Selective Electrical Silencing of Mammalian Neurons *In Vitro* by the Use of Invertebrate Ligand-Gated Chloride Channels. *The Journal of Neuroscience*, *22*(17), 7373–7379. https://doi.org/10.1523/JNEUROSCI.22-17-07373.2002

Soliman, N., Moisset, X., Ferraro, M. C., De Andrade, D. C., Baron, R., Belton, J., Bennett, D. L. H., Calvo, M., Dougherty, P., Gilron, I., Hietaharju, A. J., Hosomi, K., Kamerman, P. R., Kemp, H., Enax-Krumova, E. K., McNicol, E., Price, T. J., Raja, S. N., Rice, A. S. C., … Zunaid, M. D. (2025). Pharmacotherapy and non-invasive neuromodulation for neuropathic pain: A systematic review and meta-analysis. *The Lancet Neurology*, *24*(5), 413–428. https://doi.org/10.1016/S1474-4422(25)00068-7

Spillane, M., Ketschek, A., Merianda, T. T., Twiss, J. L., & Gallo, G. (2013). Mitochondria Coordinate Sites of Axon Branching through Localized Intra-axonal Protein Synthesis. *Cell Reports*, *5*(6), 1564–1575. https://doi.org/10.1016/j.celrep.2013.11.022

Stachniak, T. J., Ghosh, A., & Sternson, S. M. (2014). Chemogenetic Synaptic Silencing of Neural Circuits Localizes a Hypothalamus→Midbrain Pathway for Feeding Behavior. *Neuron*, *82*(4), 797–808. https://doi.org/10.1016/j.neuron.2014.04.008

Sternson, S. M., & Roth, B. L. (2014). Chemogenetic Tools to Interrogate Brain Functions. *Annual Review of Neuroscience*, *37*(1), 387–407. https://doi.org/10.1146/annurev-neuro-071013-014048

Stirling, C. L., Forlani, G., Baker, M. D., Wood, J. N., Matthews, E. A., Dickenson, A. H., & Nassar, M. A. (2005). Nociceptor-specific gene deletion using heterozygous NaV1.8-Cre recombinase mice. *Pain*, *113*(1), 27–36. https://doi.org/10.1016/j.pain.2004.08.015

Storek, B., Reinhardt, M., Wang, C., Janssen, W. G. M., Harder, N. M., Banck, M. S., Morrison, J. H., & Beutler, A. S. (2008). Sensory neuron targeting by self-complementary AAV8 via lumbar puncture for chronic pain. *Proceedings of the National Academy of Sciences*, *105*(3), 1055–1060. https://doi.org/10.1073/pnas.0708003105

Summerford, C., & Samulski, R. J. (1998). Membrane-Associated Heparan Sulfate Proteoglycan Is a Receptor for Adeno-Associated Virus Type 2 Virions. *Journal of Virology*, *72*(2), 1438–1445. https://doi.org/10.1128/JVI.72.2.1438-1445.1998

Sun, T., Huang, L., Zeng, Q., Sun, J., Wu, Z., Chen, C., & Wang, H. (2024). Blood-nerve barrier: Structure and opening. *Neurology Asia*, *29*(4), 869–886. https://doi.org/10.54029/2024kwz

Sung, K.-W., Kirby, M., McDonald, M. P., Lovinger, D. M., & Delpire, E. (2000). Abnormal $GABA_A$ Receptor-Mediated Currents in Dorsal Root Ganglion Neurons Isolated from Na–K–2Cl Cotransporter Null Mice. *The Journal of Neuroscience*, *20*(20), 7531–7538. https://doi.org/10.1523/JNEUROSCI.20-20-07531.2000

Sureda-Gibert, P., Romero-Reyes, M., & Akerman, S. (2022). Nitroglycerin as a model of migraine: Clinical and preclinical review. *Neurobiology of Pain*, *12*, 100105. https://doi.org/10.1016/j.ynpai.2022.100105

Sweeney, S. T., Broadie, K., Keane, J., Niemann, H., & O'Kane, C. J. (1995). Targeted expression of tetanus toxin light chain in Drosophila specifically eliminates

synaptic transmission and causes behavioral defects. *Neuron*, *14*(2), 341–351. https://doi.org/10.1016/0896-6273(95)90290-2

Szczot, M., Liljencrantz, J., Ghitani, N., Barik, A., Lam, R., Thompson, J. H., Bharucha-Goebel, D., Saade, D., Necaise, A., Donkervoort, S., Foley, A. R., Gordon, T., Case, L., Bushnell, M. C., Bönnemann, C. G., & Chesler, A. T. (2018). PIEZO2 mediates injury-induced tactile pain in mice and humans. *Science Translational Medicine*, *10*(462), eaat9892. https://doi.org/10.1126/scitranslmed.aat9892

Takahashi, K., Tanabe, K., Ohnuki, M., Narita, M., Ichisaka, T., Tomoda, K., & Yamanaka, S. (2007). Induction of Pluripotent Stem Cells from Adult Human Fibroblasts by Defined Factors. *Cell*, *131*(5), 861–872. https://doi.org/10.1016/j.cell.2007.11.019

Talavera, K., Startek, J. B., Alvarez-Collazo, J., Boonen, B., Alpizar, Y. A., Sanchez, A., Naert, R., & Nilius, B. (2020). Mammalian Transient Receptor Potential TRPA1 Channels: From Structure to Disease. *Physiological Reviews*, *100*(2), 725–803. https://doi.org/10.1152/physrev.00005.2019

Tan, F., Dong, Y., Qi, J., Yu, W., & Chai, R. (2025). Artificial Intelligence-Based Approaches for AAV Vector Engineering. *Advanced Science*, *12*(9), 2411062. https://doi.org/10.1002/advs.202411062

Tang, W., Ehrlich, I., Wolff, S. B. E., Michalski, A.-M., Wolfl, S., Hasan, M. T., Luthi, A., & Sprengel, R. (2009). Faithful Expression of Multiple Proteins via 2A-Peptide Self-Processing: A Versatile and Reliable Method for Manipulating Brain Circuits. *Journal of Neuroscience*, *29*(27), 8621–8629. https://doi.org/10.1523/JNEUROSCI.0359-09.2009

Tannenbaum, J., & Bennett, B. T. (2015). Russell and Burch's 3Rs Then and Now: The Need for Clarity in Definition and Purpose. *Journal of the American Association for Laboratory Animal Science*, *54*(2).

Tardiolo, G., Bramanti, P., & Mazzon, E. (2019). Migraine: Experimental Models and Novel Therapeutic Approaches. *International Journal of Molecular Sciences*, *20*(12), 2932. https://doi.org/10.3390/ijms20122932

Tasker, R. R. (1987). The Problem of Deafferentation Pain in the Management of the Patient with Cancer. *Journal of Palliative Care*, *2*(2), 8–12. https://doi.org/10.1177/082585978700200203

Tavares-Ferreira, D., Shiers, S., Ray, P. R., Wangzhou, A., Jeevakumar, V., Sankaranarayanan, I., Cervantes, A. M., Reese, J. C., Chamessian, A., Copits, B. A., Dougherty, P. M., Gereau, R. W., Burton, M. D., Dussor, G., & Price, T. J. (2022). Spatial transcriptomics of dorsal root ganglia identifies molecular signatures of human nociceptors. *Science Translational Medicine*, *14*(632), eabj8186. https://doi.org/10.1126/scitranslmed.abj8186

Tepper, S. J. (2018). History and Review of anti-Calcitonin Gene-Related Peptide (CGRP) Therapies: From Translational Research to Treatment. *Headache: The Journal of Head and Face Pain*, *58*(S3), 238–275. https://doi.org/10.1111/head.13379

Tepper, S. J., Rezai, A., Narouze, S., Steiner, C., Mohajer, P., & Ansarinia, M. (2009). Acute Treatment of Intractable Migraine With Sphenopalatine Ganglion Electrical Stimulation. *Headache: The Journal of Head and Face Pain*, *49*(7), 983–989. https://doi.org/10.1111/j.1526-4610.2009.01451.x

Terashima, T., Ogawa, N., Nakae, Y., Sato, T., Katagi, M., Okano, J., Maegawa, H., & Kojima, H. (2018). Gene Therapy for Neuropathic Pain through siRNA-IRF5

Gene Delivery with Homing Peptides to Microglia. *Molecular Therapy Nucleic Acids*, *11*, 203–215. https://doi.org/10.1016/j.omtn.2018.02.007

Tervo, D. G. R., Hwang, B.-Y., Viswanathan, S., Gaj, T., Lavzin, M., Ritola, K. D., Lindo, S., Michael, S., Kuleshova, E., Ojala, D., Huang, C.-C., Gerfen, C. R., Schiller, J., Dudman, J. T., Hantman, A. W., Looger, L. L., Schaffer, D. V., & Karpova, A. Y. (2016). A Designer AAV Variant Permits Efficient Retrograde Access to Projection Neurons. *Neuron*, *92*(2), 372–382. https://doi.org/10.1016/j.neuron.2016.09.021

Testa, L., Dotta, S., Vercelli, A., & Marvaldi, L. (2024). Communicating pain: Emerging axonal signaling in peripheral neuropathic pain. *Frontiers in Neuroanatomy*, *18*, 1398400. https://doi.org/10.3389/fnana.2024.1398400

Towne, C., Pertin, M., Beggah, A. T., Aebischer, P., & Decosterd, I. (2009). Recombinant Adeno-Associated Virus Serotype 6 (rAAV2/6)-Mediated Gene Transfer to Nociceptive Neurons through Different Routes of Delivery. *Molecular Pain*, *5*, 1744-8069-5–52. https://doi.org/10.1186/1744-8069-5-52

Tso, A. R., & Goadsby, P. J. (2017). Anti-CGRP Monoclonal Antibodies: The Next Era of Migraine Prevention? *Current Treatment Options in Neurology*, *19*(8), 27. https://doi.org/10.1007/s11940-017-0463-4

Tukker, A. M., Wijnolts, F. M. J., De Groot, A., & Westerink, R. H. S. (2018). Human iPSC-derived neuronal models for in vitro neurotoxicity assessment. *NeuroToxicology*, *67*, 215–225. https://doi.org/10.1016/j.neuro.2018.06.007

Urban, D. J., & Roth, B. L. (2015). DREADDs (Designer Receptors Exclusively Activated by Designer Drugs): Chemogenetic Tools with Therapeutic Utility. *Annual Review of Pharmacology and Toxicology*, *55*(1), 399–417. https://doi.org/10.1146/annurev-pharmtox-010814-124803

U.S. Food and Drug Administration. (2017, December 19). *LUXTURNA*. FDA. FDA. https://www.fda.gov/vaccines-blood-biologics/cellular-gene-therapy-products/luxturna

U.S. Food and Drug Administration. (2019, May 24). *FDA approves innovative gene therapy to treat pediatric patients with spinal muscular atrophy, a rare disease and leading genetic cause of infant mortality*. FDA. FDA. https://www.fda.gov/news-events/press-announcements/fda-approves-innovative-gene-therapy-treat-pediatric-patients-spinal-muscular-atrophy-rare-disease

U.S. Food and Drug Administration. (2023, June 29). *ROCTAVIAN*. FDA. FDA. https://www.fda.gov/vaccines-blood-biologics/roctavian

Usoskin, D., Furlan, A., Islam, S., Abdo, H., Lönnerberg, P., Lou, D., Hjerling-Leffler, J., Haeggström, J., Kharchenko, O., Kharchenko, P. V., Linnarsson, S., & Ernfors, P. (2015). Unbiased classification of sensory neuron types by large-scale single-cell RNA sequencing. *Nature Neuroscience*, *18*(1), 145–153. https://doi.org/10.1038/nn.3881

Van Hecke, O., Austin, S. K., Khan, R. A., Smith, B. H., & Torrance, N. (2014). Neuropathic pain in the general population: A systematic review of epidemiological studies. *Pain*, *155*(4), 654–662. https://doi.org/10.1016/j.pain.2013.11.013

Vandenberghe, L. H., Breous, E., Nam, H.-J., Gao, G., Xiao, R., Sandhu, A., Johnston, J., Debyser, Z., Agbandje-McKenna, M., & Wilson, J. M. (2009). Naturally occurring singleton residues in AAV capsid impact vector performance and illustrate structural constraints. *Gene Therapy*, *16*(12), 1416–1428. https://doi.org/10.1038/gt.2009.101

Vardy, E., Robinson, J. E., Li, C., Olsen, R. H. J., DiBerto, J. F., Giguere, P. M., Sassano, F. M., Huang, X.-P., Zhu, H., Urban, D. J., White, K. L., Rittiner, J. E., Crowley, N. A., Pleil, K. E., Mazzone, C. M., Mosier, P. D., Song, J., Kash, T. L., Malanga, C. J., … Roth, B. L. (2015). A New DREADD Facilitates the Multiplexed Chemogenetic Interrogation of Behavior. *Neuron*, *86*(4), 936–946. https://doi.org/10.1016/j.neuron.2015.03.065

Vulchanova, L., Schuster, D. J., Belur, L. R., Riedl, M. S., Podetz-Pedersen, K. M., Kitto, K. F., Wilcox, G. L., McIvor, R. S., & Fairbanks, C. A. (2010). Differential Adeno-Associated Virus Mediated Gene Transfer to Sensory Neurons following Intrathecal Delivery by Direct Lumbar Puncture. *Molecular Pain*, *6*, 1744-8069-6–31. https://doi.org/10.1186/1744-8069-6-31

Walker, M. C., & Kullmann, D. M. (2020). Optogenetic and chemogenetic therapies for epilepsy. *Neuropharmacology*, *168*, 107751. https://doi.org/10.1016/j.neuropharm.2019.107751

Warden, M. R., Cardin, J. A., & Deisseroth, K. (2014). Optical Neural Interfaces. *Annual Review of Biomedical Engineering*, *16*(1), 103–129. https://doi.org/10.1146/annurev-bioeng-071813-104733

Waxman, S. G., Kocsis, J. D., Stys, P. K., Waxman, S. G., Kocsis, J. D., & Stys, P. K. (Eds). (1995). *The Axon: Structure, Function and Pathophysiology*. Oxford University Press.

Waxman, S. G., & Zamponi, G. W. (2014). Regulating excitability of peripheral afferents: Emerging ion channel targets. *Nature Neuroscience*, *17*(2), 153–163. https://doi.org/10.1038/nn.3602

Wei, W., Liu, Y., Shen, Y., Yang, T., Dong, Y., Han, Z., Wang, Y., Liu, Z., Chai, Y., Zhang, M., Wang, H., Shen, H., Shen, Y., & Chen, M. (2024). In situ tissue profile of rat

trigeminal nerve in trigeminal neuralgia using spatial transcriptome sequencing. *International Journal of Surgery*, *110*(3), 1463–1474. https://doi.org/10.1097/JS9.0000000000001110

Weir, G. A., Middleton, S. J., Clark, A. J., Daniel, T., Khovanov, N., McMahon, S. B., & Bennett, D. L. (2017). Using an engineered glutamate-gated chloride channel to silence sensory neurons and treat neuropathic pain at the source. *Brain*, *140*(10), 2570–2585. https://doi.org/10.1093/brain/awx201

Wemmie, J. A., Chen, J., Askwith, C. C., Hruska-Hageman, A. M., Price, M. P., Nolan, B. C., Yoder, P. G., Lamani, E., Hoshi, T., Freeman, J. H., & Welsh, M. J. (2002). The Acid-Activated Ion Channel ASIC Contributes to Synaptic Plasticity, Learning, and Memory. *Neuron*, *34*(3), 463–477. https://doi.org/10.1016/S0896-6273(02)00661-X

Wess, J., Nakajima, K., & Jain, S. (2013). Novel designer receptors to probe GPCR signaling and physiology. *Trends in Pharmacological Sciences*, *34*(7), 385–392. https://doi.org/10.1016/j.tips.2013.04.006

Whitehead, J. L., Ohara, P. T., Tauscher, A. N., & LaVail, J. H. (2003). A procedure to deliver herpes simplex virus to the murine trigeminal ganglion. *Brain Research Protocols*, *12*(1), 60–66. https://doi.org/10.1016/S1385-299X(03)00072-2

Wiegert, J. S., Mahn, M., Prigge, M., Printz, Y., & Yizhar, O. (2017). Silencing Neurons: Tools, Applications, and Experimental Constraints. *Neuron*, *95*(3), 504–529. https://doi.org/10.1016/j.neuron.2017.06.050

Wilke, B. U., Kummer, K. K., Leitner, M. G., & Kress, M. (2020). Chloride – The Underrated Ion in Nociceptors. *Frontiers in Neuroscience*, *14*, 287. https://doi.org/10.3389/fnins.2020.00287

Woo, S.-H., Lukacs, V., De Nooij, J. C., Zaytseva, D., Criddle, C. R., Francisco, A., Jessell, T. M., Wilkinson, K. A., & Patapoutian, A. (2015). Piezo2 is the principal mechanotransduction channel for proprioception. *Nature Neuroscience*, *18*(12), 1756–1762. https://doi.org/10.1038/nn.4162

Woolf, C. J., & Salter, M. W. (2000). Neuronal Plasticity: Increasing the Gain in Pain. *Science*, *288*(5472), 1765–1768. https://doi.org/10.1126/science.288.5472.1765

Worm, J., Heinskou, T. B., Rochat, P., Springborg, J. B., Smilkov, E. A., Bendtsen, L., Schytz, H. W., & Maarbjerg, S. (2025). Five-year prospective outcomes of medical management and microvascular decompression in trigeminal neuralgia. *Journal of Neurology*, *272*(10), 701. https://doi.org/10.1007/s00415-025-13447-9

Wu, G., Ringkamp, M., Hartke, T. V., Murinson, B. B., Campbell, J. N., Griffin, J. W., & Meyer, R. A. (2001). Early Onset of Spontaneous Activity in Uninjured C-Fiber Nociceptors after Injury to Neighboring Nerve Fibers. *The Journal of Neuroscience*, *21*(8), RC140–RC140. https://doi.org/10.1523/JNEUROSCI.21-08-j0002.2001

Wu, Z., Zhu, Y., Xu, L., Lai, W., Chen, X., & Long, H. (2024). Development of a novel three-dimensional injection guide for trigeminal ganglia. *Journal of Neuroscience Methods*, *409*, 110197. https://doi.org/10.1016/j.jneumeth.2024.110197

Xie, Q., Bu, W., Bhatia, S., Hare, J., Somasundaram, T., Azzi, A., & Chapman, M. S. (2002). The atomic structure of adeno-associated virus (AAV-2), a vector for human gene therapy. *Proceedings of the National Academy of Sciences*, *99*(16), 10405–10410. https://doi.org/10.1073/pnas.162250899

Xiong, C., Chua, K. C., Stage, T. B., Priotti, J., Kim, J., Altman-Merino, A., Chan, D., Saraf, K., Canato Ferracini, A., Fattahi, F., & Kroetz, D. L. (2021). Human

Induced Pluripotent Stem Cell Derived Sensory Neurons are Sensitive to the Neurotoxic Effects of Paclitaxel. *Clinical and Translational Science*, *14*(2), 568–581. https://doi.org/10.1111/cts.12912

Xu, L., Wang, X., Liu, Y., Yang, G., Falconer, R. J., & Zhao, C.-X. (2022). Lipid Nanoparticles for Drug Delivery. *Advanced NanoBiomed Research*, *2*(2), 2100109. https://doi.org/10.1002/anbr.202100109

Yang, L., Xu, M., Bhuiyan, S. A., Li, J., Zhao, J., Cohrs, R. J., Susterich, J. T., Signorelli, S., Green, U., Stone, J. R., Levy, D., Lennerz, J. K., & Renthal, W. (2022). Human and mouse trigeminal ganglia cell atlas implicates multiple cell types in migraine. *Neuron*, *110*(11), 1806-1821.e8. https://doi.org/10.1016/j.neuron.2022.03.003

Yang, O. J., Robilotto, G. L., Alemán, K., Devulapally, K., Morris, A., & Mickle, A. D. (2023). Evaluating the transduction efficiency of systemically delivered AAV vectors in the rat nervous system. *Frontiers in Neuroscience*, *17*, 1001007. https://doi.org/10.3389/fnins.2023.1001007

Yu, H., Fischer, G., & Hogan, Q. H. (2016). AAV-Mediated Gene Transfer to Dorsal Root Ganglion. In F. P. Manfredsson (Ed.), *Gene Therapy for Neurological Disorders* (Vol. 1382, pp. 251–261). Springer New York. https://doi.org/10.1007/978-1-4939-3271-9_18

Yu, H., Nagi, S. S., Usoskin, D., Hu, Y., Kupari, J., Bouchatta, O., Yan, H., Cranfill, S. L., Gautam, M., Su, Y., Lu, Y., Wymer, J., Glanz, M., Albrecht, P., Song, H., Ming, G.-L., Prouty, S., Seykora, J., Wu, H., … Luo, W. (2024). Leveraging deep single-soma RNA sequencing to explore the neural basis of human somatosensation. *Nature Neuroscience*, *27*(12), 2326–2340. https://doi.org/10.1038/s41593-024-01794-1

Yuan, X., Han, S., Zhao, F., Manyande, A., Gao, F., Wang, J., Zhang, W., & Tian, X. (2023). Rapid injection of lumbar dorsal root ganglia under direct vision: Relevant anatomy, protocol, and behaviors. *Frontiers in Neurology*, *14*, 1138933. https://doi.org/10.3389/fneur.2023.1138933

Zakrzewska, J. M., & Linskey, M. E. (2014). Trigeminal neuralgia. *BMJ*, *348*(feb17 9), g474–g474. https://doi.org/10.1136/bmj.g474

Zeisel, A., Hochgerner, H., Lönnerberg, P., Johnsson, A., Memic, F., Van Der Zwan, J., Häring, M., Braun, E., Borm, L. E., La Manno, G., Codeluppi, S., Furlan, A., Lee, K., Skene, N., Harris, K. D., Hjerling-Leffler, J., Arenas, E., Ernfors, P., Marklund, U., & Linnarsson, S. (2018). Molecular Architecture of the Mouse Nervous System. *Cell*, *174*(4), 999-1014.e22. https://doi.org/10.1016/j.cell.2018.06.021

Zeng, W.-Z., Liu, D.-S., Liu, L., She, L., Wu, L.-J., & Xu, T.-L. (2015). Activation of acid-sensing ion channels by localized proton transient reveals their role in proton signaling. *Scientific Reports*, *5*(1), 14125. https://doi.org/10.1038/srep14125

Zerboni, L., & Arvin, A. (2011). Investigation of varicella-zoster virus neurotropism and neurovirulence using SCID mouse–human DRG xenografts. *Journal of NeuroVirology*, *17*(6), 570–577. https://doi.org/10.1007/s13365-011-0066-x

Zheng, H., Qiao, C., Wang, C.-H., Li, J., Li, J., Yuan, Z., Zhang, C., & Xiao, X. (2010). Efficient Retrograde Transport of Adeno-Associated Virus Type 8 to Spinal Cord and Dorsal Root Ganglion After Vector Delivery in Muscle. *Human Gene Therapy*, *21*(1), 87–97. https://doi.org/10.1089/hum.2009.131

Zheng, Y., Liu, P., Bai, L., Trimmer, J. S., Bean, B. P., & Ginty, D. D. (2019). Deep Sequencing of Somatosensory Neurons Reveals Molecular Determinants of Intrinsic Physiological Properties. *Neuron*, *103*(4), 598-616.e7. https://doi.org/10.1016/j.neuron.2019.05.039

Zhu, D., Brookes, D. H., Busia, A., Carneiro, A., Fannjiang, C., Popova, G., Shin, D., Donohue, K. C., Lin, L. F., Miller, Z. M., Williams, E. R., Chang, E. F., Nowakowski, T. J., Listgarten, J., & Schaffer, D. V. (2024). Optimal trade-off control in machine learning–based library design, with application to adeno-associated virus (AAV) for gene therapy. *Science Advances*, *10*(4), eadj3786. https://doi.org/10.1126/sciadv.adj3786

Zingg, B., Chou, X., Zhang, Z., Mesik, L., Liang, F., Tao, H. W., & Zhang, L. I. (2017). AAV-Mediated Anterograde Transsynaptic Tagging: Mapping Corticocollicular Input-Defined Neural Pathways for Defense Behaviors. *Neuron*, *93*(1), 33–47. https://doi.org/10.1016/j.neuron.2016.11.045

Zingg, B., Dong, H., Tao, H. W., & Zhang, L. I. (2022). Application of AAV1 for Anterograde Transsynaptic Circuit Mapping and Input-Dependent Neuronal Cataloging. *Current Protocols*, *2*(1), e339. https://doi.org/10.1002/cpz1.339